MASS TRANSFER

IN DISPERSE SYSTEMS

THESIS

PRESENTED FOR THE DEGREE

OF

DOCTOR OF PHILOSOPHY

DEPARTMENT OF CHEMICAL ENGINEERING

UNIVERSITY OF CANTERBURY

J.B. GLEN

1965

PREFACE

"A useful and very ingenious idea was surely that of the inventor of a short way of extracting gold and silver from the sweepings of all those arts that handle them, as well as every particle that smelters of ores might have left in the slags, and also that in some ores themselves. This is done without using great labor in smelting but by the sole means and virtue of mercury. To do this, first make a large bricked pan of stone or wood and arrange a millstone inside which rotates in the hollow of this pan like that of a flour mill. In the hollow of the pan put some of your material containing gold after it has been crushed well in a mortar and then washed and dried. Grind it in the said mill, moistening it meanwhile with vinegar or water in which sublimate, verdigris, and common salt have been dissolved. Then enough mercury to cover these materials is poured over them. They are agitated inside for an hour or two, by turning the mill either by hand or with a horse, depending on the device that you have arranged. Remember that the more the mercury and the material are rubbed together in the mill the more it can be believed that the mercury absorbs the substance that the materials contain."

This secret cost Vannoccio Biringuccio dearly, but, "This I wish to tell you not in order that you would repay me for teaching it to you, but in order that you should esteem and value it so much more."

Vannocio Biringuccio

"The Pirotechnia of Vannocio Biringuccio", circa 1500.

ACKNOWLEDGMENTS

This research has been made possible through the award of a Fellowship by the New Zealand University Grants Committee, and by their further generous financial assistance which enabled the purchase of necessary equipment. This work has been done under the direction and supervision of Dr R.B. Keey, and the staff of the Chemical Engineering Department, under Professors S.R. Siemon, and A.M. Kennedy, to all of whom grateful acknowledgment is expressed.

The writer wishes to thank Messrs J. Voot, T.P. Dobbie, and P.M. Farrier who have undertaken separate projects which form part of this work.

Finally, the writer acknowledges his appreciation of the assistance given by members of the Faculties of Chemistry and Engineering, and the technical staff of the Chemical Engineering Department, for their lending and construction of apparatus.

A University Grants Committee Research Grant 62/169, and a grant by the University of Canterbury Council, have financed the equipment necessary for this thesis.

CONTENTS

ABSTRACT

The fluid dynamic aspects of liquid extraction are investigated for the mass transfer system isooctane/o-nitrophenol (solute)/water (continuous, extractant phase), in flow mixing vessels of various geometries. Dimensional "order of magnitude" relationships, suitable for mixer scale-up, or system change, are derived from turbulence theory. The existence of locally isotropic flow, and inertial subrange control of the droplet hydrodynamics is substantiated.

The physical properties, density, viscosity, surface tension, and solute distribution are determined for the system.

Power dissipation is controlled by the impellor dimension, and is independent of the vessel diameter, for the Reynolds number range, $10^4 < Re < 10^5$.

$$P \sim N^{2.6} \cdot D_I^{3.6} \cdot D_T^{0}$$

A relationship, derived by considering the inertial subrange turbulence to control the particle fragmentation, correlates the mean drop size in the dispersion.

$$d_{sv} = 1.26 \frac{D_I^{2/5}}{(ND_I)^{6/5}} \cdot \left(\frac{D_T}{D_I}\right)^{6/5} \qquad \text{c.g.s. units}$$

The drop size distributions are log-normal, except for the maximum and minimum drop sizes that are retained in a turbulent flow. The standard deviation of the size distributions decreases with increasing power input.

The hold-up of the dispersed phase is related to the droplet slip velocity, and the mean flow velocity of the fluid.

$$\phi/\phi_f = 3.0 \frac{\rho_c^2}{\Delta\rho} \cdot \frac{\mu_c}{\sigma^{6/5}} \cdot N^{1.4} D_I^{1.6} \left(\frac{D_I}{D_T}\right)^{.9}, \quad Re_{Imp} < 7 \times 10^4$$

An internally circulating drop, combined with a turbulent sublayer mechanism, is necessary to interpret the continuous phase mass transfer correlation obtained,

$$Sh_{Imp} = 8.92 \times 10^{-4} Re_{Imp}^{1.36} \frac{1}{D_T^{.5} D_I^{.36}} - 336, \quad 10^4 < Re_{Imp} < 10^5$$

MKH units

No interfacial turbulence, or surfactant contamination of the system is noted. The continuous phase is fully mixed, for all power inputs, but the dispersed phase is substantially unmixed for the low volume fractions used, $0.025 < \phi < 0.10$.

Section 1

INTRODUCTION

The art of extraction has existed for several millenia without, as Treybal (131) observes, much knowledge of the activity coefficients, or the transfer coefficients, but within this century extraction processes have been interpreted in terms of the system and equipment variables. As the overall parameters of efficiency, power, and residence times, initially studied, failed to show uniformity in mixing processes, the theoretical and experimental investigations of fluid turbulence and solution properties, carried out in the past decade, are necessary to interpret and correlate extraction processes.

Single particle behaviour in different flow conditions has been elucidated. The effects of flow rate, interface instability, and circulation within the drop on mass transfer have been predicted and correlated. Similarly, changes of solution and solute properties with mass transfer have been determined for ideal situations, but the deviations from these simplified models, encountered in industrial extraction, are not fully correlated. Consequently, Olney and Miller, (1) (1963), observe that at present the problem of translating from one scale to another has fewer pitfalls than has the problem of predicting extraction performance from first principles.

Fluid flow within a mixer has been investigated, usually by the laborious procedure of analysing photographic traces of particles entrained in the fluid. The few mixer geometries investigated so far show that the fluid motion, particularly in the impellor zone, may be described by theories of turbulence. Taylor's (122) theory of

homogeneous and isotropic turbulence, in which the mean and fluctuating fluid velocities are independent of position and direction, does not describe mixer flow. Kolmogoroff's (60) theory of local isotropy, however, in which the small scale inertial turbulence is isotropic, although the mean flow is directional, accounts for mixer hydrodynamics, particularly near the impellor.

Thus mixing vessel processes may be correlated with the behaviour of single particles, and the theory of turbulence, when the process is controlled by fluid flow within the mixer. This implies that design from a knowledge of solution properties, and vessel geometry is possible, which would eliminate the need for pilot-scale experimental work.

This thesis considers the hydrodynamic aspects of extraction in a mixing vessel. The variables, power dissipation, particle size, dispersed phase holdup, continuous phase mass transfer coefficients, and fluid turbulence within a mixer are discussed, as separate problems. This inevitably leads to some duplication of material, but it is trusted that this disadvantage is offset by a clarification of the individual processes.

The experimental data obtained in this work, are for the simple extraction system isooctane/o-nitrophenol/water, in which the mass transfer rate is controlled by the water film transfer; but the results with different mixing vessel experiments when more complex transfer mechanisims exist, are used extensively. This thesis is in part, a survey of extraction operations in a mixing vessel.

Section 2

EXPERIMENTAL

2.1 SYSTEM SELECTION

The historic inconsistency of liquid-liquid extraction data, suggests that chemical property changes, and traces of impurities in the systems investigated, influence mass transfer rates to the same extent as mixer design (64, 70, 113). As the intent of this work is to relate liquid extraction processes to fluid flow, a simple mass transfer controlled process is necessary for experimental investigation. Other requirements for this system also exist. Continuous analysis of the solute transferred is desirable, to eliminate sampling variations, and to indicate steady state conditions within the mixer (119). In addition, the properties, volatility, corrosiveness, cost, and availibility, as well as the personnel hazards of toxicity, inflammibility, and odour have to be considered.

These conditions may be elaborated. The properties of the selected system, isooctane/o-nitrophenol (solute)/ water (continuous, extractant phase) are examined, to show how far the above criteria are fulfilled.

1 Mass transfer control of the solute transfer is to be substantially in the continuous phase.

(a) If the internal and external drop film coefficients are of the same order, the continuous phase film will control the transfer rate, provided that the solute distribution ratio strongly favours the dispersed phase. In section 7.11, the internal and external film coefficients are shown to be nearly equal, and the solute distribution coefficient,

$$m_d = \left(\frac{\text{gm. ONP}}{\text{gm.isooctane}}\right)/\left(\frac{\text{gm. ONP}}{\text{gm.water}}\right),$$

is 39.6.

(b) No chemical reaction, association, or dissociation of the solute on transfer is desired. O-nitrophenol is slightly dissociated, $K_D = 5.8 \times 10^{-8}$, in acid solutions, pH < 4.5. No chemical reaction occurs in this system, but the highly polar nature of o-nitrophenol suggests that it may act as a weak surfactant, accumulating at the liquid interface.

(c) Although not specifically mentioned, low solute concentrations are desirable, to ensure low mass transfer rates. The minimum concentration limit of o-nitrophenol which may be detected by spectroscopic means is 5×10^{-7} gm. ONP/gm. H_2O. There are no interacting transfer processes in the system, as isooctane is barely soluble in water and because the isooctane phase is recycled, it is pre-saturated with water.

(d) The interpretation of the transfer process may be simplified by interfacial stability during mass transfer. The phases densities are comparable, as are their viscosities. When transfer is from the isooctane to the aqueous phase, the interfacial tension is independent of solute concentration.

ρ_{H_2O} = 0.999 gm/cm^3 $\quad \rho_{isooctane}$ = 0.692, at 18°c

μ_{H_2O} = 1.056 cP. $\quad \mu_{isooctane}$ = 0.515, at 18°c

σ = 50.4 dynes/cm. (Isooctane + ONP)/(water + ONP)

2 Solute analysis

(a) A continuous analysis of the solute in an outlet stream is required. Associated o-nitrophenol may be analysed in the aqueous phase over the concentration range, 5×10^{-7} to 8×10^{-5} gm. ONP/gm. H_2O, using a Hilger UVSpec, with a light wave length λ = 3450 Å. A continuous Hilger - Watts absorptiometer, was modified so that a wave length, $\lambda \sim 3450$ Å could be used to follow the solute concentration in the aqueous phase as it leaves the mixer.

(b) Fast coalescence of the dispersed phase in the settling vessel is required, to minimise the mass transfer occurring during coalescence, before the solute concentration in the aqueous phase is analysed, and to reduce isooctane loss by entrainment. Substantial coalescence of the isooctane/o-nitrophenol and water/o-nitrophenol phases was found to occur within 20 seconds, after being shaken in a test tube, although a fine dispersion of isooctane remained in the aqueous phase. This dispersion settled out very slowly.

3 Further system requirements

The 'convenience' requirements are partially satisfied. Isooctane is slightly volatile at room temperature, vapour pressure ~40 mm Hg. at 20°C, and is inflammable. O-nitrophenol is toxic, but in this work, low concentrations are used. O-nitrophenol has the property that it melts at 45°C, which enables the manufacture of solid spheres by cooling liquid drops in a slightly warmed water column. The o-nitrophenol may be purified by steam distillation.

2.2 MATERIAL PURITY

The isooctane was specified by the suppliers to be 99.9% pure. A sample analysed with a Pye Argon Chromatographic Column showed a minor peak, of less than 0.5% impurity.

The o-nitrophenol supplied was technical grade, and had to be purified by steam distillation.

Melting point of o-nitrophenol (purified) = 45±.2°C

Melting point of o-nitrophenol (47) = 45°C

Tapwater, acidified with sulphuric acid to pH 3.5 ± 0.3, was used as the aqueous phase.

Dissolved solids in the tapwater = 0.01 gm/100 gm.

Sufficient quantities of distilled water were not

available, but no detrimental properties such as aeration or surfactants, were observed from the use of the artesian water.

2.3 PHYSICAL DATA

As the system isooctane/o-nitrophenol/water has not been used previously as a liquid-liquid extraction system, physical properties had to be determined experimentally.

Solute distribution coefficient

A 150 ml. flask, containing nearly 100 ml. of individually weighed o-nitrophenol, isooctane, and water, pH 3.5, was shaken for 24 hours in a temperature controlled water-bath. The two phases were separated, with a temperature-controlled separating funnel, and the aqueous phase o-nitrophenol content analysed spectroscopically, with a Hilger UVSpec, at a wavelength of $\lambda = 3450$ Å. The results, expressed as,

$$\frac{\text{gm. ONP in aqueous phase}}{\text{gm. aqueous phase}} \quad \text{and} \quad \frac{\text{gm. of ONP in isooctane phase}}{\text{gm. isooctane phase}}$$

are presented in Appendix 6; the coefficients, c and b, which best fit the relationship,

$$\left(\frac{\text{gm. ONP}}{\text{gm. aqueous phase}}\right) = c \left(\frac{\text{gm. ONP}}{\text{gm. isooctane phase}}\right)^{b}$$

are presented in Table 1. Treybal (131) observes that a straight line may be expected for such a data correlation, and this is found to be so.

As variations in temperature are not apparent, in these results, all these data are expressed for the temperature range, 17.7 - 29.4°C, as,

$$\left(\frac{\text{gm. ONP}}{\text{gm. aqueous phase}}\right) = 0.01877 \left(\frac{\text{gm. ONP}}{\text{gm. isooctane phase}}\right)^{0.9329}$$

Regression coefficient, R = 0.994.

Table 1

Temp. °C.	c	b	no.expts	R
17.7 ± .1	0.0448	0.835	8	0.986
18.0 ± .1	0.0222	0.945	8	0.978
18.0 ± .1	0.0197	0.942	20	0.995
18.3 ± .1	0.0166	0.895	9	0.993
23.6 ± .1	0.0260	1.010	6	0.999
24.8 ± .1	0.0165	0.905	8	0.980
29.4 ± .1	0.0169	0.933	7	0.999

Phase density

The density of each equilibrated phase, from the distribution experiments, was determined with a 10 ml. pyknometer. The density of the aqueous phase was essentially constant for the range of o-nitrophenol concentrations measured, 0 to 6 x 10^{-5} gm. H_2O. The isooctane phase density increased with o-nitrophenol concentration in the range 0 to 5.5 x 10^{-3} gm. ONP/gm. isooctane.

DENW = ρ_c = (1.0 - (TEMP-4.0) x 0.000111)

DENI = ρ_d = (0.7098 - (TEMP x 0.000903). (1 + CINx0.437)

Standard deviation σ_g of experimental results from correlating lines,

Aqueous phase, σ_g = 0.0004 gm/cm^3

Isooctane phase, σ_g = 0.0002 gm/cm^3

Data are presented in Appendix 7.

Phase kinematic viscosity

The kinematic viscosity of each equilibrated phase from the distribution experiments was measured with a Cannon-Fenske viscometer, range 0.4 to 1.6 cP. Within the measurement error, the kinematic viscosity of each phase was constant with increasing o-nitrophenol concentration.

$$VISW = \mu_c = 100 / (2.1482 \times (TEMP + 81.93)) - 120 \quad cP.$$

$$VISI = \mu_d = 0.0146 \exp (1036 / (TEMP + 273)) \quad cP.$$

Standard deviation σ_g of experimental results from correlating lines,

Aqueous phase, σ_g = 0.005 cP.

Isooctane phase, σ_g = 0.002 cP.

Data are presented in Appendix 8.

Surface tension

The interfacial tension of the equilibrated phases was measured by a drop-weight stalagtometer. The interfacial tensions of isooctane drops containing o-nitrophenol, rising in an aqueous solution initially containing no o-nitrophenol, as well as the reverse system of aqueous phase drops containing o-nitrophenol, were measured.

Interfacial tension correlations;

Equilibrated phase, σ = 50.4 - 220 x $\frac{\text{gm.ONP}}{\text{gm.isooctane}}$ dynes/cm,

σ_g = 0.5

Aqueous phase drops, σ = 50.3 - 75 x $\frac{\text{gm.ONP}}{\text{gm.water}}$ dynes/cm,

σ_g = 0.4

Isooctane drops, σ = 50.4 dynes/cm. σ_g = 0.2

The interfacial tension of the system isooctane/o-nitrophenol/water (continuous extractant phase) is independent of o-nitrophenol concentration in the range 0 to 5 x 10^{-3} gm.ONP/gm isooctane.

Data from surface tension measurements are presented in Appendix 9.

Diffusivity

The diffusivity of o-nitrophenol in each phase was not measured, but is estimated from Wilkes and Chang's correlation (137). The diffusivity coefficient of

o-nitrophenol in the aqueous phase is given as

$$DAB = \mathcal{D} = \frac{7.4 \times 10^{-8}(\varphi \cdot M_B)^{0.5} \cdot Temp}{\mu_c V_A^{.6}}$$

$$= 2.722 \times \frac{273.3 + TEMP}{\mu_c} \quad cm^2/sec.$$

Density, viscosity, and surface tension measurements were made, using standard equipment in controlled temperature conditions. Each piece of glassware was de-greased with potassium permanganate solution, and washed with six distilled water/acetone cycles, before being dried with an air draught.

De-ionised and de-gassed tapwater; and n-heptane, density 0.680 gm/cm^3 at 20°C, with a boiling range of 1°C., were used to calibrate the four pyknometers, two viscometers, and the stalagtometer, with which measurements of physical properties were made.

2.4 EQUIPMENT DESIGN AND EXPERIMENTAL MEASUREMENTS

A continuous-flow extraction vessel is desirable, since it eliminates the time variable, and enables easy continuous sampling of the outlet stream. It is also more likely that a continuous-flow agitated vessel will be encountered in industrial plant, than a batch vessel. As well, criteria for single-stage, flow extractors are applicable to multi-stage agitated extractors, and agitated reaction vessels.

A flow sheet, Fig. 2.1, the equipment photographs, Figs. 2.2 and 2.3, and Appendix 10, indicate the apparatus used. The mixing vessels follow the usual agitated vessel design. The phase inlets are concentric at the base of the mixing vessel, while the overflow outlet is concentric to the impellor shaft, which renders the use of a gland, unnecessary, and eliminates any gas-liquid interface in the vessel. Four baffles of width $\frac{1}{8}$th of the vessel diameter

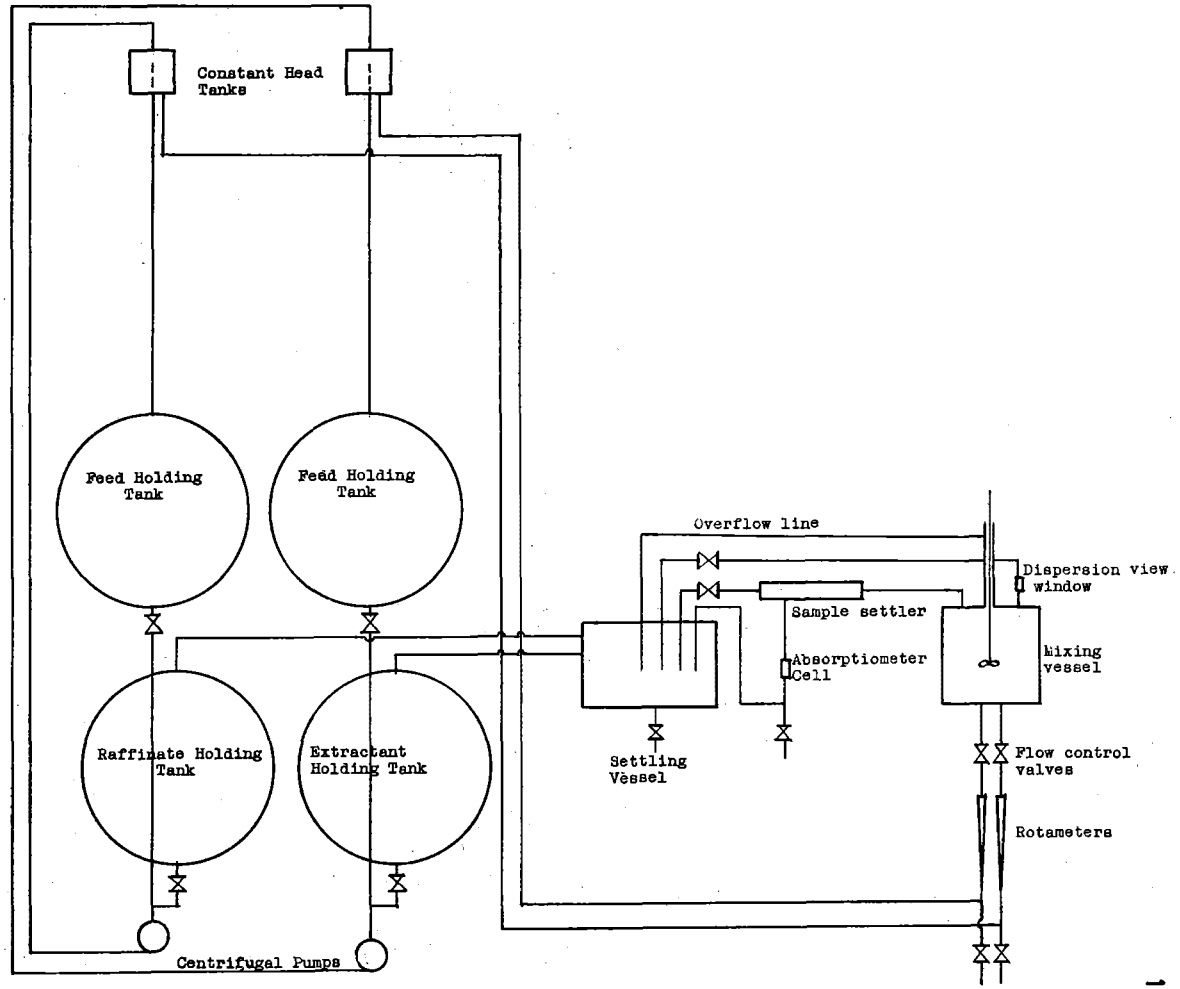

Fig. 2.1. Flow diagram of apparatus.

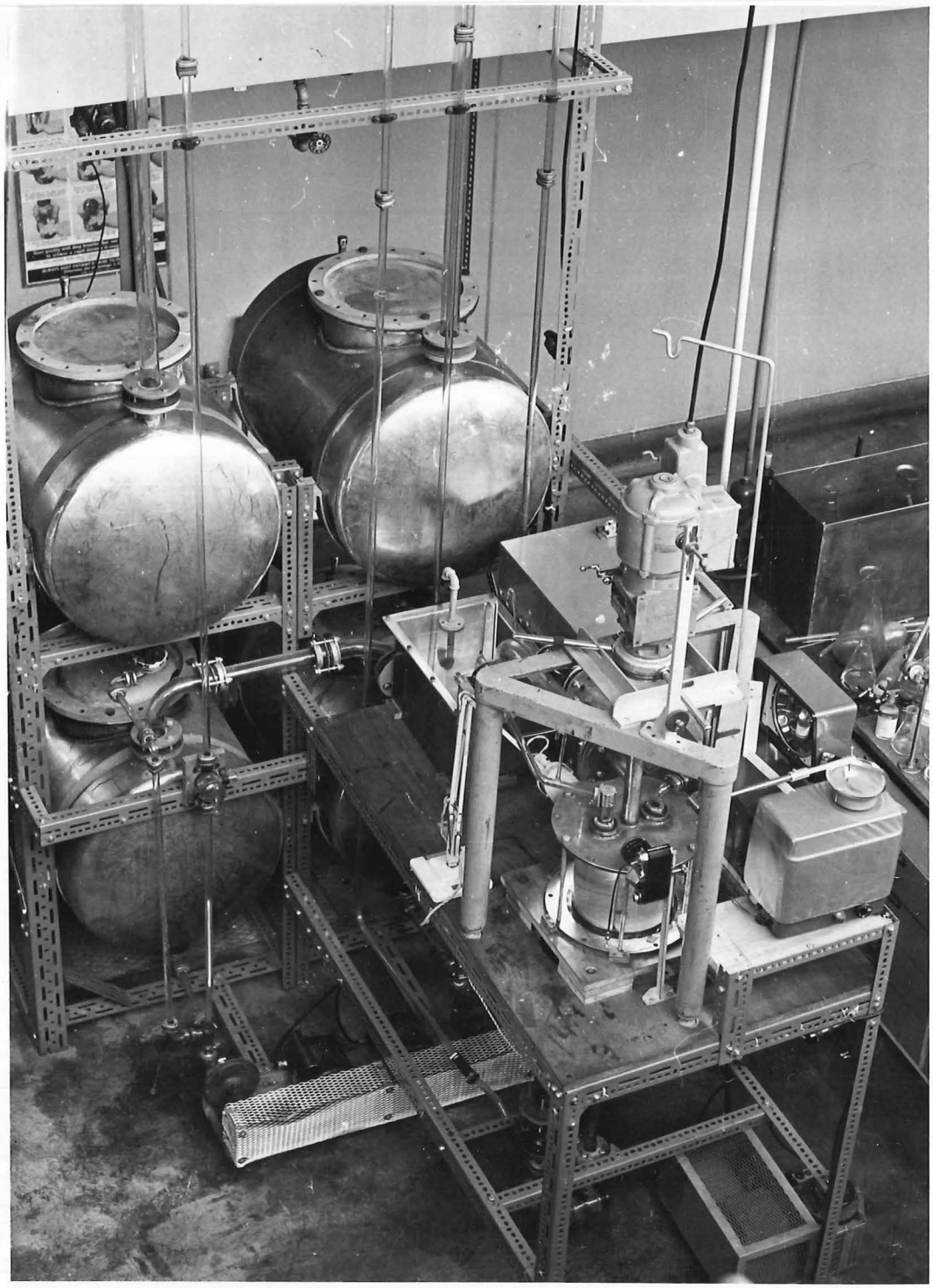

Fig. 2.2 Apparatus

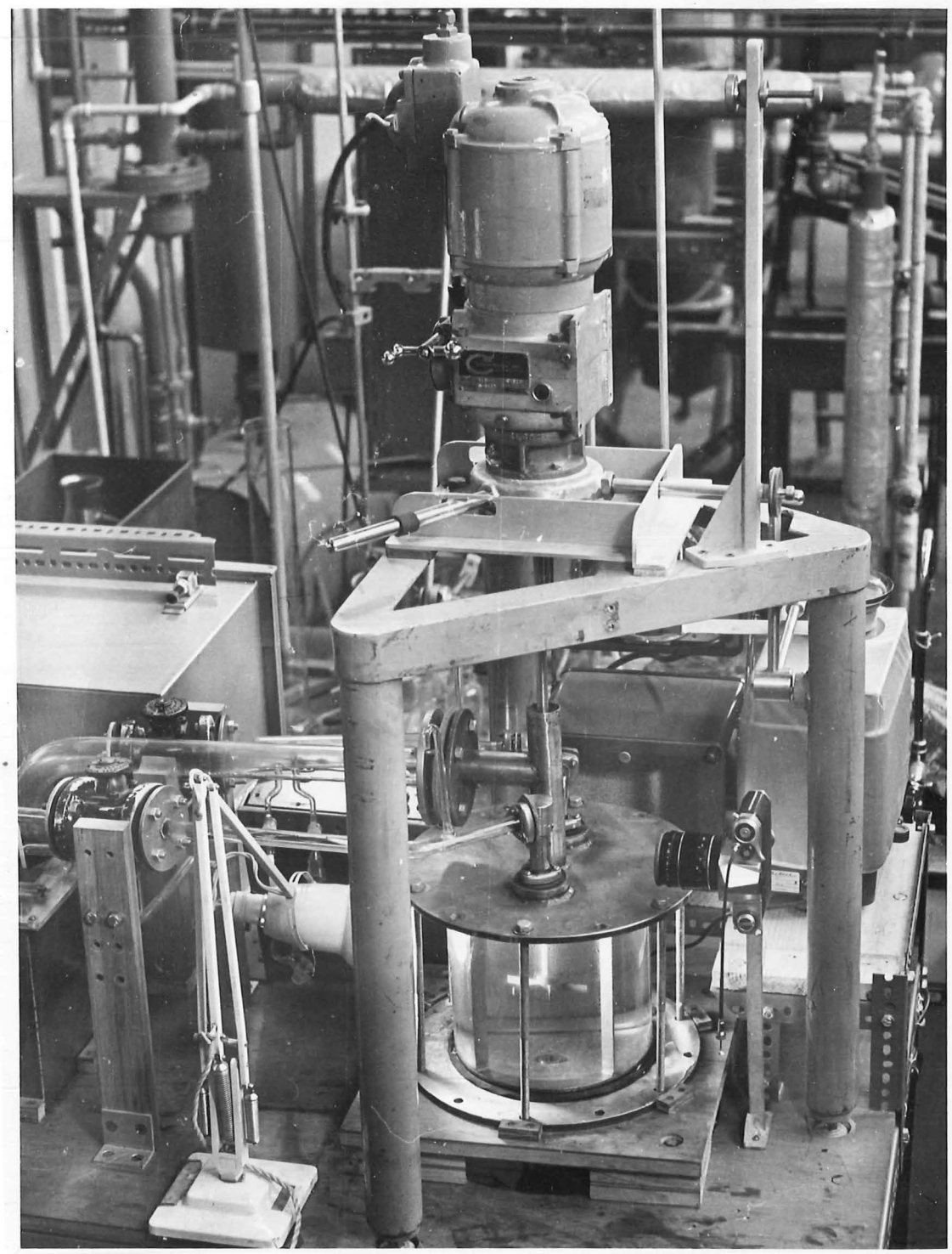

Fig. 2.3 Mixer

were set out from the vessel wall by 1/16 in., to avoid stagnant liquid regions. The impellor is set centrally in the vessel to obtain a symmetrical liquid flow pattern. See Fig. 2.4.

Fig. 2.4 Mixing Vessel

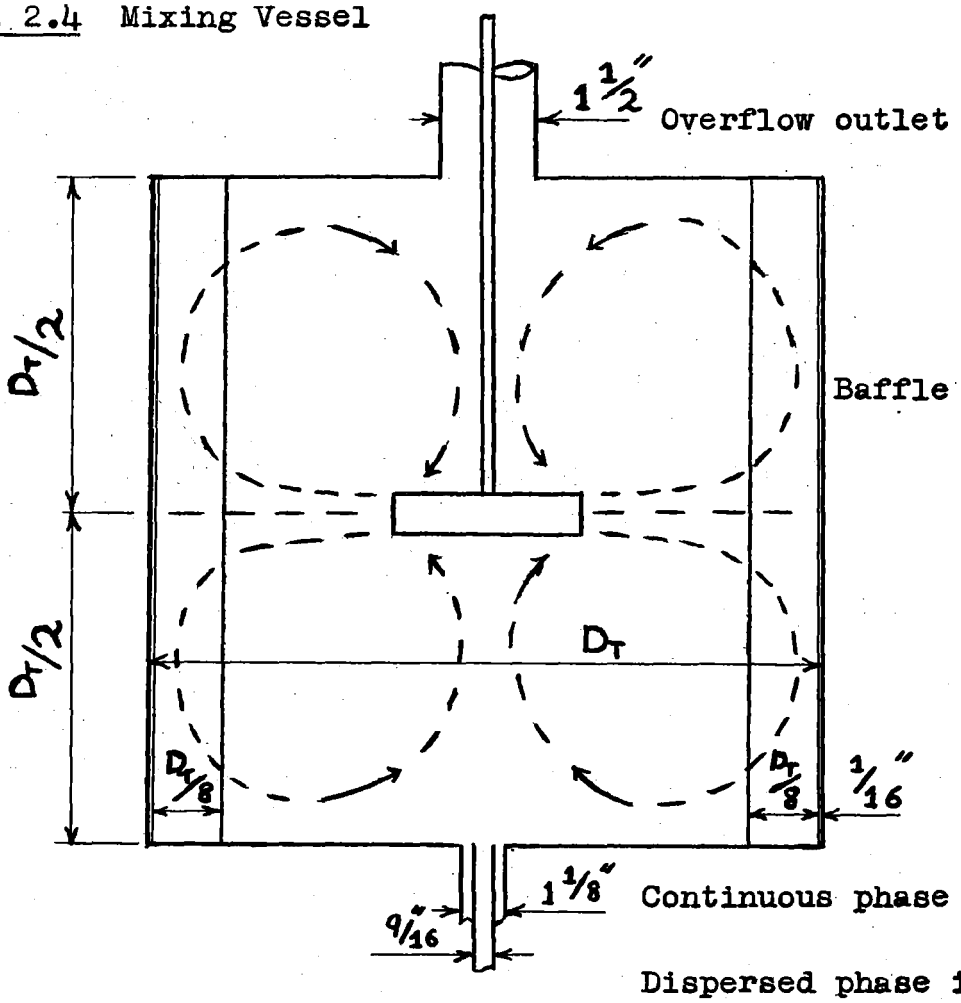

These conditions agree with the general recommendations given by Treybal (131), but in particular follow the vessel design used by Cutter (19), who has made extensive measurements of flow patterns in a baffled vessel.

The impellors used were six-bladed, flat paddles, see Fig. 2.5 some of which were supplied, with the variable speed agitator by the Chemineer Mixing Company. These impellors, and others made up in this Department, were machined to the required scale ratios. It has been found (28) that flat-bladed paddles form a flow

Fig. 2.5 Impellor

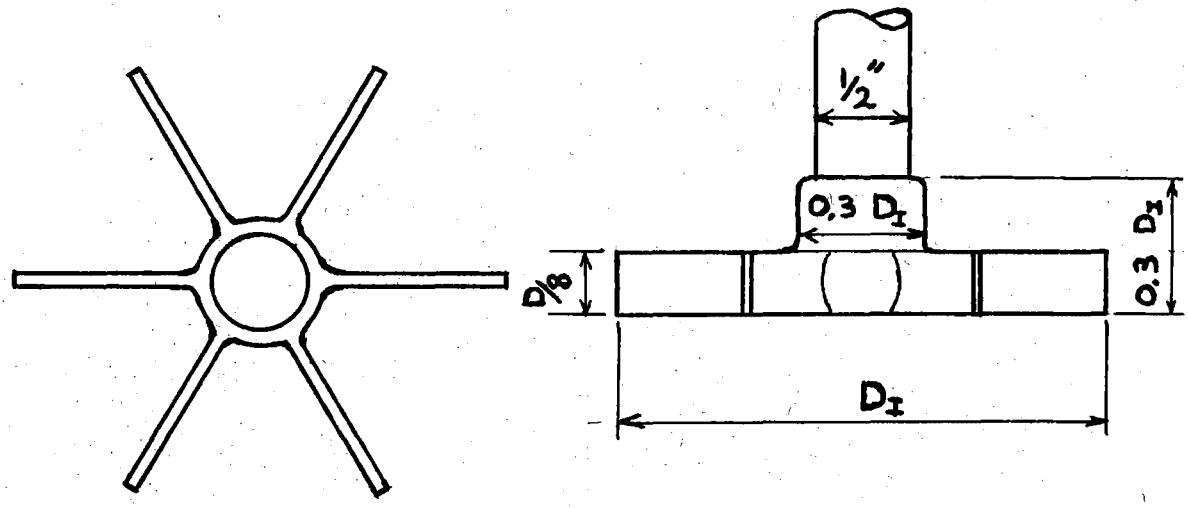

pattern slightly different from turbine impellors; the impellor stream tends to rise slightly because of the boss, but the high energy dissipating region near the impellor still exists, see Fig. 2.6.

Fig. 2.6 Impellor Stream

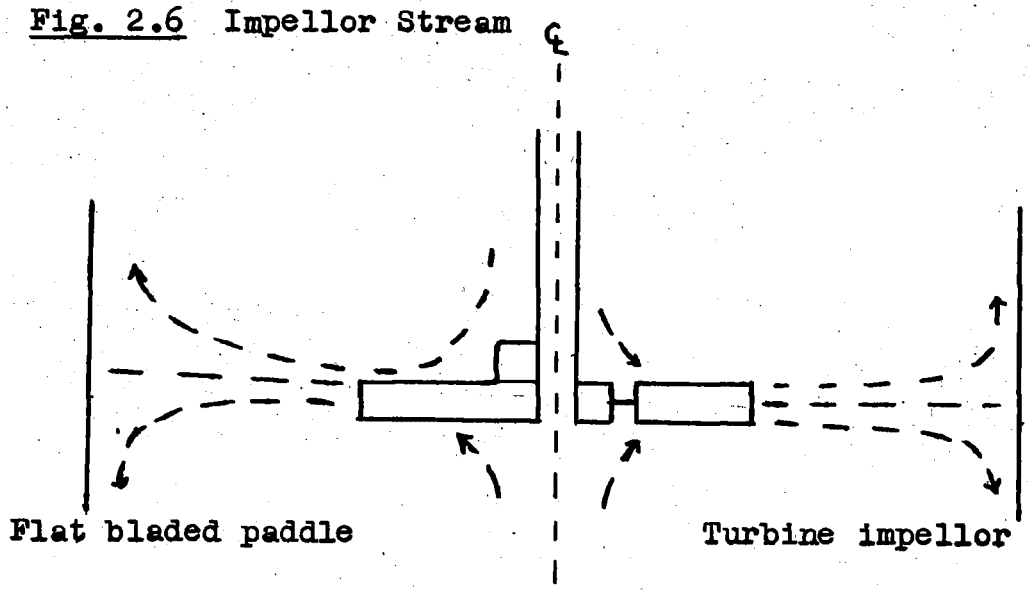

Agitator

A Chemineer agitator, Model ELB, with a continuous speed range of 0 to 915 RPM was used. The impellor speed was measured with a Dawe Stroboflash, Type No. 1200E. The impellor torque was measured by transmitting the

agitator moment with a lever arm suspended on a knife edge to the pan of a continuous digital recording Mettler balance (± 0.05 gms.), see Fig. 2.7. Reproducible torque measurements were obtained when the power cord to the agitator was clamped vertically above the impellor shaft, the agitator bearing race was horizontal and the torque lever arm was in the same position for the zero impellor torque calibration and the run torque reading. The stroboscope was calibrated against the mains frequency for each run, at a frequency within 20 cycles/min. of the impellor speed. The speed measurement error was less than ± 2%.

Fig. 2.7 Torque Lever Arm

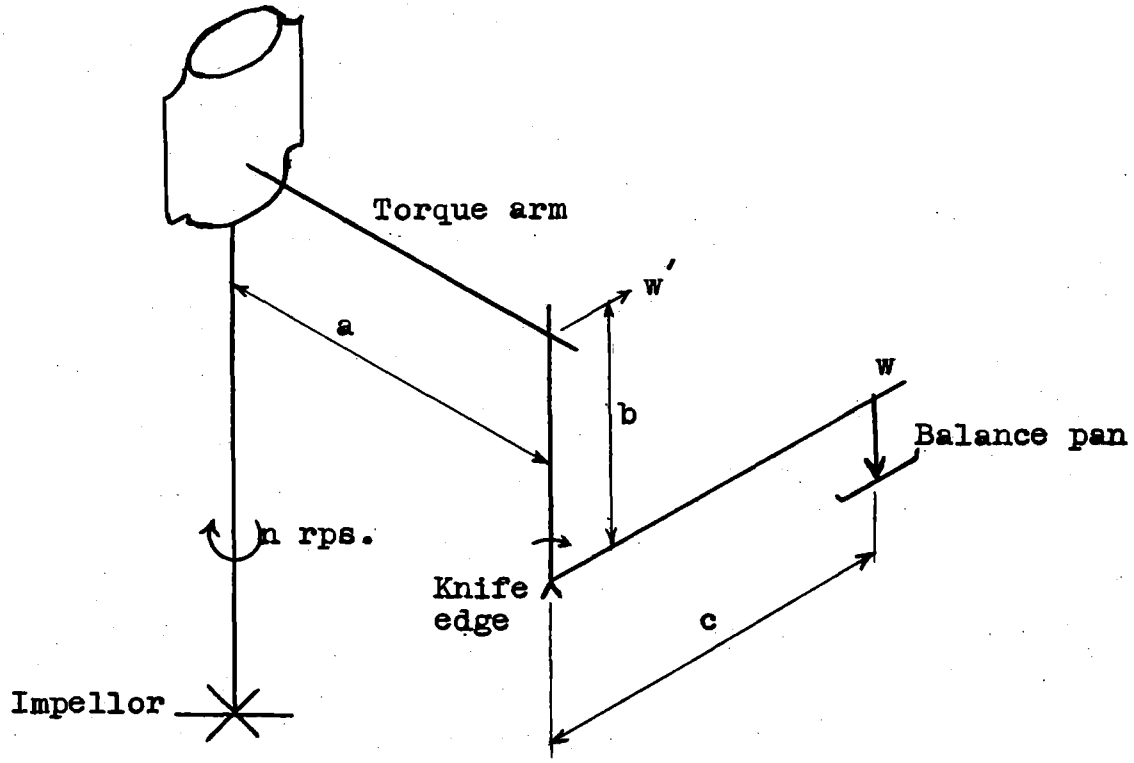

Torque applied = $T = w'.a$

but $w'.b = w.c$

Torque $T = w.\frac{ca}{b}$

Particle size

The droplets were photographed through a microscope-slide window glued to a stainless steel holder, after the dispersion had left the mixing vessel, see Fig. 2.8. The negatives were projected on to a screen, and the droplet size-distribution found by counting the number of drops in progressive increments on the screen of 0 - 3, 3 - 6, 6 - 10, 10 - 15, 15 - 25, 25 - 40, and > 40 mm. The projected scale ratio of the droplets was fixed at 15.6 by comparing the actual and projected widths of the liquid flow path.

Only a small section of the negative was analysed for the finer dispersions. An area, some 10% of the total droplet area photographed, was selected for each negative on the basis of drop definition. For the course dispersions, all the drops were counted, the criterion being that approximately 400 drops were counted from each negative. Eight negatives were analysed for each dispersion.

Fig. 2.8 Particle Size Analysis

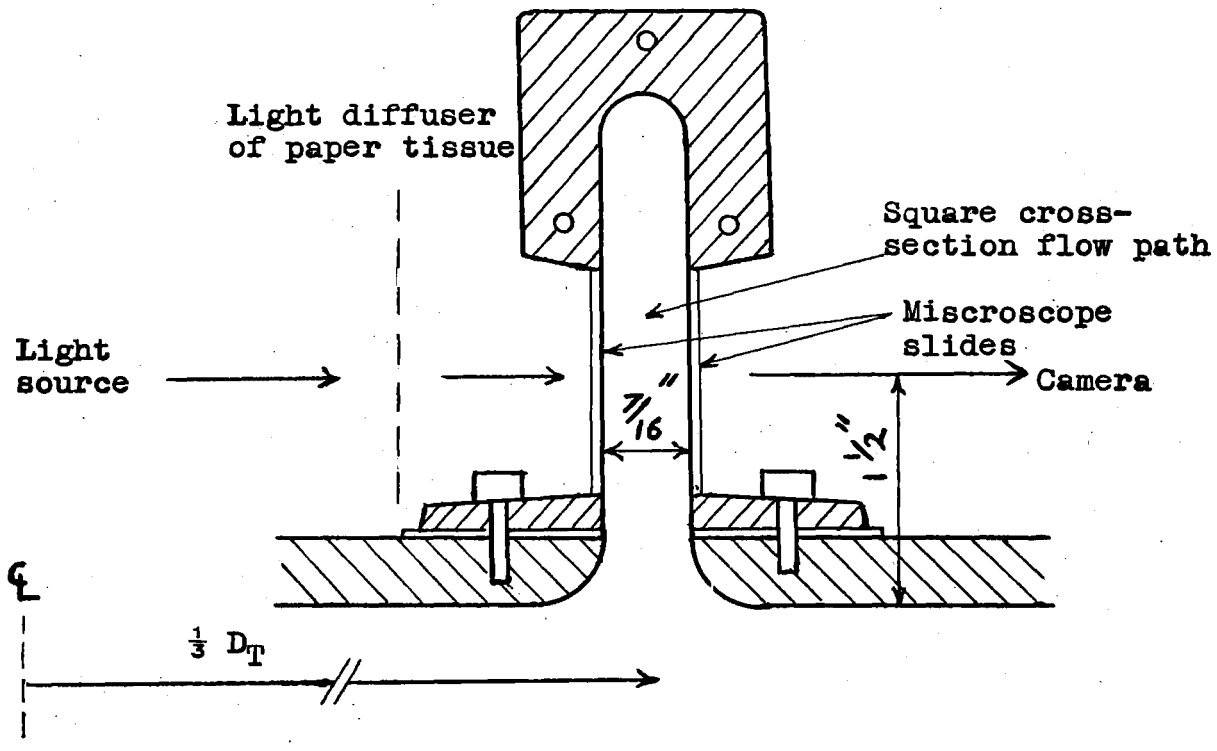

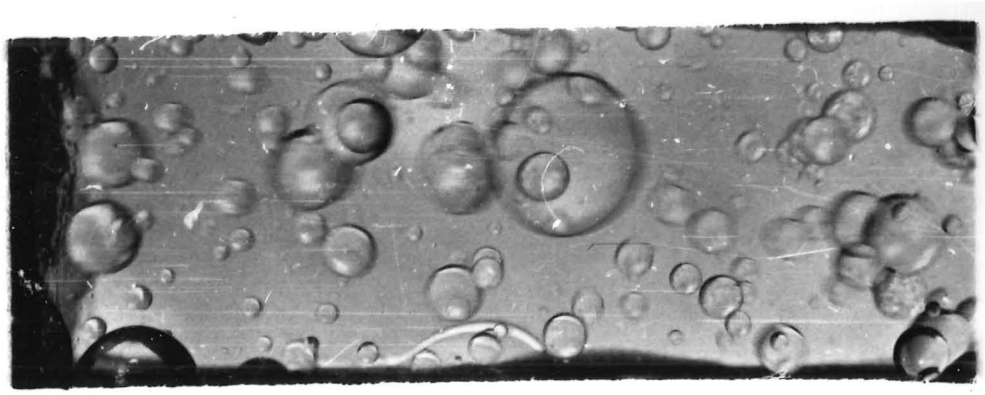

Run 69 Scale x 6

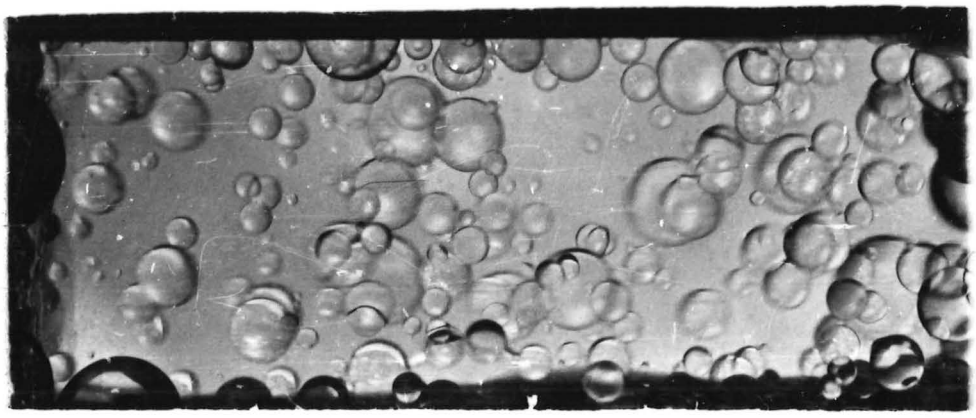

Fig. 2.9 Isooctane dispersion

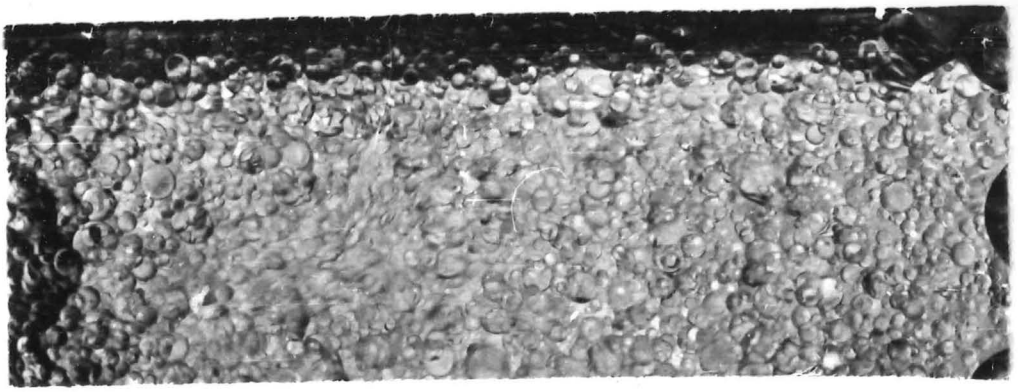

Run 79 Scale x 6

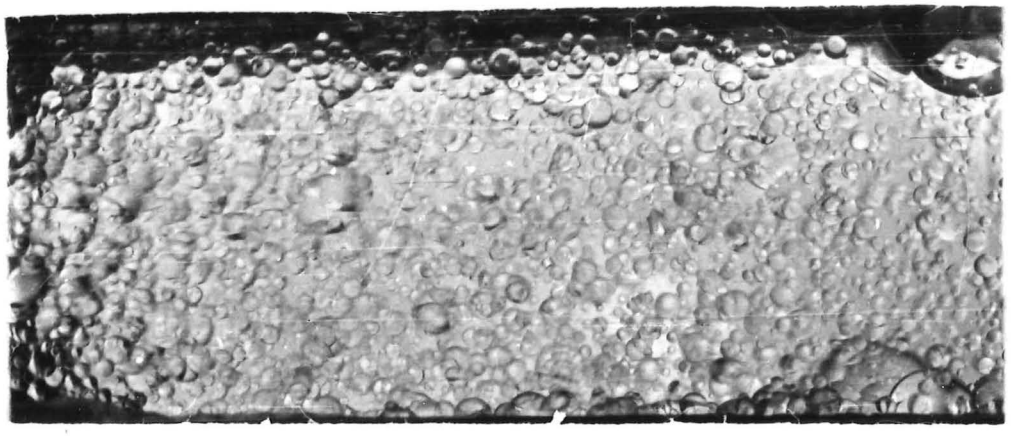

Fig. 2.9 Isooctane dispersion

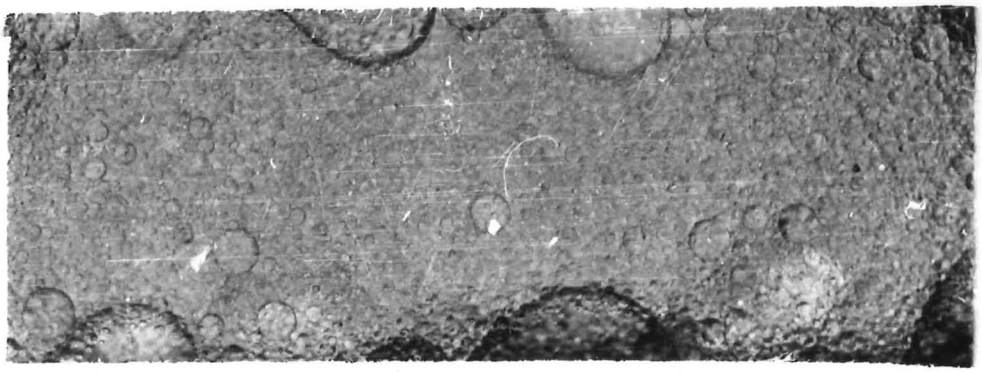

Run 77 Scale x 6

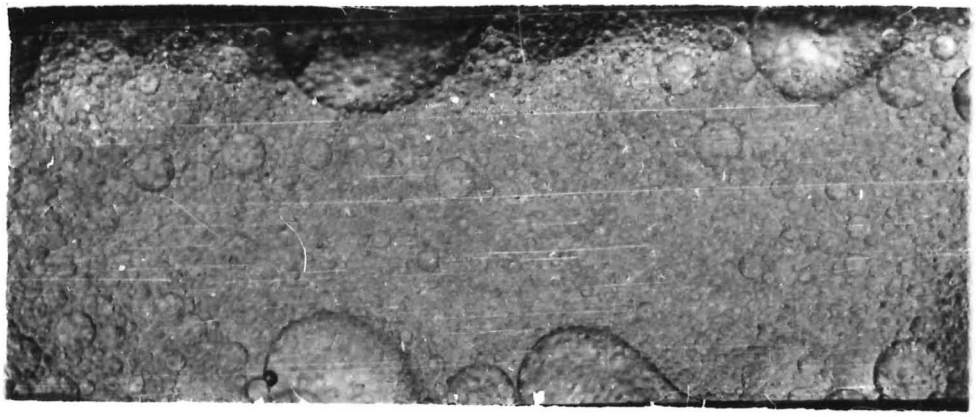

Fig. 2.9 Isooctane dispersion

For the finer dispersions, the flow past the view window was momentarily stopped, to obtain a less blurred photographic image, but even at a 500th of a second exposure time, considerable blurring occurred, see Fig. 2.9.

The size distribution data are presented in Appendix 11.

Camera:- Asahi Pentax
Exposure:- 500th at f8, HP 3 film
Lighting:- 100 watts with reflector, with a single Snowtex tissue as a back-lit screen.

Holdup of dispersed phase

At the end of each run the two inlet flows were stopped simultaneously. The agitator was then turned off, and the two phases were allowed to settle. When the phases had cleared, some aqueous phase was run out from the bottom of the vessel, to lower the isooctane-air interface. The isooctane height was then measured with a scale held outside the glass vessel, by sighting along the two interfaces.

Although little parallax error occurred with the glass wall, error arose from a lack of clarity of the liquid-liquid meniscus. When allowed to settle slowly, the interface could be clearly seen, but when the liquid interface was lowered to make the liquid-gas interface visible, the liquid-liquid meniscus was deformed, making sighting along the interface difficult. The measurement error was $\pm$ 0.07 cms. for each interface.

The holdup measurements made during the mass transfer runs had to be repeated. Isooctane in the two sampling lines drained back into the vessel when the interface was lowered, and differing volumes of isooctane between the inlet flow control valve and the mixing vessel were displaced by the aqueous phase, when the inlet flows were stopped after each run. The inlet error was minimised by siting the isooctane inlet control valve next to the mixing vessel and determining a constant correction for the isooctane

two outlet sample lines were blanked off from the vessel, and the runs repeated, with the measurement of power, impellor speed, and dispersed phase holdup, for otherwise similar conditions.

These data are presented in Appendix 12. The holdup for each mass transfer run is estimated from graphs of these results.

Solute concentration

A sample line from the top of the mixing vessel led to a settling tube, 10 in. long by 1½ in. diameter. A fraction (~ 2 ml./sec.) of the settled aqueous phase was continuously drawn off through a light absorptiometer cell, see Fig. 2.10.

A Hilger Watts continuous absorptiometer, H954, was modified by introducing a 200 watt mercury-arc light source, which necessitated modified optical paths and a cooling fan. Heat filters and Wood's glass filters were placed in the reference and analysis optical paths, to allow a light transmittance of wavelength near 3500 Å. A 40% total light transmittance filter was also included in the reference-cell optical path to protect the photocell. The isooctane and aqueous phases do not absorb in the region of 3500 Å, and the dissociated o-nitrophenol absorption peak is nearly 5800 Å, (12). The difference in millivolt output from the two photocells (± 40 mV. max.) was recorded with a Philips single point recorder, Type PR2210, see Fig. 2.10.

The spectrophotometer millivolt output was sensitive to the mains voltage fluctuations and the cooling fan operation. Fast oscillations of the mercury arc had no effect on the recorded spectrophotometer output, but during the day-time, 5 millivolt fluctuations of nearly 0.5 minute periods, occurred. These fluctuations disappeared during the evening when the experiments were carried out, but slow drifts of the zero concentration line still

o-nitrophenol concentration reading between each run. The continuous phase in the analysis line was drained, providing a sample for an analysis check with the Hilger UVSpec. The line was washed and filled with water pH 3.5, from which the zero o-nitrophenol concentration reading was obtained.

The concentration of o-nitrophenol in the isooctane phase before extraction was kept near 4×10^{-3} gms. ONP/gm. isooctane, by adding o-nitrophenol dissolved in isooctane to the raffinate, before it was used as feed again. The actual feed concentration was determined from four samples. The o-nitrophenol in each sample was extracted into KOH solution pH > 12; complete extraction being indicated when no colouration of fresh alkaline solution occurred. The extractant was then diluted, acidified to pH 3.5 and analysed by the Hilger UVSpec.

The continuous spectrophotometer and the UVSpec were both calibrated with solutions of known o-nitrophenol concentrations, before and after each series of runs.

The mass transfer data are presented in Appendix 13.

Settling Vessels

The main settling vessel had a volume of 5 gals., which gave a minimum aqueous phase residence time of 36 seconds. The design, see Fig. 2.11, based on the coalescence time in a test-tube being less than 20 seconds, with mixer flow rates of nearly a half of those used, was insufficient to allow total coalescence of the fine dispersions occurring with high power inputs to the mixing vessel. Isooctane was entrained in the non-recycled aqueous phase at a rate of 1 to 2 gal. per hr.

The sample settling tube, see Fig. 2.10 operated satisfactorily with a fluid residence time of 20 seconds. Any fine isooctane drops that were still entrained in the aqueous phase did not affect the concentration analysis, because their small cross-sectional area intercepted a negligible

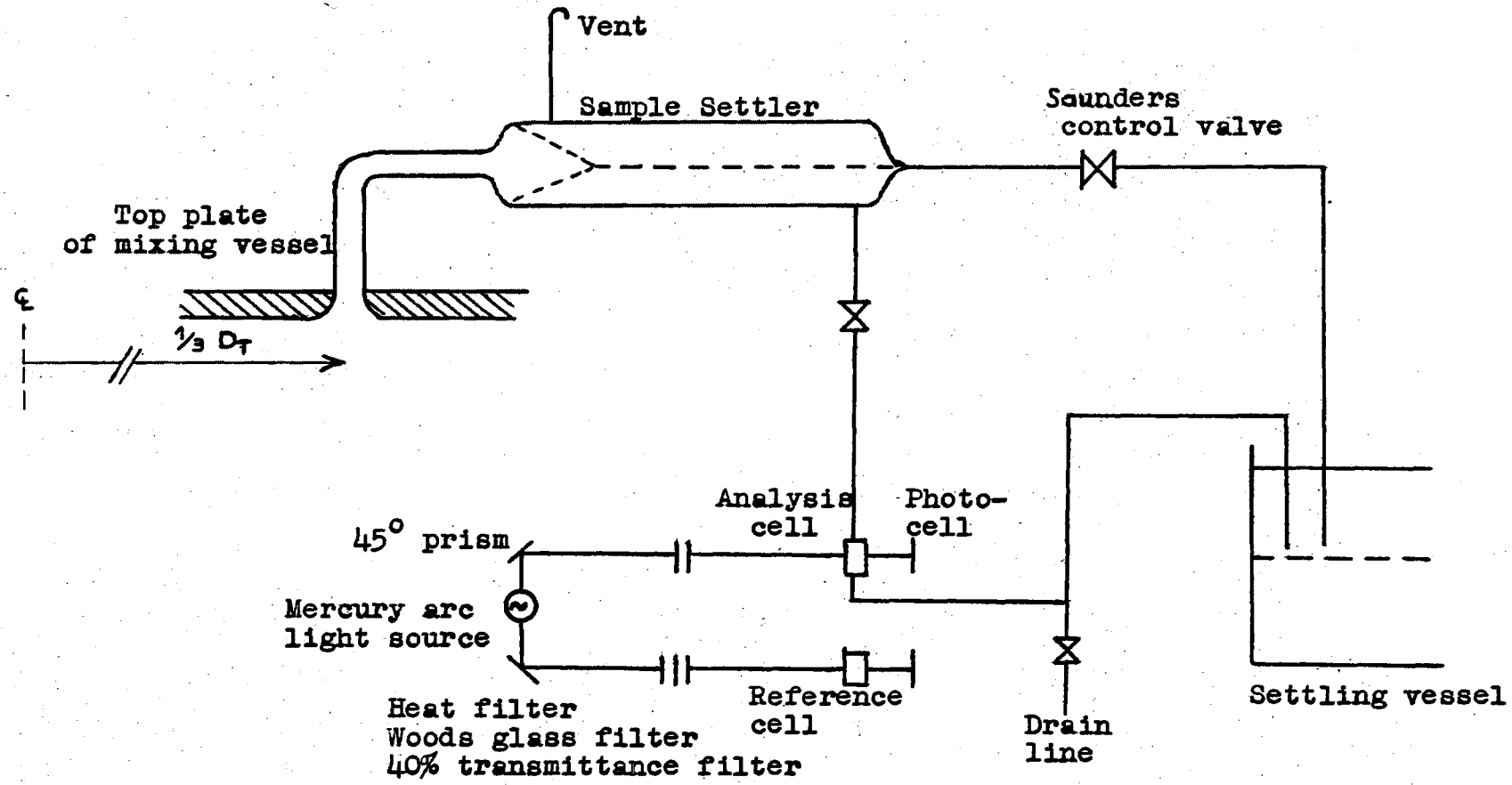

Fig. 2.10 Settling Vessel for Concentration Sample

mixing vessel.

Temperature

The temperature of the mixing vessel was not controlled, but the temperature of the dispersion was measured in the settling vessel. The physical properties, density, viscosity, and diffusivity, were calculated from the measured temperatures, which were in the range 16.2 to 17.8 °C.

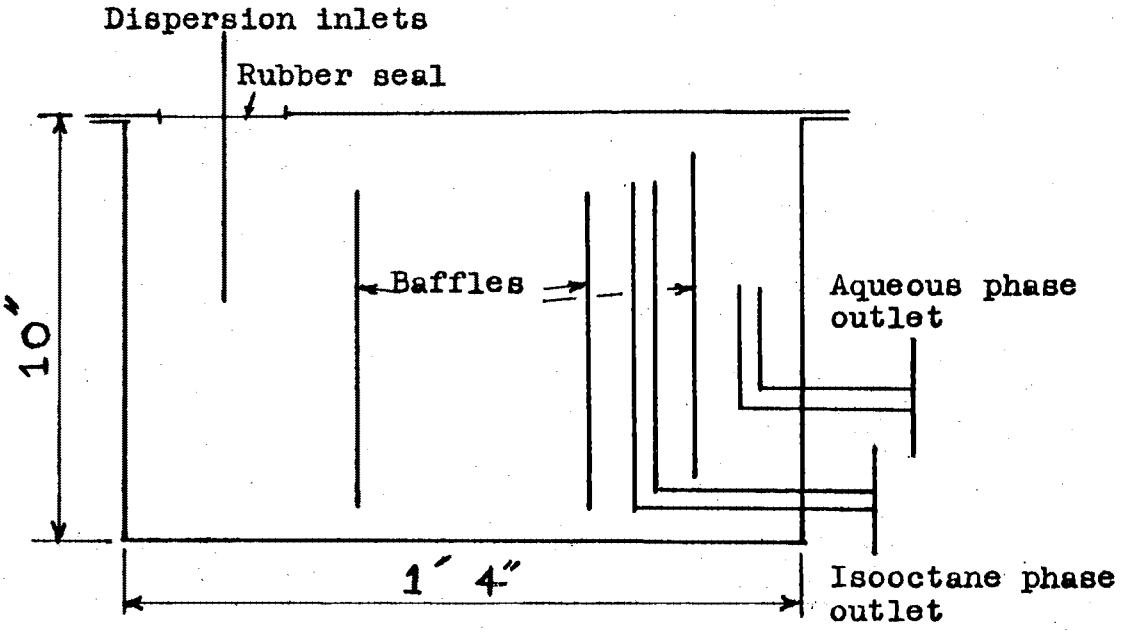

Fig. 2.11 Main Settling Vessel

2.5 MATERIALS OF CONSTRUCTION

In liquid-liquid extraction investigations, as contamination of the phases is particularly troublesome, glass and F.M.B. stainless steel were used as construction materials. Teflon gasket inserts and nitrile rubber gaskets were used as jointing materials. The o-nitrophenol and acid solutions used are midly corrosive, but other ternary systems may be used in the equipment without risk

The stainless steel equipment, constructed by "Mercers Limited" and "Oakleys Limited", Christchurch, was cleaned with acetone to remove all dirt and grease. The Q.V.F. glassware was de-greased with potassium permanganate and acetone washes. Water and a low boiling point straight-chain petroleum fraction, Shellsol-7, were circulated through the assembled apparatus. These fluids were drained, and the equipment dried with air before the isooctane and aqueous phases were introduced.

In cleaning all the equipment used in this work, care was taken not to introduce surface active materials, which might contaminate the solutions in later experiments.

Plant list

Plant No.	No.off.	Description	Matl.of Const.
1	4	Holding tank, 47 gals	F.M.B. S/S
2	2	Constant head tank, 2 gals	"
3	1	Settling vessel, 5 gals	"
4	3	Vessel end plates	"
5	4	Baffle sets, 4, width $\frac{1}{6}$th dia.	"
6	7	6 bladed flat paddles	SS or Ni plated
7	2	Brown Centrifugal pumps $\frac{3}{4}$"	F.S.T. S/S
8	70'	Q.V.F. $\frac{5}{8}$" Pipe line	Glass
9	20'	Q.V.F. $1\frac{1}{2}$" Pipe line	"
10	4	Mixing vessel $5\frac{1}{2}$", $7\frac{3}{4}$",$8\frac{3}{4}$" 12"	"
11	2	Metric rotameters No's 14 & 24	"
12	8	Saunders control valves	Glass lined
13	9	Draincocks Q.V.F. $\frac{5}{8}$"	Glass
14	1	Light Absorptiometer Hilger Watts H954	
15	1	Mercury Arc Source, 200 watt	
16	1	Philips recorder, PR2210 A/21	
17	1	Agitator, Chemineer, Model ELB	
18	1	Mettler balance, type K7T	
19	1	Dawe Stroboflash, type 1200E	

2.6 CALIBRATION EXPERIMENTS

The volumes of the assembled mixing vessels were found by filling each with a measured volume of water. The rotameter calibrations were then checked by measuring the time required for a constant inlet flow rate to fill the $8\frac{3}{4}$" vessel. The calibration chart for the aqueous phase rotameter was found to be accurate, but the isooctane phase rotameter had to be calibrated experimentally. The discrepancy arose because a large water drop from the mixing vessel always settled on the rotameter bob.

The breakup and rise of the dispersed phase between the inlet and the impellor zone was photographed with a motion camera, see Fig. 2.12, to estimate the inlet "end effect", and observe the particle breakup mechanism.

Camera, Bolex HR16.
Film, Ferrani ASA 40. 24 frames/second.
Exposure 240th at f4.5.
Side lighting, 2000 watts.

Table 2 Inlet Conditions

Flow rate		Impellor speed	Particle size	Rise velocity
Aqueous phase	Isooctane phase	3" Imp.	Mean	Ins./sec.
$0.4536 M^3/hr$	$0.0583 M^3/hr$	0 RPM	0.276 ins	17
"	"	240 "	"	20
1.1430 "	0.0893 "	0 "	0.087 "	23
"	"	240 "	(.05-.16)"	26

Height of dispersed phase column before breakup.

$$\text{Height} = 11.66 - 5.83 \times 10^{-3} \times \text{FLOI} \quad \text{cms.}$$

The dispersion in the sample settler was also photographed to estimate the outlet "end effect". Droplet size entrained in the aqueous phase:

Mean = 0.0033 ins.

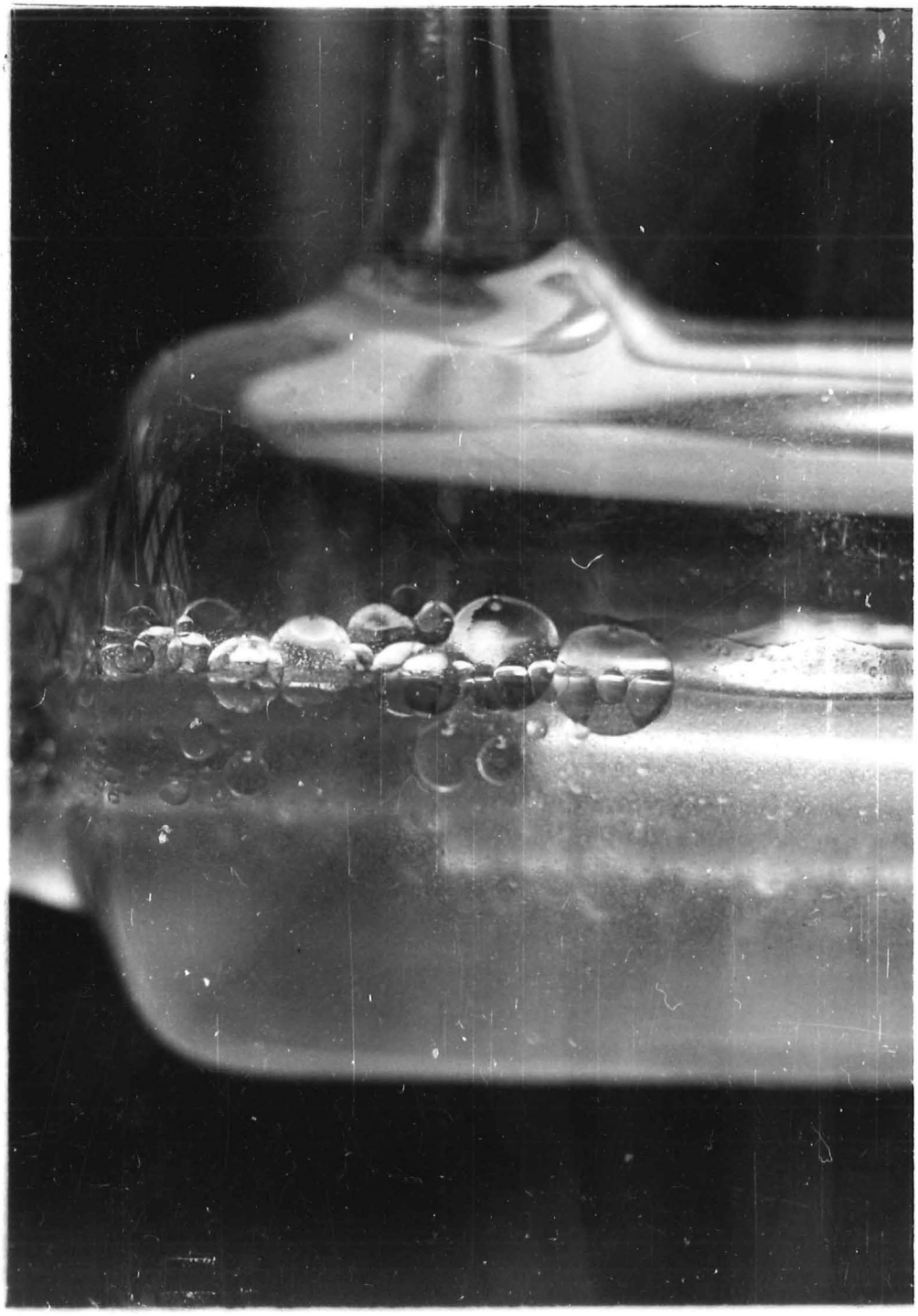

Fig. 2.12 Entrainment in the sample settler

Scale x 3

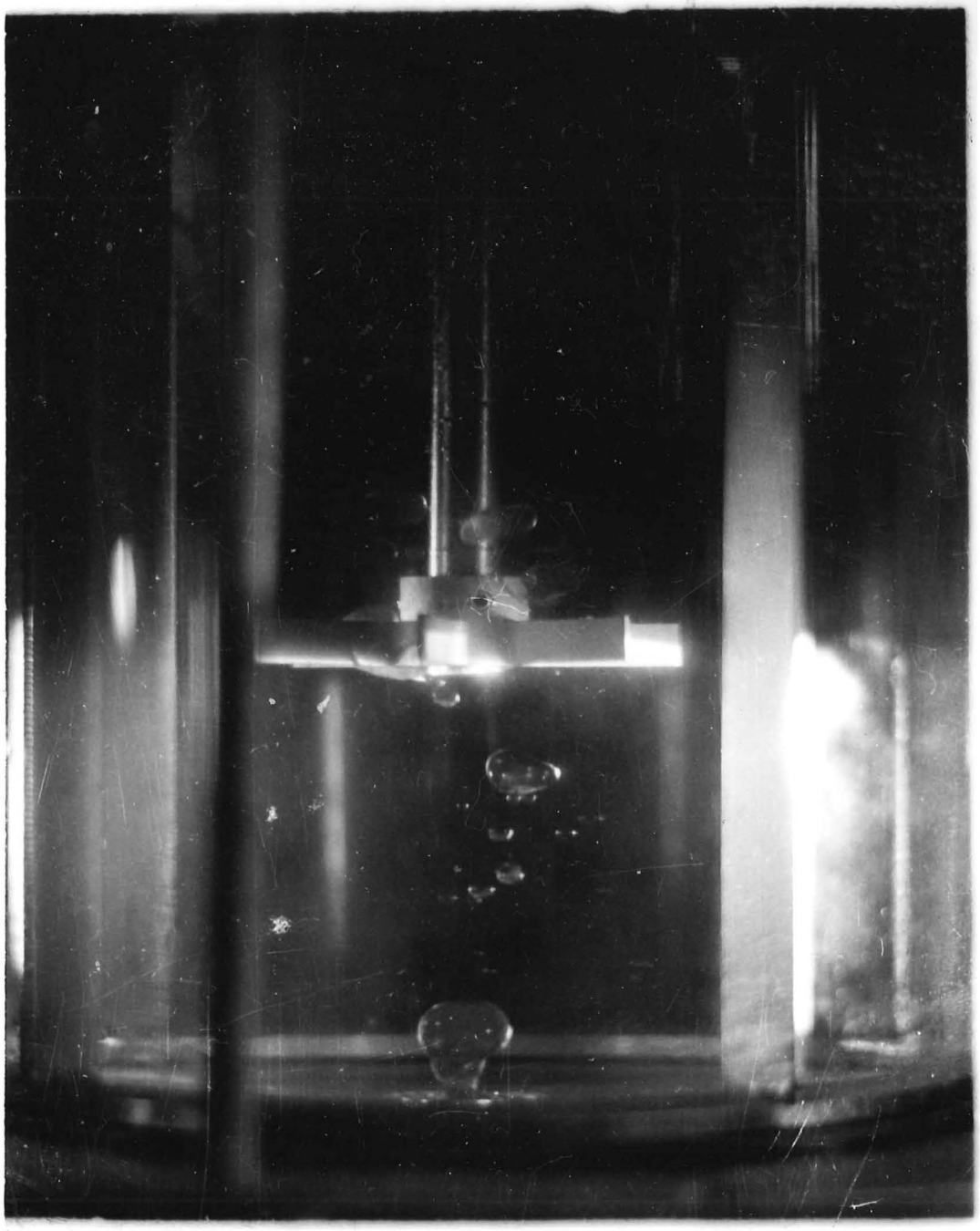

Fig. 2.12 Dispersion at the liquid inlet

3" Imp. 250 RPM. Flow isooctane 0.0583 $M^3/hr.$
water 0.454 $M^3/hr.$

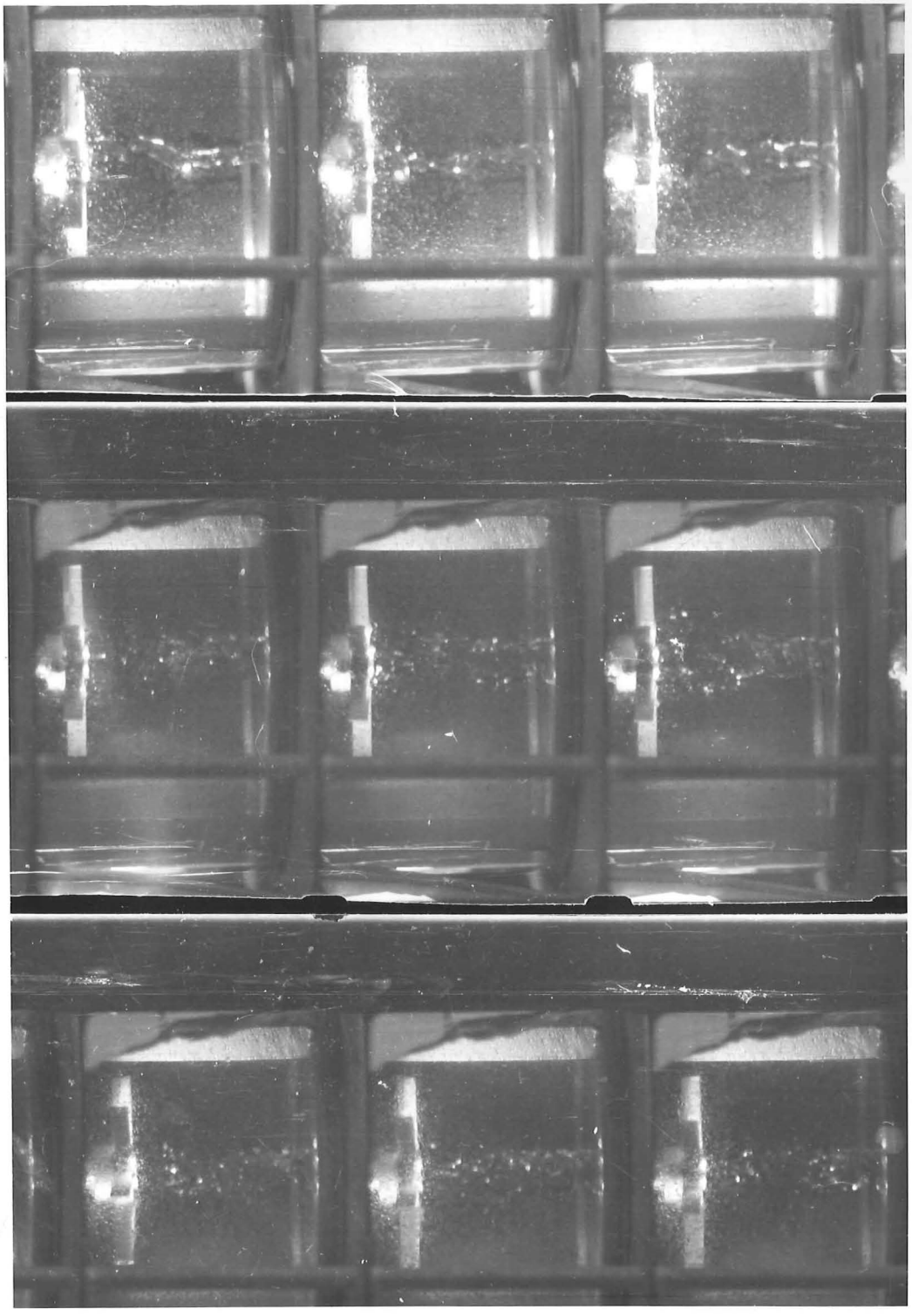

Fig. 2.12 Inlet flow 24 f.p.s.

The liquid residence time in the settler was determined with the aid of a stopwatch, by watching the fine droplets entrained in the aqueous phase, see Fig. 2.12.

Residence time in the settler = 15 - 20 seconds.

Time for liquid to flow from mixer to sample settler = 2 - 3 seconds.

Camera, Asahi Pentax
Lighting, 1000 watts, Film HP 3, Exposure 500th at f8.

The inlet and outlet dispersions, which had low dispersed phase volume fractions, could be photographed only by using intense side lighting. Any further work of this type would be assisted by the use of polarising filters.

Section 3

FLUID DYNAMICS IN A MIXER

3.1 INTRODUCTION

The fluid motion within a mixer has been used to correlate specific mixer operations. In mixing miscible liquids in trubulent conditions, van de Vusse (134), and Aiba (2), found that mixing times were a function of the impellor pumping capacity, $(ND_I) \cdot (D_I)^2$, but Fox and Gex (30) found mixing times to be a function of the fluid momenteum flux $(ND_I)^2 \cdot (D_I)^2$. The breakup of drops has been shown by Pavlushenko, (93) and Rodger, Trice, and Rushton, (101), to depend on the ratio of fluid inertia force to the surface tension force. Mass transfer with fixed and freely circulating particles has been correlated by the fluid flow, as shown by Treybal (131).

These examples show that a knowledge of the fluid flow within a mixer would aid the prediction of mixer performance.

3.2 DESCRIPTION OF MIXER FLUID FLOW

In an unbaffled vessel, the flow is mostly tangential to the impellor; this is also true for a baffled vessel with laminar flow, $Re_{Imp} < 400$, Sach and Rushton (110). Baffles tend to increase the radial and vertical flows with a substantial decrease in the tangential velocity, except in the region of the impellor tips. Thus a turbine impellor sets up a high velocity stream with a large radial component near the impellor tips. This stream, which is slightly wider than the impellor, extends to the vessel wall. The flow in the vessel may be described as two weakly defined

torroids, one above and one below the impellor, Farrier (28), see Fig. 3.1.

A turbine impellor in a baffled vessel appears to generate turbulence in two ways. Vortex sheets are set up in the wake of each blade. With increasing distance from the blade, these rapidly degenerate into increasingly random turbulence. Further turbulence is generated by the entrainment of the bulk fluid by the faster moving impellor stream. In addition to this random turbulence, regular velocity fluctuations precede each turbine blade. The intensity of these fluctuations decreases with the number of blades. These regular fluctuations also degenerate into random turbulence with increasing distance from the impellor.

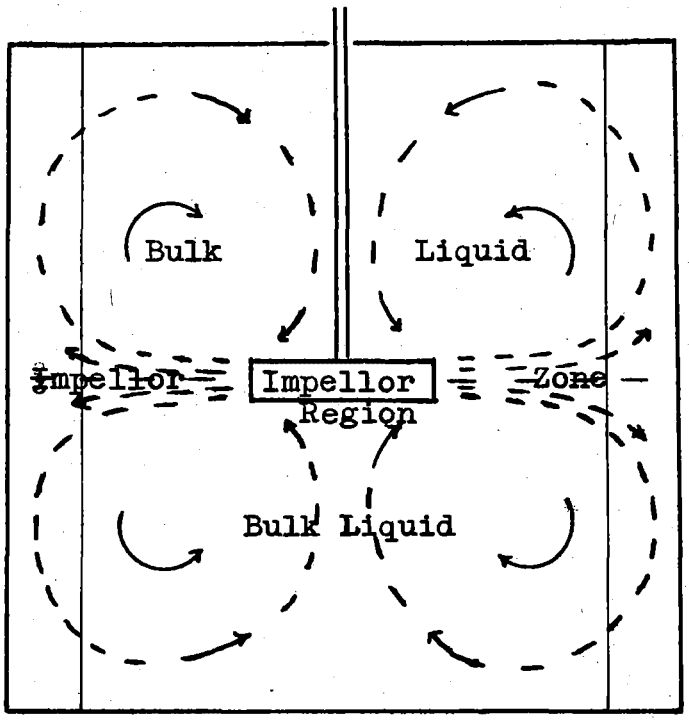

Fig. 3.1 Flow regions in a mixing vessel

An exact solution of the Navier-Stokes and Continuity equations describing these flow conditions has not been derived. An approximate solution, for turbulent flow in the impellor stream has been developed by S.K. Friedlander,

and is to be found in Cutter's thesis, (19).

The solution of the radial direction component is developed here to show the approximations required.

w_x = Fluctuating tangential flow component, direction x.
v_r = Fluctuating radial flow component, direction r.
u_y = Fluctuating vertical flow component, direction y.
$\bar{}$ superscript indicates the mean component.

Navier-Stokes equation in cylindrical polar co-ordinates.

$$\bar{u}_y \frac{\partial \bar{v}_r}{\partial x} + \frac{1}{r}\frac{\partial r\bar{v}_r^2}{\partial r} - \frac{\bar{w}_x^2}{r} = -\frac{1}{\rho}\cdot\frac{\partial P}{\partial r} - \left(\frac{\partial u_y v_r}{\partial x} + \frac{1}{r}\frac{\partial r v_r^2}{\partial r} - \frac{w_x^2}{r}\right) + \nu\left(\nabla^2 \bar{v}_r - \frac{\bar{v}_r}{r^2}\right)$$

Continuity equation

$$\frac{\partial \bar{u}_y}{\partial x} + \frac{1}{r}\frac{\partial r\bar{v}_r}{\partial r} = 0$$

$\frac{p}{\rho} = \frac{P_o}{\rho} - u_y^2$, is substituted, and the viscous terms neglected compared with the inertial terms.

P_o = pressure outside the impellor stream.

$$\frac{\partial \bar{u}_y \bar{v}_r}{\partial x} + \frac{1}{r}\frac{\partial r\bar{v}_r^2}{\partial r} - \frac{\bar{w}_x^2}{r} = -\frac{\partial u_y^2}{\partial r} - \left(\frac{\partial u_y v_r}{\partial x} + \frac{1}{r}\frac{\partial r v_r^2}{\partial r} - \frac{w_x^2}{r}\right)$$

Substitute $\frac{\partial u_y^2}{\partial r} = \frac{\partial u_y^2 r}{r\partial r} - \frac{u_y^2}{r}$, and integrate the equation at constant r, from x = 0 to x = ∞.

Boundary conditions, $\bar{u}_y = u_y v_r = 0$, at x = 0,

all velocities = 0, at x = ∞.

$$\int_o^\infty \left(\frac{\partial \bar{u}_y \bar{v}_r + \partial u_y v_r}{\partial x}\right) dx + \frac{1}{r}\frac{\partial r}{\partial r}\int_o^\infty (\bar{v}_r^2 + v_r^2 - u_y^2)\, dx =$$

$$= \int_o^\infty (\bar{w}_x^2 + w_x^2 - u_y^2)\, dx$$

The first term is zero, from the first boundary condition,

$$\int_o^\infty (\bar{v}_r^2 + v_r^2 - u_y^2)\, dx = \int_o^\infty (\bar{w}_x^2 + w_x^2 - u_y^2)\, dx$$

If the turbulence approaches isotropy,

$$w_x^2 \sim u_y^2 \sim u_r^2$$

$$\int_o^\infty \bar{v}_r^2 \, dx = \int_o^\infty \bar{w}^2 \, dx \qquad (3.1)$$

Tangential and vertical equations of motion are obtained similarly, the vertical direction yields,

$$\int_o^\infty \frac{\partial u_y^2}{\partial x} \, dx = -\frac{1}{\rho} \int_o^\infty \frac{\partial P}{\partial x} \, dx \qquad (3.2)$$

Boundary conditions $u_y^2 = 0$, at $x = \infty$

$P = P_o$, at $x = \infty$

The tangential equation is,

$$\int_o^\infty (\bar{w}_x \, r^2 \bar{v}_r + r^2 v_r w_x) \, dx = \text{const.} \qquad (3.3)$$

Equations 3.1, 3.2 and 3.3 are expressions for the conservation of angular momenteum. The energy equation obtained is,

$$\int_o^\infty \epsilon \, dx = \frac{2\pi r dr}{r dr} \int_o^\infty (k^2 \bar{v}_r + 2 \bar{w}_x \, v_r w_x) \, dx \qquad (3.4)$$

where $k^2 = (\bar{u}_y^2 + \bar{v}_r^2 + \bar{w}_x^2) + (u_y^2 + v_r^2 + w_x^2)$

The approximations require that:

1. All velocities outside the impellor stream are negligible.
2. The mean vertical velocity is neglected when compared with the mean radial and tangential velocities, in the impellor stream.
3. Circular symmetry and symmetry about the horizontal centre plane are assumed for all velocity components.
4. The mixer flow has reached a statistically steady state.

These simple solutions (eqns. 3.1 to 3.4), are interesting, but because of these approximations, are not of great practical value.

3.3 THEORIES OF TURBULENCE

A more useful approach is to characterise the fluid flow within a mixer according to different regions of energy dissipation, see Fig. 3.2.

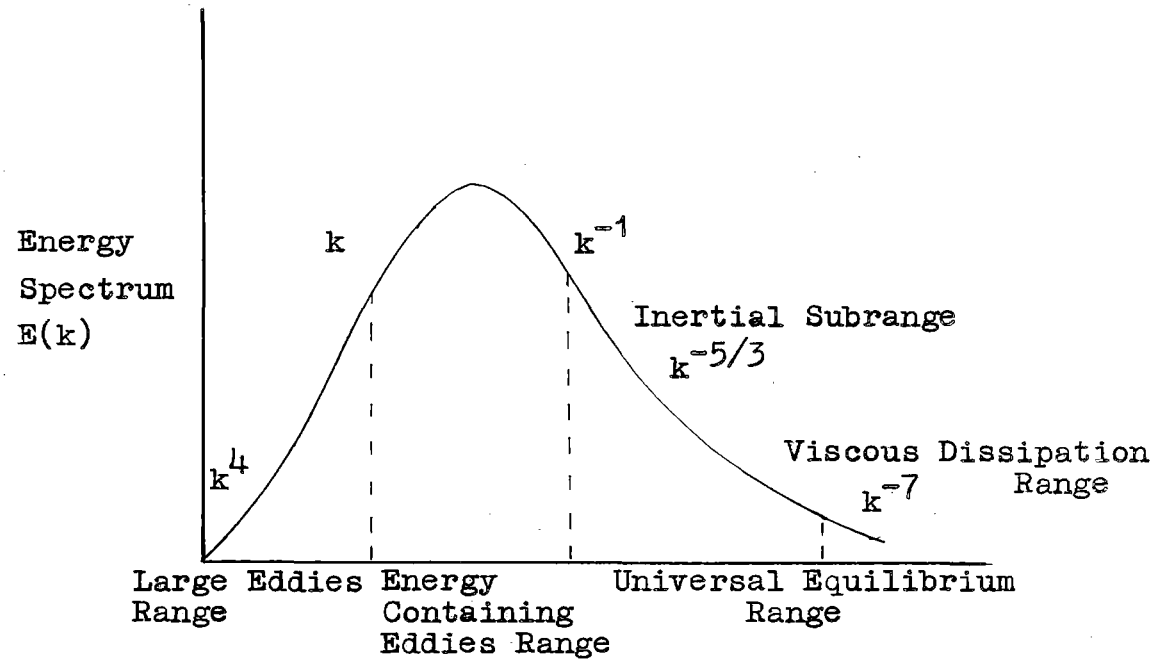

Fig. 3.2

The Fourier transform of the Karman-Howarth energy equation, of which eqn. 3.4 is part, yields the energy spectrum equation,

$$\frac{\partial}{\partial t} E(k,t) = W(k,t) - 2\nu k^2 E(k,t) \qquad (3.5)$$

As W, the energy transfer function, is indeterminate, eqn. 3.5 is intractable. Two methods of avoiding this difficulty have been employed. Batchelor (4), and Lin (66), by discarding this equation and drawing conclusions about the functional form of E from the similarity hypothesis, showed that $E(k) \sim k^4$, describing a 'large eddies' range. Von Karmen and Lin (53) postulated a parameter D_o to characterise the energy transfer mechanism. Dimensional

analysis then showed $E(k) \sim D_o^2 k$, for a section of the 'energy containing' eddies range. Kolmogoroff (60) introduced the concept of local isotropy, and the two similarity hypotheses from which he derived $E(k) \sim k^{-5}/3$ for the inertial subrange in the universal equilibrium range. An explicit functional form of W was assumed by Heisenberg (42), who showed $E(k) \sim k^{-7}$ in the viscous dissipation subrange, and Tchen (123) who divided the equilibrium range into three subranges and showed, by a harmonic analysis, that E(k) is proportional to k^{-1}, $k^{-5}/3$, and k^{-7}, respectively. These relationships, which have also been derived by other workers, are summarised in Fig. 3.2, from Kim and Manning (56).

In isotropic flow, the rate of decrease of kinetic energy during an initial period of decay, when the inertia forces are appreciable, is found $\sim u^3/l$ (5).

$$\text{i.e.} \quad \frac{du^2}{dt} = - C. \frac{u^3}{l} \qquad (3.6)$$

where C is a constant of order unity.

A choice of the scale length l which permits direct measurement, is the longitudinal integral scale,

$$L_p(t) = \frac{\int_o^\infty R_{11}(r,0,0,t)dr}{R_{11}(0,0,0,t)}$$

where $R_{ij}(r)$ is the velocity correlation tensor for two points separated by the space vector r.

For isotropic turbulence,

$$L_p(t) = \int_o^\infty f(r,t)dr = \frac{3\pi}{4} \frac{\int_o^\infty k^{-1} E(k,t)dk}{\int_o^\infty E(k,t)dk}$$

The length $L_p(t)$ is not directly representative of the part of the function E(k,t) that makes the major contribution to the total energy $\int_o^\infty E(k,t)dk$, as it slightly overweights small values of k. However, $L_p(t)$ is taken as a length parameter that characterises the turbulence, as it is measurable.

A second hypothesis on the independence of Fourier

components for distant wave-numbers, which like the relationship $L_p(t) = 1$, has been verified for turbulence behind grids, is introduced. At Reynolds number, and for values of the wave-number k such that the Fourier coefficients dz(k,t) are determined principally by the non-linear inertia term in the energy equation 3.5 and not by the viscous damping term, dz(k,t) is statistically independent of $dz(k',t)$, if $|k| \gg |k'|$ or $|k| \ll |k'|$.

The wave-number magnitude at which the viscous terms are significant may be measured by the value k_o, at which the maximum contribution to the dissipation integral, $\epsilon = 2\mu . \int_o^\infty k^2 E(k,t)dk$ occurs. If the energy containing eddies are confined to the region k_1 $(\sim \frac{1}{l})$, so that k_1 is the lower limit of the wave-numbers taking part in the inertial exchange, then the hypothesis would apply if $k_1 \ll k_o$. Taylor (122), by calculating $\int_o^\infty E(k,t)dk$ and $\int_o^\infty k^2 E(k,t)dk$ from measured spectrum curves showed that these integrals were determined by non-overlapping ranges of k, for high Reynolds numbers.

This result shows that the rate of decay is given by the rate at which energy is transferred by inertia forces, from the energy-containing range of wave-numbers to higher wave-numbers. Thus, changes in the kinematic viscosity, which are accompanied by changes in the motion associated with the dissipation range of wave-numbers, have no effect on the rate of energy transfer from the lower wave-numbers.

Equation (3.6), $du^2/dt = - C. u^2 \frac{u}{l}$ suggests that the energy transfer occurs chiefly by inertial interaction of wave-numbers of the same order of magnitude, since u^2 is the order of magnitude of the Reynolds stresses produced by the energy containing range of wave-numbers and u/l is the order of magnitude of the rate of shearing produced by the same range. Similarly, $du^2/dt = - C\, ul.\, u^2/l^2$ suggests that an eddy viscosity of order ul, acts on the shear to cause a decay of energy from the energy containing eddies to the smaller eddies.

It has been shown that the inertia forces spread the

turbulence energy over an increasing wave-number range, which is checked only by the stronger viscous damping at large wave-lengths. For a finite but high flow Reynolds number, the spectral density of energy in the turbulent flow will decrease sharply at some large wave-number, which marks the onset of the viscous dissipation range. The region of wave-numbers which is within this range moves towards $k=\infty$, as the flow Reynolds number increases.

These hypotheses and conclusions may be summarised by the following relationships,

$$\epsilon = \rho \frac{du^2}{dt} \sim \rho . \nu_{turb} \left(\frac{\Delta u}{l}\right)^2 \sim \rho \frac{(\Delta u)^3}{l} \qquad (3.7)$$

where $\nu_{turb} \sim \Delta u . l$

and $\mu_{turb} \sim \rho \Delta u . l \qquad (3.8)$

The order of the turbulent kinematic viscosity may be estimated, as,

$$\frac{\nu}{\nu_{turb}} \sim \frac{\nu}{\Delta u . l} \sim \frac{1}{Re} \ll 1$$

If the approximation $\Delta u \sim l \frac{\partial u}{\partial l}$, is made, the shear stress τ may be determined,

$$\tau = F/S = \mu_{turb} \frac{\Delta u}{l} \sim \rho l \left(\frac{\partial u}{\partial l}\right)^2 = \alpha \rho l^2 \left(\frac{\partial u}{\partial l}\right)^2 \qquad (3.9)$$

where α is a numerical constant of order unity.

3.4 THE UNIVERSAL EQUILIBRIUM

The conditions necessary for the existence of the equilibrium range of wave-numbers, have been described. The energy is self-adjusting within the range through the inertia forces, and depends only on the parameters which describe external effects. These are only two,- the removal

of energy by viscous dissipation over the whole, but mostly at the upper wave-number end of the range, and the imput of energy by inertial transfer at the lower end. The imput and removal of energy must be at the same rate,

$$\epsilon = -\tfrac{3}{2} C\rho \frac{du^2}{dt} = 2\mu \int_0^\infty k^2 E(k,t)dk;$$

thus energy is one of the external parameters. The kinematic viscosity is the other external parameter which, besides the spectrum function $E(k,t)$, describes the dissipation of energy over the range. In view of their statistical independence, these two parameters specify the equilibrium range. Thus a hypothesis for Universal Equilibrium may be written. "The motion associated with the equilibrium range of wave-numbers is uniquely determined statistically by the parameters ϵ/ρ and ν". A statistically independent equilibrium range may exist only when,

$$k_1 \ll 1/\lambda = (\epsilon/\rho\nu^3)^{\frac{1}{4}}$$

$$1/l \ll \left(\frac{u^3}{l\nu}\right)^{\frac{1}{4}} \quad \text{or} \quad \left(\frac{ul}{\nu}\right)^{\frac{3}{4}} \gg 1 \qquad (3.10)$$

The eddy velocity and length scales may be determined dimensionally from the two parameters ϵ/ρ and ν.

Thus: Eddy length, $\lambda \sim \left(\frac{\nu^3\rho}{\epsilon}\right)^{\frac{1}{4}}$ (3.11)

Eddy velocity, $v_\lambda \sim (\nu\epsilon/\rho)^{\frac{1}{4}}$ (3.12)

$\sim (\lambda\epsilon/\rho)^{\frac{1}{3}}$ (3.13)

The relative liquid velocity at two points, distance λ apart is given, (5), for the Universal Equilibrium range as,

$$\overline{|u(x+\lambda,t) - u(x,t)|^2} = \int_0^\infty E(k,t).\left(1 - \frac{\sin k\lambda}{k\lambda}\right) dk, \qquad (3.14)$$

For $k_o \gg k \gg k_1$ the intergrand is suppressed by small values of $\left(1 - \frac{\sin k\lambda}{k\lambda}\right)$ when k is of the order k_1. When k is

of the order k_o, the intergrand is suppressed by small values of $E(k,t)$. With the condition $E(k,t) = \alpha (\frac{\epsilon}{\rho})^{-\frac{2}{3}} k^{-5/3}$, applicable in the Universal Equilibrium range, Batchelor (5) shows eqn. 3.14 to be approximated by,

$$\overline{|u(x+\lambda,t) - u(x,t)|^2} \sim 4\int_o^\infty \alpha \ (\frac{\epsilon}{\rho})^{-\frac{2}{3}} k^{-5/3} \ (1 - \frac{\sin k\lambda}{k\lambda})dk$$

$$\sim 9/5 \ \Gamma\tfrac{1}{3} \ . \alpha (\epsilon\lambda)^{\frac{2}{3}} \qquad (3.15)$$

Equation 3.15 may be written in the form,

$$v_\lambda^2 \sim (\frac{(\Delta u)^3}{l} . \lambda)^{\frac{2}{3}}$$

or $$v_\lambda \sim \Delta u . (\frac{\lambda}{l})^{\frac{1}{3}} \qquad (3.16)$$

For motion of scale λ, the eddy velocity is smaller than the velocity of the main flow by the factor $(\frac{\lambda}{l})^{\frac{1}{3}}$. With the reduction in scale the corresponding eddy Reynolds number becomes,

$$Re_\lambda = \frac{v_\lambda . \lambda}{\nu} \sim Re \ (\frac{\lambda}{l})^{4/3} \qquad (3.17)$$

The wave-number defining the change from the inertial to the dissipation ranges is given by (5).

$$k_o = (\frac{3}{8}\frac{\gamma^2\epsilon}{\nu^3\rho})^{\frac{1}{4}}$$

or $$\lambda_o = \frac{1}{k_o} \sim (\frac{8\rho\nu^3}{3\gamma^2\epsilon})^{\frac{1}{4}}$$

As γ is a constant, of order unity,

$$\lambda_o \sim (\frac{\rho\nu^3}{\epsilon})^{\frac{1}{4}} \qquad (3.18)$$

Kolmogoroff (60) originally formulated the Universal Equilibrium hypothesis in terms of the probability distribution of velocity differences. The Fourier derivation, presented for instance by Batchelor (5), is at present more acceptable, but the relationships so derived have to be transposed to the equivalent velocity difference expressions, to be useful in physically describing mixer flow conditions.

3.5 EDDY DECAY NEAR A WALL

A turbulent fluid flowing past a flat plate of infinite extent in the plane y = 0, has an average velocity in a plane parallel to the plate. This average velocity, derived from the shear relationship, eqn. 3.9, is a function of distance from the plate.

$$U_p = \sqrt{\frac{v_o^2}{\alpha}} \int \frac{dy}{l(y)} + \text{constant} \qquad (3.19)$$

$$v_o = \sqrt{\frac{\tau}{\rho}}$$

For momentum transfer to a curved surface, the shear stress over the surface is not constant, due to the pressure drop in the boundary layer of a bluff body and the viscous energy dissipation in the boundary layer. Nevertheless, the analysis developed for a flat surface is applicable as an order analysis of the hydrodynamic effects about a particle.

If the dimensional assumption that the eddy scale increases with distance from the solid wall, $l_{(y)} \sim y$ is made, Levich (63), then eqn. 3.19 becomes,

$$U_p = \sqrt{\frac{\tau}{\rho\alpha}} \ln \left(\frac{y}{b\nu} \cdot \sqrt{\frac{\tau}{\rho}}\right) \qquad (3.20)$$

The constant in eqn. 3.19 is eliminated by the condition that $Re_{\lambda_o} \sim 1$, at $y = \delta_o$, the onset of the energy dissipation range.

$$\text{i.e.} \quad \frac{v_o \lambda_o}{\nu} \sim 1$$

$$\text{or} \quad \delta_o = b\,\nu/v_o \qquad (3.22)$$

There is no single hydrodynamic viewpoint regarding eddy decay in the viscous sublayer. Prandtl's widely accepted hypothesis, (see 35), which is based on the Reynolds number being less than unity for $y < \delta_o$, states that the fluid motion is entirely laminar in the region $y < \delta_o$. This gives rise to a laminar sublayer concept. Von Karmen (see 35) proposed a buffer layer in which the turbulence is damped as it approaches the solid wall. The turbulent flow relationship, $l_{(y)} \sim y$,

is used in this region, where the viscosity becomes appreciable. Thus, Prandtl's and von Karmen's hypotheses yield three zones, a bulk turbulence region, a buffer layer, and a laminar sublayer, which may be fitted to the average velocity profile for turbulent flow past a plate.

A third hypothesis, by Landau and Levich (63), considers that the turbulent motion in the viscous sublayer does not suddenly disappear, but is gradually damped as it approaches a wall. This hypothesis yields the relationships,

$$\tau_{turb} \sim \rho \cdot \nu_{turb} \cdot \frac{du}{dy} \sim \rho \cdot v_y \cdot l \frac{du}{dy} \sim \frac{\rho v_o y^4}{\delta_o^3} \cdot \frac{du}{dy}$$

$$\text{or} \quad \nu_{turb} \sim \frac{v_o y^4}{\delta_o^3} \sim \nu \left(\frac{y}{\delta_o}\right)^4 \qquad (3.22)$$

For $y < \delta_o$, the momentum transfer by eddies is less than the momentum transfer by molecular viscosity as the eddy viscosity is less than the molecular viscosity, μ. Thus, for the region $y < \delta_o$, the shear stress τ approximates to the quantity τ_o and the average velocity profile is given by the equation $\tau_o = \rho\mu \frac{\partial u}{\partial y}$. As turbulence eddies exist up to the surface, they affect the processes of heat and mass transfer, when the Schmidt number is greater than unity.

Lin, Mouton and Putnam (67) develop a variation of Landau-Levich's hypothesis. The turbulence eddies are damped out in the viscous sublayer according to the turbulent zone relationship $l_{(y)} \sim y$, rather than $l_{(y)} \sim y^2$, as postulated in (63). The eddy viscosity derived from $l_{(y)} \sim y$ is $\nu_{turb} \sim \nu \left(\frac{y}{\delta_o}\right)^3$. In deriving this, and Landau and Levich's relationship for the velocity profile in the viscous sublayer, the transfer of momentum is assumed to be accomplished by turbulence eddies which have already been affected by viscosity. The relationship $\nu_{turb} \sim \nu^{y/\delta_o}$, for the eddy viscosity decay in the viscous sublayer is not applicable in the buffer zone, so an interpolation formula first proposed by Piterskikh (see ref. 63) for the coefficient of eddy viscosity, is used for this region.

$$\nu_{turb} = b\nu \left(\frac{y}{\delta_o}\right)^2 \qquad (3.23)$$

The average velocity in the buffer zone is thus given by,

$$U_p = \frac{v_o}{\sqrt{b}} \operatorname{arctg}\sqrt{b} \cdot \frac{y}{\delta_o} + \text{constant},$$

which matches the velocity decay profile for this region, (63).

These turbulence decay relationships are summarised in Table 3.

Table 3

	Postulate	Viscosity	Range	Flow region
Prandtl	$l_{(y)} = 0$	ν = constant	$0 \leqslant y^* \leqslant 5$	Laminar sublayer
Von Karmen	$l_{(y)} \sim y$	$\nu_{turb} \sim \frac{y}{\delta_o}$	$5 \leqslant y^* \leqslant 30$	Buffer layer
	"	"	$y^* > 30$	Turbulence
Levich	$l_{(y)} \sim y^2$	$\nu_{turb} \sim \nu\left(\frac{y}{\delta_o}\right)^4$	$0 \leqslant y^* \leqslant 5$	Viscous sublayer
Lin et al.	$l_{(y)} \sim y$	$\nu_{turb} \sim \nu\left(\frac{y}{\delta_o}\right)^3$	$0 \leqslant y^* \leqslant 5$	"
Piterskikh		$\nu_{turb} \sim \nu\left(\frac{y}{\delta_o}\right)^2$	$5 \leqslant y^* \leqslant 30$	Buffer layer

The drag force F, acting on unit surface area is, from eqn. 3.9,

$$F = \iint \tau \cdot ds \sim k_f \cdot \rho_c \cdot \frac{(\Delta u)^2}{2} \times \text{unit area}$$

To estimate mass transfer coefficients, it is necessary to relate the skin friction velocity v_o to the bulk flow velocity U.

$$v_o = \sqrt{\frac{\tau}{\rho_c}} \sim \sqrt{\frac{k_f \cdot (\Delta u)^2 \cdot \rho}{2\rho}}$$

$$v_o \sim \sqrt{\frac{k_f}{2}} \cdot \Delta u \sim \sqrt{\frac{k_f}{2}} \cdot U \qquad (3.24)$$

3.6 PARTICLE ENTRAINMENT IN TURBULENT FLOW

If a particle moving with a velocity u_1, is fully entrained in a fluid with a velocity u, ($u_1 = u$) it experiences the same force as would the fluid enclosed in the same volume, that is $\rho_c V\frac{du}{dt}$. For partial entrainment, the fluid may be considered to flow past the particle at a velocity v, ($v = u_1 - u$) and the particle experiences a drag-force, F_{drag}. If the gravitational force is neglected the total force F, experienced by the particle, is given by,

$$F = \rho_c V\frac{du}{dt} + F_{drag} \qquad (3.25)$$

The relative velocity v and the drag-force, F_{drag} ($= - k_f \rho_c S v^2$), applicable for a particle diameter $2a > \lambda_o$ and $Re_{particle} \gg 1$, are introduced into eqn. 3.25,

$$\rho_d V\frac{dv}{dt} = (\rho_c - \rho_d) V\frac{du}{dt} - k_f \rho_c S v^2 + F_{react} \qquad (3.26)$$

F_{react}, the supplemental reaction term, denotes the higher drag force experienced by an accelerating particle (128). This term has been shown (96) to be proportional to the relative acceleration of the particle and the density of the medium, $F_{react} \sim \rho_c/2\ V\frac{dv}{dt}$, it may be included dimensionally with the particle acceleration term $\rho_d V\frac{dv}{dt}$.

$$\rho_d V\frac{dv}{dt} \sim (\rho_c - \rho_d) V\frac{dv}{dt} - k_f \rho_c S v^2 \qquad (3.27)$$

The acceleration of the particle may be written,

$$\frac{dv}{dt} = \frac{v}{T_\lambda}$$

Where T_λ is the period of motion of the particle corresponding to the velocity v, and the scale of motion λ, of the particle under the influence of the entraining turbulence.

$$T_\lambda \sim \frac{\lambda}{v_\lambda}$$

hence $$\frac{dv}{dt} \sim \frac{v_\lambda^2}{\lambda}$$

In the Universal Equilibrium range of wave-numbers, T_λ must be described dimensionally by the terms ϵ/ρ and ν, from which,

$$T_\lambda \sim \left(\frac{\lambda^2 \rho}{\epsilon}\right)^{\frac{1}{3}} \sim \frac{\lambda}{v_\lambda}$$

The acceleration of an eddy, scale λ, may be written,

$$\omega_\lambda = \frac{dv_\lambda}{dt} \sim \frac{v_\lambda}{T_\lambda} \sim \frac{\lambda}{T_\lambda^2} \sim \left(\frac{\epsilon}{\rho}\right)^{\frac{2}{3}} \times \left(\frac{1}{\lambda}\right)^{\frac{1}{3}} \qquad (3.29)$$

Equations 3.2, 3.28 and 3.29, yield,

$$\rho_d V \frac{v^2}{\lambda} \sim (\rho_d - \rho_c) V \left(\frac{\epsilon}{\rho_c}\right)^{\frac{2}{3}} \left(\frac{1}{\lambda}\right)^{\frac{1}{3}} - k_f \rho_c S v^2$$

The relative velocity v may then be obtained as,

$$v \sim \left((\rho_d - \rho_c) V\right)^{\frac{1}{2}} \frac{(\epsilon\lambda)^{\frac{1}{3}}}{\rho_c^{\frac{1}{3}} (\rho_d V + k_f \rho_c S \lambda)^{\frac{1}{2}}} \qquad (3.30)$$

The derivative $\frac{dv}{dt}$, shows a maximum relative velocity v_{max}, for an eddy length, $(\lambda) v_{max} = {}^2/k_f \cdot \rho_d V/\rho_c S$

$$v_{max} = \frac{1}{\sqrt{3}} \left(\frac{\rho_d - \rho_c}{\rho_d}\right)^{\frac{1}{2}} \left(\frac{V}{S}\right)^{\frac{1}{3}} \left(\frac{\epsilon}{\rho_c}\right)^{\frac{1}{3}} \left(\frac{\rho_d}{\rho_c}\right)^{\frac{1}{3}} \left(\frac{2}{k_f}\right)^{\frac{1}{3}}$$

which may be written, for spherical particles with $\rho_c \sim \rho_d$,

$$v_{max} \sim \frac{1}{3^{5/6} k_f^{\frac{1}{3}}} \left(\frac{\rho_d - \rho_c}{\rho_d}\right)^{\frac{1}{2}} (2a)^{\frac{1}{3}} \left(\frac{\epsilon}{\rho_c}\right)^{\frac{1}{3}} \qquad (3.31)$$

A comparison of equations 3.6, 3.13 and 3.31, shows,

$$v_{max} \sim u_{\lambda=2a} \text{ for } \rho_d \sim \rho_c \qquad (3.32)$$

Different flow conditions control the relative velocity of a particle, diameter 2a, when $2a < \lambda_o$. For this case, Levich (63) shows the maximum relative particle velocity to be,

$$v_{max} \sim \frac{2}{3^{3/2}} \left(\frac{\rho_d - \rho_c}{\rho_d}\right) \frac{\epsilon_o^{3/4}}{\nu^{5/4}} \qquad (3.33)$$

A relative velocity expression may also be derived for

the motion of an internally circulating liquid drop. If the gravitational and supplemental reaction terms are neglected, the particle force balance equation may be written, (63).

$$\frac{4\pi}{3} \cdot \rho_d a^3 \cdot \frac{v}{T_\lambda} = \frac{4\pi}{3} a^3 (\rho_c - \rho_d) \sqrt{\frac{\epsilon}{\rho_c T_p}} - 12\pi\mu a v \qquad (3.34)$$

The maximum relative velocity between the particle and the fluid may be determined from eqn. 3.34 as,

$$v_{max} \sim \frac{\rho_c - \rho_d}{\rho_d} a \left(\frac{\epsilon}{\rho_c \nu_c}\right)^{\frac{1}{2}} \qquad (3.35)$$

Even with circulation of the drop interface caused by the relative motion of the drop with the surrounding fluid, there still exists a weak viscous term, $12\pi\mu av$. Thus, there is a velocity gradient in the continuous fluid, close to the interface. For a drop with full internal circulation, this viscous term, however, causes only the slightest wake region, even at drop Reynolds numbers of 700, (63).

3.7 REPORTED MEASUREMENTS OF MIXER HYDRODYNAMICS

Fluid velocities within a mixer have been inferred from photographic traces of particles entrained in the fluid. It is apparent that considerable tedium is involved, Cutter (19); and that such measurements show only the large scale flow, although the high energy dissipating regions may be deduced from the mean velocity gradients measured. Cutter (19) used a lycopodium emulsion with a mean particle diameter of approximately 3×10^{-5} cm. but other workers (2, 86, 110) have used particles of order 0.05 cm. diameter. The dissipation scale of turbulence, λ_o, is stated by Levich (63) to be $10^{-2} > \lambda_o > 10^{-3}$ cms. while Cutter (19) suggests $\lambda_o \sim 5 \times 10^{-5}$ cms. Recently, Kim and Manning (56) have used a transducer probe, developed by Eagleson (27), which is sensitive to small pressure fluctuations, and directly measures the equilibrium range turbulence in the impellor zone.

Most of these velocity measurements have been made in the impellor stream generated by a six-bladed turbine impellor. The bulk vessel flow is virtually uninvestigated, although some work has been done in this Department (28).

For the impellor zone and the bulk flow, it has been established experimentally that the mean velocities are proportional to the impellor tip speed (2, 19, 28, 56, 76, 110, 124). In the impellor tip region the radial and tangential velocities are equal, in accordance with eqn. 3.1, (19), but the tangential velocity decreases to nearly half the radial velocity near the vessel wall. The vertical mean velocity is zero in the horizontal plane through the centre of the impellor blades, (19).

The fluctuating velocity components have been found to be proportional to the impellor speed, and have the same magnitude as the mean flow, in the impellor stream, $u_y \sim v_r \sim w_x \sim ND_I$, (2, 19, 56, 86, 110). The regular velocity fluctuations that follow each blade are rapidly damped out before reaching the baffle ring, (19, 56, 110). With a four-bladed turbine, a 38% radial velocity increase

precedes each rotating blade by nearly 50°, while the associated tangential velocity increase of 20% precedes the blade by nearly 60°, (110).

The correlation coefficients, f and g, and the scales calculated from them, are independent of impellor speed (19). Near the impellor tips the tangential correlation coefficient g, found experimentally, equals the value calculated from the radial correlation coefficient f, supporting the postulate of isotropic flow in this region.

$$f(r) = \frac{\overline{w_x(x) \cdot w_x(x+r)}}{\overline{w_x^2}}, \quad g(r) = \frac{\overline{v_r(x) \cdot v_r(x+r)}}{\overline{v_r^2}}$$

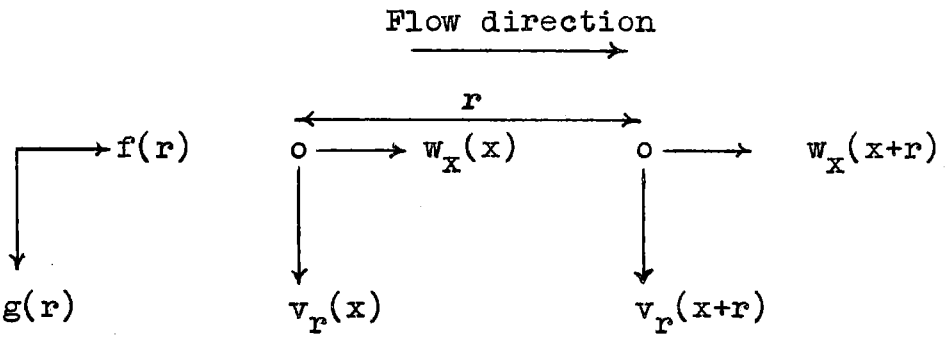

For isotropic turbulence, $g = f + \frac{r}{2}\frac{\partial f}{\partial r}$.

The Eulerian coefficient, $L_p \equiv \int_0^{\infty} R dr$, was found by Cutter (19) for a single vessel geometry, to be equal to the impellor diameter. Similarity between the mixing vessel turbulence decay profile and that obtained for grids (18), suggests that eqn. 3.6 is applicable to mixer flow. This intuitive, but simplifying conclusion is substantiated at high impellor Reynolds numbers, $Re_{Imp} > 10^5$, when a constant Power number is found.

Most of the energy dissipation is due to turbulence breakdown, rather than viscous dissipation of the mean flow (2). The local energy dissipation rate, which is a maximum in the impellor region, decreases with increasing radial distance in the impellor stream, and is comparatively low in the bulk vessel (19). The extent of the high dissipation region depends on the solution properties as well as the vessel geometry (2, 76). For a Newtonian fluid in a fully

baffled vessel, approximately 20% of the total energy imput is dissipated within the impellor, 50% is dissipated in the impellor stream, and the remaining 30% is dissipated in the bulk flow regions which occupy nearly 90% of the total volume of the vessel, (19, 124).

The ratio of the local to the average energy dissipation rate ϵ/ϵ_{av}, varies from nearly 70 at the impellor tips, to 3.5 in the impellor stream near the vessel wall, and is approximately 0.26 in the bulk fluid. In the constant Power number region, the local values of ϵ/ϵ_{av} are independent of impellor speed (19). Thus, the mixer fluid may be divided into two regions, a bulk flow zone of inertial flow and an impellor zone, where high energy dissipation rates occur.

In the impellor zone, Kim and Manning (56), found $E(k,t) \sim k^{-5/3}$, for wave-numbers $19 < k < 100$ ft.$^{-1}$, and $E(k,t) \sim k^{-10/3}$ for $100 < k < 1000$ ft.$^{-1}$. An energy peak occurs at the turbulence generating frequency, defined as Impellor speed x Number blades/second, which approximately separates the two ~~second~~ wave-number regions. The wave-number energy spectrum function curves, $E(k,t)$, show the decay to be self-preserving, as it is independent of impellor dimensions, speed, and position in the vessel. The wave-number results do not exactly support the postulate of an isotropic inertial subrange in the impellor stream, which would require $E(k,t) \sim k^{5/3}$, for the higher wave-numbers, but the existence of a self-preserving higher wave-number subrange, is substantiated.

The energy spectrum curves shown (56), are similar to the concentration spectra obtained by Manning and Wilhelm (72), for the impellor zone. Corrsin theoretically shows, (16), by applying the turbulence theory of local isotropy to an ideal mixer, that the mixing time for homogeneous materials is dependent on the turbulence scale and the power imput. This prediction has been verified experimentally for fully developed turbulence in mixers, (2, 61, 134).

3.8 CONCLUSION

These experimental results suggest that turbulence theory cannot be rigorously applied to the entire mixer. However, any process that takes place mainly in the impellor zone may be correlated by an expression derived from a dimensional 'order of magnitude' analysis; by assuming the existence of an inertial subrange.

A summary of the mixer conditions necessary for scale-up or direct prediction by turbulence theory is given:

1. An equilibrium range exists when the particle Reynolds number is much greater than unity,

$$\frac{v_\lambda \cdot \lambda}{\nu} \gg 1$$

$$\text{or } Re_{Imp} \cdot \left(\frac{\lambda}{D_I}\right)^{4/3} \gg 1$$

For an eddy wave-length λ = 0.1 cms., an equilibrium range could exist when the impellor Reynolds number is greater than 10^4.

2. Inertial subrange turbulence will control a mixer process only if the process is dependent on the microscopic fluid velocity fluctuations. The inertial subrange eddy lengths depend on the local rate of energy dissipation and the fluid kinematic viscosity.

At an impellor Reynolds number of 10^4, the dissipation scale of turbulence is given by,

$$\lambda_o \sim \left(\frac{\rho \nu^3}{\epsilon}\right)^{\frac{1}{4}} \qquad (3.18)$$

When $\epsilon \sim 300$ kg.M/hr and $\nu \sim 0.01$ cS.,

$\lambda_o \sim 0.005$ cms.

In liquid-liquid extraction, the average particle diameter is of order 0.1 cms., which is larger than the dissipation scale of turbulence λ_o, by more than an order of magnitude.

For rigorous mixerscale-up, the ratio of the local to the average energy dissipation rate must be independent of vessel size and impellor speed. For baffled vessels, a constant power number region, which is necessary for ϵ/ϵ_{av} to be constant, is predicted for $Re_{Imp} > 10^4$. Some mixer processes are also dependent on the time spent in a quiescent flow region. The rate of fluid mixing, as well as energy dissipation, must be considered for the scale-up of such a process.

Section 4

POWER DISSIPATION IN A MIXING VESSEL

4.1 CORRELATIONS OF POWER INPUT

The rate of energy dissipation in mixing vessel may be estimatedfrom the simplified energy relationship, eqn.3.4, which was derived from the Navier-Stokes and Continuity equations.

$$\int_o^\infty \epsilon \, dx = \frac{2\pi \, dr}{r dr} \int_o^\infty (k^2 . \bar{v}_r + 2\bar{w}_z . v_r . w_z) \, dx \quad (3.4)$$

$$k^2 = (v_r^2 + w_z^2 + u_y^2) + (\bar{v}_r^2 + \bar{w}_x^2 + \bar{u}_y^2)$$

In section 3.7 it was shown that,

$$u_y^2 \sim v_r^2 \sim w_x^2 \sim \bar{u}_y^2 \sim \bar{v}_r^2 \sim \bar{w}_x^2 \sim (ND_I)^2$$

From which, substitution in eqn. 3.4 yields,

$$\int_o^\infty \epsilon \, dx \sim \frac{2\pi}{r} \int_o^\infty 8(ND_I)^3 \, dx$$

or $$P_o \equiv \frac{P.g}{D_I^5 n^3 \rho} = \text{Constant} \quad (4.1)$$

A similar relationship may be derived from the inertial energy equation,

$$\epsilon \sim \rho \frac{(\Delta u)^3}{l} \quad (3.6)$$

When local isotropy exists, $\Delta u \sim ND_I$, and $l \sim D_I$, thus,

$$\epsilon = \frac{P.g}{D_I^3} \sim \rho \, N^3 D_I^2$$

or $$\frac{P.g}{D_I^5 N^3 \rho} = \text{Constant} \quad (4.1)$$

Equation 4.1 applies only to fully developed turbulent flow, when the viscous energy terms may be neglected compared with the inertial terms.

An energy relationship may also be derived from the Navier-Stokes and Continuity equations, when the inertia terms are negligible compared with the viscous terms,

$$\int_o^\infty \epsilon \, dx = -\nu \int_o^\infty (\nabla^2(\overline{v}_r^2 + \overline{w}_x^2 + \overline{u}_y^2) - \frac{1}{r^2}(\overline{v}_r^2 + \overline{w}_x^2)) \, dx$$

For viscous flow the second order differential velocity terms may be neglected,

$$\int_o^\infty \epsilon \, dx \sim -\nu \int_o^\infty (ND_I)^2 \, dx$$

$$\text{or} \qquad P_o \sim Re_{Imp}^{-1} \qquad (4.2)$$

Turbulence theory does not numerically predict the power dissipated in a stirred vessel, so the semi-empirical approach of dimensionless analysis is necessary. The mixer variables that may affect power dissipation may be expressed as a functional relationship

$$f(P, D_I, D_T, N, H_t, H_I, S_b, B_I, B_b, L_b, g, \rho, \mu) = 0$$

These parameters are combined into dimensionless groups by use of the Buckingham Pi theory, (108)

$$\left(\frac{P g_c}{D_I^5 N^3 \rho}\right) = \text{const.} \left(\frac{D_I^2 N}{\nu}\right)^m \left(\frac{D_I N^2}{g}\right)^n \left(\frac{D_T}{D_I}\right)^t \left(\frac{H_T}{D_I}\right)^h \left(\frac{H_I}{D_I}\right)^c \left(\frac{S_b}{D_I}\right)^s \cdot \left(\frac{B_I}{D_I}\right)^b \left(\frac{B_b}{D_I}\right)^w \left(\frac{L_B}{D_I}\right)^j \cdot (\text{No. of blades})^a (\text{No. of baffles})^r \qquad (4.3)$$

D_T	=	Tank diameter	B_I	=	Width of impellor blades
D_I	=	Impellor diameter	B_b	=	Width of baffles
H_T	=	Height of liquid	L	=	Length of impellor blades
H_I	=	Height of impellor	S_b	=	Pitch of impellor blades

For geometric similarity eqn. 4.3 reduces to

$$P_o = \text{Const.}\ Re_{Imp}^{m}.\ Fr^{n} \qquad (4.4)$$

where m, n and the constant may be determined experimentally.

The Froude number exponent n, is zero at high impellor Reynolds numbers, unless a forced vortex occurs in the vessel, when n becomes approximately equal to -0.22, for $10^2 < Re_{Imp} < 10^4$, (108).

In a mixer, viscous flow is predominant for $Re_{Imp} < 10$, when the power relationship derived from the viscous energy equation is found to apply (108).

$$P_o \sim Re_{Imp}^{-1}$$

A transition power region exists for $10 < Re_{Imp} < 10^4$, in which the Power number becomes increasingly dependent upon the mixer geometry. A minimum point occurs in the Power-Reynolds numbers plot at $Re_{Imp} \sim 400$ for a baffled vessel, but a point of inflexion occurs in the plot for an unbaffled vessel. The constant Power number region, predicted by eqn. 4.1 which requires the viscous forces to be negligible compared with the inertia forces in the vessel, does not occur until $Re_{Imp} \sim 10^4$, (108).

A turbine stirred vessel is usually operated in the Reynolds number range $10^3 < Re_{Imp} < 10^7$, where the Power number is essentially constant. The numerical value of this constant may be found only by measurement with the vessel, or with a scaled model. Power number scale-up, which requires the ratio of the local to the average energy dissipation rate ϵ/ϵ_{av} to be constant for the model and the prototype vessels, necessitates kinematic as well as geometric similarity. However, any deviation from exact geometric similarity may be allowed for by the dimensionless scale ratios in eqn. 4.3,

$(\frac{D_T}{D_I})$, $(\frac{H_T}{D_I})$, $(\frac{L_b}{D_I})$, $(\frac{S_b}{D_I})$, $(\frac{B_I}{D_I})$, $(\frac{B_b}{D_I})$, $(\frac{H_I}{D_I})$ (No. of blades),

(No. of baffles).

Turbulence theory, which is summarised in Section 3 of this thesis, neglects these scale ratios, but for fully developed turbulence a Power number range of 10 is found for different vessel geometries, even when no forced vortex occurs, (108). Early workers in mixer design endeavoured to correlate Power numbers against these scale ratios. Some of these correlations and that obtained in this thesis, are tabulated in Table 4.

Corrsin (17) predicts the power scale-up requirements for similar degrees of liquid mixing, in two vessels, from inertial turbulence theory. The relationship derived shows that exact scale-up does not lead to identical "mixedness" of the liquids in the two vessels. Corrsin's paper, it appears, predicts the experimental observation that scale-up with a scale ratio greater than 10 is unlikely to be accurate, (68).

4.2 PHYSICAL PROPERTIES OF A TWO PHASE FLUID

The Power number - Reynolds number correlations summarised in Table 4 are for single phase fluids. By superimposing Power-Reynolds numbers plots for single and two phase fluids, Laity and Treybal (62) determined the most suitable density and viscosity correlations to give the best data agreement.

The density so found is the weighted mean density, ρ_{soln},

$$\rho_{soln} = \phi.\rho_d + (1 - \phi)\rho_c \qquad (4.4)$$

The most suitable bulk viscosity, μ_{soln} is,

$$\mu_{soln} = \frac{\mu_d}{1-\phi}\left(1 + \frac{1.5\,\phi\,\mu_d}{\mu_c + \mu_d}\right) \qquad (4.5)$$

This expression is an extension, (100), for concentrated solutions, of Taylor's viscosity for dilute emulsions in laminar flow conditions, (121).

$$\mu_{soln} = \mu_c\left(1 + \phi\,\frac{\mu_c + 2.5\,\mu_d}{\mu_c + \mu_d}\right)$$

4.3 EXPERIMENTAL MEASUREMENTS OF POWER INPUT

The impellor torque was measured for each of the mass transfer runs and for the repeat hold-up measurements. The torque was transmitted from the agitator by a lever arm, supported on a knife edge, to a continuously indicating digital balance. The apparatus is shown diagrammatically in Fig. 2.7, and is described in Section 2.4.

Agitator torque, T = Balance Wt. x $\frac{ca}{b}$

Agitator power, P = Torque . $2\pi N$

$2\pi N$ = radial velocity of impellor, $sec.^{-1}$

$\frac{ca}{b}$ = lever arm ratio.

The weight measurement introduced an error into the power estimation, although the balance was accurate to ± 0.02 gms. The low torque estimates are affected by the 'balance weight' being a difference quantity, $\sim$ 6 gms., of two large measurements, $\sim$ 160 gms. The high torque measurements suffer from a reading error introduced because of fast fluctuations of the balance reading ± 3 gms., for a 'balance weight' of about 150 gms. Combined with the stroboscope error of $\pm 2\%$, the total error in the power measured becomes nearly 4%.

The lever arm support gave no measurable torque loss, but the low torque measurements were susceptible to the errors described in Section 2.4, if care was not taken in setting up the agitator.

The experimental results are tabulated in Appendices 12, 13, and presented in Figs. 4.1, 4.2, 4.3. The line of best data correlation, found by log-log regression is,

$$P \sim N^{2.51} D_I^{3.66} \qquad (4.7)$$

Regression coefficient = 0.996

The density and viscosity correlations recommended by Treybal (62), Section 4.2, are used to estimate the two phase fluid properties. The graphs involving power, impellor speed,

and diameter assume a constant density and viscosity for all runs. Appendix 13 shows this approximation to be tenable, particularly for the solution density.

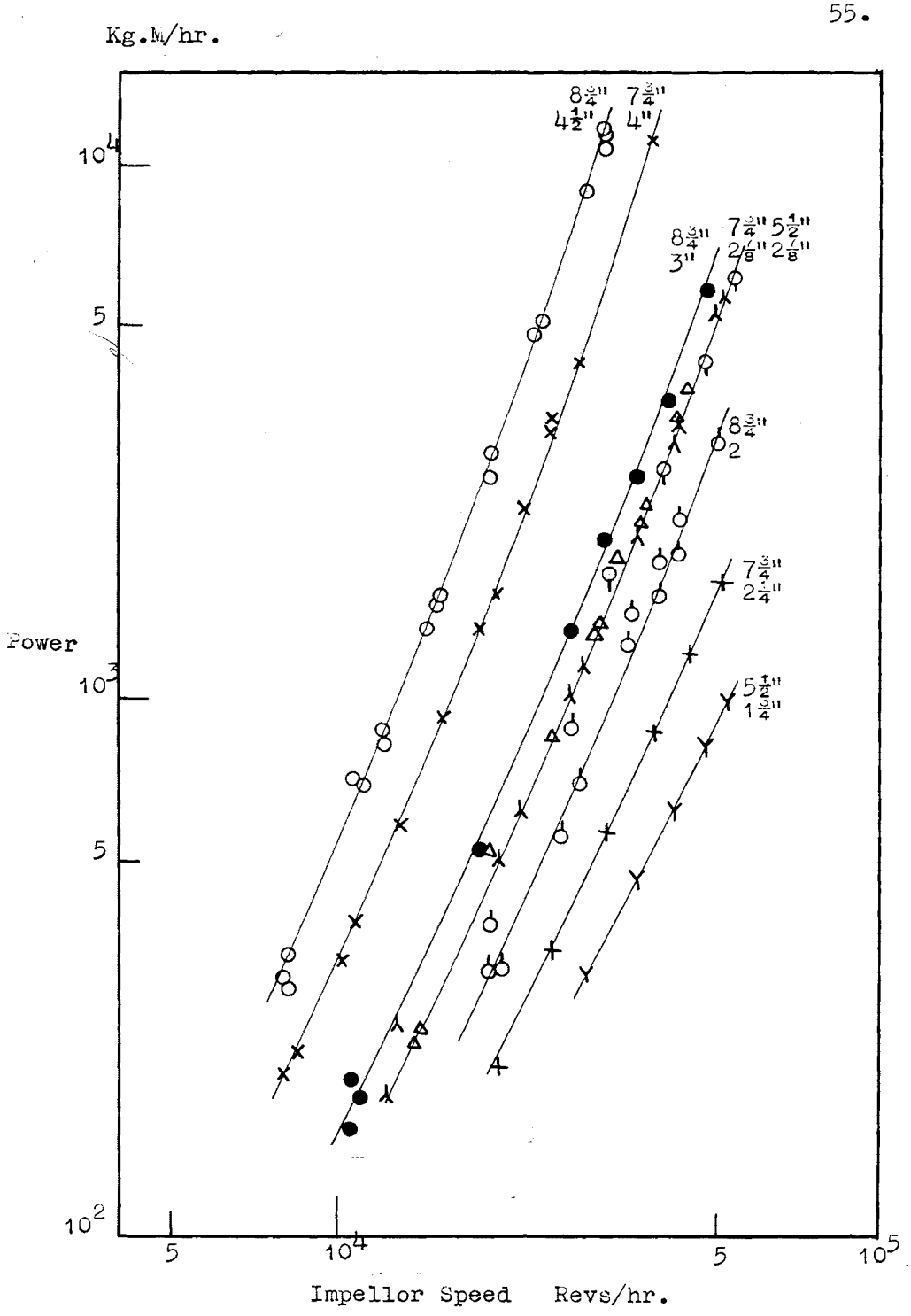

Fig. 4.1 Mixing vessel power input versus impellor speed.

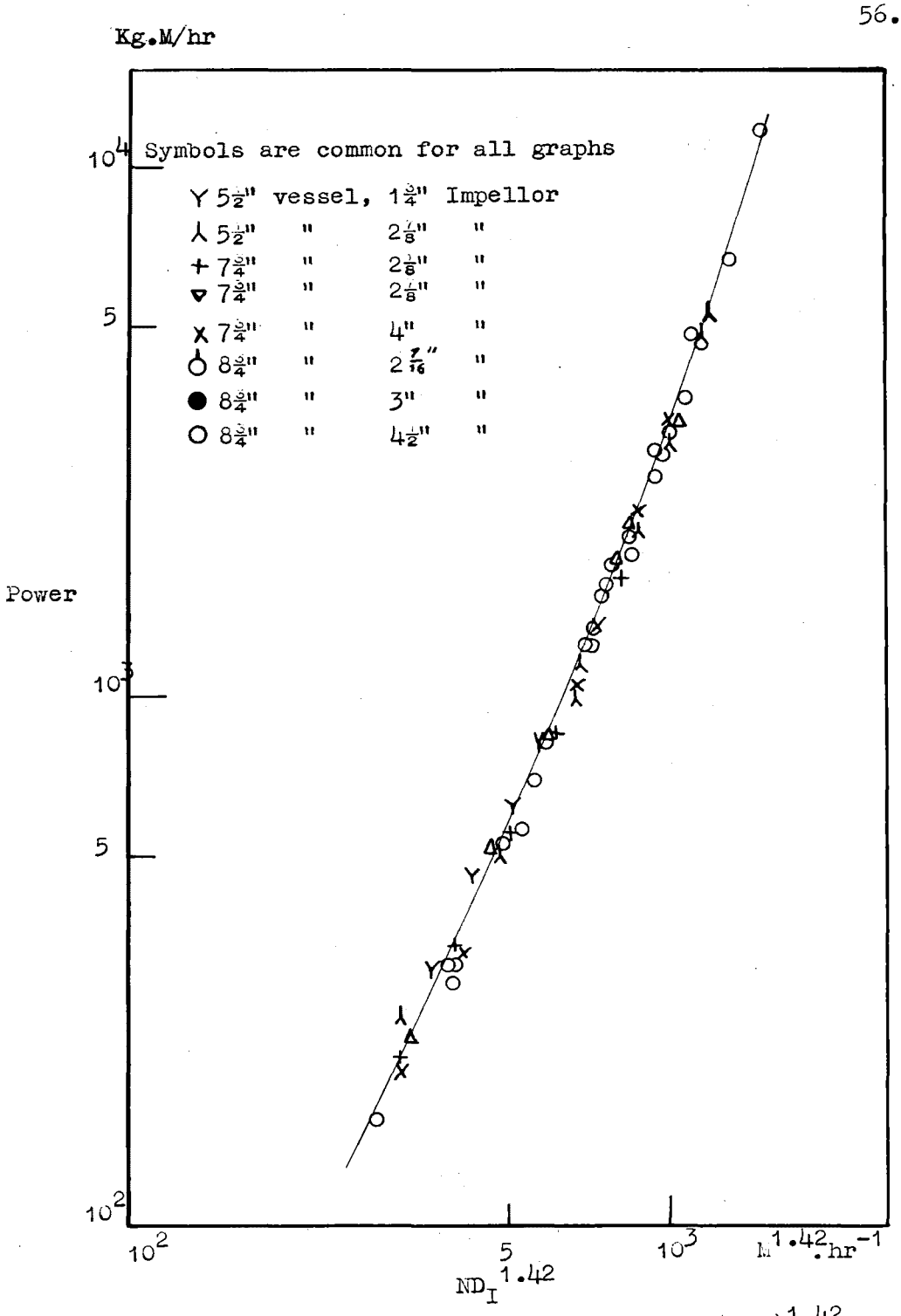

Fig. 4.2 Line of best fit for power data, power vs $(ND_I)^{1.42}$

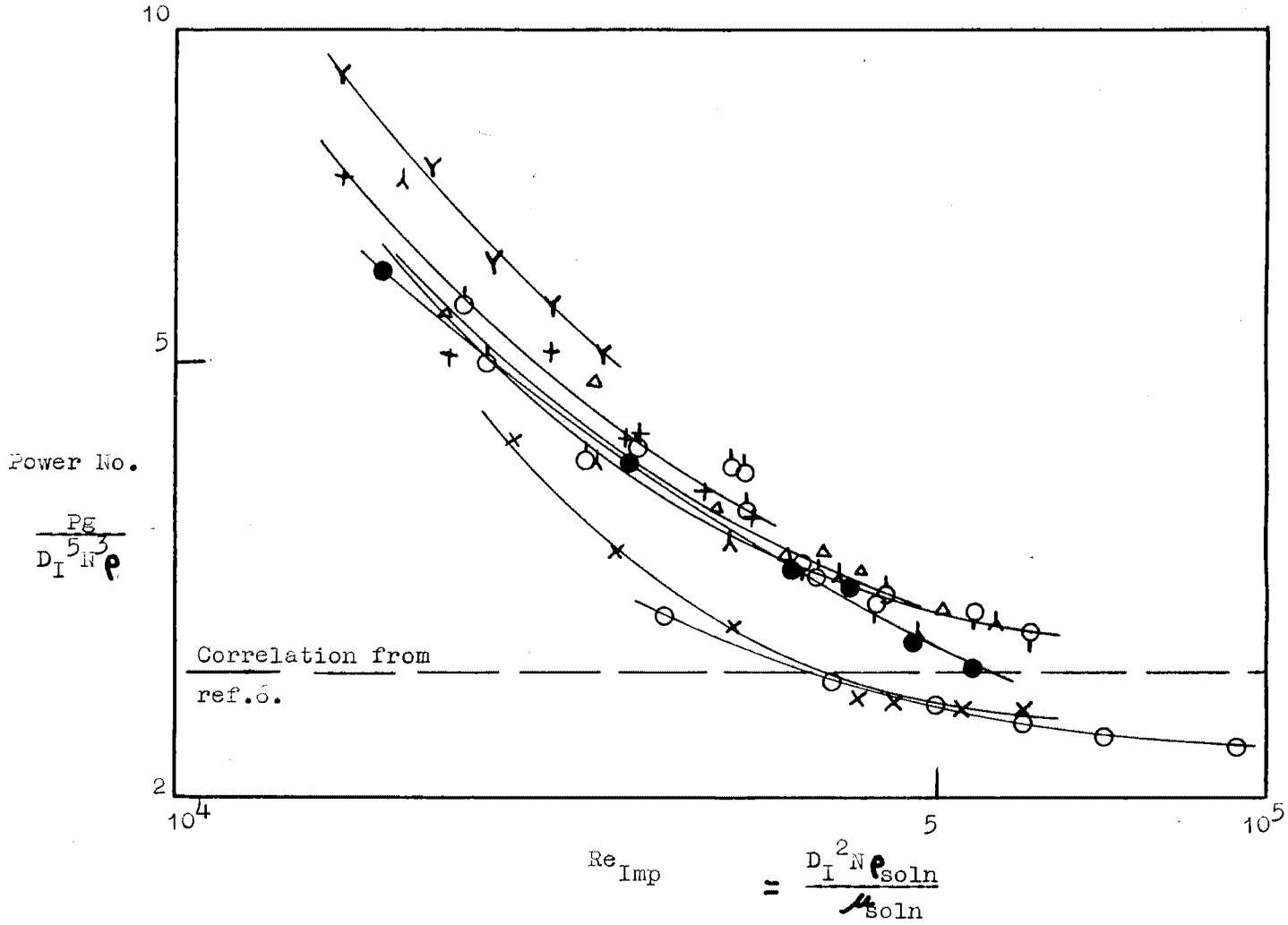

Fig. 4.3 Power number versus Reynolds number for partial geometric similarity

4.4 DISCUSSION

In this work the power imput to the mixing vessel is measured for each run, so that interfacial area and mass transfer relationships, involving the term, energy dissipated/unit volume, may be evaluated. Consequently, a small range of the variables, impellor diameter, tank diameter, and impellor speed have been investigated, while the liquid properties, density, and viscosity, are essentially constant. Thus, these results do not represent a full investigation into power dissipation in a mixer, although the results are comparable with a limited section of the published data.

The impellor diameter is found to be the significant correlating length, for power dissipation, eqn. 4.7. This result is common to all mixer power measurements, (7, 108) and is in accordance with the observation that 70% of the power dissipation occurs in the impellor stream (19). The term, power dissipated/unit volume, should involve the impellor volume, rather than the total vessel volume, which is more usual in correlating interfacial areas (13).

Table 4 summarises the experimental values for m, n, t, d, v, and h, see eqn. 4.3, that have been obtained when mixer geometric similarity did not occur.

$$P \sim D_I^{\,m} . N^n . D_T^t . \rho^d . \mu^v . H_T^{\,h} \qquad (4.3)$$

Graphs of the literature data summarised in Table 4, are presented by Rushton and co-workers (108), and Bates and co-workers (6). The exponents m, and n, for the impellor diameter D_I, and speed N, found in this work are in agreement with those in published correlations, when there is no geometric similarity between vessels, but no effect of vessel diameter, D_T, is found in this work, Figs. 4.1, 4.2. The vessel diameters used, $5\frac{1}{2}$", $7\frac{3}{4}$" and $8\frac{3}{4}$", would be expected to show a diameter dependence if it occurred.

Table 4

Six-bladed impellors in a baffled vessel

Author	Impellor type	m	t	n	h	d	v
Hooker	turbine, fully baffled	3.65	0.75	3.0	0.6	1.0	0
Olney & Carlson	Flat bladed paddles,"	3.3	0.5	2.85	0.6	.85	.15
Rushton & co-workers	" " " "	3.75	0	3.0	0	1.0	0
Laity & Treybal	" " " "	5.0	0	3.0	0	1.0	0
O'Connel & Mark	Paddle, baffled	3.65	1.09	3.0		1.0	0
this work	Flat bladed paddle,"	3.6	0	2.6			

A blank space indicates that the parameter was not investigated.

The graph of Power number versus Reynolds number, Fig. 4.3, shows the Power number to decrease with increasing Reynolds number for each vessel geometry, in the range $10^4 < Re_{Imp} < 10^5$. A graph for the same impellor geometry as used in this work (6), shows the Power number to be constant in the range $10^3 < Re_{Imp} < 10^5$. The experimental power results obtained in this thesis are contrary to published data for similar vessel geometries, and coincide more with Power-Reynolds number plots for paddles in an unbaffled vessel (136), or propellors in a baffled vessel (108).

Published graphs (108, 136) do not usually show data points, but a plot of Power versus Reynolds numbers for a propellor operating in an unbaffled vessel shows that a constant Power number region may only be obtained for the range $10^3 < Re_{Imp} < 10^5$, by varying the solution viscosity, which would not be expected to affect the Power number, see Section 4.1. The constant viscosity plots for a single vessel geometry diverge markedly from the published over-all plots for a propellor in an unbaffled vessel.

The baffle width to vessel diameter ratio used in this work, $B_b/D_T = 1/8$, may suggest that the vessel was over-baffled, causing a decrease in power dissipation, (83). The literature is somewhat divided on the effect of baffles, (6), but it is apparent that the effects of baffle width, impellor

diameter, and vessel diameter, are sufficiently interrelated to mask the effect of vessel diameter on power dissipation in a mixing vessel.

In this Department, Farrier, (28), has found the impellor stream from the paddle-type impellor used in this work, to have a mean vertical velocity component, as well as radial and tangential components, see fig.2.6. To a slight extent, flat-bladed paddles with comparatively large bosses act as propellors.

A weak, Power = f(Liquid residence time x Impellor speed), correlation is found by Laity and Treybal (62). In this thesis the maximum energy of the inlet liquid streams is 45KG.M/hr, which is 1 - 2% of the total energy imput to the mixer, so the residence time term would, if included, make a negligible contribution to the mixer power correlation.

4.5 CONCLUSION

At present, it is not possible to predict power dissipation in a mixing vessel. In consequence, a large volume of experimental data has been collected, which enables power scale-up for different vessels to be made by dimensionless group correlations. Thus power prediction is possible for limited geometric scale ratios, which have been extended by recent turbulence theory analyses.

The Power number - Reynolds number plots obtained in this work do not show a constant Power number region for the Reynolds number range $10^4 < Re_{Imp} < 10^5$, as is shown in published data for similar vessel geometries. The explanation is considered to be that the over-all published plots have achieved a Reynolds number range by altering the solution viscosity, a term which the power dissipation rate is independent of, for $Re_{Imp} > 10^3$.

The dimensional correlation,

$$P \sim D_I^{3.6} \cdot N^{2.6} \cdot D_T^{0} \qquad (4.8)$$

is in agreement with those obtained when geometric similarity does not exist between vessels. The independence of power on the tank diameter is caused by the inter-relation of the impellor diameters, the baffle widths, and the vessel diameters.

It is found that the parameter, energy dissipated/unit volume, is more accurately described by power dissipated/ unit impellor volume, than by power dissipated/unit vessel volume, for processes controlled by high rates of energy dissipation.

The hypotheses required for local isotropy, which are valid in the constant Power number region, do not fully apply to this work. Since relationships derived from these hypotheses closely describe the mixer fluid turbulence at the higher Reynolds numbers, $Re_{Imp} > 10^5$, the hypotheses and the simplifications implied are retained.

Section 5

INTERFACIAL AREA IN A TWO PHASE SYSTEM

5.1 INTRODUCTION

The area of contact between two phases may be calculated from two parameters, the mean surface-volume particle diameter, and the dispersed phase volume fraction. For spherical particles, the interfacial area A, is given by,

$$A = \frac{6\phi}{d_{sv}} \qquad (5.1)$$

The particle size range existing in a mixing vessel results from fragmentation of the larger particles in the higher energy dissipating regions and coalescence of the smaller particles in the lower energy dissipating regions, (79, 111). The maximum and minimum stable drop sizes that exist in locally isotropic flow may be predicted by turbulence theory. The average particle size measured in a mixing vessel frequently may be correlated by one of these two mechanisms, as either coalescence or dispersion may control the particle size in the mixer region from which the particles are sampled, (1, 115, 131).

5.2 PARTICLE FRAGMENTATION CAUSED BY INTERNAL CIRCULATION OF THE DROP

In a theoretical analysis, fragmentation is considered to occur when the surface disrupting force exceeds the surface tension force. The disruptive force may result from internal circulation of the drop, or pressure fluctuations over the drop surface resulting from velocity gradients in the external fluid.

Large drops moving through another phase tend to flatten

perpendicularly to the direction of motion (25). Fragmentation of these drops occurs when the internal circulation pressure causes the liquid forming the central dome to rupture, forming many fine droplets.

The surrounding torus then breaks into several comparatively large drops.

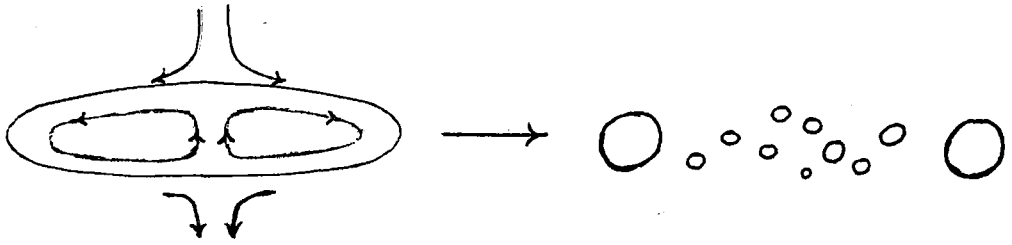

Let $Re = \frac{ua}{\nu_c}$ = External Reynolds number of the drop.

$Re = \frac{ua}{\nu_d}$ = Internal circulation Reynolds number of the drop.

$V = \frac{4}{3}\pi a^3 \sim \pi q^2 h$ = Volume of the drop as an ellipsoid, $h << q$.

The internal circulation pressure of the drop is given by $k_f' \rho_d (u')^2/2$. A minimum surface tension pressure occurs at the maximum radius of curvature of the drop. The condition for drop fragmentation at this point may be written,

$$k_f' \rho_d \frac{u'^2}{2} > \frac{\sigma h}{q^2} = \frac{\sigma \pi h^2}{V} \qquad (5.2)$$

The surface tension and pressure forces for the drop are related by the equation,

$$\Delta p . S_a . \delta h + \sigma . \delta S_a = 0 \qquad (5.3)$$

S_a = maximum cross-sectional area of the drop.

$S_a h = \frac{4}{3}\pi a^3 = V$, drop volume, which is constant.

The pressure difference across the drop may be written,

$$\Delta p \sim \rho_c \frac{u^2}{2} \qquad (5.4)$$

Substitution of eqn. 5.4 in 5.3 yields,

$$h = \frac{\sigma}{\Delta p} \sim \frac{2\sigma}{\rho_c u^2} \qquad (5.5)$$

h may be substituted in eqn. 5.2, to yield,

$$k_f' \frac{\rho_d (u'_{cr})^2}{2} = \frac{\pi h^2 \sigma}{V} \sim \frac{4\pi\sigma \cdot \sigma^2}{\rho_c^2 u_{cr}^4 \cdot \frac{4}{3}\pi a_{cr}^3} \qquad (5.6)$$

u_{cr} = critical external fluid velocity for particle fragmentation.

a_{cr} = critical drop radius for fragmentation.

To determine an order of magnitude relationship between u and u', the Navier-Stokes equation is solved for the limiting case of negligible viscous terms.

$$u' \cdot \Delta u' = -\frac{1}{\rho_d} \cdot \Delta p' + \nu_d \Delta u'$$

$$\frac{(u')^2}{L} \sim \frac{P}{\rho_d L}$$

L = characteristic length dimension of the drop.

$$(u')^2 \cdot \rho_d \sim p \sim u^2 \cdot \rho_c \qquad (5.7)$$

The critical drop radius may be obtained from eqns 5.6 and 5.7,

$$k_f' \cdot \rho_d \cdot \frac{(u')^2}{2} \sim k_f \cdot \rho_c \cdot \frac{u^2}{2} \sim \frac{2\sigma^3}{\rho_c \cdot a_{cr}^3 \cdot u_{cr}^4}$$

$$\text{or} \quad a_{cr} \sim \sqrt[3]{\frac{6}{k_f}} \cdot \frac{\sigma}{\rho_c \cdot u_{cr}^2} \qquad (5.8)$$

A similar expression may be obtained for the fragmentation of gas bubbles (63),

$$a_{cr} \sim \sqrt[3]{\frac{6}{k_f}} \cdot \frac{\sigma}{\rho_c \cdot u_{cr}^2} \cdot \left(\frac{\rho_c}{\rho_d}\right)^{\frac{1}{3}}$$

If the Navier-Stokes equation for the drop is solved for the viscous terms, it is found that an induction period is required, before the drop fragments by an internal circulation mechanism. The induction time required to establish circulation within the drop, may be written

approximately as,

$$\frac{\nabla p}{\rho_c} \sim \nu \Delta u$$

$$\text{or} \quad \frac{\sigma}{a^2 \rho_c} \sim \nu_c \frac{u}{a^2} \sim \frac{\nu_c}{a t_i}, \quad t_i \sim \rho_c a \nu / \sigma \qquad (5.9)$$

t_i = characteristic time for displacement of the material in the drop.

Although a viscosity term does not appear in the fragmentation condition, eqn. 5.8, a correlation of the sizes of drops fragmented by this mechanism may include a viscous term. The effect of this term is controlled by the time that the drops remain in the high energy dissipating regions of the fluid.

5.3 PARTICLE FRAGMENTATION CAUSED BY TURBULENCE IN THE EXTERNAL FLUID

If the velocity fluctuations in the external fluid cause the pressure differences across a drop to exceed the surface tension pressure, the drop will fragment. The maximum relative velocity between a particle and the fluid occurs with turbulence of eddy length $\lambda = 2a$, $\lambda_1 > \lambda > \lambda_o$, see Section 3.6. The maximum pressure difference across the drop is thus caused by inertial subrange turbulence with eddy length $\lambda = 2a$.

The pressure difference over a diameter of a particle may be written,

$$Q = k_f \cdot \rho_c \left(\frac{u_1^2 - u_2^2}{2}\right) \qquad (5.10)$$

$$\sim k_f \cdot \rho_c \cdot \frac{v_\lambda^2}{2}$$

Equations 3.6 and 3.13 are substituted in the fragmentation condition,

$$\frac{\sigma}{a_{cr}} = Q = k_f \rho_c \left(\frac{u_1^2 - u_2^2}{2}\right) \qquad (5.11)$$

The equation for turbulence fragmentation, derived

independently by Kolmogoroff (59) and Hinze (45), is obtained as,

$$a_{cr} = \left(\frac{\sigma}{\rho_c k_f}\right)^{3/5} \cdot \epsilon^{-2/5} \qquad (5.12)$$

Approximations that may be made for locally isotropic flow in a mixing vessel, $\Delta u \sim ND_I$, $\lambda_I \sim D_I$, are substituted,

$$a_{cr} \sim \left(\frac{\sigma}{\rho_c k_f}\right)^{3/5} \cdot \frac{D_I^{2/5}}{(ND_I)^{6/5}} \qquad (5.13)$$

The equivalent expression for bubble fragmentation is (63),

$$a_{cr} \sim \left(\frac{\sigma}{k_f \rho_c}\right)^{3/5} \frac{D_I^{2/5}}{(ND_I)^{6/5}} \cdot \left(\frac{\rho_c}{\rho_d}\right)^{1/3}$$

The quadratic pressure relationship $\Delta p \sim \rho_c \frac{(\Delta u)^2}{2}$, used to derive eqn. 5.13, requires that $Re \geq 10$. Thus, a minimum drop diameter, a_{min}, that may be formed by a pressure fluctuation mechanism, is given by,

$$Re = \frac{v \cdot 2a_{min}}{\nu_c} \sim 10$$

$$\frac{\rho_c \alpha^2 \nu^2}{a_{min}^2} \sim \frac{\sigma}{a_{min}}$$

or $$a_{min} \sim \frac{\rho_c \alpha^2 \nu^2}{\sigma} \qquad (5.14)$$

Levich (63) notes that smaller drops cannot be formed in a turbulent fluid. Viscous eddies, where $Re_\lambda < 1$, for $2a < \lambda_o$, do not cause drop fragmentation.

5.4 FRAGMENTATION OF DROPS NEAR A WALL

Near a solid surface, the liquid velocity profile may be written,

$$U = \frac{v_o}{\sqrt{\alpha}} \cdot \ln \frac{y}{\delta_o}$$

y = distance out from a wall.

For $y \sim \delta_o$, the velocity gradient is greater than the maximum in the bulk turbulence, giving further particle fragmentation close to the wall.

For $2a < y$, the pressure difference over a drop diameter may be written,

$$Q = 6\,\rho_c\, v_o^2 \left(\ln^2\left(\frac{y+2a}{\delta_o}\right) - \ln^2\left(\frac{y}{\delta_o}\right)\right)$$

$$\sim 6\,\rho_c\, v_o^2\, \frac{4a}{y}\, \ln\frac{y}{\delta_o}$$

The skin friction velocity v_o, is related to the mean flow velocity U, by eqn. 3.24, $v_o \sim \sqrt{k_f/2}.U$, which is substituted in the fragmentation condition,

$$\frac{\sigma}{a_{cr}} = 6\,\rho_c\, v_o^2\, \frac{4a_{cr}}{y}\, \ln\frac{y}{\delta_o}$$

to give,

$$a_{cr} \sim \frac{1}{U}\sqrt{\frac{\sigma}{\rho_c}} \cdot \sqrt{y/\ln y/\delta_o} \qquad (5.15)$$

The minimum drop size that may be formed by this mechanism is given when $Re_\lambda = 1$, at $y = \delta_o$. Smaller particles are not formed in the viscous boundary layer, when $Re_\lambda < 1$, (63).

5.5 PARTICLE SIZE WITH COALESCENCE MECHANISMS

Shinnar, (114) postulated that at a minimum particle diameter, $2a_{min}$, the energy of the turbulent velocity fluctuations is equal to the energy of droplet adhesion. The turbulence energy is then insufficient to displace smaller drops, which are separated by only a thin film. The force of adhesion for small drops is given by Deryagnin (23) as,

$$F_a(h_o) = \frac{\pi r}{2}\int_{h_o}^{\infty}\int_{h}^{\infty} f(h).\,dh.\,dh'$$

h_o = separation distance of the drops.

For equi-diameter drops, separation may occur for droplet diameters given by,

$$\rho_c\, \frac{v_{2a}^2 \cdot (2a)^2}{S(h_o)} = \text{Constant} \qquad (5.16)$$

In isotropic flow, eqn. 5.16 may be written,

$$\rho_c\, \epsilon^{2/3}\, a^{8/3}/F_a\left(\frac{h_o}{2a}\right) = \text{Constant}$$

$$\text{or} \quad a_{min} \sim \epsilon^{-\frac{1}{4}} \cdot \rho_c^{-\frac{3}{8}} \cdot S\left(\frac{h_o}{2a}\right) \qquad (5.17)$$

For $\frac{h_o}{2a} < 1$, $F_a\left(\frac{h_o}{2a}\right)$ is constant.

In turbulent flow, there is also a maximum particle diameter which may be entrained by the turbulence. Rearrangement of an expression derived by Kneule (58), for solid particles, shows the maximum particle diameter that will be retained in mixer flow to be,

$$a_{max} = \text{constant} \cdot \epsilon^2 \left(\frac{\rho_c}{\rho_c - \rho_d}\right)^3 \cdot \frac{1}{g_c^2} \cdot f(\phi), \qquad (5.18)$$

$f(\phi)$ = empirical phase volume ratio.

Equation 5.18 is in some doubt, (116), but in this work it is only used qualitatively to show the maximum entrained particle size effect.

5.6 PARTICLE SIZE DISTRIBUTION IN A MIXER

In a mixing vessel, a considerable range of particle sizes is found, but at present there is no method of calculating this spread, (1). However, if the particle diameters found in a mixer are plotted against the impellor speed, the diameter spread should lie in a region of stability, given by the equations derived in the preceding sections, see Fig. 5.1.

5.7 FREQUENCY OF PARTICLE COLLISIONS

There are several postulates on which is based the prediction of particle collision frequency. For small particles with diameter $2a < \lambda_o$, the number of particle collisions, which are predominantly caused by Brownian motion, may be calculated by Smoluchowski's theory, (see 63). Such a random collision mechanism, however, applies only to aerosols and colloidal

suspensions. Levich (63) considers other mechanisms that cause collisions, for particles with small diameters $2a < \lambda_o$. The mechanisms of 'gradient coagulation' where particles following adjacent streamlines near a wall collide, 'diffusion' of particles towards each other, and 'incomplete entrainment' of the particle in turbulent flow, are considered. For larger diameter particles $\lambda_1 > 2a > \lambda_o$, most of the particle collisions result from incomplete entrainment in the turbulence, although other mechanisms for collision still occur.

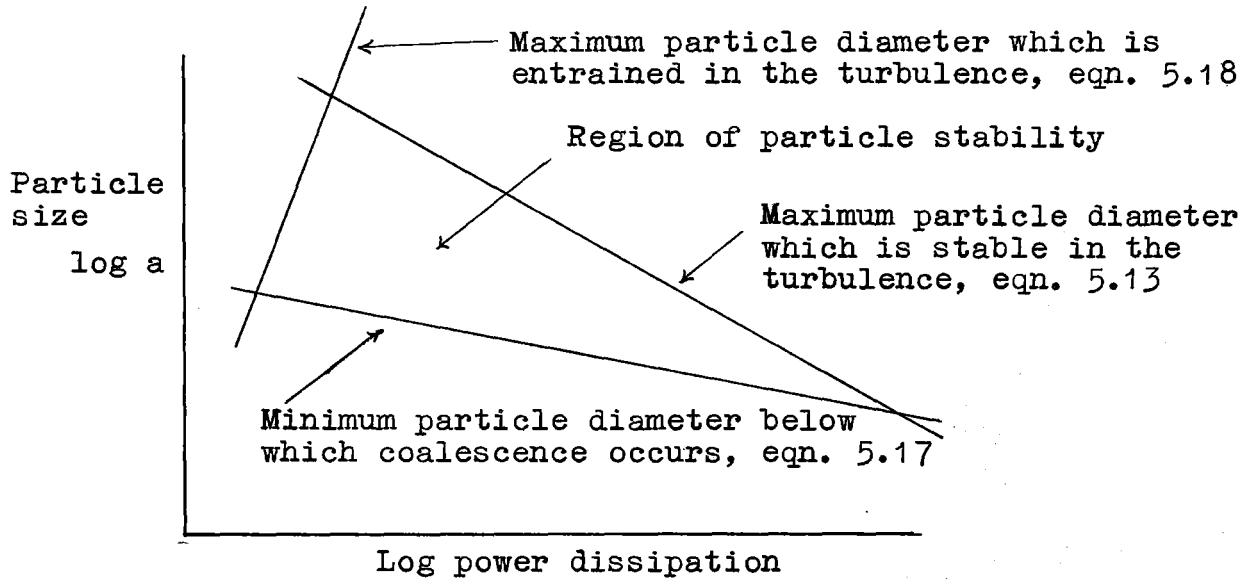

Fig. 5.1 Stable Particle Size Region in a Mixer

The maximum relative velocity between a particle and the surrounding fluid is given by eqn. 3.31 for particles, $\lambda_1 > 2a > \lambda_o$,

$$v_{max} = \frac{1}{3^{5/6} \cdot \sqrt[3]{k_f}} \cdot \left(\frac{\rho_d - \rho_c}{\rho_d}\right)^{\frac{1}{2}} (2a)^{\frac{1}{3}} \left(\frac{\epsilon}{\rho_c}\right)^{\frac{1}{3}} \qquad (3.31)$$

The maximum relative velocity between two particles is approximately given by the difference between the relative velocities of each particle with the surrounding fluid $v_{rel} = v_{max}(a) - v_{max}(r)$. The number of collisions, n_c, of particles radius a, with those of radius r, per unit time, is given by,

$$n_c = n_o \pi (a+r)^2 \cdot ((2a)^{\frac{1}{3}} - (2r)^{\frac{1}{3}}) \left(\frac{\epsilon}{\rho_c}\right)^{\frac{1}{3}} \left(\frac{\rho_d - \rho_c}{\rho_c}\right)^{\frac{1}{2}} \quad (5.19)$$

n_o = number of particles/unit volume.

$(a+r)^2$ = area swept by a particle, radius a, relative to a particle, radius r.

The total number of collisions of particles, radius a, with smaller particles is equal to,

$$\int_o^a \pi (a+r)^2 \cdot (a^{\frac{1}{3}} - r^{\frac{1}{3}})\, n_o \cdot f(r) \cdot \left(\frac{\epsilon}{\rho_c}\right)^{\frac{1}{3}} \left(\frac{\rho_d - \rho_c}{\rho_c}\right)^{\frac{1}{2}}$$

$f(r)$ = particle size distribution.

The total number of collisions in unit volume per unit time is given by,

$$N_o \sim \overline{(a+r)^2 (a^{\frac{1}{3}} - r^{\frac{1}{3}})}\, n_o^2 \left(\frac{\rho_d - \rho_c}{\rho_c}\right)^{\frac{1}{2}} \left(\frac{\epsilon}{\rho_c}\right)^{\frac{1}{3}} \quad (5.20)$$

Dimensionally, the term $\overline{(a+r)^2 \cdot (a^{\frac{1}{3}} - r^{\frac{1}{3}})}$ may be replaced by $a^{7/3}$.

$$N_o \sim n_o^2 \left(\frac{\rho_d - \rho_c}{\rho_d}\right)^{\frac{1}{2}} \left(\frac{\epsilon}{\rho_c}\right)^{\frac{1}{3}} a^{7/3} \quad (5.21)$$

Experimentally measured coalescence rates have been reported as w_i (37, 70, 77), where w_i = (vol. of dispersed phase coalesced/vol. of dispersed phase x min.))

For spherical particles, w_i may be written in terms of N_o.

$$w_i = N_o \cdot \tfrac{4}{3} \pi a^3 / \phi$$

Equation 5.21 may be written as,

$$w_i \sim \left(\frac{\rho_d - \rho_c}{\rho_d}\right)^{\frac{1}{2}} \left(\frac{\epsilon}{\rho_c}\right)^{\frac{1}{3}} a^{-\frac{2}{3}} \phi \quad (5.22)$$

The drop diameter 2a, may be substituted by eqn. 5.12,

$$w_i \sim \left(\frac{\rho_d - \rho_c}{\rho_d}\right)^{\frac{1}{2}} \frac{\epsilon^{3/5}}{\sigma^{2/5}} \cdot k_f^{3/5} \phi \quad (5.23)$$

This mechanism predicts that no coalescence occurs with equal diameter particles. Similarly, no coalescence is predicted if the dispersed and continuous phases have the same density, but in mixers, some collisions may occur by gradient coagulation.

Two other models predicting particle collision frequency have been proposed, (49, 118), but these are based on Smoluchowski's theory for random motion of particles with diameter $2a < \lambda_0$.

5.8 AFFECT OF INTERFACIAL PHENOMENA ON PARTICLE COALESCENCE RATES

Photographs obtained by Groothius and Zuiterweg (36) show that droplet pairs, although colliding, need not coalesce. Inertia of the continuous medium between the drops, a surface stabilising film, or a static charge on the drops may reduce drop coalescence rates, while interfacial tension gradients around the drops' surfaces may induce coalescence. As mass transfer proceeds, a reduction of surface tension increases the probability of coalescence on the approach of another drop, by reducing the drop stability and decreasing the buffer effect of the liquid between the drops. Conversely, if the surface tension increases with transfer of solute, the probability of drop coalescence decreases, see Fig. 5.2. Recent selective surveys of interfacial phenomena and their effects on liquid-liquid extraction are given in (1) and (25).

Descriptions of the curious behaviour of non-equilibrated liquids when brought together are given in (113, 120), while mathematical models based on roll-cells are developed by Sternling and Scriven, (120), and Ruckenstein and Berbente, (107), to predict these interfacial instabilities. The use of these models requires extensive physical data for the system. For example, one parameter is 'the concentration coefficient of interfacial tension' which, for the system used in this work, is zero, see Section 2.3. Ruckenstein and Berbente's model, (107), predicts that no interfacial

disturbances occur in the system isooctane/o-nitrophenol/ water, (continuous, extractant phase), and this was observed while measuring the interfacial tension of the system.

Fig. 5.2 Diagram showing that coalescence rates may be increased by interfacial tension gradients caused by solute transfer around a drop.

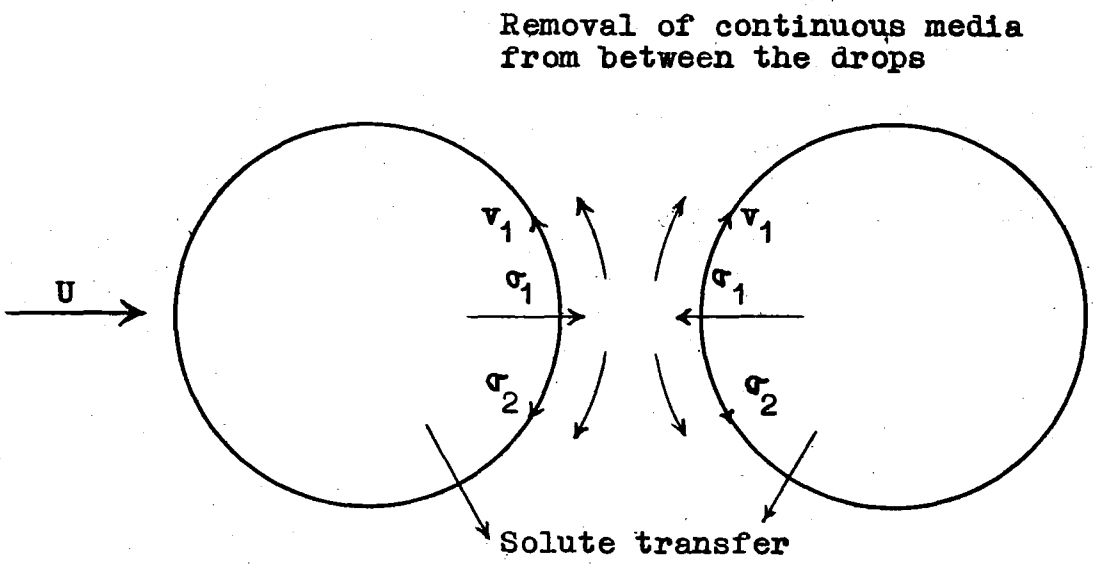

U = relative velocity of drops

v_1 = internal circulation velocity of drops

$\sigma_1 < \sigma_2$

5.9 EXPERIMENTAL MEASUREMENT OF PARTICLE SIZE

In each experimental run, approximately eight photographs of the dispersion leaving the mixer were taken, after the recorded o-nitrophenol concentration in the outlet aqueous phase had reached a steady value. Each photograph was projected on to a marked screen and the diameters of approximately 400 drops were measured. The experimental apparatus and operation are described in Section 2.4.

All but the largest drops (> 2.5 mm dia.) were observed to be circular. Any clearly defined smaller drop that was not circular was not counted, as consecutive photographs showed these drops to be attached to the glass surface. The criterion for measuring a drop was that a full diameter could be seen, although a portion of the drop might have been obscured.

The mean surface-volume particle diameter d_{sv}, was calculated for each dispersion from the definition,

$$d_{sv} = \frac{\Sigma nd^3}{\Sigma nd^2} \qquad (5.24)$$

d = mean diameter of the size increment.
n = normalised drop fraction in the increment.

A log. (diameter)-frequency plot for each run showed the particle sizes to have a log. normal distribution. Drop diameters greater than d_{98} tended to scatter and at low power inputs to the mixer, the smallest size increment occured over-frequently, making the graph slightly convex. The remaining points indicated a log. normal particle size distribution for each run, see Fig. 5.3. Thus, assuming a log. normal distribution of particle sizes, a second estimate of the mean surface volume diameter could be obtained.

$$\log d_{sv} = \log d_{50} + 5.757 \log^2 \sigma_g \qquad (5.25)$$

The counting of the number of drops in the smallest size increment was not accurate, because of blurring and overlapping

of the drop images. For the screen size of 3 mm., an accuracy of $\pm$ 20% could be expected, but the large number of particles counted for each run ($\sim$ 3000) and the incremental nature of the d_{sv} calculations would reduce the error of each d_{sv} estimate considerably.

Errors caused by inexact screen magnification, lens and film distortion, although present, are negligible compared with that caused by particle coalescence in the sampling line before the dispersion was photographed.

Experimental data are tabulated in Appendix 11. Correlations of the data are presented in Figs. 5.4 to 5.8.

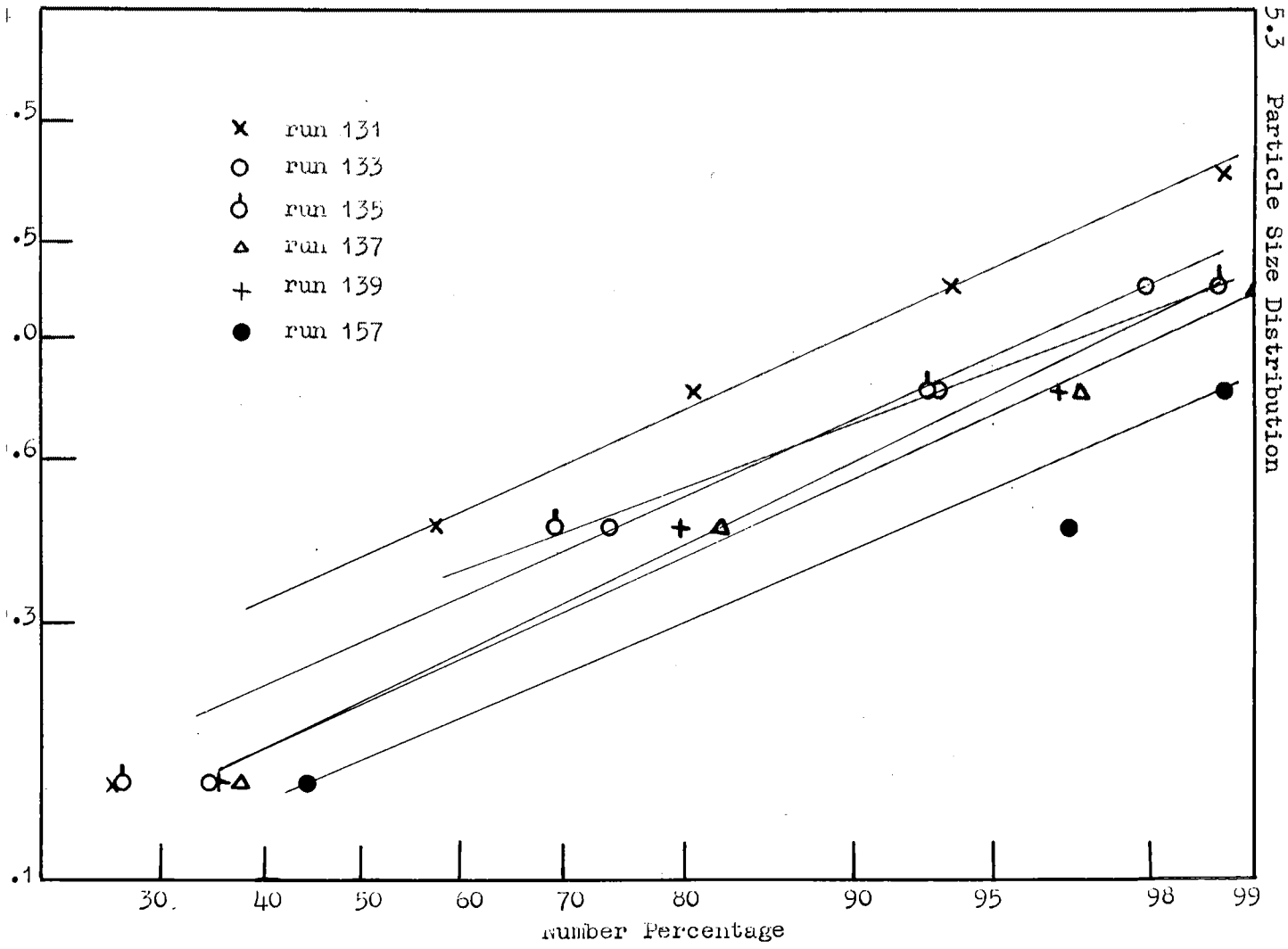

5.3 Particle Size Distribution

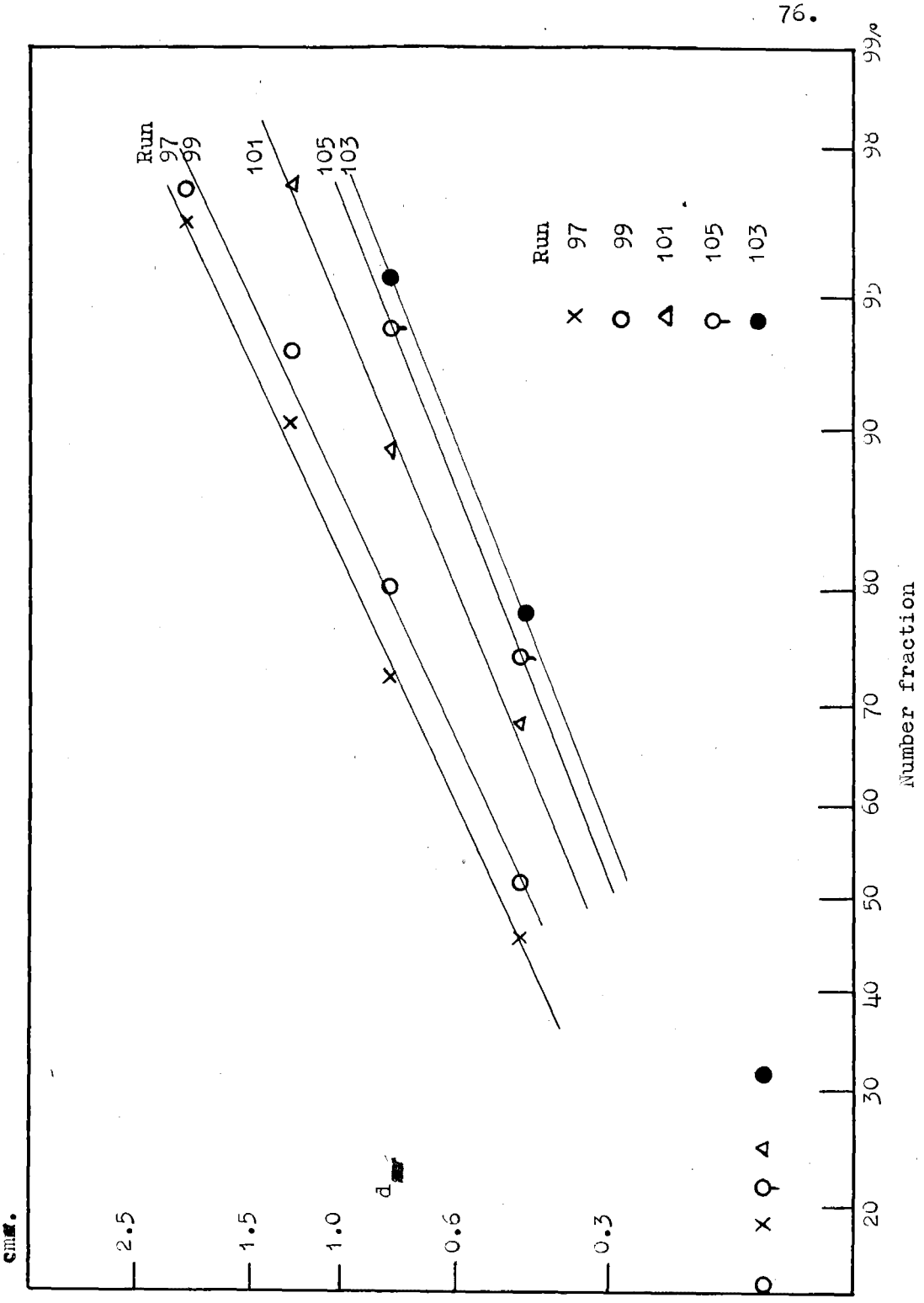

Fig. 5.3 Particle size distribution, Runs 97-105

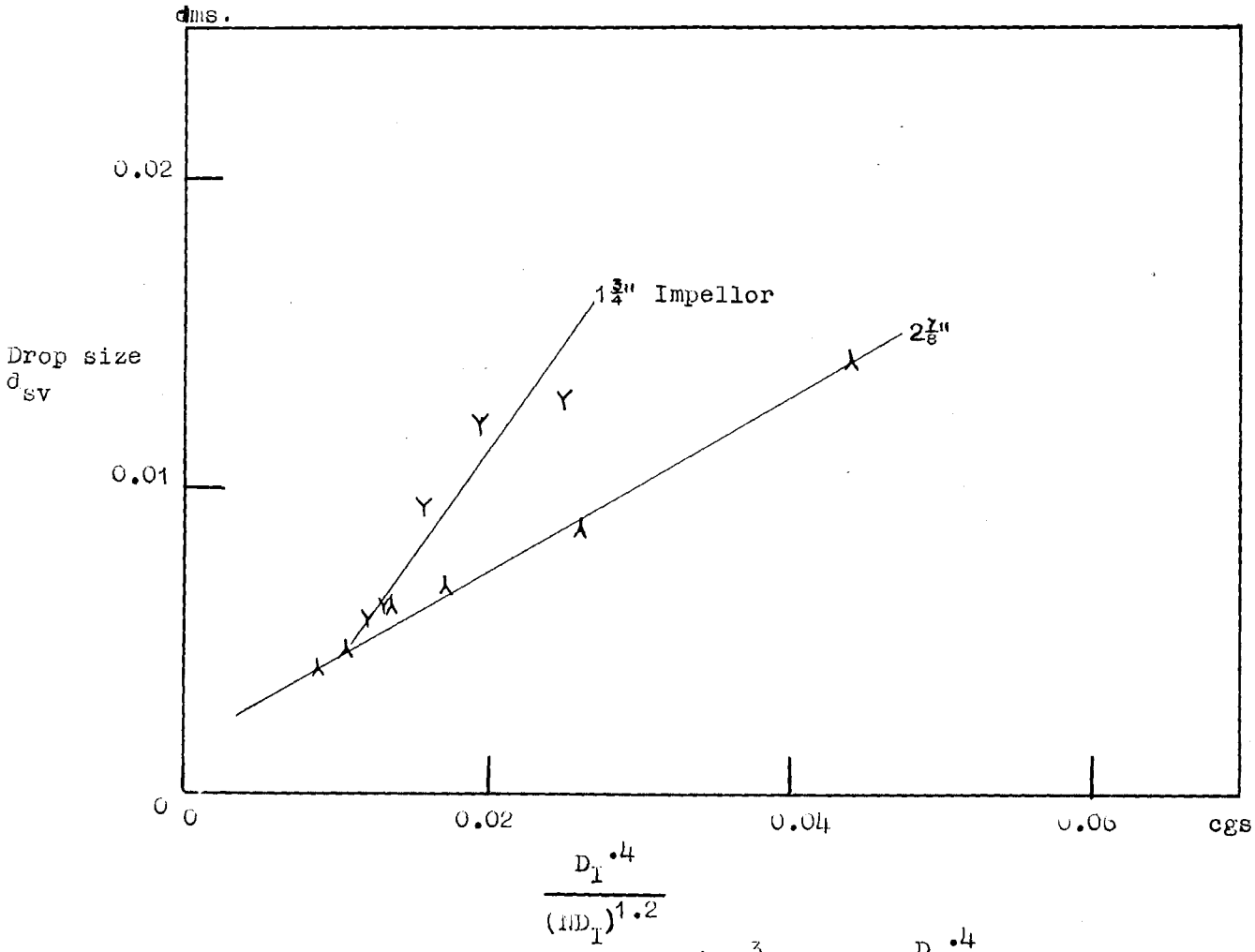

Fig. 5.41 Mean drop size $d_{sv} = \frac{\Sigma nd^3}{\Sigma nd^2}$ versus $\frac{D_I^{.4}}{(ND_I)^{1.2}}$ for the $5\frac{1}{2}$" vessel

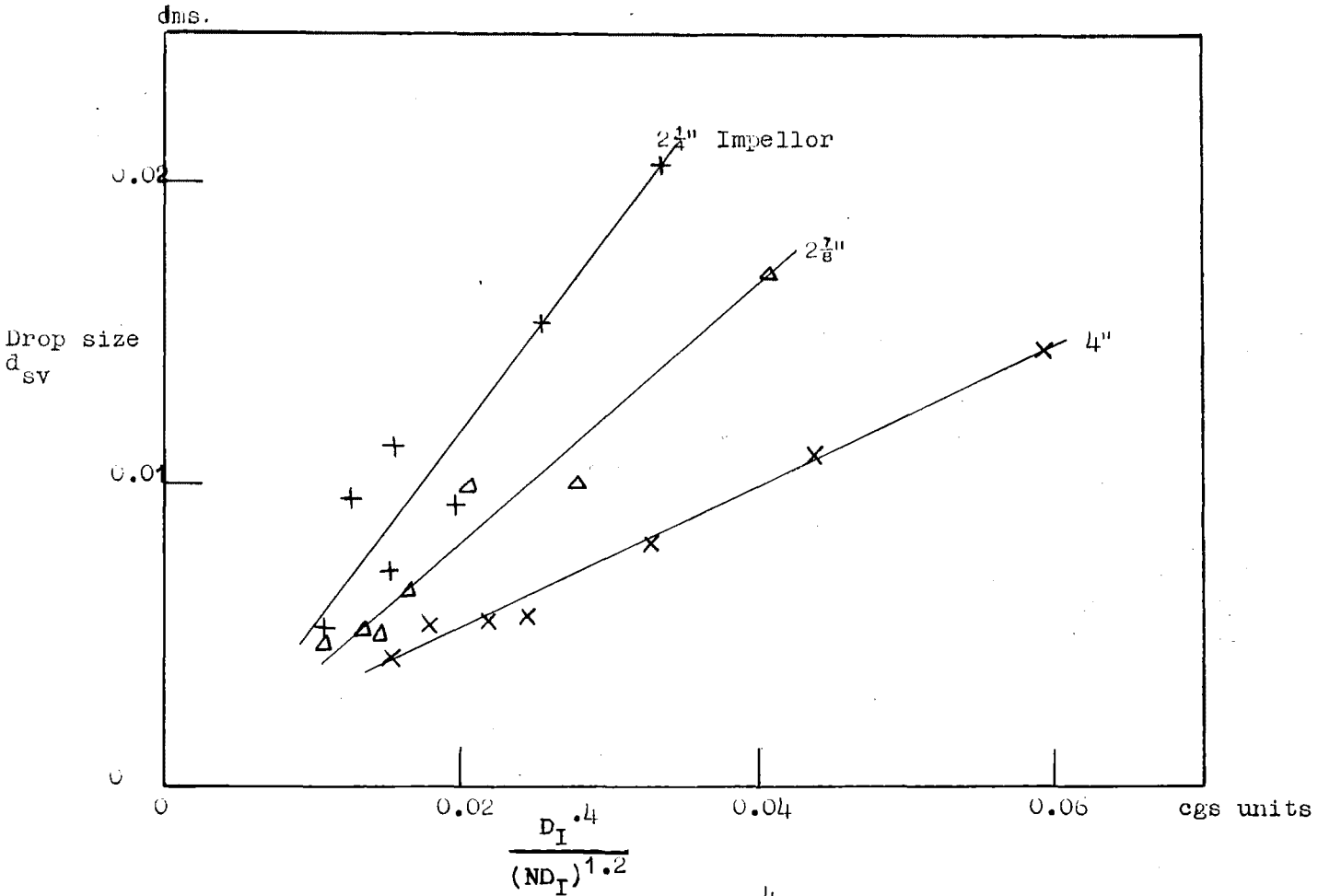

Fig. 5.42 Mean drop size $d_{sv} = \frac{\Sigma nd^3}{\Sigma nd^2}$ versus $\frac{D_I^{.4}}{(ND_I)^{1.2}}$ for the $7\frac{3}{4}$" vessel

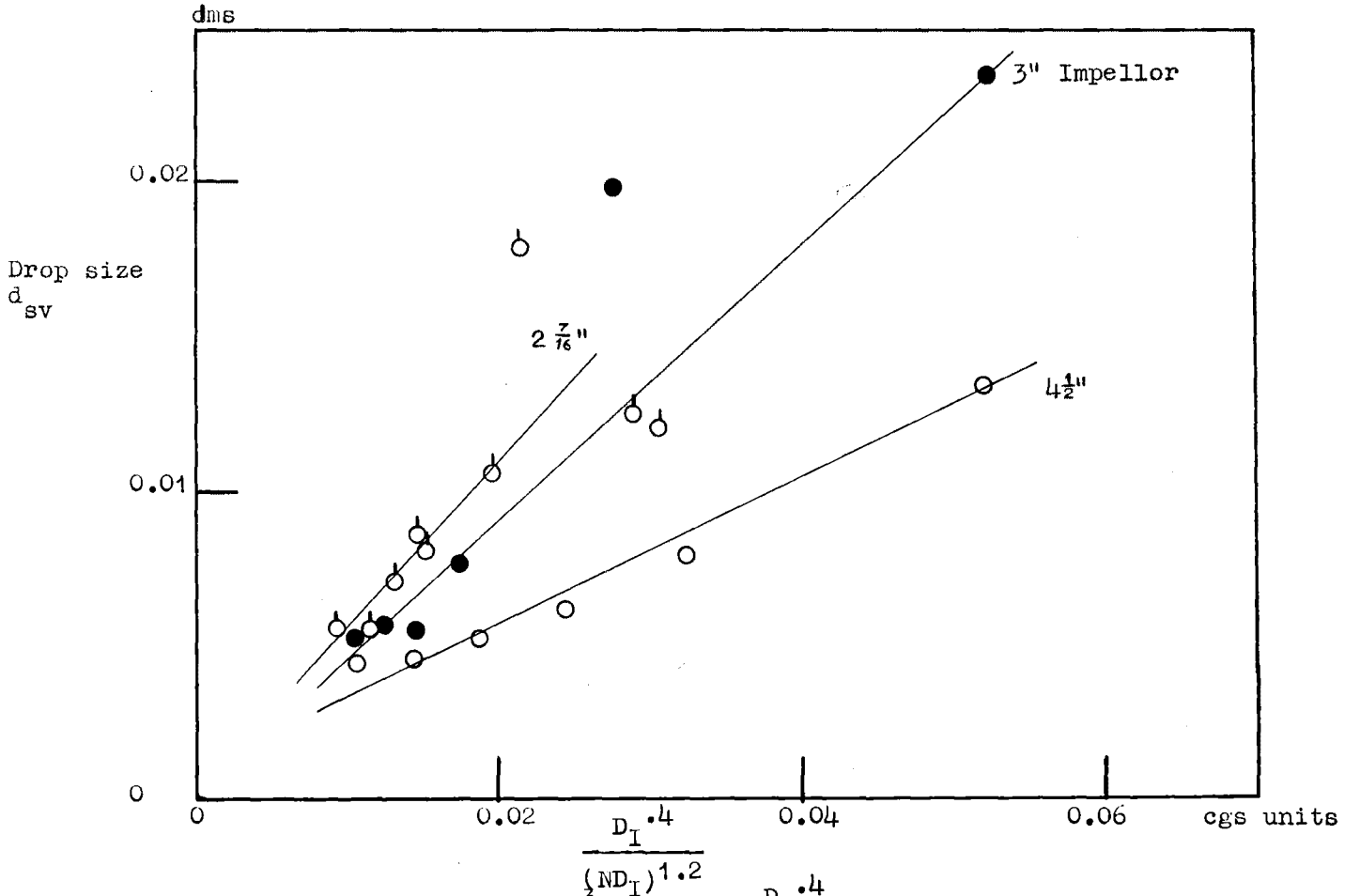

Fig. 5.43 Mean drop size $d_{sv} = \frac{\Sigma nd^3}{\Sigma nd^2}$ versus $\frac{D_I \cdot 4}{(ND_I)^{1.2}}$ for the $8\frac{3}{4}$" vessel

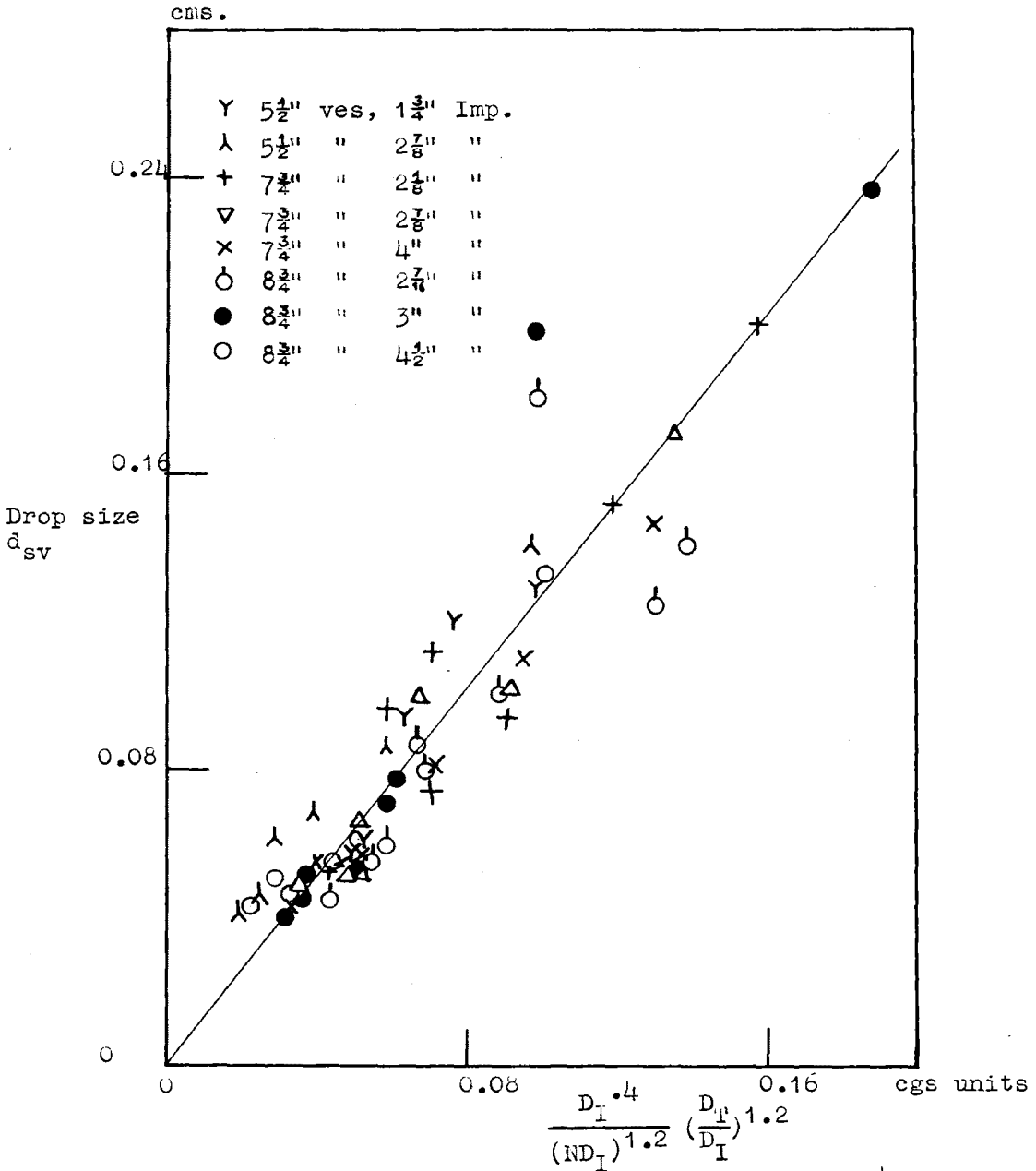

Fig. 5.5 Mean Drop diameter $d_{sv} = \frac{\Sigma nd^3}{\Sigma nd^2}$ versus $\frac{D_I^{.4}}{(ND_I)^{1.2}} \cdot \left(\frac{D_T}{D_I}\right)^{1.2}$,

Line of best fit.

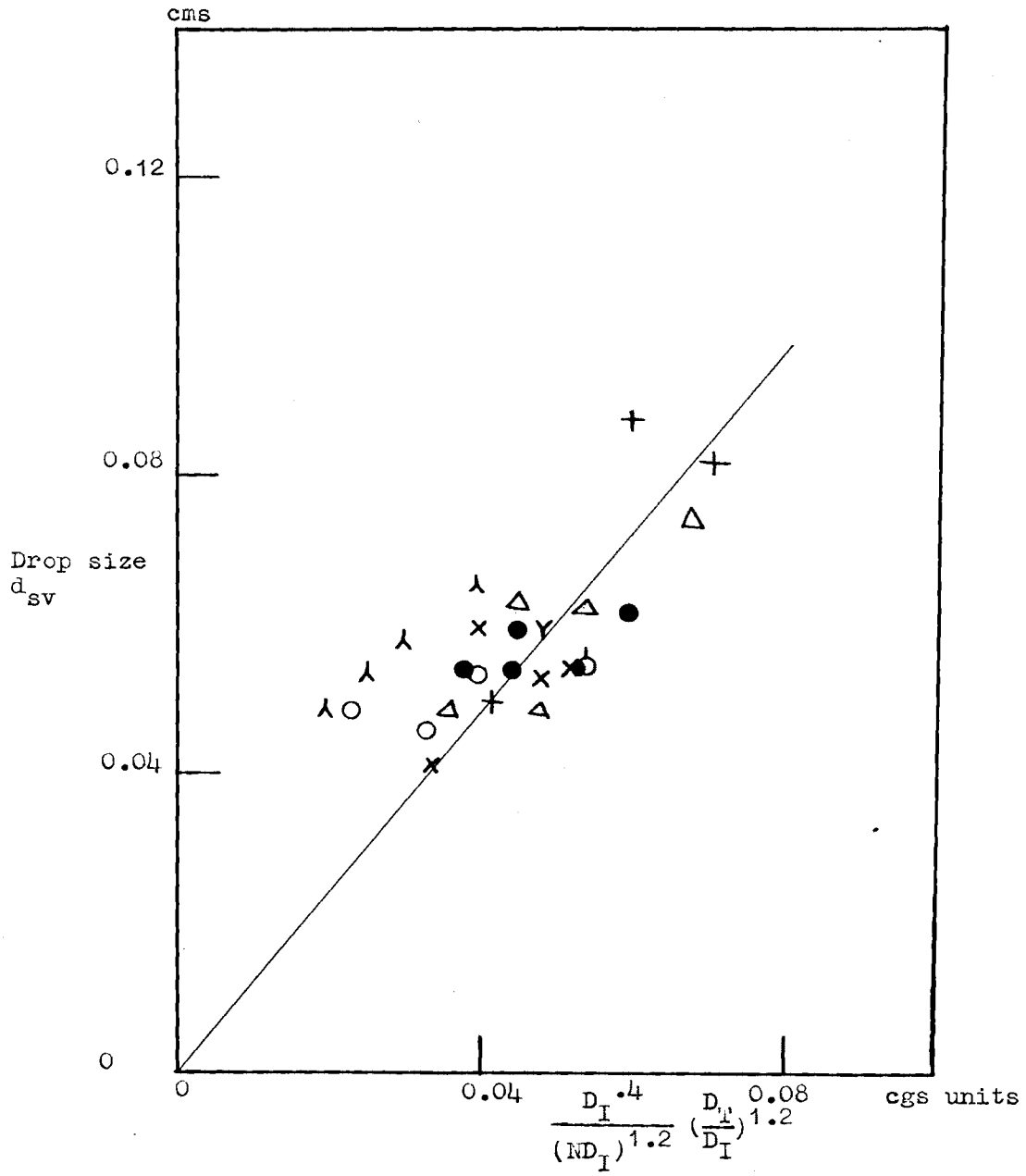

Fig. 5.6 Mean Drop diameter d_{sv}, obtained from a log normal relationship, versus $\frac{D_I^{.4}}{(ND_I)^{1.2}} \cdot (\frac{D_I}{D_I})^{1.2}$

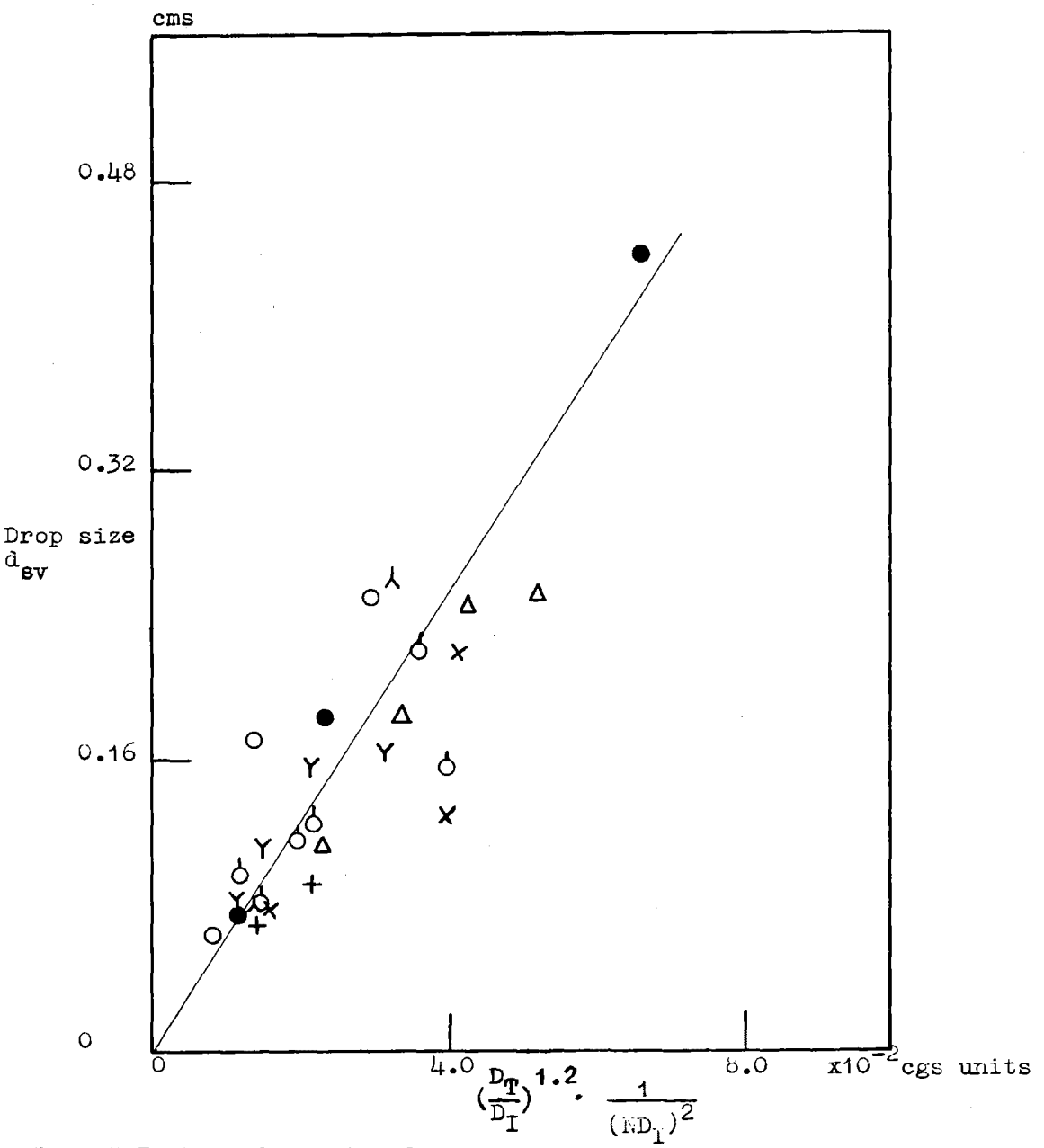

Fig. 5.7 Mean drop size d_{sv}, from the log-normal relationship, for low flow throughputs of the vessel versus $(\frac{D_T}{D_I})^{1.2}\frac{1}{(ND_I)^2}$

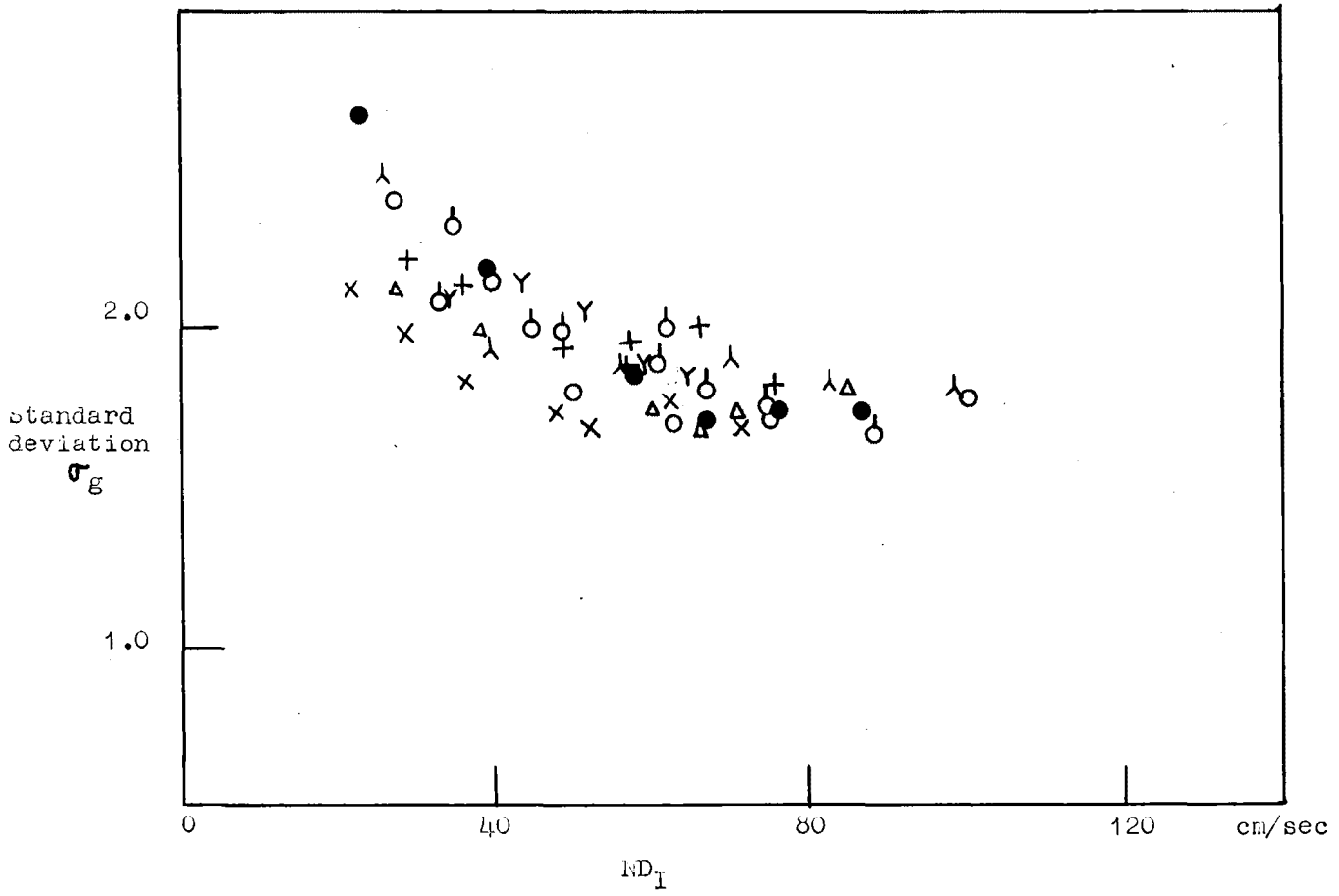

Fig. 5.8 Standard deviation of the droplet size distribution versus impellor tip speed.

5.10 DISCUSSION

If no particle coalescence occurred in the sample line before the dispersion was photographed, the particle size distribution obtained would be representative of that in the vessel. However, to obtain less blurred images of the finer dispersions, the sample line flow rate was momentarily stopped. Coalescence that occurred during this time, and the difficulty of analysing the photographs of the finer dispersions, as well as the error resulting from the analysis of the clearest portions of the photographs caused the nearly constant mean drop size which was obtained with the high mixer power inputs, see Fig. 5.5. The normalised drop frequency data, tabulated in Appendix 11, show the size distribution for each photograph in a run to be similar. Figs. 5.3, show the particle size distributions to be log. normal. These observations suggest that the dispersions had not partially coalesced before being photographed, but this conclusion is probably erroneous for the finer dispersions. The drop coalescence times at a plane interface for the system isooctane/water are extremely short, 0.5 to 5 secs., (51).

The two methods of calculating the surface volume diameter d_{sv}, (eqns. 5.24 and 5.25), from the data give similar estimates of d_{sv} for the higher inlet flow rates, Fig. 5.6, but show marked differences for the lower inlet flow rates, Figs. 5.5 and 5.7. The estimates of d_{sv} obtained by using the definition, $d_{sv} = \sum nd^3 / \sum nd^2$ are correlated by the turbulent fluctuation mechanism for particle fragmentation, eqn. 5.13, except that an additional term $(D_T/D_I)^{1.2}$ is necessary. This result is in agreement with the published correlations for d_{sv}, obtained by direct measurement of the dispersed phase interfacial area, using light scattering techniques. Vermeulen, Williams and Langlois, (132) approximately correlate their data by,

$$d_{sv} \sim \left(\frac{\sigma}{\rho_c}\right)^{3/5} \cdot \frac{(D_I)^{2/5}}{(ND_I)^{6/5}} \cdot \phi^{0.3}$$

in the dispersed phase volume range, ϕ = 0.2 to 0.4. Other workers (13, 52, 102, 116) correlate the mean surface-volume particle diameters in a mixing vessel by the turbulence fragmentation mechanism eqn. 5.13, but the additional terms $(D_T/D_I)^{1.2}$, ϕ^n and $(\mu_c/\mu_d)^m$ are necessary,

n = 0 to 0.6

m = 0 to 0.25

Alternatively, some of the published correlations (93, 101, 116), support the coalescence controlled relationship, eqn. 5.18. For example, Rodger, Trice and Rushton (101) correlate their data as,

$$A = \frac{\text{Const}}{D_I} \left(\frac{D_I^3 N \rho_c}{\sigma}\right)^{0.36} \left(\frac{D_I}{D_T}\right)^k \left(\frac{\nu_c}{\nu_d}\right)^{1/5} \left(\frac{\theta_d}{\theta_c}\right)^{1/6} \exp \left(\frac{3.6 \Delta p}{\rho_c} \phi\right)$$

where k = f(We) = 0.75 to 1.4.

When k = 1,

$$d_{sv} \sim \left(\frac{\sigma}{\rho_c}\right)^{0.36} \frac{D_I}{(ND_I)^{0.72}} \left(\frac{D_T}{D_I}\right) \left(\frac{\nu_d}{\nu_c}\right)^{1/5}$$

The parameters D_T/D_I, ϕ and μ_c/μ_d, which were not predicted by the fragmentation mechanisms, but are necessary to correlate the experimental data, arise from the particle break-up not being solely controlled by a single mechanism. The phase volume ratio term ϕ^m, correlates the coalescence that occurs between the region of particle break-up and the measuring probes. The viscous term $(\mu_c/\mu_d)^n$ denotes a drop resistance to deformation before fragmentation.

These two effects were not investigated in this work, but the scale length term $(D_T/D_I)^{1.2}$ is found in this and other works. Calderbank, (13), notes that the term ϵ, in eqn. 5.12 should be substituted by "power dissipated/vessel volume". which suggests that particle fragmentation occurs

$(D_T/D_I)^{1.2}$ in eqn. 5.13. In Section 4.5 of this work it is concluded that the term ϵ should be substituted by 'power dissipated/impellor volume' for a process controlled by high rates of energy dissipation. If this substitution is correct, the term $(D_T/D_I)^{1.2}$ may only be accounted for belatedly, as a correction for the liquid velocity gradient near the impellor region, where particle break-up was observed to occur.

The alternative method of calculating d_{sv} from the log. normal relationship eqn. 5.25, yields estimates of d_{sv} different to those obtained from eqn. 5.24, for the lower inlet flow velocities, ($\leqslant$ 0.75 M^3/hr., aqueous phase and $\leqslant$ 0.072 M^3/hr., isooctane phase), although the size distribution data appear to be log. normal. Fig. 5.7 shows data estimated by eqn. 5.25 to be correlated by $d_{sv} \sim (ND_I)^2 (D_T/D_I)^{1.2}$, which suggests that particle break-up for the lower inlet flow rates occurs by an internal circulation pressure mechanism, eqn. 5.8.

With the lower inlet flow rates, the large isooctane drops were observed to deform in their rise from the liquid inlet to the impellor zone, Figs. 2.12 and 5.9. These drops fragmented into numerous small droplets and several larger drops as postulated in the theoretical mechanism developed in Section 5.2. The larger drops formed were then further fragmented on recirculation through the impellor zone. The isooctane drops initially formed at the liquid inlet were spherical for the higher flow rates, and fragmented in the impellor region by the turbulence mechanism, eqn. 5.13.

A circulation break-up mechanism accounts for the high number of small particles found for the low mixer power inputs, but even if the drops were initially broken by this mechanism, the measured particle size for a mixer would indicate the secondary turbulent break-up of the particles. The circulation break-up correlation found, results from the log. normal estimate of d_{sv} at lower power inputs becoming increasingly inaccurate as the standard deviation of the particle size distribution increases, see Fig. 5.8. A maximum particle size which is stable in the turbulence and is entrained in

the flow exists in the vessel, but a log. normal size distribution requires even larger particles to exist in the vessel, and the inclusion of these particles leads to the erroneous estimate of d_{sv} obtained. As σ_g decreases, the number of large particles which are implied by a log. normal size distribution that are not present in the mixer decreases, causing the two estimates of d_{sv} from eqns. 5.24 and 5.25 to coincide, see Appendix 13.

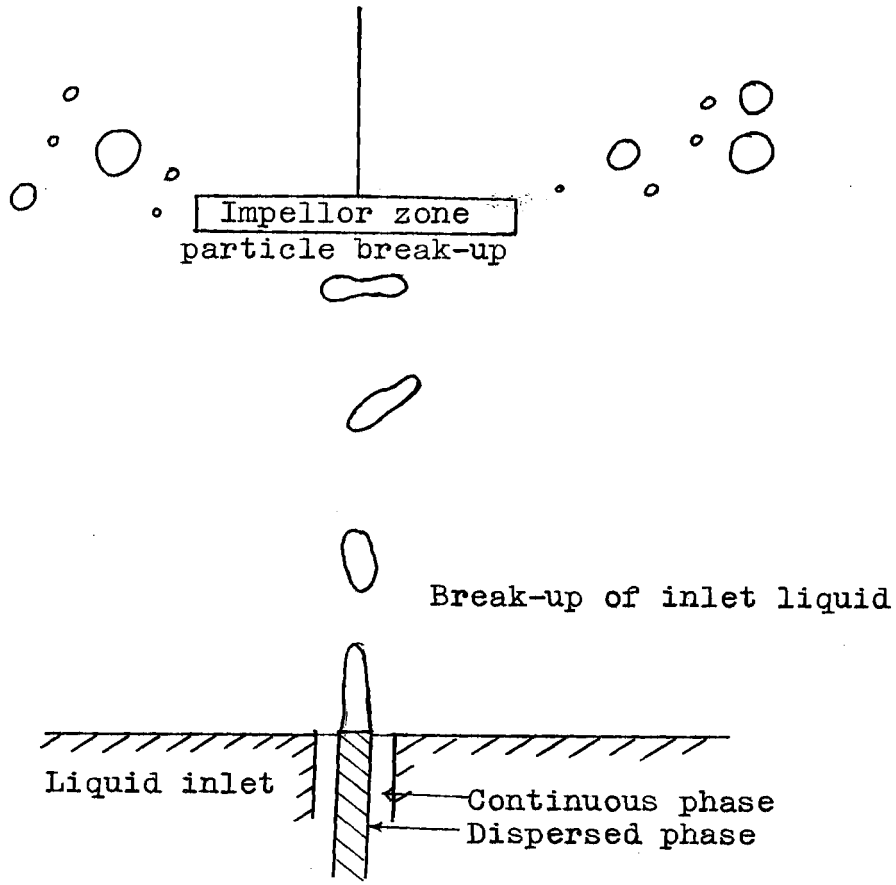

Fig. 5.10 Break-up of Inlet Liquid Stream

In fact, there are no data available to support an internal circulation pressure mechanism for particle fragmentation. However, inspection of Sleicher's data (117), which are interpreted as representing drop break-up being caused by shear forces near a wall, suggests that Sleicher's correlation,

$$\frac{a\rho_c u^2}{\sigma} = 19\sqrt{\frac{\sigma}{\mu_c u}}\left(1 + 0.7\left[\frac{\mu_d 2au}{\sigma}\right]^{0.7}\right)$$

may be reinterpreted in terms of an internal circulation break-up mechanism.

Particle size distribution data which have been obtained by photographic analysis of mixing vessel dispersions, as in this work, have been reported by other workers, (50, 81, 111). The skew size distribution favouring the larger particles in Setzer and Treybal's work, (111), suggests that coalescence occurred in the mixing vessel, but Huttig and Stadler's data, (50), and Nagata and Yamaguchi's, (81), show a log. normal particle size distribution for mixer dispersion. Limited coalescence between the larger and smaller particles, $> d_{85}$ and $< d_2$, and incomplete entrainment are suggested to occur in the batch vessel used by (50). A log. normal size distribution is obtained, as in this work, for the particle size range measured, $d_7 \lesssim d \lesssim d_{97}$,(81).

In the two works (50, 81) and in this thesis, the standard deviation of the particle size distribution σ_g decreases with the mean particle size, see Fig. 5.8. A qualitative explanation may be seen in Fig. 5.1, with the convergence of the coalescence and fragmentation limits at higher power inputs. For similar vessel geometries, but different liquid systems, σ_g's obtained in this work and Nagata's, (81) correspond.

The expedient of using theoretical predictions for the maximum or minimum particle size in a dispersion to correlate the mean particle size, is used in this work, as in all previous interfacial area correlations. A range of particle size standard deviations is found experimentally in this work, $2.6 > \sigma_g > 1.7$, see Fig. 5.8. Thus the assumption that $a_{max} \sim a_{min} \sim d_{sv}/2$ is only approximate. However, it becomes tenable for higher power inputs to the mixer.

Coalescence in the sample line has been discussed in this section; it was noted that the phases isooctane/water are fast coalescing in a non-agitated system. Within the vessel,

however, no drop coalescence was observed in the low dispersed phase volume fractions used, $0.02 < \phi < 0.1$. It appears to be customary to consider each phase as being 'fully mixed', particularly when estimating mass transfer driving forces, (131). The mixing rates of dispersed phases in a mixer have been measured, (37, 70, 74, 77). Matsuzawa and Migauchi, (74), report that no coalescence of ferric and stannous chloride solutions occurred, when dispersed in an organic phase. Other workers find that w_i = vol. dispersed phase coalesced/vol. dispersed phase present x min. is given by,

$$w_i \sim \epsilon^{0.5 \rightarrow 1.1} . \phi^{0.5 \rightarrow 1.1}$$

where w_i = 1 to 100 min^{-1}
for ϵ = 1 to 100 HP/1000 gals.

The theoretically obtained equation

$$w_i \sim \epsilon^{0.6} . \phi \qquad (5.23)$$

indicates the orders of the correlating terms. In the derivation of the coalescence model, it was found that large and small drops would coalesce most frequently in turbulent flow. For an air-water system, this has been observed experimentally, (97).

In any dispersion, the coalescence rate is sensitive to the system and the vessel geometry, but data given by Miller and co-workers, (77), for the system 64% isooctane and 36% carbon tetrachloride in water may be extrapolated to this work. With a volume ratio range of the dispersed phase of $0.02 \rightarrow 0.1$, the coalescence rate w_i, in a baffled turbine stirred vessel is calculated to be of the order $0.1 \rightarrow 1.0$ min^{-1}. In this work, the dispersed phase residence time ranged from $0.1 \rightarrow 0.5$ min., so little effective dispersed phase mixing is predicted to occur. For a pure isooctane phase, the coalescence rate would be even less, (77). This result, that little dispersed phase mixing occurs, is contrary to the fast coalescence noted for non-agitated systems, (51), but is

supported by the particle break-up mechanism found, and by observations of the dispersions in the mixing vessels.

5.11 CONCLUSION

The order of magnitude relationships may be developed from the theories of turbulence, assuming locally isotropic flow, to predict the maximum and minimum particle sizes that exist in a mixing vessel. If a single particle-size controlling mechanism occurs in the vessel, these relationships have been shown to describe the mean particle diameter in a dispersion.

The particle sizes determined in this work have been shown to be representative of those existing in the vessel, except for the finest dispersions, for which the photographic techniques used are unsuitable.

A log. normal distribution of particle sizes was found; except for the large diameter dispersions, where the effect of a maximum particle diameter that is stable in the vessel becomes significant. The standard deviation, σ_g, of the particle size distribution decreases slightly with decreasing particle size. This decrease in σ_g is predicted by the convergence of the maximum and minimum particle sizes that may exist in the higher energy dissipating flows.

The estimate of the surface volume diameter obtained, using the definition $d_{sv} = \sum nd^3 / \sum nd^2$, is considered to be more accurate than that obtained by using log. normal relationships because of the maximum size "cut-off" occurring in the size distribution. Estimates of d_{sv} obtained by the two methods converge at the higher energy dissipation rates.

In agreement with much of the published literature, the mean d_{sv} particle sizes obtained, are correlated by a turbulence fragmentation mechanism.

$$d_{sv} = 1.26 \cdot \frac{D_I^{2/5}}{(ND_I)^{6/5}} \cdot \left(\frac{D_T}{D_I}\right)^{6/5} \text{ cgs. units} \qquad (5.26)$$

However, it is suggested that an internal circulation mechanism controls the initial fragmentation of large drops, but this observation cannot be verified experimentally.

The additional parameters, hold-up ratio, ϕ , and

viscosity, μ_c/μ_d, necessary to correlate particle-size data of previous workers were not investigated in this work. The appearance of the parameter $(D_T/D_I)^{1.2}$ introduces a dichotomy in reasoning.

Fast coalescence is considered to occur in the system isooctane/water, when it is not agitated. In the mixing vessel conditions, the dispersed phase isooctane approached more closely a non-coalesced condition than the customarily assumed fully mixed condition. This conclusion is substantiated by the mass transfer results, see Section 7.11.

The fragmentation of liquid drops in a mixing vessel has been shown to be similar to other comminution processes, notably those of solids, in that a log. normal size distribution of the products is obtained. There would appear to be a universality in the probability of a particular size reduction ratio being formed, but liquid dispersions show the effect of a maximum particle-size that may exist in the environment.

Section 6

VOLUME FRACTION OF THE DISPERSED PHASE

6.1 ENTRAINMENT OF PARTICLES IN A TURBULENT FLUID

The second parameter necessary to calculate the interfacial area between two phases, eqn. 5.1, is the dispersed phase volume fraction, or 'hold-up',

$$A = \frac{6\,\phi}{d_{sv}} \qquad (5.1)$$

In a batch mixer, the hold-up is constant, and is given by the volume of the phases initially in the vessel,

$$\phi = \frac{\text{Volume dispersed phase}}{\text{Vol. dispersed phase + Vol. continuous phase}}$$

except when local changes in the uniformity of mixing are considered. For flow mixers, however, the hold-up is not given simply as,

$$\phi = \frac{\text{Volume flow rate dispersed phase}}{\text{Total vol. flow rate to the mixer}}$$

because different mean residence times for each phase in the vessel result from incomplete entrainment of the dispersed phase. The hold-up in a flow mixing vessel is usually correlated in terms of the hold-up ratio ϕ/ϕ_f, which is dependent on the system properties, the vessel design, and its operation.

$$\phi/\phi_f = \left(\frac{\text{Vol. dispersed phase in the vessel}}{\text{Total vol. of vessel}}\right) / \left(\frac{\text{Total inlet flow rate}}{\text{Dispersed phase inlet flow rate}}\right)$$

In most experimental work, the mixers have had overflow liquid outlets, see Fig. 2.4, and have been operated

with the lighter phase dispersed. Consequently, the hold-up ratio approaches unity, $\phi/\phi_f \leqslant 1.0$ only at higher power inputs, (131).

An equation predicting the maximum particle size entrained in a turbulent fluid, eqn. 5.18, has been presented, (58).

$$a_{max} = \text{const} \cdot \epsilon^2 \left(\frac{\rho_c}{\rho_c - \rho_d}\right) g_c^{-2} \cdot f(\phi) \qquad (5.18)$$

$f(\phi)$ = empirical hold-up ratio.

Since the derivation of eqn. 5.18 is in doubt, (116), a hold-up correlation based on the particle entrainment properties of the turbulence is developed. It is assumed that the liquid hold-up ratio is given by,

$$\phi/\phi_f \sim \frac{\text{Average flow velocity in the mixer}}{\text{Relative velocity between the particle and the fluid}}$$

To this approximation must be added the additional condition that the hold-up ratio is equal to one when the dispersed phase becomes fully entrained.

The maximum relative velocity between a particle and the fluid which was found by differentiating eqn. 3.30,

$$v \sim ((\rho_d - \rho_c)V)^{\frac{1}{2}} \frac{(\epsilon\lambda)^{\frac{1}{3}}}{\rho_c^{\frac{1}{3}}(\rho_c V + k_f \rho_c S\lambda)^{\frac{1}{2}}} \qquad (3.30)$$

occurs with turbulence of the same eddy length as the particle diameter. In entrainment, when the large scale and mean velocity flows retain the drops within the mixer, the small scale turbulence is not important. Thus, the relative magnitudes of the two terms, $\rho_c V$ and $k_f \rho_c S\lambda$ in eqn. 3.30, become important. For Stokes flow of the fluid, $Re_\lambda < 1.0$, $k_f \rho_c S\lambda$ is greater than $\rho_c V$, for $\lambda_1 \sim D_I$ and $k_f = 24/Re_\lambda$. In the constant drag region, $Re_\lambda > 700$, $\rho_c V$ is greater than $k_f \rho_c S\lambda$, where $\lambda_1 \sim D_I$. A numerical solution could also be obtained for the transition region, where the two terms are of the same magnitude.

In the Stokes flow region eqn. 3.30 may be written,

$$v \sim ((\rho_d - \rho_c)V)^{\frac{1}{2}} \frac{(\epsilon\lambda)^{\frac{1}{3}}}{\rho_c^{\frac{1}{3}}(k_f \rho_c S\lambda)^{\frac{1}{2}}} \qquad (6.1)$$

The drag coefficient k_f may be substituted by,

$$k_f \sim \frac{1}{Re_\lambda}$$

and the eddy wave-length λ, for the large scale flow, may be written as,

$$\lambda \sim D_I$$

$$v \sim (\frac{\Delta\rho}{\rho_c})^{\frac{1}{2}} \cdot (\frac{V}{S})^{\frac{1}{2}} \cdot \frac{(\epsilon D_I)^{\frac{1}{3}}}{\rho_c^{\frac{1}{3}} D_I^{\frac{1}{2}}} \cdot (\frac{v \cdot 2a}{\nu_c})^{\frac{1}{2}}$$

$$\text{or} \quad v \sim \frac{\Delta\rho}{\rho_c} \cdot \frac{a^2 \epsilon^{\frac{2}{3}}}{\rho_c^{\frac{2}{3}} \nu_c D_I^{\frac{1}{3}}} \qquad (6.2)$$

a, may be substituted by eqn. 5.26, to give,

$$v \sim \frac{\Delta\rho}{\rho_c^{5/3}} \cdot (\frac{\sigma}{k_f' \rho_c})^{6/5} \cdot \frac{\epsilon^{-.13}}{D_I^{1/3} \nu_c}$$

The drag coefficient k_f' is related to the particle break-up, and is not substituted by the Stokes relationship. k_f' is the particle drag coefficient with respect to the inertial subrange turbulence, and as such is in the constant drag coefficient region.

The relative velocity V is obtained by substituting eqn. 3.7, for ϵ,

$$v \sim \frac{\Delta\rho}{\rho_c^2} \cdot \frac{\sigma^{6/5}}{\mu_c} \cdot \frac{1}{(ND_I)^{.39} D_I^{.2}}$$

The hold-up ratio ϕ/ϕ_f is given by,

$$\phi/\phi_f \sim \frac{ND_I}{v} \sim \frac{\rho_c^2}{\Delta\rho} \cdot \frac{\mu_c}{\sigma^{6/5}} \cdot N^{1.4} D_I^{1.6} \qquad (6.3)$$

In eqn. 3.30, when $\rho_c V \gg k_f \rho_c S \lambda$, the particle drag coefficient k_f will approach a minimum value, or be in the constant drag coefficient region, $700 < Re_\lambda < 10^5$. This suggests that the particles are fully entrained by the large scale flow, as entrainment by the inertial subrange turbulence is occurring. For this extreme case eqn. 3.30, may be written,

$$v \sim ((\rho_c - \rho_d) V)^{\frac{1}{2}} \cdot \frac{(\epsilon\lambda)^{\frac{1}{3}}}{\rho_c^{\frac{1}{3}} (\rho_c V)^{\frac{1}{2}}} \qquad (6.4)$$

With the substitutions $\lambda_1 \sim D_I$, and $\epsilon \sim \rho_c (\Delta u)^3 / D_I$ eqn. 6.4 becomes,

$$v \sim \left(\frac{\rho_c - \rho_d}{\rho_c}\right)^{\frac{1}{2}} \cdot \Delta u$$

The hold-up ratio may be determined as,

$$\phi/\phi_f \sim \frac{ND_I}{v} \sim \left(\frac{\rho_c}{\rho_c - \rho_d}\right)^{\frac{1}{2}} \qquad (6.5)$$

With complete entrainment, the hold-up ratio becomes one. The numerical value of the constant obtained for any system $(\rho_c/(\rho_c - \rho_d))^{\frac{1}{2}}$, has little significance, except to show that complete entrainment may be more easily obtained with systems having a small density difference between the two phases.

This analysis does not evaluate the hold-up 'end correction' for a non-agitated vessel, but for the system and vessels used in this work, this correction is small compared with the measurement errors.

6.2 EXPERIMENTAL MEASUREMENTS OF DISPERSED PHASE VOLUME FRACTION

The volume of the dispersed phase in a mixer was measured at the end of each run. The two inlet flows were stopped simultaneously, and the agitator was turned off. The two phases were allowed to settle, and the dispersed phase height in the vessel was measured by comparison with a scale held outside the vessel.

These measurements were found to be inaccurate, and apparatus modifications were made after the mass transfer runs to eliminate the sources of error. The flow control valve for the dispersed phase was moved from below the rotameter to immediately below the mixing vessel, and the two overhead sample lines were blanked off. The volume of isooctane that was still displaced from the short inlet line, after the isooctane flow stopped, was measured experimentally and found to be constant.

The repeated runs were for the same conditions as the mass transfer runs, but only the impellor torque and speed, and the dispersed phase hold-up were measured. A complete description of the apparatus and its operation is given in Section 2.4. The measurement error noted gives a 20% error for the lowest hold-up measured, and 9% error for the highest hold-up.

The experimental data are tabulated in Appendix 12, and are presented in Figs. 6.1 and 6.2.

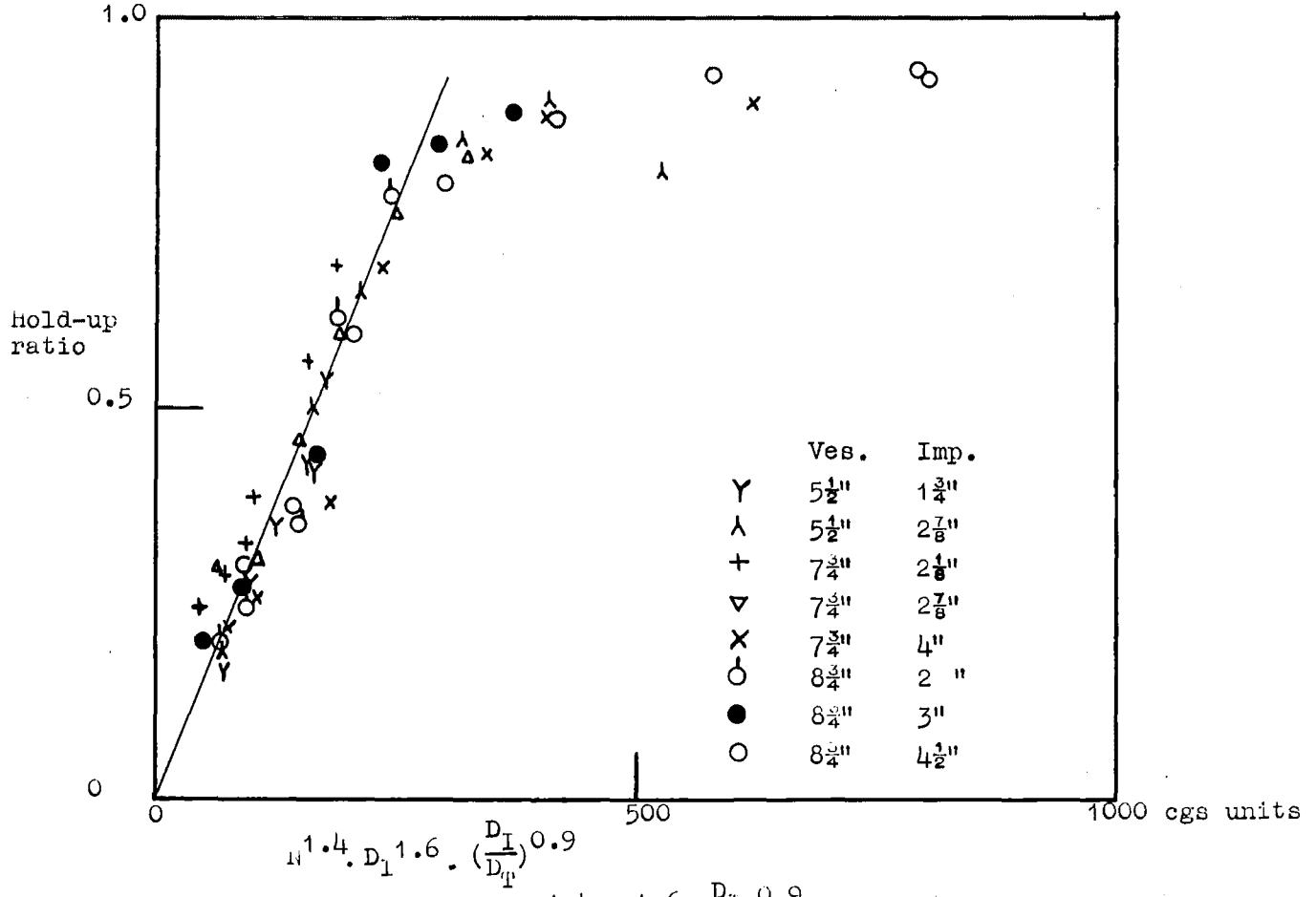

Fig. 6.1 Hold-up ratio vs $N^{1.4} \cdot D_I^{1.6} \cdot (\frac{D_I}{D_T})^{0.9}$. Line of best data correlation for low power inputs to the mixing vessel.

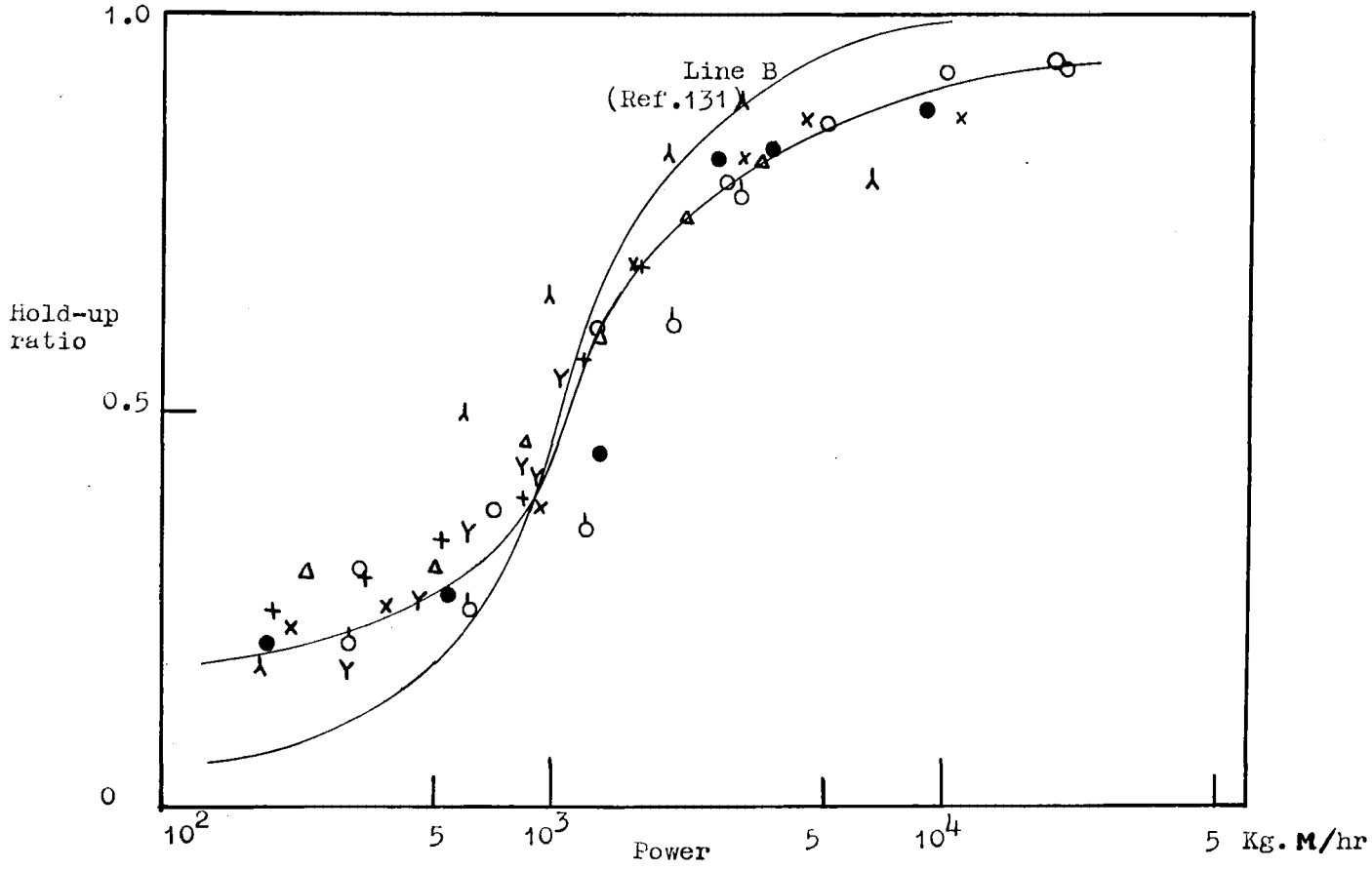

Fig. 6.2 Hold-up versus Power Graph. Line B, Data line from ref. 131.

6.3 DISCUSSION

The dispersed phase volume fractions in the mass transfer runs were determined from the graphed results of the repeated hold-up measurements. In these runs the two phases were recycled to eliminate isooctane loss by entrainment in the non-recycled aqueous phase, which occurred during the mass transfer runs. Consequently, in the repeated experiments, the o-nitrophenol concentrations in the two phases were in equilibrium, with a concentration of 3×10^{-5} gm. ONP/gm. H_2O in the aqueous phase. The interfacial tension of this system is 50.2 dynes/cm., while it was 50.4 dynes/cm. in the mass transfer runs, see Appendix 9. This decrease, and the changes of the other phase properties, density, and viscosity, are considered negligible.

The graphs of hold-up versus power input, Fig. 6.2, are similar to those already published, (78, 130). Treybal, (131), notes that the impellor speed at which the initial rise in hold-up occurs is given by Nagata and co-workers' correlation, (84). This equation was originally obtained as the impellor speed at which two phases became fully mixed in an unbaffled vessel. A similar correlation for baffled vessels, (92), is more satisfactory in correlating the 'rise point' impellor speed in this work, contrary to Treybal's observation that it 'seems unrealistically low'.

$$\text{At rise point } Re_{Imp} = 2.85 \left(\frac{D_T^3 \rho_c g}{\mu_c^2}\right)^{0.3} \left(\frac{Re_{Imp}^2}{We}\right)^{0.15} \left(\frac{\mu_d}{\mu_c}\right)^{0.04} \left(\frac{\Delta\rho}{\rho_c}\right)^{0.08} \left(\frac{D_I}{D_T}\right)^{0.92} \quad \text{Ref. (92)}$$

The two asymptotic hold-up relationships derived in Section 6.1, eqns. 6.3 and 6.5, are found to correlate the data, see Fig. 6.1, although a wide scatter is apparent. This scatter does not entirely lie within the error limits of the techniques used. The correlating equation found is,

$$\text{Hold-up ratio, } \phi/\phi_f = 0.003\, N^{1.4}\, D_I^{1.6} \left(\frac{D_I}{D_T}\right)^{0.9} \qquad (6.6)$$

for low mixing vessel power inputs. c.g.s. units

$$\phi/\phi_f \rightarrow 1.0 \qquad (6.7)$$

for high mixing vessel power inputs.

The parameter $(D_T/D_I)^{0.9}$, necessary to correlate the experimental data is not predicted in the derivation of eqn. 6.3. The same scale ratio, to the power of 1.2, $(D_T/D_I)^{1.2}$, occurred unpredicted in the particle diameter correlation, see Section 5.10. The appearance of $(D_I/D_T)^{1.2}$ is related to the dimensionless scale term, D_T/D_I, being necessary in the dimensional expressions for the energy dissipation rate ϵ, but this is neither predicted, nor found experimentally in this work, see Section 4.4.

A numerical solution to eqn. 3.30, could be fitted to the data in the transition region, but such a solution would not constitute an improved theoretical approach.

The system parameters predicted in eqn. 6.3,

$$\phi/\phi_f \sim \frac{\rho_c^2}{\Delta\rho} \cdot \frac{\rho_c}{\sigma^{6/5}}$$

qualitatively correlate the hold-up ratios for different systems, obtained with low power inputs in the same mixer, (131). However, insufficient data are given to check this result numerically. Equation 6.6 may be written, in c.g.s. units as,

$$\text{Hold-up ratio} \quad \phi/\phi_f = 3.0 \frac{\rho_c^2}{\Delta\rho} \cdot \frac{\mu_c}{\sigma^{6/5}} \cdot N^{1.4} D_I^{1.6} \left(\frac{D_I}{D_T}\right)^{0.9} \qquad (6.8)$$

6.4 CONCLUSION

Complete entrainment of the dispersed phase in the turbulent flow occurs only for $Re_{Imp} > 10^5$. The hold-up ratios for lower Reynolds numbers are predicted by turbulence theory by determining the relative velocity between a particle and the turbulent fluid.

The initial rise in hold-up, shown in the graphs of hold-up versus power, is correlated by Pavlushenko's equation (92), rather than Nagata's (84), but little further information is obtained from this approach.

A semi-empirical expression derived from the particle slip velocity in turbulent flow is found to describe the dispersed phase hold-up, in the low power dissipation range,

$$\phi/\phi_f = 3.0 \frac{\rho_c^2}{\Delta\rho} \frac{\mu_c}{\sigma^{6/5}} N^{1.4} D_I^{1.6} \left(\frac{D_I}{D_T}\right)^{0.9} \qquad (6.8)$$

A constant hold-up region is predicted and found experimentally for high mixer power inputs.

$$\phi/\phi_f \longrightarrow 1.0 \qquad (6.7)$$

With incomplete entrainment, the larger particles tend to by-pass the mixing vessel, and contribute little to transfer processes. The extent of this by-passing is shown by the interfacial area variations, in the different mixing vessel regions, (111).

A Stokes drag force relationship for the particles is substituted in the derivation of eqn. 6.3. However, much higher particle Reynolds numbers occur with the inertial subrange turbulence, see Section 3.6. It is thus likely that transfer processes with freely circulating particles in a mixer are controlled by the inertial subrange turbulence, and not by the bulk flow conditions.

Section 7

MASS TRANSFER

7.1 MASS TRANSFER PROCESSES IN THE CONTINUOUS PHASE

Transfer processes with solid particles held in a fluid with a known velocity distribution have been predicted and measured with, as recent review articles show, substantial agreement, (55, 104). These articles concur with the concept that the boundary layer around a solid particle changes with an increase in the mean velocity and the turbulent fluctuations of the external fluid. A similar review article, (39), shows that experimental measurements of transfer processes with fluid interfaces may be correlated either by a selected surface renewal, or by a boundary layer mechanism.

In mixers, where a large number of drops occur, the effects of fluid turbulence, drop interference, and fragmentation may modify these single particle correlations. Although these effects have been observed, little theoretical extension of single particle equations to multiple drops has been achieved. As a result, transfer processes in mixing vessels have been related to overall vessel parameters, (129). Recently, data have been correlated in terms of dimensionless groups, relating the overall mass transfer to the vessel and system properties. This semi-empirical approach has yielded vastly different transfer correlations, as shown by two examples given below.

$$Sh_T = 0.02\ Re_{Imp}^{0.833}\ Sc^{0.5} \qquad \text{Ref. (3)}$$

$$\frac{k_c \phi_s D_T}{\pi \mathcal{D}} = 3.6\times10^{12}\ Re_{Imp}^{p}\ Sc^{q}\ \left(\frac{\mathcal{D}}{D_T^3 g}\right)^{0.627}\left(\frac{D_p}{D_T}\right)^{3.08}\left(\frac{\Delta\rho}{\rho_c}\right)^{2.82} \qquad \text{Ref. (82)}$$

$$p = 0.0802 \left(\frac{\mathcal{D}^3 g \rho_c^2}{\mu_c^2}\right)^{0.077} \cdot \left(\log\left(\frac{\Delta\rho}{\rho_c}\right) + 0.043\right) - 10^{(-10.5 \cdot D_p/D_T)}$$

$$q = 14.4 \cdot \frac{D_P}{D_T} + 1.84 \left(\frac{\Delta\rho}{\rho_c}\right)^{0.116}$$

$$\phi_s = \frac{A}{D_P^2} = \pi, \quad \text{for a sphere.}$$

The effects of mixer parameters and solution properties are shown in surveys of the rates of dissolution of solids in mixers, (24, 40, 73). Few data for liquid extraction processes controlled by the continuous phase transfer resistance in a mixing vessel have been published. The added effect of interfacial phenomena, which often results from mass transfer across an interface, (25), tends to diversify such data beyond the scatter obtained in the dissolution of solids. A more realistic approach is to derive mass transfer relationships, applicable for the transfer controlling mechanism existing in the mixer.

The prediction of continuous phase mass transfer rates may involve either boundary layer theories, or surface renewal models. Both these methods consider the total material transfer resistance to be within a region close to the interface. Within this region molecular diffusion occurs through a thin laminar layer next to the interface. Dissimilarity between the two methods arises from the boundary layer theories averaging the time dependent diffusivity term, while the surface renewal models average the mass transfer rate. Otherwise the two methods are similar.

The boundary layer approach is developed in this thesis, because the derived surface renewal relationships depend on parameters which at present are indeterminate. The surface renewal correlations analogous to the derived boundary layer equations are noted.

7.2 LAMINAR BOUNDARY LAYERS

Mass transfer correlations derived by considering laminar boundary layers are discussed in a paper presented by Dr R.B. Keey and the author of this thesis, see Appendix 1.

7.3 TURBULENT BOUNDARY LAYERS

The fluid region next to a surface is divided into the zones summarised in Table 3. The solute diffusion rate is derived from the viscous decay mechanism for each zone.

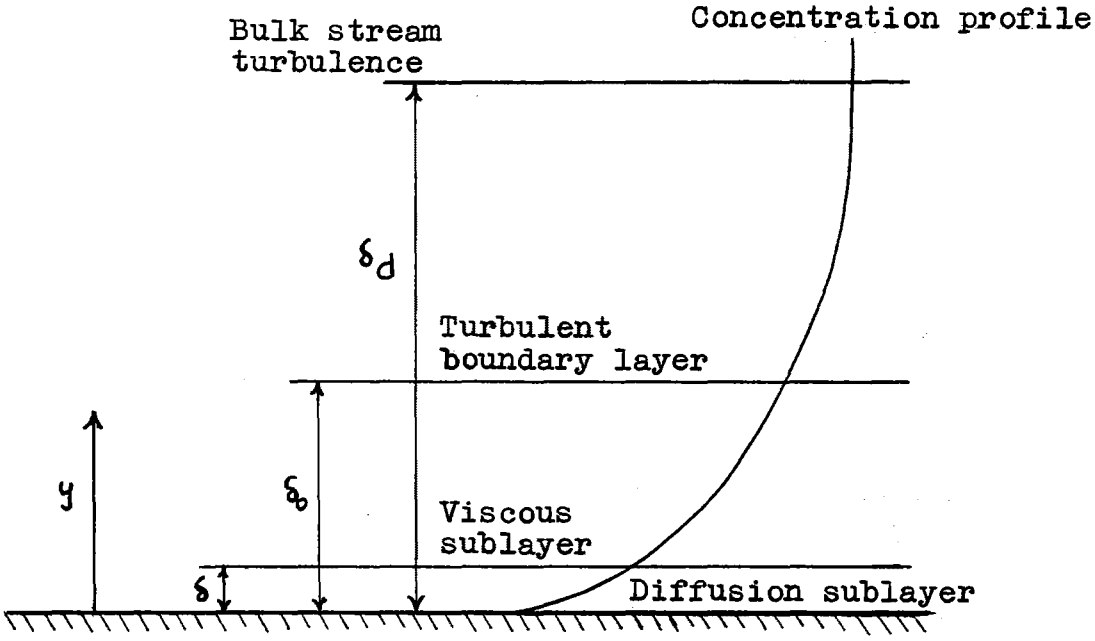

Hydrodynamic and Mass Transfer Boundary Layers

Diffusion Sublayer, $0 < y < \delta$.

The diffusion sublayer is defined as the region in which the molecular diffusion exceeds the eddy diffusion. In some derivations, (55, 67), the eddy and molecular

diffusivities are added,

$$\mathcal{D} = (\mathcal{D}_{mol} + \mathcal{D}_{turb})$$

but considerable mathematical difficulties are caused, with little improvement in the transfer mechanism. Therefore,

$$J = - \mathcal{D}_{mol} \frac{\partial c}{\partial y} \qquad (7.1)$$

is used.

Viscous Sublayer, $\quad \delta < y < \delta_o$

The diffusion rate for this region of the viscous sublayer is given by the eddy diffusivity, as this exceeds the molecular diffusivity. The viscous damping relation used, $\nu_{turb} \sim \nu(y/\delta_o)^4$, yields,

$$J = - \gamma v_o \frac{\delta^4}{\delta_o^3} \cdot \frac{\partial c}{\partial y} \qquad (7.2)$$

γ = constant of order unity

Turbulent Boundary Layer, $\quad \delta_o < y < \delta_d$.

Von Karmen's viscous damping relationship $l(y) \sim y$ is used, from which $\mathcal{D}_{turb} \sim y^2 \partial c/\partial y$

$$J = - \beta v_o y \frac{\partial c}{\partial y} \qquad (7.3)$$

β = constant.

Bulk Liquid, $\quad \delta_d < y$.

It is postulated that the concentration in the bulk liquid is constant, for Sc $\gg$ 1, due to turbulent mixing.

The concentrations, c_d at y = d, c_{δ_o} at $y = \delta_o$, c_δ at $y = \delta$, and c_o at y = 0, are substituted at their respective boundaries. For constant mass flux through each zone, eqns. 7.1, 7.2 and 7.3 yield,

$$J = \frac{(c_d - c_o)}{- \frac{\mathcal{D}}{\beta v_o} \ln \delta_o/d + \frac{\delta_o^3}{3 v_o \gamma}\left(\frac{1}{\delta^3} - \frac{1}{\delta_o^3}\right) + \delta} \qquad (7.4)$$

At $y = \delta$, eqn. 7.2 may be written,

$$\mathcal{D}_{mol} = \mathcal{D}_{turb} = \gamma v_o \cdot \frac{\delta^4}{\delta_o^3} \qquad (7.5)$$

Equation 3.21, $\delta_o = b\,\nu/v_o$ may be substituted in eqn. 7.5 to give,

$$\delta = \left(\frac{\mathcal{D}\,\delta_o^3}{\gamma v_o}\right)^{\frac{1}{4}} \sim \frac{\delta_o}{Sc^{\frac{1}{4}} \cdot \sqrt[4]{10\gamma}} \sim \frac{10^{\frac{3}{4}} \cdot \nu}{Sc^{\frac{1}{4}} \cdot \gamma^{\frac{1}{4}} \cdot v_o} \qquad (7.6)$$

Substitution of eqn. 7.6 in eqn. 7.4 yields,

$$J = \frac{(c_d - c_o)}{\delta\left(1 + \frac{1}{30.\gamma.Sc}\left(10.\gamma.Sc - \sqrt[4]{10\gamma\,Sc}\right) - \frac{\delta_o}{10\,\beta Sc\,\delta}\ln\frac{\delta_o}{d}\right)} \qquad (7.7)$$

The coefficients β and γ, have been shown to be of order unity, (63). For $Sc \gg I$, eqn. 7.7 may be approximated by,

$$J = \frac{\mathcal{D}(c_d - c_o)}{4/3\,\delta} \sim \frac{v_o(c_d - c_o)}{\alpha\, Sc^{3/4}}$$

$$\alpha = \frac{4}{3} \cdot 10^{3/4}\, \gamma^{-1/4}$$

Equation 3.24, relating v_o and U may be substituted to give finally,

$$k_c \sim \sqrt{k_f} \cdot U \cdot Sc^{-3/4} \qquad (7.8)$$

For the particle Reynolds number range, $700 < Re_\lambda < 10^5$ the total drag force coefficient is nearly constant at 0.5.

An alternative viscous damping relationship for the viscous sublayer, used by Lin, Moulton and Putnam, (67), see Table 3, leads to the expression, (see 63),

$$k_c \sim \sqrt{k_f} \cdot U \cdot Sc^{2/3} \qquad (7.9)$$

The maximum turbulence slip velocity for the particle, is substituted as the velocity term, in the turbulent mass transfer relationships, eqns. 7.8 and 7.9. In mixers the

dispersed phase particle diameters are frequently greater than the inner turbulence scale, $2a > \lambda_o$. Thus eqn. 3.31 is substituted as the velocity term. k_f may also be substituted for, as $k_f \sim N^{\frac{1}{4}}$ (55).

7.4 TRANSFER WITH AN INTERNALLY CIRCULATING DROP

Exact solutions for the continuous phase transfer rates from an internally circulating drop have been obtained for viscous flow, (10, 63, 106). Levich's solution, (63), may be written,

$$I = 8\frac{\sqrt{\pi}}{2} \cdot \left(\frac{\vartheta u}{a}\right)^{\frac{1}{2}} a^2 (c_d - c_o) \qquad (7.10)$$

The velocity u is substituted by the maximum drop slip velocity eqn. 3.35, to yield, with approximations applicable for locally isotropic flow in mixers,

$$Sh_T = \frac{kD_T}{\vartheta} = \text{Const} \cdot \left(\frac{\rho_c - \rho_d}{\rho_d}\right)^{\frac{1}{2}} Re_{Imp}^{\frac{3}{4}} Sc^{\frac{1}{2}} \qquad (7.11)$$

An equation, interpolating between eqn. 7.10 and eqn. 3, (Appendix 1) is developed by Ruckenstein, (106). For steady flow, this equation shows the changing importance of the Schmidt number, with the change in the ratio of the internal circulation velocity to the external fluid velocity, (v'/v).

$$0.849 \cdot \frac{v'}{v} \cdot Sh^{-2} \cdot Re + 0.278 \left(\frac{3}{2} - \frac{v'}{v}\right)\left(\frac{3}{2} + \frac{v'}{v}\right)^{\frac{1}{2}} Re^{3/2}\, Sh^{-3} = Sc^{-1}$$

An estimate of the parameter v'/v is obtained from a graph presented by Boye-Christenson and Terjeson, (11), which relates v'/v to the concentration of surfactants in the continuous phase. Except in clean liquids where the surfactant concentration is less than 2.10^{-6} gms. surfactant/gm. solvent, the ratio v'/v is in the range $0.1 < v'/v < 0.3$ for most liquids. A similar result has been derived theoretically, (63).

Piterskikh's relationship, eqn. 3.23,

$$\nu_{turb} = b\nu \left(\frac{y}{\delta_o}\right)^2 \qquad (3.23)$$

b = constant $\sim$ 0.01 (63), does not describe turbulence damping in the viscous sublayer next to a solid wall, but may apply at a mobile drop interface, at which the energy loss through viscous dissipation in the boundary layer is considerably less, (63). A relationship, similar to eqns. 7.8 and 7.9, may be derived by considering a turbulent boundary layer mechanism.

$$k_c \sim \sqrt{k_f'} \cdot U \cdot Sc^{-\frac{1}{2}} \qquad (7.12)$$

k_f' = external drag coefficient for an internally circulating drop.

The slip velocity for an internally circulating drop may be substituted for U in eqn. 7.12. The equation obtained is similar to the transfer relationship derived by considering surface tension damping at the interface, see Appendix 5.

$$k_c \sim \sqrt{k_f'} \; \frac{\rho_c - \rho_d}{\rho_d} \cdot (ND_I)^{3/2} \cdot a \cdot \frac{Sc^{-1/2}}{(D_I \nu_c)^{1/2}} \qquad (7.13)$$

These transfer relationships, which have been derived from boundary layer considerations, are summarised in Table 5.

The extent to which any experimental correlation approaches a limiting theoretical relationship is dependent upon the controlling parameters, particle size, interface mobility, and boundary layer turbulence.

Numerical coefficients are not derived in a dimensional 'order analysis' approach. From eqn. 7.6, however, it is apparent that the mass transfer rate increases with surface mobility. For steady flow conditions, Harriott, (39), shows that,

$$\frac{Sh_{drop}}{Sh_{solid}} \sim 5.9,$$

at $Sc \sim 10^3$, when a drop has full internal circulation.

Table 5 Transfer relationships for rigid interfaces.

Laminar boundary layer, $2a > \lambda_o$, eqn. 1 Appendix 1.

$$Sh = 2 + 0.58\ Re^{\frac{1}{2}}\ Sc^{\frac{1}{3}} \qquad (7.14)$$

Turbulent boundary layer, $2a > \lambda_o$, eqn. 7.8

$$k_c \sim \sqrt{k_f}.U.Sc^{-\frac{3}{4}} \qquad Sh_{Imp} \sim \left(\frac{\Delta\rho}{\rho_d}\right)^{\frac{1}{3}} \left(\frac{2a}{D_I}\right)^{\frac{1}{3}} Re_{Imp}\ Sc^{\frac{1}{4}} \qquad (7.15)$$

Turbulent flow, $2a < \lambda_o$, eqn. 2 Appendix 1.

$$k_c \sim \left(\frac{\delta^2 u}{a^2}\right)^{\frac{1}{3}} Sc^{-\frac{2}{3}} \qquad Sh_{Imp} \sim 0.5\ Re_{Imp}^{\ \frac{3}{4}}\ Sc^{\frac{1}{3}} \left(\frac{\Delta\rho}{\rho_d}\right)^{\frac{1}{3}} \qquad (7.16)$$

Transfer relationships for mobile interfaces.

Turbulent flow, $2a > \lambda_o$, eqn. 7.12

$$k_c \sim \sqrt{k_f'}.U.Sc^{-\frac{1}{2}} \qquad Sh_{Imp} \sim \sqrt{k_f'}\ \frac{\Delta\rho}{\rho_d}\ Re_{Imp}^{\ 3/2}.\left(\frac{a}{D_I}\right).\ Sc^{\frac{1}{2}} \qquad (7.17)$$

Steady flow in the external fluid, $2a > \lambda_o$, eqn. 7.11

$$k_c \sim 8\ \frac{\sqrt{\pi}}{2}\left(\frac{\partial u}{a}\right)^{\frac{1}{2}} \qquad Sh_{Imp} \sim \left(\frac{\Delta\rho}{\rho_c}\right)^{\frac{1}{2}} Re_{Imp}^{\ \frac{3}{4}}\ Sc^{\frac{1}{2}} \qquad (7.11)$$

The correct viscous damping postulate has not been determined. Investigations of the effect of molecular diffusivity, in mass transfer, have failed to select any particular postulate, and velocity fluctuations sufficiently close to solid and mobile interfaces have not been measured. However, the Schmidt number exponent of $\frac{1}{3}$ for transfer from solid surfaces is accepted, (55) by American workers, from laminar boundary layer considerations, (67), while $\frac{1}{2}$ is accepted for mobile interfaces, on the basis of penetration theory, (39). In contrast, Russian workers consider $Sc^{\frac{1}{4}}$ applies for solid surfaces in turbulent flow, (63).

7.5 SURFACE RENEWAL MODELS

Mass transfer relationships derived from surface renewal models (41, 105, 126, 127), have been developed using Higbie's concept (44) of molecular diffusion into a fluid film next to an interface. The more comprehensive models are proposed by Harriott (41) and Ruckenstein (105).

Harriott computed the average mass transfer rate, for normal and skew distributions, as well as constant values of the renewal times and penetration distances. The mass transfer coefficients are found to be little affected by the time distributions used, but increases by a factor of five occur for different distributions of penetration distances, having the same mean value.

The transfer relationship derived,

$$St = Sh.\ Re^{-1}\ Sc^{-1} \sim Sc^{-n}$$

$n \sim 0.7$ at $Sc = 10^3$, $n \sim 0.85$ at $Sc = 10^5$, shows a continuously changing Schmidt number exponent, rather than the discrete values obtained from viscous damping postulates. The result $Sh \sim Sc^{0.3}$, at $Sc = 10^3$, is intermediate between Levich's and Lin's postulates for turbulence damping at rigid interfaces. As velocity gradients in the diffusion layer are not considered in the derivation, comparison of this result with internally circulating drops is unsound.

Ruckenstein (105) derives two models in which the interface fluid is divided into two layers. The outer layer is renewed more frequently than the inner, $x_2 = \theta_2 u_2 < x_1 = \theta_1 u_1$.

θ = renewal time.

X = length of contact layer.

Z = depth of contact layer.

The first model is based on the hydrodynamic and transfer boundary layers lying within the inner fluid turbulence zone $0 < \delta < \delta_0 < Z_1$. The equation for diffusion from a semi-infinite fluid flowing over a path length x_1, is applicable.

$$k_c = 0.68 \left(\frac{u_2}{\delta\, x_1}\right)^{\frac{1}{2}} \left(\frac{\nu}{\mathcal{D}}\right)^{-\frac{2}{3}} \qquad (7.18)$$

The parameters x_1 and u_2 are derived dimensionally from the hydrodynamic parameters τ, ν and ρ.

$$x_1 = b' \nu / \sqrt{\tau/\rho} \quad , \qquad u_2 = b_1 \sqrt{\tau/\rho}$$

Equation 7.18 is comparable with Lin and co-workers' equation for turbulent transfer processes at a rigid interface, eqn.7.9.

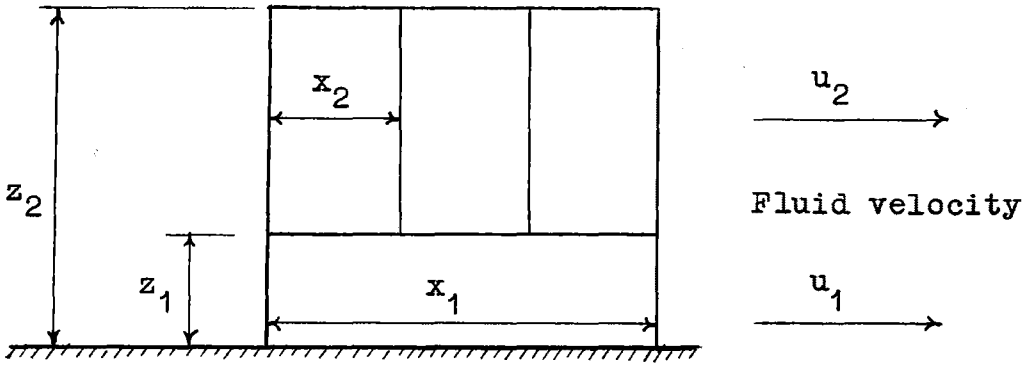

Surface Renewal Model

Ruckenstein's second model is based upon the hydrodynamic and mass transfer boundary layers lying in the outer renewal layer, $z_1 < \delta < \delta_0 < z_2$. An approximate solution for the transfer coefficient is obtained.

$$k_c = \frac{\sqrt{\tau/\rho}}{\beta'(\nu/\mathcal{D}) + \frac{1}{2}\left[\frac{630\beta_2}{74\beta_1 + 115\beta''}\right]^{\frac{1}{2}} \cdot \nu/\mathcal{D} \cdot Sc^{-n}} \qquad (7.19)$$

$$z_1 = \beta_1 \nu/\sqrt{\tau_0/\rho} \qquad u_1 = \beta'' \sqrt{\tau_0/\rho}$$

$$x_2 = \beta_2 \nu/\sqrt{\tau_0/\rho} \qquad u_2 = \beta' \sqrt{\tau_0/\rho}$$

For a rigid interface $\left(\frac{\beta''}{\beta'} \longrightarrow 0\right)$, $n \sim \frac{1}{3}$

For a mobile interface $\left(\frac{\beta''}{\beta'} \longrightarrow 1\right)$, $n \sim \frac{1}{2}$

Equation 7.19 yields no further information on the correct Schmidt number exponent, as the parameters, β_1, β_2, β' and β'', are indeterminate. For particular values of n,

eqn. 7.19 is equivalent to the turbulent boundary layer equations derived, eqns. 7.8, 7.9 and 7.12.

7.6 DROP INTERACTION

The volume fraction of dispersed phase, at which particle interaction affects the overall mass transfer rate, has not been determined for mixers. With turbulent boundary layers, it is unlikely that particle proximity will have a significant effect. For particles with laminar boundary layers, however, a marked change in transfer rates could occur, as shown by packed bed studies, (98).

For a surface renewal model of mass transfer, Ruckenstein (105) calculates that there is no particle interaction when the drop separation distance h_o is given by,

$$\frac{h_o}{\sqrt{\mathcal{D}\theta}} \geqslant 2 \qquad (7.20)$$

For internally circulating drops in a mixer, eqn. 7.20 shows negligible interaction for a phase volume ratio less than 0.5, for $2a \sim 0.1$ cms., $\theta = \frac{2a}{v}$, where $v \sim v_\lambda \sim 20$ cm/sec, eqn. 3.35. A value 0.5 seems high, even for turbulent flow. Evidently, the surface renewal requirement of "fresh bulk liquid", must be modified.

The dispersed phase volume fractions in this work are in the range 0.02 - 0.1, and the mass transfer coefficients are correlated by a turbulent boundary layer mechanism, see Section 7.10. Thus particle interaction is considered to have had negligible effect on the continuous phase mass transfer coefficients.

7.7 INTERFACIAL PHENOMENA

Surface absorbed films tend to increase the skin friction drag around a drop, see Section 7.4, and interfacial tension gradients have been shown to affect drop

coalescence rates, see Section 5.8. These two aspects of interfacial phenomena influence the overall mass transfer in a mixer. Interfacial turbulence also augments the mass transfer rate by disrupting the fluid boundary layers and causing local mixing. Two papers, which have been noted (107, 120), relate the occurrence of interfacial turbulence with the phase properties and the solute transfer rate. Interfacial tension gradients for dilute acid solutes may also be calculated, (112), but increases in mass transfer rates, caused by interfacial turbulence, remain unpredicted.

As a large precentage of liquid extraction literature has been devoted to interfacial phenomena, a selective note on this effect is necessary in this work. In a mixing section of a Scheibel column, Karr and Scheibel (54) found the transfer rate to depend on the direction of solute transfer and the phase dispersed. Mixer cells, which retain a continuous fluid interface with differential agitation of each phase, have yielded similar mass transfer results, (20, 64, 88, 113). Sherwood and Wei,(113) observed that interfacial behaviour affected the mass transfer rate to the same extent as the mixer cell dimensions. This observation is supported by Lewis's classification of systems according to their interfacial behaviour.

The complexities of extraction data may be interpreted, qualitatively at least, by recent theoretical work on interfacial behaviour. For example, the effects of surfactants on transfer with single drops are related to the boundary layer mobility. Thus, data obtained by Boye-Christensen and Tergeson (11), and Garner (31), may be correlated. However, solute purity has been found to affect the dissolution rate of cinnamic acid spheres (33), a process which is independent of interface mobility.

Solute purity	Transfer relationship
98%	$Sh \sim Re^{0.55}\ Sc^{0.46}$
99^{+}%	$Sh \sim Re^{0.75}\ Sc^{0.29}$

With the increase in solute purity, the mean increase in k_c is approximately 50%. A surface resistance for the

lower purity solute may have resulted from accumulated impurities at the interface. This effect has been noted previously (26), to complement surface mobility effects.

This note suggests that consistent fluid turbulence controlled transfer-data may best be obtained in the absence of interfacial phenomena effects. A clean apparatus, purified materials, and a stable liquid interface with mass transfer are apparently necessary. The selection of a system, and the cleaning of the apparatus, for this work, are described in Sections 2.1, and 2.5. The interfacial stability of the system used, isooctane/o-nitrophenol/water (continuous, extractant phase), is noted in Section 5.10.

Thus, as far as is possible in extraction with large scale experimental apparatus, these interfacial phenomena have been eliminated.

7.8 MASS TRANSFER DURING DROP DISPERSION AND COALESCENCE

Mass transfer rates during drop formation in a stagnant liquid are best correlated, for slow drop formation periods 1 to 15 seconds, by Ilkovic's equation (95),

$$N_A = \text{Constant} \cdot (c_d - c_o) \cdot (\pi \mathcal{D})^{\frac{1}{2}} d_f^{\,2} \, t_f^{-\frac{2}{3}} \, t^{7/6}$$

Constant = 6/7 to 24/7, depending on the transfer mechanism.

d_f = drop diameter at the end of the formation period, t_f.

Although not directly applicable to drop dispersion, this correlation suggests that the total solute transferred during drop dispersion is small, contrary to Garner and Lane's conclusion (32), that high transfer rates occur for the initial absorption of gases by suspended droplets.

In the system used in this investigation, negligible coalescence of the dispersed phase occurs in the mixing vessel, see Section 5.10. As the transfer resistance is substantially in the continuous phase, the dispersion and

coalescence that does occur will have little affect on the overall transfer rate, unless internal circulation is induced in otherwise non-circulating drops.

There are inherent "end effects" in mixer operation. These "end effects" define the mass transfer occurring during the initial phase dispersion, and the transfer occurring during coalescence in the settling vessel. As fluid turbulence in mixers is being investigated, the end effect corrections are calculated as the mass transfer from the dispersed phase jet before it breaks up, and the transfer in the settling vessel, before the aqueous phase is analysed for solute concentration. These corrections are subtracted from the total transfer measured, to give the transfer that occurs with the dispersion in the mixer.

For spray towers, Licht and Conway (65) found "end effects", as stage efficiencies, in the range $0.05 < e_s < 0.30$. The magnitude of the "end effect" is dependent on the drop size, as well as the extraction system.

7.9 DRIVING POTENTIAL FOR TRANSFER PROCESSES IN MIXERS

A driving potential based on the difference in solute concentrations in the outlet phases is accepted for calculating mixer vessel transfer rates, despite activity coefficients being more rigorous as driving force potentials from a thermodynamic standpoint, (34). Except in Karr and Scheibel's paper (54), concentration driving forces have been used for extraction, although a solute discontinuity occurs at the interface. In this work, the solute concentration in the continuous phase is sufficiently low, $< 10^{-5}$ Mol. fraction, to cause little deviation from the ideal, (22), and with the accuracy of solute concentration obtained, activity driving forces are not warranted.

The solute concentration at the interface is considered to be at equilibrium, except for high mass transfer rates, (9). Some workers, notably Kishinevskii and Kornienko (57),

claim that an interfacial resistance caused by a solute absorption layer, occurs with low mass transfer rates, although Davies and Waggill (21) consider that monomolecular film resistances are caused by damping of interfacial instabilities. Also, a theoretical analysis (43) shows that the bulk phase concentrations may not lie on the equilibrium curve, because of differing material transfer rates, in an extraction process. However, interfacial equilibrium is here assumed, although the polar solute, o-nitrophenol, may have been absorpted on the interface.

Each phase in a mixing vessel is normally assumed to be fully mixed. Treybal and Setzer,(111) found that data for isobutanol transfer into water, when the dispersed isobutanol phase was presaturated with water, are more consistent, when the driving forces with low mixer power inputs are based on plug flow of the continuous phase. Some knowledge of the continuous phase mixing rate is available, flow models for mixing vessels have been developed (85, 135), and theoretical studies of inertial subrange turbulence mixing have been made (17, 103). Rosenweig (103) develops an explicit relationship for the degree of"unmixedness", ψ / Ψ.

$$\frac{\psi^2}{\Psi(1-\Psi)} = \left(1 + N_c \left(\lambda_d^2 \; g_c \epsilon\right)^{\frac{1}{3}} \Theta\right)^{-1} \qquad (7.21)$$

$$N_c = \frac{2\sqrt{5/6}}{\sqrt{1/3}} \cdot \frac{1}{c_\gamma} = \frac{0.48}{c_\gamma}$$

Ψ = final mean concentration, (or volume fraction).

ψ = local fluctuations from the mean concentration, (or vol. fraction).

λ_d = characteristic wave-length of large eddies, length^{-1}.

Θ = mean residence time.

ϵ = energy input cascade $= -\frac{3}{2gc} \cdot \frac{dv_\lambda^2}{dt}$

c_γ = universal constant for the inertial subrange, (103)
$= k^{5/3} G(k_1) (g_c \epsilon)^{1/3} \; \epsilon_o^{-1} \sim 0.4$

Substitution in eqn. 7.21 shows the 'degree of unmixedness'

in this work to range from 1.2% (minimum) in the $8\frac{3}{4}$ in. vessel, to 7.5% (maximum) in the $5\frac{1}{2}$ in. vessel.

Mixing rate experiments (75) for vessel geometries similar to those used here also suggest that a high degree of continuous phase mixing occurs. Rice, Toor and Manning, (99), observed that complete neutralisation of a NaOH and phenolpthalein solution, introduced into the eye of an impellor occurred in the impellor stream, the circulating bulk liquid being acid, H_2SO_4. Biggs (8) introduced a tracer pulse into the mixer inlet feed stream. The mixing in the vessel was indicated by the outlet stream concentration which approached 95% of the final concentration in time t_{95}. For a paddle type impellor in a $9\frac{5}{8}$ in. vessel,

$$t_{95} = 3.5 \left(\frac{D_T}{D_I}\right)^{11/6} \cdot g_c^{-1/6} N^{-2/3}, \text{ for, } 10^4 < Re_{Imp} < 10^5.$$

The ratio, mixing time to the fluid residence time t_{95}/θ, for the $8\frac{3}{4}$ in. vessel used is in the range $0.05 < t_{95}/\theta < 0.13$. This result also shows the continuous phase to be nearly fully mixed.

In Section 5.10, it is shown that negligible coalescence of the dispersed phase, isooctane, occurs in the mixing vessel. Thus, the change in the solute concentration of the dispersed phase must be included in the mass transfer driving force potential.

The mean driving force potential is numerically calculated. For each run it is based on the constant outlet solute concentration in the continuous phase, and a decreasing solute concentration in the dispersed phase, the limits of which are given by the inlet and outlet concentrations.

7.10 RESULTS OF MASS TRANSFER EXPERIMENTS

A full description of the apparatus and its operation is given in Section 2. A summary of this section, and the data processing program, in Appendix 14, is given here.

A sample of the dispersion leaving the mixer coalesced in the tube settler, see Fig. 2.10. The o-nitrophenol content in a portion of the coalesced aqueous phase was analysed, while flowing through a light absorptiometer cell. The differential millivolt output from the measuring and reference photometer cells was recorded. At the end of each run, a sample, circa 50 ml., was collected from the sample settler for a check spectroscopic analysis, using a Beckmann DK2 spectrophotometer. The two analyses of the outlet concentrations were in agreement $\pm$ 4%, except when some isooctane was inadvertently included in the aqueous sample. The mass transfer coefficients are calculated from the continuous analysis concentrations, except for runs 113 and 115, where a heat filter in the continuous absorptiometer cracked, making the calibration curve inaccurate. Both absorptiometers were calibrated with solutions of known solute concentration.

The inlet aqueous phase contained no solute, being tapwater. The solute concentration in the inlet isooctane phase was calculated from the spectrophotomically measured concentration of water samples, into which all the solute in an isooctane sample had been extracted, see Section 2.4. The raffinate solute concentration was calculated from a mass balance.

The scale reading error for the two concentration analysis methods is $\pm$ 3%, for an extraction stage efficiency of 0.5. The error in the mass transfer coefficient, however, is $\pm$ 6%, as the outlet aqueous phase concentration is used to estimate the total solute transferred, as well as the driving force.

$$\text{FLOW.}\ (c_b - c_o) = k_c . VA . (c_b^* - c_o)$$

(Aqueous phase flow rate).(Concentration change) = (Mass transfer coefficient).(Interfacial area).(Driving force)

The percentage error in the mass transfer coefficient, resulting from the concentration measurement errors, increases as the stage efficiency tends towards 0 or 1.0. At an efficiency of 0.85, the mass transfer error becomes ± 12%.

The computational steps in a computer program used to calculate the mass transfer coefficients, see Appendix 14, are summarised here.

The solution properties, density, viscosity, and diffusivity are calculated from relationships given in Section 2.3.

The extraction stage efficiency is calculated, and the end effect corrections made. The mass transferred from the undispersed isooctane jet, see Fig. 5.9, is calculated, using a transfer coefficient based on penetration theory.

$$k_c = \sqrt{\frac{4\mathcal{D}}{\pi\theta}}$$

A contact time, θ was estimated from the jet height and rise velocity, which were measured, see Section 2.6. The outlet end effect was calculated as two effects. Transfer through the slowly moving interface in the settler was estimated from a relationship obtained for a similar flow configuration, (80).

$$Sh = 0.522 . We^{0.67} . \left(\frac{\mu_c}{\mu_d}\right)^{0.254} . Sc^{-1.46} . \left(\frac{D_F G_c}{\mu_c}\right)^{0.397}$$

D_F = diameter of flow path.

G_c = flow rate, mass/(length^2 x time).

The second contribution, of mass transfer from the entrained dispersed phase drops, is estimated from Ward and co-workers' correlation, see Appendix 1.

$$Sh = 0.98\ Re^{\frac{1}{3}}\ Sc^{\frac{1}{3}}$$

which is applicable for small drops in viscous flow. This end effect is negligible as the small, non-coalesced drops, which are considered to be formed in the initial dispersion, contribute little to the transfer processes in a mixer. The number of these drops present in the sample settler is estimated by matching the mean particle size found in the settler, Section 2.6, with the number of that size in the mixing vessel. The solute transfer that occurred in 0.5 - 1.5 seconds before the phases became substantially coalesced, after leaving the mixer, is not estimated.

The sum of these end effect corrections is small, stage efficiency < 0.02, and is less than the errors due to solute concentration measurements. However, the inlet and outlet concentrations are corrected to exclude these end effects, as they always add to the transfer occurring with the dispersion in the mixing vessel.

The transfer coefficient COA, based on the corrected outlet solute concentrations is calculated, as well as the transfer coefficient COIA, based on the corrected continuous phase outlet concentration and the change in dispersed phase concentration between the corrected inlet and outlet concentrations, see Section 7.9. For the latter case, the mean driving force is calculated by a numerical integration involving 100 to 150 steps.

The film coefficients for the continuous phase CO and COI, are calculated from the transfer coefficients COA and COIA, and the measured interfacial area of the dispersion.

$$CO = COA/AREA, \qquad COI = COIA/AREA$$

The interfacial area, $AREA = 6\phi / d_{SV}$ is obtained from the dispersed phase hold-up, and the surface-volume particle diameter, see Sections 5 and 6.

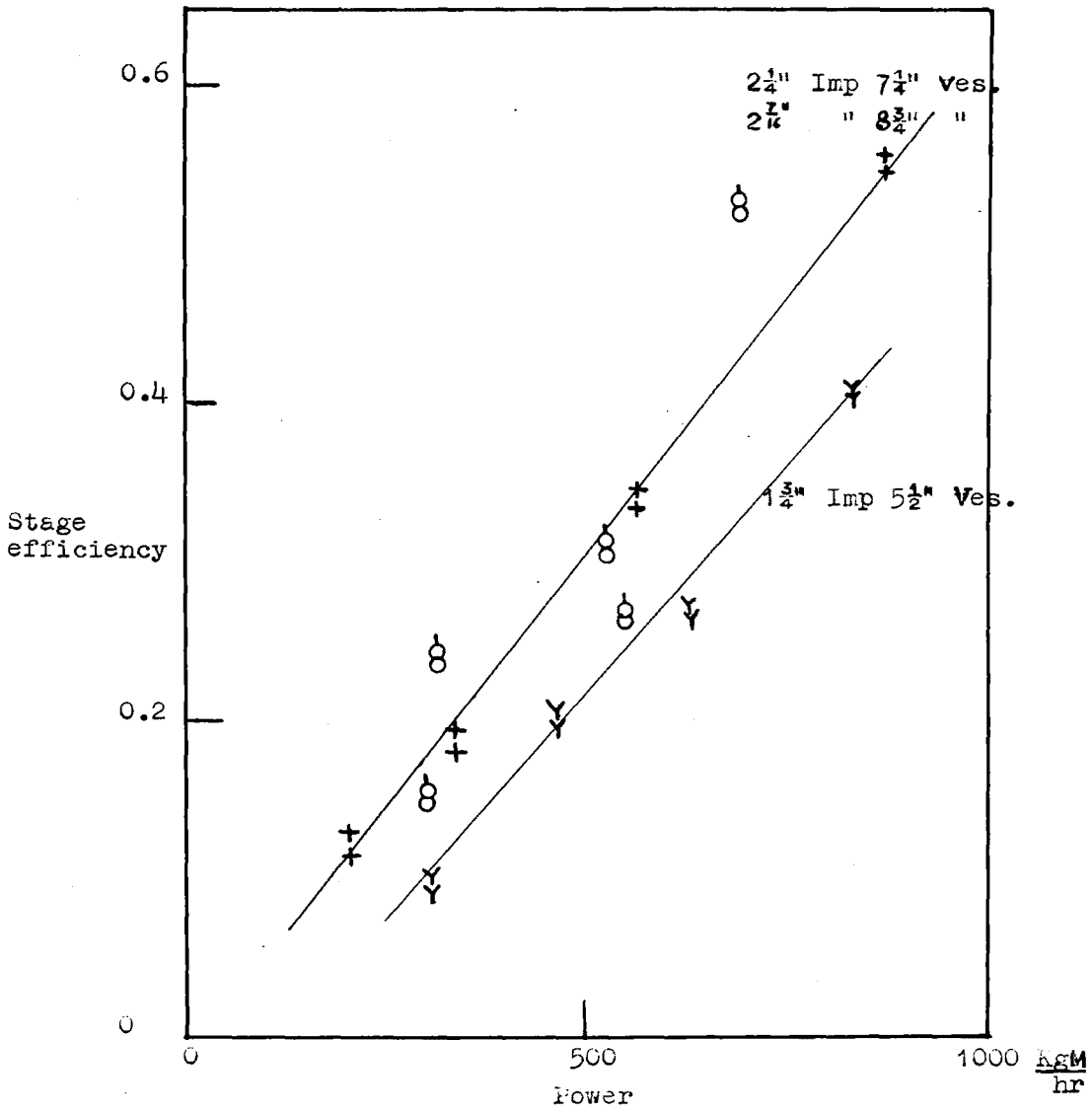

Upper value = total overall efficiency.
Lower value = overall efficiency resulting from transfer to the dispersion in the mixing vessel.

Fig. 7.1 End Effect Corrections.

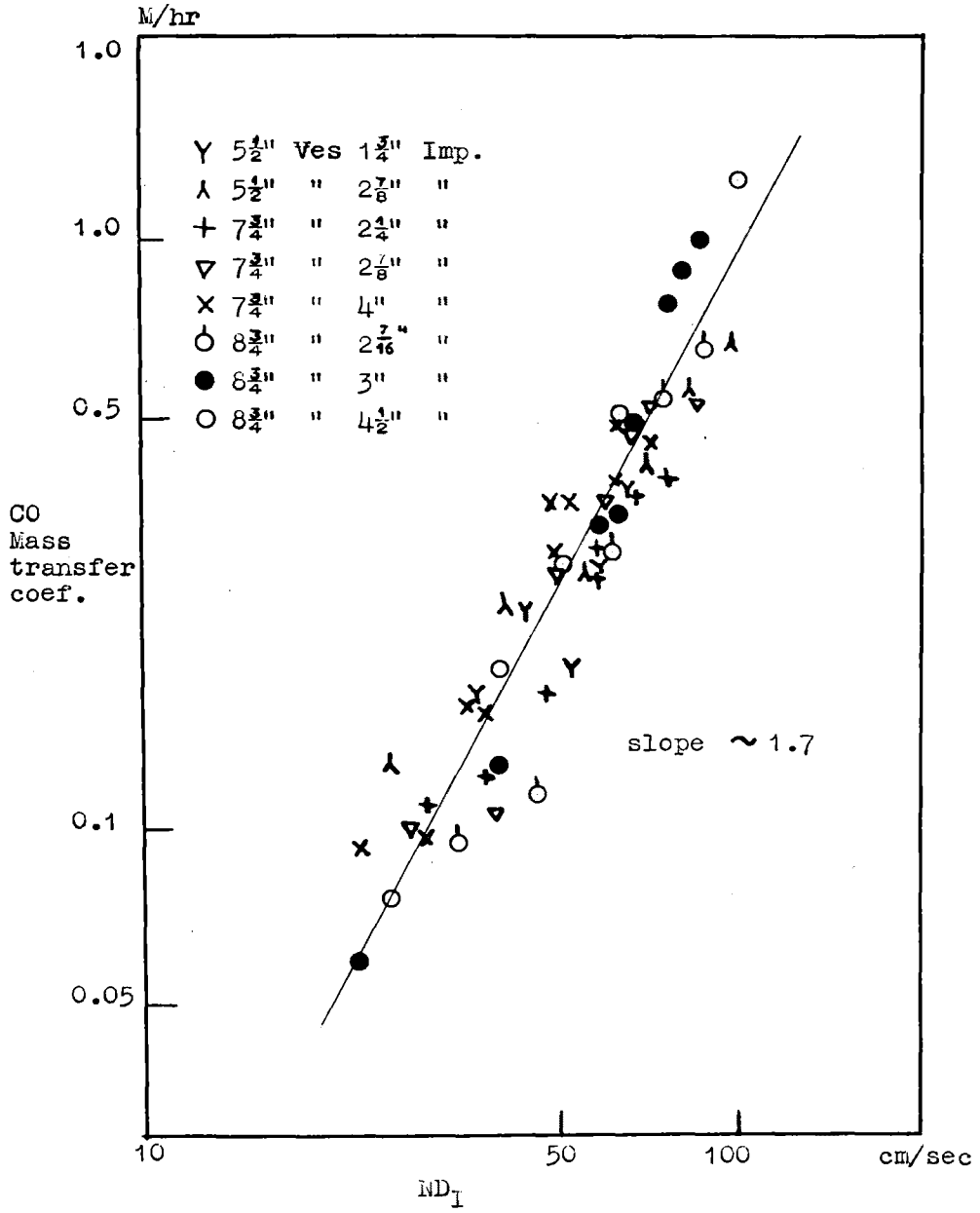

Fig. 7.2 Mass transfer coefficient based on both phases being fully mixed in the agitated vessel versus impellor tip velocity.

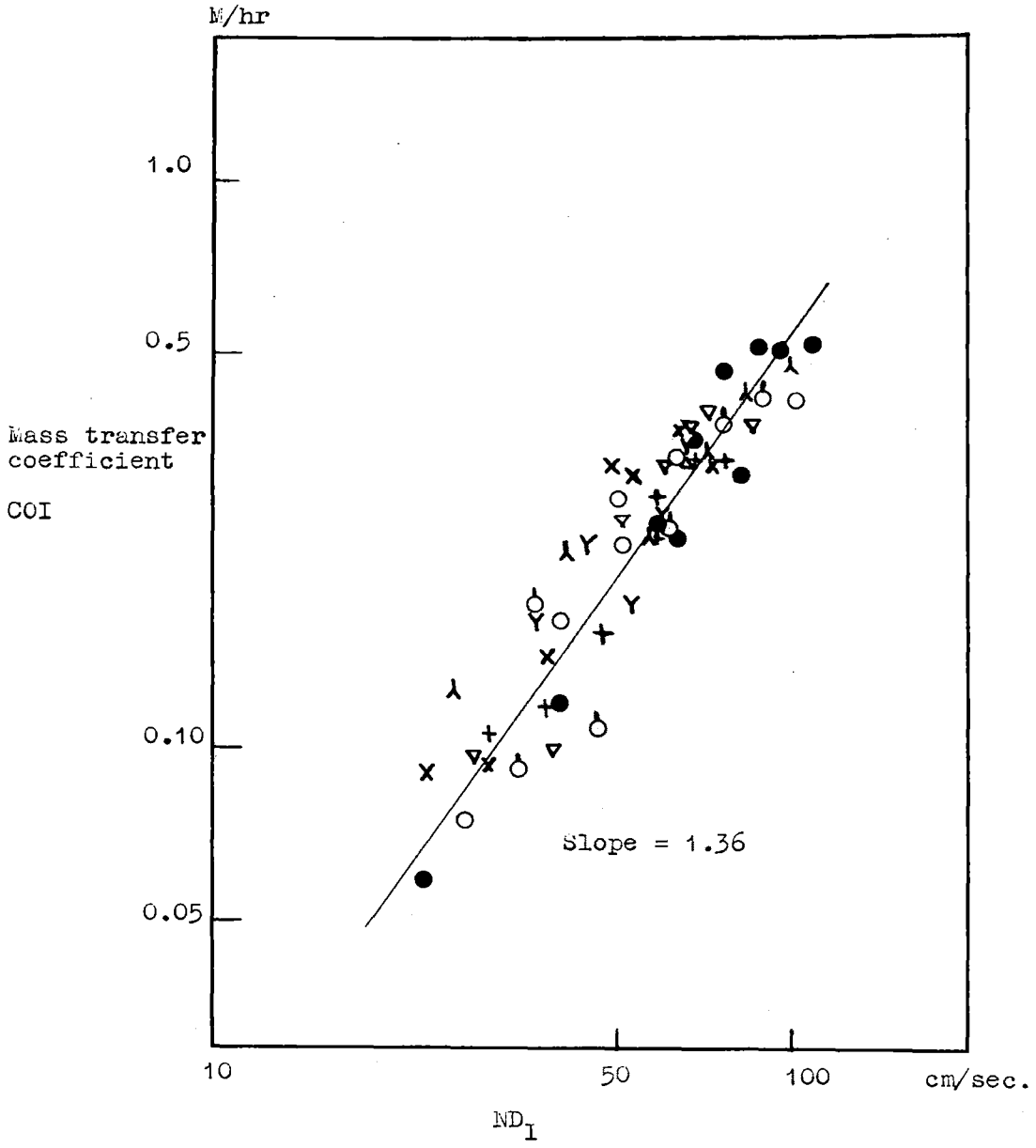

Fig. 7.3 COI, Mass transfer coefficient based on a non-mixed dispersed phase versus impellor tip velocity.

Fig. 7.4 Graphical determination of the line of best fit for the mass transfer data.

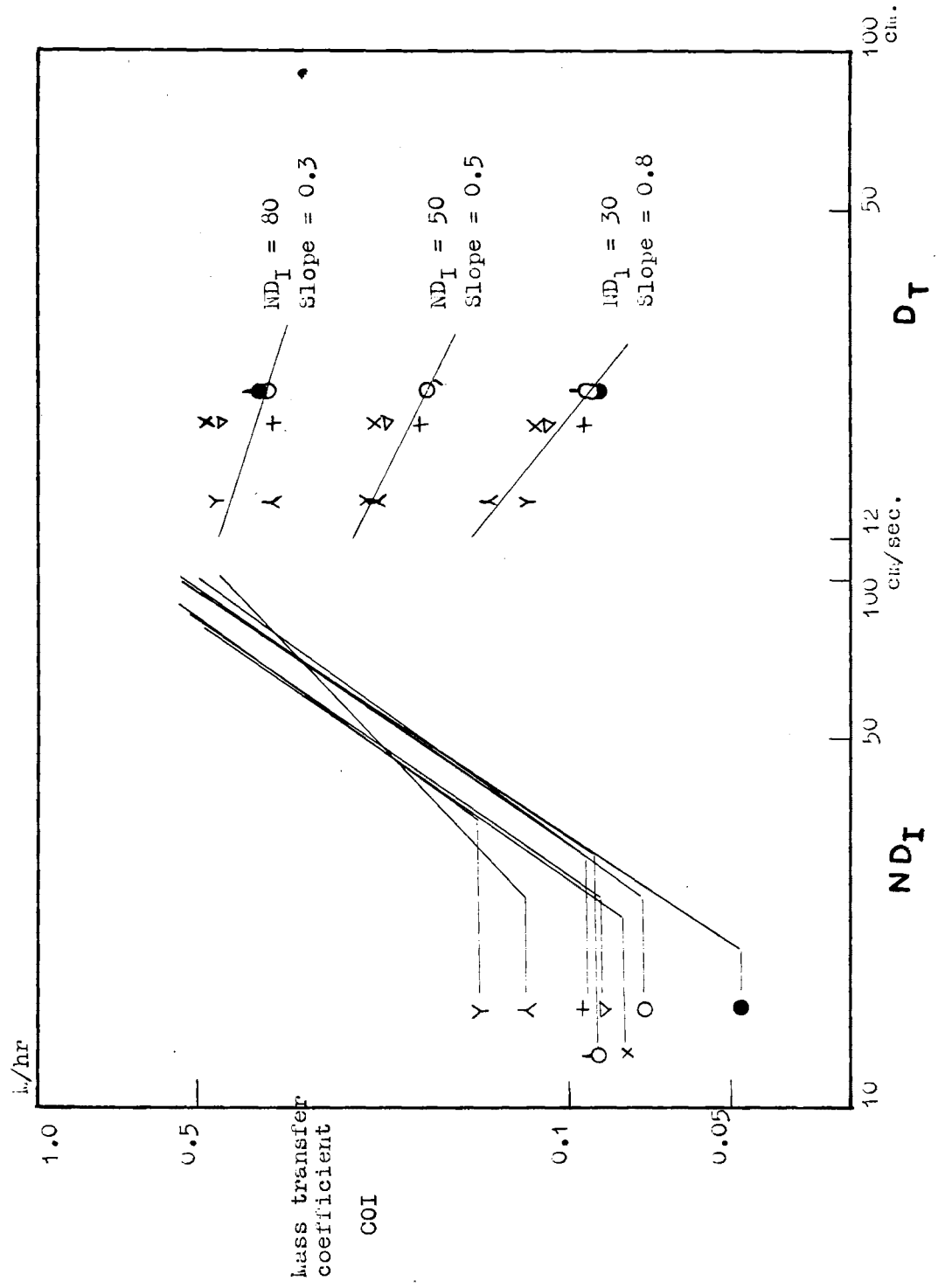

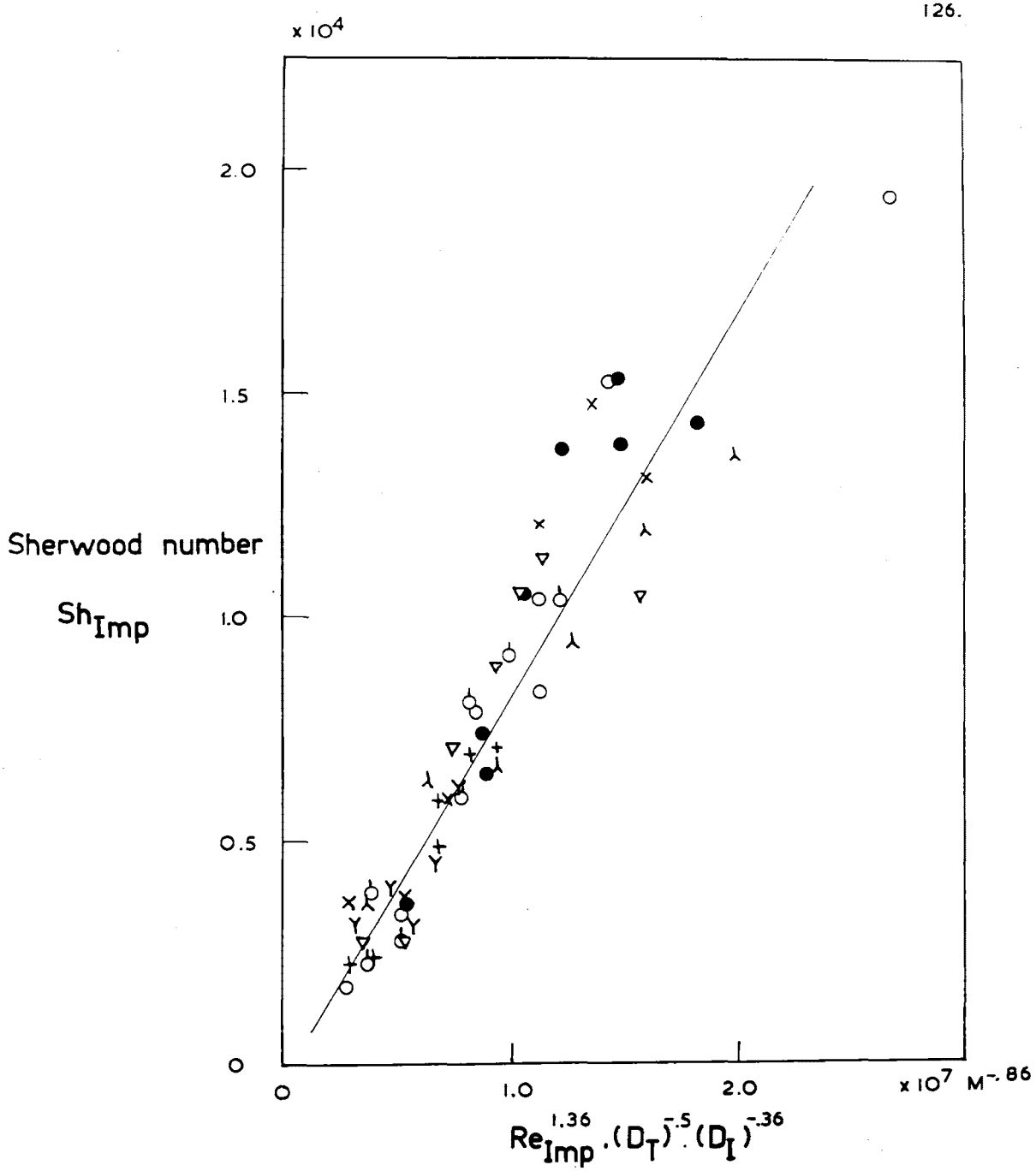

Fig. 7.5 Line of best fit for mass transfer data, regression coefficient R = 0.931

$$Sh_{Imp} = 8.92 \times 10^{-4} Re_{Imp}^{1.36} . (D_T)^{-.5} . (D_I)^{-.36} - 336, \quad \text{MKH units}$$

7.11 DISCUSSION

The stage efficiency calculated for each run, indicates the fractional approach to equilibrium of the extraction phases. The efficiency range was limited by using different liquid residence times in the mixing vessel, to minimise the errors in the mass transfer coefficients, introduced by errors in the concentration analysis. However, high and low efficiencies were unavoidable with the apparatus and the impellor Reynolds number range used, Appendix 13. Except for the inlet end effect (29), the inlet flow rate does not influence the mass transfer within the mixing vessel, (130).

The end effect corrections, for the mass transfer that occurs before the dispersed phase liquid is broken up, and the transfer occurring outside the mixing vessel before the aqueous phase solute concentration is analysed, are estimated as stage efficiencies, see Appendix 13. The maximum total end effect calculated equals a stage efficiency of 0.011, but Flynn and Treybal (29) found end effect corrections, expressed as Murphree efficiencies, of 0.2 to 0.9, for mixing vessels. The relatively low inlet flow rates and the fast dispersion coalescence in the settling vessel, have resulted in the small end effects estimated. Extrapolation of the data in Fig. 7.1 to zero power inputs shows the calculated end effect corrections to be realistic, and less than the errors in the experimental determination of the overall efficiency. The geometries graphed are selected on the basis that there are more than three comparable data points in each graph.

The overall mass transfer coefficients CO and COI, are calculated from the expression,

$$\text{Transfer rate, } N_A = CO.\ AV_v.\ \overline{DF}$$

A = interfacial area/unit volume.
V_v = volume of vessel.
$\overline{DF}$ = mean driving force.

A more correct relationship is,(9),

$$\frac{N_{Ay}}{AV_v} = CO.\ \overline{DF} + x_A\,(N_{Ay} + N_{By})$$

which reduces to,

$$N_{Ay}/AV_v = CO.\ \overline{DF} \quad \text{when } x_A \ll 1 \qquad (7.22)$$

For the low solute transfer rates occurring in this work, $0.8 \times 10^{-9} <$ transfer flux $< 1.3 \times 10^{-9}$, mols solute/cm. sec., eqn. 7.22 may be used to estimate accurate values of CO and COI.

The overall mass transfer coefficient will approximate to the continuous phase film resistance, when there is negligible interfacial resistance to solute transfer.

$$\frac{1}{K_c} = \frac{1}{k_c} + \frac{1}{m_d\, k_d} \quad \text{if } (1-x_c) \sim (1-x_d) \sim 1 \qquad (7.23)$$

If the dispersed phase transfer term is much less than the continuous phase term $\frac{1}{m_d\, k_d} \ll \frac{1}{k_c}$ then,

$$\frac{1}{K_c} \longrightarrow \frac{1}{k_c}$$

m_d = gradient of the equilibrium curve over the concentration range considered.

K_c = overall coefficient, based on the continuous extractant phase.

k_c = film coefficient, based on the continuous extractant phase.

The internal mass transfer coefficient for a drop may be calculated for the extreme conditions of maximum or zero internal circulation. As it is shown in this section that the dispersed phase drops were circulating internally, this condition is considered in the comparison of k_d and k_c.

For an internally circulating drop, with $Re_{drop} > 50$, Handlos and Baron,(38) found the internal mass transfer coefficient to be correlated by,

$$k_d = \frac{0.00375\ v_t}{1 + \mu_d/\mu_c} \qquad (7.24)$$

which yields, for isooctane drops in water,

$$k_d = 0.0912\ v_t, M/_{hr}.$$

v_t may be substituted by eqn. 3.35,

$$v_t = v_{max} \sim \frac{\rho_c - \rho_d}{\rho_d} \cdot a \left(\frac{\epsilon}{\rho_c\ \nu_c}\right)^{\frac{1}{2}} \qquad (3.35)$$

to yield, for mixer conditions,

$$k_d \sim 1.0 - 2.0\ M/_{hr} \qquad (7.25)$$

For rigid drops, k_d becomes,

$$k_d \sim 0.4 - 0.9\ M/_{hr}$$

The gradient of the solute equilibrium curve, for the mixer operating conditions, is obtained from Table 1 as,

$$\frac{1}{m_d} \sim 0.025\ , \left(\frac{\text{gm ONP}}{\text{gm } H_2O}\right) / \left(\frac{\text{gm ONP}}{\text{gm isooctane}}\right) \qquad (7.26)$$

Within the accuracy of the experimental measurements of the solute concentration, the continuous phase mass transfer film coefficient, is equal to the overall mass transfer coefficient. The error introduced $\left(\frac{1}{m_d k_d}\right)/\left(\frac{1}{k_c}\right)$ is less than 0.025, by comparison of eqns. 7.25 and 7.26 with Appendix 13, and, as with the possibility of interfacial resistance, is neglected.

The mass transfer coefficients, CO and COI, obtained are plotted versus the impellor tip velocity ND_I, in Figs. 7.2 and 7.3. For each vessel geometry the graphs show,

$$CO \sim (ND_I)^{1.7} \qquad (7.27)$$

$$COI \sim (ND_I)^{1.36} \qquad (7.28)$$

CO = mass transfer coefficient when the driving force is based on each phase being fully mixed.

COI = mass transfer coefficient when the driving force is based on a fully mixed continuous phase but an unmixed dispersed phase.

The relationship $CO \sim (ND_I)^{1.7}$ is not explained by the laminar or turbulent boundary layer relationships, summarised in Table 5. This disparity lends weight to the conclusion that the dispersed phase is not fully mixed in the extraction vessel, see Section 5.10. The velocity exponent in the relationship $COI \sim (ND_I)^{1.36}$ approaches that predicted for a drop that has high interfacial mobility in turbulent flow, eqn. 7.17. The data for COI are best correlated as, see Fig. 7.4,

$$COI = 4.10 \times 10^{-6} (ND_I)^{1.36} \cdot \left(\frac{1}{D_T}\right)^{(-.016\ ND_I + 1.211)} \quad (7.29)$$

MKH units

which may be approximated by, see Fig. 7.5,

$$Sh_{Imp} = 0.000892 \cdot Re_{Imp}^{1.36} \cdot \frac{1}{D_I^{.36}\ D_T^{.5}} - 336 \quad (7.30)$$

MKH units

The comparable mobile interfacial relationship eqn. 7.17, may be written,

$$Sh_{Imp} \sim \sqrt{k_f'}\ \frac{\Delta\rho}{\rho_d} \cdot Re_{Imp}^{1.5} \cdot \left(\frac{a}{D_I}\right) \cdot Sc^{\frac{1}{2}} \quad (7.31)$$

The solution property terms in eqn. 7.31, cannot be compared with the experimental results, as these terms are not being investigated.

The experimentally determined Reynolds number exponent shows that extensive drop interfacial motion occurs, as well as turbulence in the continuous phase boundary layer. The theoretical velocity exponent of 1.5 (eqn. 7.31) may arise from internal circulation in a drop, with turbulence damping in the surrounding boundary layer, or from interfacial turbulence caused by interfacial tension gradients, see Appendix 5. The latter mechanism is not applicable to the system isooctane/o-nitrophenol/water (extractant phase), see Section 5.8; thus the velocity exponent of 1.36 may only be interpreted by internal drop circulation and turbulence damping mechanisms.

The predicted length ratio, a/D_I, partially occurs as the term $\frac{1}{D_I^{.36} D_T^{.5}}$. The particle diameter term, a, is not found experimentally. It arises in the predicted transfer relationship, eqn. 7.17 from considering the mass transfer to be caused entirely by the inertial subrange turbulence of eddy length $\lambda = 2a$. Besides some transfer occurring with all the fluid velocity components, a range of particle diameters is found for each dispersion in a mixer. The length parameter $\frac{1}{D_I^{.36} D_T^{.5}}$, eqn. 7.30, is dimensionally similar to $\frac{1}{D_I}$, eqn. 7.31. The combined length term arises from the energy dissipation region, and the mass transfer region extending to the vessel walls. The energy dissipation relationship, eqn. 3.7, substituted in the theoretical prediction of the transfer rate, shows the energy dissipation to occur entirely within the impellor volume, see Section 6.3.

The Sherwood number in eqn. 7.30 is based on the impellor diameter, as suggested in Section 4.5, but the experimental correlation could equally well be written,

$$Sh_T = 8.92 \times 10^{-4} Re_{Imp}^{1.36} \cdot \frac{D_T^{.5}}{D_I^{1.36}} - 1100 \quad M^{-.86} \qquad (7.32)$$

The relevant vessel length is not established, but it is apparent that the particle diameter is not the correlating length parameter, in mixing vessel extraction. This result is contrary to that obtained for mass transfer with spheres in steady flow conditions, see Appendices 1 and 2.

Three subsections of this work have been completed as projects, in this Department. T.P. Dobbie (24) investigated the dissolution of freely circulating o-nitrophenol particles in mixing vessels. The particles used were nearly spherical, with a range of diameters of $0.047 < 2a < 0.147$ cms., $d_{sv} = 0.098$ cms. These data are correlated by the relationship,

$$Sh_T = 0.072 \quad Re_{Imp}^{0.81} \cdot Sc^{\frac{1}{3}}, \qquad (7.33$$

which is similar to other correlations for slow rates of the dissolution of solids in mixing vessels (24). However, the continuous phase controlled transfer coefficients for the isooctane drops in this thesis are significantly higher than the transfer coefficients for solids' dissolution; although the particle sizes, the solute, the transfer controlling phase, and the mixing vessels are the same. The difference in phase densities is greater for the solids' dissolution,

$$(\rho_{\text{o-nitrophenol}} - \rho_{H_2O}) = 0.658, \text{ and } (\rho_{\text{isooctane}} - \rho_{H_2O}) = -0.310 \text{ gm/cm}^3$$

at 20°C, but from eqn. 7.15, a transfer coefficient decrease is predicted for the isooctane dispersed phase.

Re_{Imp}	k_c liquid extraction	k_c solids dissolution
10^4	0.045 $M/_{hr}$	0.019 $M/_{hr}$
10^5	1.18 $M/_{hr}$	0.12 $M/_{hr}$

Solute impurities may have depressed the o-nitrophenol dissolution rates (33), but the principal increase can arise only from differences of interface mobility, (25). The higher transfer rates for the liquid dispersed phase support the conclusion, deduced from the velocity exponent in eqn. 7.28, that the drop interfaces were mobile.

The extent of the internal drop circulation required to give this mass transfer increase has not been predicted for turbulent boundary layer conditions. For a drop in steady flow, $10 < Re_{drop} < 10^3$ and $Sc = 6.7 \times 10^4$, Ruckenstein's relationship, (106),

$$0.849 \frac{v'}{v} Sh^{-2} Re + 0.278 \left(\frac{3}{2} + \frac{v'}{v}\right)^{\frac{1}{2}} Re^{3/2} Sh^{-3} = Sc^{-1}$$

shows that a mass transfer increase of four may be obtained with $v'/v = 0.7$. The maximum possible value of v'/v is 1.5. Although Ruckenstein's relationship is not directly applicable to this work, it suggests that high drop interfacial circulation occurred. This is not expected in large scale

experimental apparatus which is difficult to clean (11), although v'/v values near 1.5 have been achieved in falling drop investigations (25).

Two other projects have shown that the transfer rate with particles held in a mixer are controlled by boundary layers, different from those around freely circulating particles. J. Voot (133) followed the dissolution of large o-nitrophenol spheres, 0.6 > 2a > 0.2 cms., held by a thin wire passing through a diameter. The transfer data, obtained from a region just above the impellor, is correlated by,

$$k_c = 0.0048.\ a.\ (ND_I)^{0.7} \qquad \text{cgs units} \qquad (7.34)$$

P.M. Farrier (28) investigated the mass transfer controlled electrochemical reduction of ferricyanide ions in an indifferent electrolyte, see Appendices 2 and 4. The transfer rates, in a grid of mixer positions, were measured at the surface of an 0.143 cm. diameter copper-plated sphere. The mass transfer coefficients are correlated by,

$$\text{Impellor zone,} \quad k_c = 0.00221\ N^{0.45} \quad \text{cgs units} \qquad (7.35)$$

$$\text{Bulk fluid,} \quad k_c = 0.00115\ N^{0.53} \quad \text{cgs units}$$

Farrier's results, eqns. 7.35, are evidence that a laminar boundary layer exists around a sphere, even in the high energy dissipating impellor zone. This boundary layer develops for the mean flow and the larger eddies; the relative velocities of the inertial subrange turbulence, with respect to a fixed sphere, are much smaller, see eqn. 3.16. Consequently, the inertial subrange turbulence does not greatly affect the total mass transfer rate from a fixed sphere, a conclusion that is contrary to that found for freely circulating particles, see Appendices 2, 3, and 4. Voot's data (133) shows that the large diameter spheres are more influenced by turbulence, and possibly the method of particle support, (55).

These three projects show that transfer processes with fixed and freely circulating spheres cannot be compared for

mixer conditions. Thus, experimental correlations of mass transfer with particles held in a water tunnel, although useful in showing boundary layer processes, do not yield transfer data that may be scaled to mixers, even for particle dissolution.

Comparison of results with published data

With number, correlations of extraction mass transfer have increased in diversity rather than in conformity, although some classification according to transfer mechanisms has been possible. As it is likely that any new correlation will be simultaneously supported and contradicted by existing correlations, the generalised relationships proposed in review articles are used for the comparison of transfer correlations obtained in this and T.P. Dobbie's work.

The rates of the dissolution of solids have been satisfactorily correlated with the dimensionless groups, Sh_T, Re_{Imp}, Sc.

$$Sh_T = \frac{k_c D_T}{\mathcal{D}}$$

$$Re_{Imp} = \frac{N D_I^2 \rho_c}{\mu_c}$$

$$Sc = \frac{\nu_c}{\mathcal{D}}$$

A survey of solids' dissolution data (73), shows that an average transfer relationship may be written for mixers,

$$Sh_T = 0.402\ Re_{Imp}^{0.65}\ Sc^{0.33} \qquad (7.36)$$

This correlation includes some diversity of data; the continuous phase transfer for ion exchange beads is given as $Sh_T \sim Re_{Imp}^{0.1 \to 0.5}$, (40, 71), while solids' dissolution rates in a mixer are given as $Sh_T \sim Re_{Imp}^{0.5 \to 0.9}$ (3, 24, 40). Dobbie's correlation,

$$Sh_T = 0.072\ Re_{Imp}^{0.81}\ Sc^{0.33} \qquad (7.33)$$

for $10^4 < Re_{Imp} < 2 \times 10^5$ is in agreement with Marangozis and

Johnson's correlation, eqn. 7.36, at $Re_{Imp} = 5 \times 10^4$.

There is a dearth of comparable extraction data (131). Mostly, liquid-liquid transfer data have been presented as efficiency relationships, for example, (90),

$$1. - e_s = \frac{3.18 \times 10^{15}}{Re_{Imp}^{3.2}\ Po^{1.37}} \cdot \left(\frac{D_T}{D_I}\right)^t$$

$t = 1.6$ unbaffled vessel, $t = 0$ baffled vessel. Other works (29, 38, 46), show the Murphree efficiency to be proportional to the mixing vessel power input, but these correlations do not distinguish between the resistances in each phase.

Overall transfer coefficients, Ka, for systems with the transfer resistance substantially in the continuous phase have been measured. Rushton, Nagata and Rooney (109) found, for a single mixer geometry,

$$Ka = 1.05 \times 10^{-4} \cdot N^{2.1} \cdot \mu_d^{-0.6} \cdot \mu_c^{-0.55} \quad sec^{-1}$$

Equation 5.13 for the interfacial area, may be substituted in this equation, to yield,

$$k_c \sim N^{0.9}$$

Berestovai and Romanov (7) found for several systems, with predominantly continuous phase control, in a flow mixing vessel,

$$Ka = \frac{0.94 \times 10^{-4}\ G_c^{0.54}\ G_d^{0.2}\ N^{1.36}\ D_I^{3.0}\ \rho_c^{3.32}\ \mu_d^{0.5}}{\Delta\rho^{0.5}\ \mu_c^{1.5}\ \sigma^{0.82}}$$

$\frac{Kg}{M^3\ sec}$

The volumetric flow rates, G_c and G_d, probably occur in the interfacial area term, but as the holdup and mean drop diameters were not determined, the dependence of the mass transfer coefficient k_c, on the impellor speed N, is not apparent.

Nagata and Yamaguchi's data (81) for continuous phase transfer processes show a weak dependence of the mass transfer rate on the impellor speed. The dependence is a function of the phase density difference.

$k \sim N^{0}$ for $\rho = 0$ gm/cm^3

$k \sim N^{0.5}$ for $\rho = 0.219$ gm/cm^3

A density, impellor speed inter-relation is also found for solids dissolution, but for higher density differences, the exponent of the impellor speed changes in the opposite manner, (71).

Limited mass transfer data for the dissolution of isobutanol drops in water, obtained for mixer conditions similar to those in this work (111), are too scattered to permit correlation.

The diversity of these published correlations, necessitates the estimation of continuous phase mass transfer coefficients in mixer extraction, from stirrer cell, falling drop, and solids' dissolution data.

Transfer from falling drops in a stagnant medium, may be correlated by Sh = f(Re.Sc) relationships, such as those obtained by Thorsen and Tergeson (125),

$$Sh = -178 + 3.62\ Re^{\frac{1}{2}}\ Sc^{\frac{1}{3}} \qquad Re > 23,\ Sc \gg 1$$

for carefully purified liquids,

$$Sh = 2 + 0.95\ Re^{\frac{1}{2}}\ Sc^{\frac{1}{3}}$$

for surfactant contaminated systems. These relationships cannot be directly used in mixer correlations, see Appendix 4. Mass transfer with freely circulating drops is controlled by the inertial subrange turbulence, and involves the vessel geometry, but falling drop relationships are based on the drop velocity and diameter, and are independent of the vessel geometry.

More relevent to mixers are film transfer data obtained from stirrer cell measurements. In these cells, each phase is agitated, but the interface remains continuous, except for

surface eruptions. Davies, (25) correlates these data by an empirical relationship found by McManamey, (69),

$$k_2 = 6.4 \times 10^{-4}. \ \nu_2. \ Sc^{-0.3} \ Re_2^{0.9} \ (1 + \frac{\mu_1 Re_1}{\mu_2 Re_2}) \quad (7.37)$$

At least, the numerical constant will depend upon the system, (113). Lewis's data (64), which Davies recorrelates with eqn. 7.37, was originally presented in the form,

$$k_2 = 1.13 \times 10^{-7}. \ \nu_2 \ (Re_2 + Re_1 \frac{\mu_1}{\mu_2})^{1.65} + 0.0167 \ \nu_2 \quad (7.38)$$

Data obtained by Zhelcznyak and Brounshtein (138) for the system, heptane/toluene/diethylene glycol, may be cited in support of Lewis's correlation, eqn. 7.38,

$$k_h = A' \ (N_h \ D_{Imp.h} + N_d \ D_{Imp.d})^{1.43}$$

$$k_d = 0.46 \times 10^{-4}. \ N_d^{1.43}$$

A' increases slightly with concentration.

Subscripts h and d refer to the heptane and diethylene glycol phases.

Data from other types of agitated extraction equipment may be cited in support of a range of mass transfer-velocity correlations. For example,

$k_c \sim N^0$ Ref. 14.

$k_c \sim N^{2.55}$ Ref. 91.

It is sufficient to observe the results of Karr and Scheibel (54), who investigated transfer in the system, methyl isobutyl ketone/acetic acid/water, in a single section of a Scheibel column. With the organic phase dispersed, transfer to the continuous phase is correlated by,

$$\frac{K'a.\ D_I}{G\ (\Delta\rho/\sigma)^{1.5}} = 3.67 \times 10^{-7}\ (ND_I)^4 \qquad (7.39)$$

while the numerical constant for transfer into the dispersed phase is 1.06×10^{-7}. For transfer in either direction when the aqueous phase is dispersed,

$$\frac{Ka\ D_I^{0.3}}{G\ (\Delta\rho/\sigma)^{1.5}} = 7.9 \times 10^{-6}\ (ND_I)^3$$

Substitution of eqns. 5.13 and 6.3, in eqn. 7.39 shows,

$$k' \sim k_c \sim (ND_I)^{1.4}/D_I^{0.8} \qquad (7.40)$$

Karr and Scheibel attribute the high transfer coefficients in eqn. 7.39, to a drop coalescence resistance, and a high degree of holdup. For the system used it is suggested that interfacial circulation also contributed to the increased velocity exponent, in eqn. 7.40.

7.12 CONCLUSION

Mass transfer relationships may be predicted for single particles, in viscous, steady, and turbulent flow conditions. The diversity of the derived relationships arises from considering surface mobility and fluid turbulence as well as the average flow parameters. These predicted relationships have not been extended to include the effect of particle interaction, but for low dispersed phase volume fractions in turbulent flow this effect is considered negligible.

In this work the overall mass transfer coefficient is shown to be substantially controlled, within the measurement error, by the continuous phase film resistance. Calculated corrections for the mass transfer, occurring before the dispersed phase fragments, and after the dispersion leaves the mixing vessel, are subtracted from the total measured transfer, to obtain the transfer due to the continuous phase turbulence in the mixer.

The scatter in the mass transfer data arises from two sources: the errors in solute concentration analysis and the errors in interfacial area estimation. The interfacial area was calculated from smoothed curves of the mean particle diameter d_{sv}, and the holdup ϕ, but errors due to a lack of uniformity in the dispersion at low mixer power inputs, and inadequate analysis techniques at high mixer power inputs still occur.

The mass transfer-velocity relationship obtained when both phases are considered to be fully mixed, and when only the continuous phase is fully mixed, substantiates the conclusion that the dispersed phase does not coalesce in the mixer, see Section 5.11.

The experimental mass transfer correlation found,

$$COI = 4.10 \times 10^{-6} (ND_I)^{1.36} \frac{1}{D_T{}^{.5}} - 0.012 \quad , \quad 10^4 < Re_{Imp} < 10^5$$

MKH units

approaches that predicted using interface mobility and turbulent boundary layer mechanisms. Interface mobility,

which influences the continuous phase transfer rate, is shown to arise from viscous drag in the boundary layer leading to partial internal circulation of the drops. The mechanism of drop interface mobility is necessary to interpret the differences in the transfer data for liquid-liquid extraction, and the data for solids dissolution, in the same mixing vessels, for the same solute and continuous phase.

The experimental data do not indicate whether the impellor diameter or the vessel diameter is the correlating length in the Sherwood number. The particle diameter, which is predicted to be necessary for the correlation of transfer data for drops with surface mobility and a turbulent boundary layer, does not appear in the experimental relationship. The diameter effect, if real, is considered to be diminished by the range of particle sizes and turbulence eddy lengths. The dimensional term $\frac{1}{D_T^{.5}}$ is found to correlate the transfer data rather than the predicted term $\frac{1}{D_I^{.5}}$. Dimensionally, these terms are similar, but the vessel diameter term found in this work shows that the mass transfer, although predominantly occurring in the impellor region, also occurs in the bulk vessel.

Experimental measurements of mass transfer with particles or drops in controlled, steady flow conditions, are shown to be inadequate for predicting transfer from particles or drops in a mixer. The mean fluid velocity controls transfer with a held particle, whereas the inertial subrange turbulence controls the mass transfer from a particle or a drop moving with the bulk flow. The controlled flow experiments, however, do yield information about bulk flow and surface behaviour. In contrast, stirrer cells appear to be satisfactory mixing vessel models, for mass transfer rates.

The dependence of the mass transfer coefficient on the solution properties is predicted in surface renewal models and boundary layer theories. With turbulent boundary layers, the relationship derived is dependent on the viscous damping

postulate considered. The effect of solution properties on the mass transfer rates is not investigated in this work, so these parameters are not included in the experimental correlations obtained.

Section 8

MIXING VESSEL DESIGN

This thesis, by surveying existing literature and presenting new data, has shown mixing vessel processes to be controlled by the fluid motion. Dimensional relationships derived from the concepts of local isotropy in turbulent motion, correlate data for power dissipation, particle size, coalescence rate, dispersed phase entrainment, and continuous phase mass transfer rates in a mixer. These relationships have involved order of magnitude approximations which render them suitable either for scale-up or data correlation, but direct mixer design from first principles is not yet possible.

Published correlations of mixer data suggest a turbulence theory approach, but secondary system properties often alter the rate-controlling mechanism, rendering the predicted correlation invalid. The data obtained in this work for the system isooctane/o-nitrophenol/water, may be correlated by the relationships predicted from turbulence theory. This system, however, has introduced properties that may be considered to be uncommon for most extraction systems. These properties are summarised:

1. Low rates of mass transfer, with most of the transfer resistance in the continuous phase boundary layer.
2. No interaction of material when it is being transferred through the interface.
3. Interface mobility and partial internal drop circulation occur, which are related to the absence of surfactants in the system.
4. No interfacial turbulence is caused by surface tension gradients induced by mass transfer.

5. In the mixer the continuous phase is fully mixed, but the dispersed phase is substantially unmixed.

The power dissipation data obtained in this work do not extend the understanding of this process. The problems are shown to be more complex than is apparent from the literature.

The correlations of particle size, distribution, and coalescence rates, although not extended to industrial-sized mixers, are established for pilot scale mixers. A knowledge of particle sizes is important not only in the estimation of extractor efficiency, but in the prediction of emulsification and solvent losses, through entrainment of smaller particles.

It is unlikely that total non-coalescence of the dispersed phase will occur in industrial mixing vessels, but some degree of 'unmixedness' will occur with low dispersed phase hold-up, or low power inputs.

The mass transfer dependence on the impellor Reynolds number is uncommonly high, but boundary layer relationships suggest that this and other high Reynolds number correlations that have been obtained, show real effects. The mechanism of internal drop circulation for the system used in this work is unlikely to occur industrially, but high transfer rates caused by surface tension gradients are a likely occurrence.

Thus, the exact prediction of mixer processes from first principles, has not been achieved; but if the interfacial behaviour of an extraction system is known, the relationships derived from turbulence theory will enable more exact scale-up of an existing process, or translation from one system to another.

Section 9

NOMENCLATURE

Roman alphabet, small letters

a	Particle radius
a_{cr}	Critical drop radius for fragmentation
b	Hydrodynamic constant
b_1, b_2	Renewal theory constants
c	Solute concentration
c_b	Solute concentration in the bulk solution
c_o	Solute concentration at the interface
c_{δ_d}, c_{δ_o}, c_δ	Solute concentrations at distances δ_d, δ_o, δ, from an interface
c^*	Equilibrium concentration of the solute at the interface.
d	Mean diameter of a particle size range, subscript indicates the number percentage of drops which are smaller than this size.
d_f	Drop diameter at the end of the drop formation period
e_s	Extraction stage efficiency
f	Correlation coefficient
g	Correlation coefficient
g_c	Gravtational constant
h	Minor axis of drop as an ellipsoid
k	Wave-number
k'	Derivative of k
k_c	Mass transfer coefficient for the continuous phase
k_d	Mass transfer coefficient for the dispersed phase.
k_f	Drag coefficient for skin friction
k_l	Large scale generated wave-number
k_o	Energy dissipation wave-number
l	Length dimension

m	Reynolds number exponent
m_d	Solute distribution coefficient
n	Schmidt number exponent, normalised number-fraction of particles in a size increment.
n_c	Number of collisions of particles of radius a with those of radius r per unit time and volume
n_o	Number of particles per unit volume
p	Pressure
Δp	Pressure difference
q	Major axis of a deformed drop as an ellipsoid
r	Radial direction, radius of drop, space vector
t	Time
t_f	Time required for drop formation
t_i	Characteristic time for displacement of material in a drop
t_{95}	Liquid residence time in a mixer to reach 95% of the equilibrium concentration, after a step change in the inlet conditions.
u	Velocity at a point
u_{cr}	Critical velocity for particle fragmentation
u_y	Velocity component in a vertical direction
u_1, u_2	Velocity of liquid in surface renewal zones 1 and 2.
Δu	Change in velocity at a point with time
v	Slip velocity of the liquid with respect to a partially entrained particle.
v_{max}	Maximum slip velocity of the liquid with respect to a partially entrained particle
v_o	Skin friction velocity
v_r	Velocity component in the radial direction, r
v_t	Terminal velocity of a particle in a stagnant fluid
v_λ	Velocity change in an eddy of wave-length λ .
v'	Velocity of internal circulation for a drop
w_i	Volume fraction of dispersed phase coalesced per minute.
w_x	Velocity component in the tangential direction x
x	Tangential direction
x_1, x_2	Liquid contact lengths for surface renewal models

y	Vertical direction, distance out from a wall
y^*	Dimensionless distance, $= \frac{v_o y}{\nu} \sim y/\delta_o$
z_1, z_2	Depths of renewal liquid zones in surface renewal theories

Roman alphabet, capitals

A	Interfacial area of dispersion per unit volume
B_b	Width of a single baffle
B_I	Width of an impellor blade
C	Const. constants
CIN	Solute concentration (o-nitrophenol) in the inlet dispersed phase (isooctane).
CIT	Solute concentration (o-nitrophenol) in the outlet dispersed phase (isootance).
CO	Continuous phase mass transfer coefficient, based on each phase being fully mixed, in the mixer.
COA	CO x Interfacial area (coefficient)
COI	Continuous phase mass transfer, based on the continuous phase being fully mixed and the dispersed phase being not mixed, in the mixing vessel.
COIA	COI x Interfacial area
CWN	Solute concentration in the continuous phase at the vessel inlet.
CWT	Solute concentration in the continuous phase at the vessel outlet.
D_F	Diameter of flow path
D_I	Impellor diameter
D_O	Characteristic energy transfer function
D_P	Diameter of a particle
D_T	Diameter of a mixing vessel
DAB	Solute diffusion coefficient, o-nitrophenol in water
DENI	Density of the isooctane phase
DENW	Density of the aqueous phase
$\overline{DF}$	Average driving force for mass transfer
E	Energy spectrum of wave numbers
F	Shear force, skin friction drag on a surface

F_a	Force of adhesion of two drops, distance h_o apart
F_{react}	Supplemental drag force for an accelerating particle
FLOI	Flow of isooctane phase to the mixer (volume/time)
FLOW	Flow of aqueous phase to the mixer, (volume/time)
Fr	Froude number = $\frac{DN^2}{g}$
G	Liquid flow rate
H_I	Impellor height off the bottom of the mixing vessel
H_T	Height of liquid in the mixing vessel
I	Total mass transferred from a drop per unit time
J	Mass transfer flux
K	Overall mass transfer coefficient per unit interfacial area
K_D	O-nitrophenol dissociation constant
Ka	Overall mass transfer coefficient
L	Characteristic length dimension of a drop
L_b	Length of a turbine impellor blade
L_p	Eulerian coefficient or the longitudinal integral scale
N	Stirrer speed
N_A	Number of mols. of A transferred per unit time
N_{AY}, N_{BY}	Number of mols. of A or B transferred in the y direction per unit time
N_o	Total number of particle collisions in unit volume per unit time
P	Power input to the mixing vessel
Po	Power number, = $\frac{Pg_c}{D_I^5 N^3 \rho}$
Q	Pressure difference between two points
R	Regression coefficient
R_{ij}	Velocity correlation tensor
Re	Reynolds number = $\frac{v.2a.\rho}{\nu}$ = Re_{drop} $\frac{ND_I^2 \rho_{Soln}}{\nu_{soln}}$
Re_{Imp}	Reynolds number of the impellor =

$Re\lambda_o$	Reynolds number of dissipation eddy lengths, ~ 1
S	Unit surface area
S_a	Cross section area of a drop
S_b	Pitch of impellor blades
Sc	Schmidt number = $\nu/\mathfrak{D}$
Sh	Sherwood number, for particles, = $\frac{k_c\, 2a}{\mathfrak{D}}$
Sh_{Imp}	Sherwood number based on the impellor diameter, = $\frac{k_c D_I}{\mathfrak{D}}$
Sh_T	Sherwood number based on the tank diameter, = $\frac{k_c D_T}{\mathfrak{D}}$
St	Stanton number, = Sh. Re^{-1}. Sc^{-1}.
T	Agitator torque
T_p	Period of motion of particles in a turbulent flow
TEMP	Temperature, ^oC
U	Average velocity of the fluid at a point
U_p	Fluid velocity profile next to a surface
V	Volume of a particle
V_v	Volume of a mixing vessel
VISI	Viscosity of the isooctane phase
VISW	Viscosity of the aqueous phase
W	Energy transfer function
We	Weber number, = $\frac{\rho v^2 l}{\sigma}$

Greek alphabet

α	Hydrodynamic constant
β	Hydrodynamic constant
β_1, β_2, β', β''	Constants for the surface renewal theories
γ	Hydrodynamic constant
$\mathfrak{D}$	Diffusion coefficient
δ	Mass transfer boundary layer thickness
δ_d	Buffer layer thickness
δ_o	Hydrodynamic boundary layer thickness

ϵ	Energy transfer rate per unit fluid volume
ϵ_{av}	Average energy dissipation rate per unit volume
ϵ_o	Energy dissipation rate per unit volume, at the wave-length λ_o.
θ	Liquid residence or contact time
θ_1, θ_2	Liquid contact times in surface renewal theories
λ	Eddy wave-length, distance
λ_1	Wave-length of large scale, or generated eddies
λ_o	Wave-length of dissipation eddies
μ	Fluid viscosity
ν	Fluid kinematic viscosity
ρ	Fluid density
ρ_{sol}	Density of a two phase solution
σ	Interfacial tension
σ_g	Standard deviation
τ	Shear stress
ϕ	Volumetric fraction of dispersed phase
ϕ_f	Volumetric fraction of the dispersed phase in the inlet flow to a mixing vessel
ϕ_s	Shape factor of a particle
ψ	Fluctuations of concentration about a mean
Ψ	Final or mean fluid concentration
ω_λ	acceleration of particles, size λ.

Superscripts

$\bar{}$	Average value
$'$	Circulating drop

Subscripts

c	Continuous phase
d	Dispersed phase
Imp	Impellor
T	vessel
turb	Turbulent
λ	With respect to eddy length λ.

Section 10

BIBLIOGRAPHY

1. Acrivos, A., "Modern Chemical Engineering", Volume 1, Reinhold Publishing Corporation (1963).
2. Aiba, S., A.I.Ch.E. Journal, 4, 485 (1958).
3. Barker, J.J. and Treybal, R.E., A.I.Ch.E. Journal, 6, 289 (1960).
4. Batchelor, G.K., Proc. Roy. Soc. (Lon)., A 195, 513 (1949).
5. Batchelor, G.K., "Homogeneous Turbulence", Cambridge University Press (1953).
6. Bates, R.L., Fondy, P.L. and Corpstein, R.R., Ind. Eng. Chem. fund., 2, 311 (1963).
7. Berestovai, A.M. and Romanov, P.G., Zhur. Priklad, Khim., 38, 319 (1965).
8. Biggs, R.D., A.I.Ch.E. Journal, 9, 636 (1963).
9. Bird, R.B., Stewart, W.E. and Lightfoot, E.N., "Transport Phenomena" John Wiley & Sons, Inc. (1960).
10. Boussinesq, J., Maths Pure Appld., 6, 285 (1905).
11. Boye-Christensen, G. and Terjeson, S.G., Chem. Eng. Sci., 7, 22 (1958), 9, 225 (1959).
12. Burawoy, A. and Chamberlain, J.T., J. Chem. Soc., 155, 2310, 3734 (1952).
13. Calderbank, P.H., Trans. Inst. Chem. Engrs., 36, T443 (1958).
14. Calderbank, P.H., Trans Inst. Chem. Engrs., 37, T173 (1959).
15. Calderbank, P.H. and Moo-Young, M.B., Chem. Eng. Sci, 16, 39 (1961).
16. Corrsin, S., A.I.Ch.E. Journal, 3, 329 (1957).
17. Corrsin, S., A.I.Ch.E. Journal, 10, 870 (1964).
18. Corrsin, S. and Uberoi, M.S., Natl. Advisory Comm. Aeornaut. Tech. Rept., No. 998 (1950).
19. Cutter, L.A., Eng. Sci. Doc. thesis, Columbia Univ., New York, (1960).

20. Davies, J.T., Chem. Eng. Sci., 16, 55 (1961).

21. Davies, J.T. and Waggill, J.B., Proc. Roy. Soc. (Lon.) A 255, 277 (1960).

22. Denbigh, K., "The Principles of Chemical Equilibrium", University Press, Cambridge (1961).

23. Deryagnin, B., Kolloidzschr, 69, 135 (1934).

24. Dobbie, T.P., B.E. Project Report, Dept. of Chem. Eng., University of Canterbury, N.Z., (1964).

25. Drew, T.B., Hopes, J.W. and Vermeulen, T., editors, "Advances in Chemical Engineering" Vol.4., Academic Press, New York, (1963).

26. Drickamer, H.G., Scott, E.J. and Tung, L.H., J. Chem. Phys., 19, 1075 (1951), 20, 6 (1952).

27. Eagleson, P.S., Huval, D.J. and Perkins, F.E., Mass. Inst. Technol. Hydrodynamics Lab., Tech. Rept. No. 46. (1961).

28. Farrier, P.M., B.E. Project Report, Dept. of Chem. Eng., Univ. of Canterbury, N.Z. (1965).

29. Flynn, A.W. and Treybal, R.E., A.I.Ch.E. Journal, 1, 324 (1955).

30. Fox, E.A. and Gex, V.E., A.I.Ch.E. Journal, 2, 539 (1956).

31. Garner, F.H., J. App. Chem., 9, 315 (1959).

32. Garner, F.H. and Lane, G.G., Trans. Inst. Chem. Engrs., 37, 162 (1959).

33. Ghosh, G.N. and Perlmutter, D.D., A.I.Ch.E. Journal, 9, 474 (1963).

34. Glasstone, S., Laidler, K.J. and Eyring, H., "The Theory of Rate Processes", McGraw-Hill Book Co. Inc., New York, (1941).

35. Goldstein, S., "Modern Developments in Fluid Dynamics", Vol.I and II, Clarendon Press, Oxford, (1938).

36. Groothius, H. and Zuiderweg, F.J., Chem. Eng. Sci., 12, 288 (1960).

37. Groothius, H. and Zuiderweg, F.J., Chem. Eng. Sci., 19, 63 (1964).

38. Handlos, A.E. and Baron, T., A.I.Ch.E. Journal, 3, 127 (1957).

39. Harriott, P., Can. Jour. Chem. Eng., 40, 60 (1962).

40. Harriott, P., A.I.Ch.E. Journal, 8, 93 (1962).

41. Harriott, P., Chem. Eng. Sci., 17, 149 (1962).

42. Heizenberg, W.Z., Proc. Roy. Soc. (Lon.), A195, 402 (1948).

43. Hennico, A. and Vermeulen, T., A.I.Ch.E. Journal 8, 394 (1962).

44. Higbie, R., T.Am.I.Ch.E., 31, 365 (1935).

45. Hinze, J.O., A.I.Ch.E. Journal, 1, 289 (1955).

46. Hixon, A.W. and Smith, I.M., Ind. Eng. Chem., 41, 973 (1949).

47. Hodgman, C.D., editor, "Handbook of Chemistry and Physics", 40th edn., Chemical Rubber Publishing Co., Cleverland, Ohio, (1958-59).

48. Hooker, T., Chem. Eng. Prog., 44, 837 (1948).

49. Howarth, W.J., Chem. Eng. Sci., 19, 33 (1964).

50. Huttig, G.F. and Stadler, H., Monatsch, 88, 150 (1957).

51. Jeffreys, G.V. and Hawksley, J.L., A.I.Ch.E. Journal, 11 413 (1965).

52. Kafarov, V.V. and Babanov, B.M., Zhur. Priklad, Khim., 32, 789 (1959).

53. Von Karman, T. and Lin, C.C., Rev. Modern Phys., 21, 516 (1949).

54. Karr, A.E. and Scheibel, E.G., Chem. Eng. Prog. Symp. No. 10, 73 (1954).

55. Keey, R.B. and Glen, J.B., Can. Jour. Chem. Eng., 42, 227 (1964).

56. Kim, W.J. and Manning, F.S., A.I.Ch.E. Journal 10, 747 (1964).

57. Kishinevskii, M.Kh. and Kornienko, T.S., Zhur. Priklad. Khim., 36, 1008, 2681 (1963).

58. Kneule, F., Chem. Ing. Tech., 28, 221 (1956).

59. Kolmogoroff, A.N., Doklady Akad. Nauk., S.S.S.R. 66,825 (1949).

60. Kolmogoroff, A.N., C.R. Acad. Sci. S.S.S.R. 30, 31 (1941), see Batchelor, ref. 5.

61. Kramers, H., Baars, G.M. and Knott, W.H., Chem. Eng. Sci., 2, 1 (1953).

62. Laity, D.S. and Treybal, R.E., A.I.Ch.E. Journal, 3 176 (1957).

63. Levich, V.G., "Physicochemical Hydrodynamics", Prentice-Hall, Inc. Englewood Cliffs, N.J. (1962).

64. Lewis, J.B., Chem. Eng. Sci., 3, 248, 260 (1954).

65. Licht, W. and Conway, J.B., Ind. Eng. Chem., 42, 1151 (1950).

66. Lin, C.C., First Symp. Appl. Math., Am. Math. Soc.,(1947).

67. Lin, C.C., Moulton, R. and Putnam, G., Ind. Eng. Chem., 45, 636 (1953).

68. Mack, D.E. and Kroll, A.E., T. Am.I.Ch.E., 44, 189,(1948).

69. McManamey, W.J., Chem. Eng. Sci., 15, 251 (1961).

70. Madden, A.J. and Damerell, G.L., A.I.Ch.E. Journal, 8, 233 (1962).

71. Madden, A.J. and Nelson, D.G., A.I.Ch.E. Journal, 10, 415 (1964).

72. Manning, F.S. and Wilhelm, R.N., A.I.Ch.E. Journal, 9, 12 (1963).

73. Marangozis, J. and Johnson, A.I., Can. Jour. Chem. Eng., 40, 231 (1962).

74. Matsuzawa, H. and Migauchi, T., Kagaku Kogaku, 25, No.8 582 (1961).

75. Mattern, R.V., Bilous, O. and Piret, E.L., A.I.Ch.E. Journal, 3, 497 (1957).

76. Metzner, A.B. and Taylor, J.S., A.I.Ch.E. Journal, 6, 109 (1960).

77. Miller, R.S., Ralph, J.L., Curl, R.L. and Towell, G.D. A.I.Ch.E. Journal, 9, 196 (1963).

78. Miller, S.A. and Mann, C.A., T.Am.I.Ch.E., 40, 709 (1944).

79. Misek, T., Collection Czeck. Chem. Comm., 29, 2089 (1964).

80. Murphy, N.F., Lastovica, J.E. and Skrzec, A.E., A.I.Ch.E. Journal, 2, 451 (1956).

81. Nagata, S. and Yamaguchi, I., Mem. Fac. Eng., Kyoto Univ., 22, 249 (1960).

82. Nagata, S. Yamaguchi, I., Yabetta, S. and Havanda, M., Kagaku Kogaku, 24, 618 (1960).

83. Nagata, S., Yokoyama, T. and Maeda, H., Mem. Fac. Eng., Kyoto Univ. Japan, 18, 13 (1956).

84. Nagata, S., Yoshioka, N., Yokoyama, T. and Teramoto, D., Trans. Soc. Chem. Engrs. (Japan), 8, 43 (1950).

85. Naor, P. and Shinnar, R., Ind. Eng. Chem. (fund.), 2, 278 (1963).

86. Nielson, H.J., See Cutter, L.A., see ref. 19.

87. O'Connel, F.D. and Mack, D.E., Chem. Eng. Prog., 46, 358 (1950).

88. Olander, D.R. and Reddy, L.B., Chem. Eng. Sci., 19, 67 (1964).

89. Olney, R.B. and Carlson, G.J., Chem. Eng. Prog., 43, 473 (1947).

90. Overcashier, R.H., Kingsley, H.A. and Olney, R.B., A.I.Ch.E. Journal, 2, 529 (1956).

91. Pavlushenko, I.S., Braginskii, L.N. and Brylov, V.D., Zhur. Priklad, Khim., 34, 805 (1961).

92. Pavlushenko, I.S. and Yanishevskii, A.V., Zhur. Priklad. Khim., 31, 1348 (1958).

93. Pavlushenko, I.S. and Yanishevskii, A.V., Zhur. Priklad. Khim., 32, 1495 (1959).

94. Perry, J.H., editor, "Chemical Engineers Handbook", McGraw-Hill Book Company, Inc., (1950).

95. Popovich, A.J., Jervis, R.E. and Trass, O., Chem. Eng. Sci., 19, 357 (1964).

96. Prandtl, L., "Essentials of Fluid Mechanics", Blackie, London (1952).

97. Preen, B.V., Ph.D. thesis, Univ. of Durham, S.A., (1961), see Westerterp, K.R., van Dierendonck, L.L. and de Kraa, J.A., Chem. Eng. Sci., 18, 157 (1963).

98. Rhodes, J.M. and Peebles, F.N., A.I.Ch.E. Journal, 11, 481 (1965).

99. Rice, A.W., Toor, H.L. and Manning, F.S., A.I.Ch.E. Journal, 10, 125 (1964).

100. Robinson, J.V., J. Phys. Coll. Chem., 53, 1042 (1949).

101. Rodger, W.A., Trice, V.G. and Rushton, J.H., Chem. Eng. Prog., 52, 515 (1956).

102. Rodriquez, F., Grotz, L.C. and Engle, P.L., A.I.Ch.E. Journal, 7, 663 (1961).

103. Rosenweig, R.E., A.I.Ch.E. Journal, 10, 91 (1964).

104. Rowe, P.N., Claxton, K.T. and Lewis, J.B., Trans. Inst. Chem. Engrs., 43, T14 (1965).

105. Ruckenstein, E., Chem. Eng. Sci., 18, 231 (1963).

106. Ruckenstein, E., Chem. Eng. Sci., 19, 131 (1964).

107. Ruckenstein, E. and Berbente, C., Chem. Eng. Sci., 19, 329 (1964).

108. Rushton, J.H., Costich, E.W. and Everett, H.J., Chem. Eng. Prog., 46, 395 (1950).

109. Rushton, J.H. Nagata, S. and Rooney, T.B., A.I.Ch.E. Journal, 10, 298 (1964).

110. Sach, J.P. and Rushton, J.H., Chem. Eng. Prog., 50, 597 (1954).

111. Setzer, H.J. and Treybal, R.E., Symp. on Bubble and Drop Phenomena, II, A.I.Ch.E., (1963).

112. Shain, S.A. and Prausnitz, J.M., A.I.Ch.E. Journal, 10, 766 (1964).

113. Sherwood, T.K. and Wei, J.C., Ind. Eng. Chem., 49, 1030 (1957).

114. Shinnar, R., Jour. Fluid. Mech., 10, 256 (1961).

115. Shinnar, R. and Church, J.M. Ind. Eng. Chem., 52, 253 (1960).

116. Shinnar, R. and Church, J.M., Ind. Eng. Chem., 53, 479 (1961).

117. Sleicher, C.A., A.I.Ch.E. Journal, 6, 529, (1960).

118. Smith, A.R., Caswell, J.E. and Larsons, P.P., Can. Jour. Chem. Eng., 41, 150 (1963).

119. Staffin, K. and Ju Chin Chu., A.I.Ch.E. Journal, 10, 98 (1964).

120. Sternling, C.V. and Scriven, L.E., A.I.Ch.E. Journal, 5, 514 (1959).

121. Taylor, G.I., Proc. Roy. Soc. (Lon.) A138, 41 (1932).

122. Taylor, G.I., Proc. Roy. Soc. (Lon.) A164, 476 (1938).

123. Tchen, C.M., J. Res. Natl. Bur. Standards, 50, No. 1, 51 (1953) See ref. 56.

124. Tennant, B.W., M.Sc. Thesis, Illinois Inst. Technol, Chicago, (1952), see ref. 19.

125. Thorsen, G. and Terjeson, S.G., Chem. Eng. Sci., 17, 137 (1962).

126. Toor, H.L. and Marchello, J.M., A.I.Ch.E. Journal, 4, 97 (1958).

127. Toor, H.L. and Marchello, J.M. Ind. Eng. Chem. fund., 2, 8 (1963).

128. Torobin, L.B. and Gauvin, H., Can. Jour. Chem. Eng., 38, 189 (1960).

129. Treybal, R.E., A.I.Ch.E. Journal, 4, 202 (1958).

130. Treybal, R.E., Ind. Eng. Chem., 53, 592 (1961).

131. Treybal, R.E., "Liquid Extraction", 2nd edn., McGraw-Hill Book Company, Inc., (1963).

132. Vermeulen, T., Williams, G.M. and Langlois, G.F., Chem. Eng. Prog., 51, 85F (1955).

133. Voot, J., B.E. Project Report, Dept. of Chem. Eng., Univ. of Canterbury, N.Z., (1963).

134. van de Vusse, J.G., Chem. Eng. Sci., 4, 178, 209 (1955).

135. van de Vusse, J.G., Chem. Eng. Sci., 17, 507 (1962).

136. White, A.McL. and Sumerford, G.D., Chem. and Met. Eng., 43, 370 (1936).

137. Wilkes, C.R. and Pin Chang, A.I.Ch.E. Journal, 1, 264 (1955).

138. Zheleznyak, A.S. and Brounshtein, B.I., Zhur, Priklad. Khim., 36, 2437 (1963).

Keey, R. B., & Glen, J. B. (1964). Mass transfer from solid spheres. The Canadian Journal of Chemical Engineering, 42(5), 227-232

Glen, J. B., & Keey, R. B. (1965). Mass transfer by forced convection at the front pole of a sphere. Chemical Engineering Science, 20(5), 444-447.

APPENDIX 3

COMMENTS ON "HEAT AND MASS TRANSFER IN AN EXTENSIVE FLOWING FLUID", BY P.N. ROWE AND CO-WORKERS[1]

by R.B. KEEY, B.Sc., PH.D. (Associate Member)* and
J.B. GLEN, B.E., B.Sc*

In a recent paper, Rowe, Claxton and Lewis[1] survey published data on heat and mass transfer from single spheres mainly in the range $10 < \underline{Re} < 10^4$ and have described new experiments over a more limited range ($20 < \underline{Re} < 2000$). The present note discusses several points that arise from that paper and, particularly, that transport rates from bluff bodies are sensitive to the intensity of turbulence of the continuous medium.

The authors are to be congratulated on their extensive overview which should prove of great value to workers interested in transport phenomena around isolated spheres. However, it is disappointing to see mass-transfer coefficients defined in an analogous way to heat-transfer coefficients without any comment on the limitations of the definition. Not only must it be assumed that the fluid properties be constant, as pointed out by the authors, but also if the analogy between the transport processes is to be maintained then the bulk-flow effects must be negligible and the solute concentrations small[2]. While such conditions may have prevailed in the experiments described by Rowe et al, those wishing to use their data should be forewarned of such limitations.

There appear to be some misconceptions about the experimental work done by the late Professor Garner and one of us (R.B.K.)[3]. An air-lift pump was not used for recirculating the liquid; a small centrifugal pump was used and the air-lift was employed solely for raising the water into the tunnel at start-up. Evolution of air did not appear to be a problem; bubbles of radii greater than 0.001 in. could be detected by the experimental techniques employed. The theoretical equation developed was composed with Garner and Suckling's[4] data (for the range $80 < \underline{Re} < 900$) and the agreement between theory and experiment was invoked to justify the use of the theoretical equation as a datum. The criticism of the choice of diffusivity is difficult to understand, for Wilke and Chang's[5] correlation predicts values intermediate in magnitude to the two ranges of values proposed by Rowe and coworkers[1].

The authors note that the loss in weight could be measured to within $\pm$ 0.5 mg and that weight losses due to handling and other factors were less than this. As this error is about 1/10,000th of the sphere mass for a $\frac{1}{2}$" diameter sphere, great care must have been exercised in handling the spheres after exposure to the fluid. While the velocity

measurements are less critical, if the data are to be regressed in terms of the square root of the velocity, some indication of the repeatability of the velocity determinations would be helpful, especially as six experimenters were involved. For example, in the dye-trace method of finding the water velocities was diffusion of the trace a problem, as the residence time in the water-trough could be nearly 6 minutes at the lowest flows? In the wind-tunnel experiments, as the calibration of the sliding outlet valve was presumably non-linear, what flow reproducibility was possible at the highest velocity of 3 ft/sec?

More significantly there appears to be a dichotomy between the authors' comments in the discussion and their remarks in the previous sections of their paper. Initially the authors are concerned to show that whenever a Reynolds number index $n \neq \frac{1}{2}$ is reported, either such an exponent is explicable through experimental error, or the data would be equally well correlated by $n = \frac{1}{2}$. For example, in Table III they set out to show that the differences in the residual error variances for the least-square equations for their data over the range $0.4 < n < 0.6$ are not significant compared with the F-test for 73 degrees of freedom at the 5 and 1% probability levels. In the discussion, however, the authors state: "In spite of the scatter and uncertainty surrounding the exponent there is no doubt that it increases with Reynolds Number."

This conclusion is obtained by a general observation "that the 'best' exponent tends to increase with the average value of Reynolds number in the range explored", the increasing influence of the wake at higher Reynolds numbers and the variation of total drag with Reynolds number. In view of the statistical evidence adduced by the authors, little weight presumably can be given to the change of the "best" exponent with Reynolds number.

The quantitative effect of increasing wake transfer with increasing Reynolds number is difficult to predict. There is some evidence[6] to suggest that

$$\underline{Sh} = \left[B_1 \ \underline{Re}^{\frac{1}{2}} + B_2 \ \underline{Re}^{\frac{2}{3}} \right] \underline{Sc}^{\frac{1}{3}} \qquad (1)$$

and that the latitude at which separation of the forward flow occurs is given by

$$\theta_s = 83 + 191 \ \underline{Re}^{-\frac{1}{3}} \qquad (2)$$

The first term in equation (1) derives from the contribution for the forward-flow area and the second term from that aft of separation. Since below $\underline{Re} \sim 10^5$ the average transfer flux over the forward flow area is some 60% greater than the average flux in the wake[4] it seems likely that $B_1 \gg B_2$. Inspection of both equations (1) and (2) would suggest the variation of a lumped exponent n is small up to $\underline{Re} \sim 10^4$.

The analogy between drag force and heat (or mass) transfer cited by the authors is not wholly convincing. It appears that the authors have calculated the exponent for velocity from the total drag on a sphere, but changes in form-drag coefficient are insignificant only in the range $10^4 < \underline{Re} < \underline{Re}_{crit}$. Further, the analogy between momentum and heat (or mass) transfer is unacceptable unless:

(a) the flow is one-dimensional
(b) $\underline{Pr}$ (or $\underline{Sc}$) ~ 1, so that the hydrodynamic and heat- (or mass-) transfer boundary-layers are nearly equal.

On the other hand, there is some evidence[6] from boundary-layer theories to suggest that the exponent n is a function of Reynolds number.

TABLE 1

Theoretical Values of Reynolds Number Exponent

n	Re Range	Theoretical Assumptions
$\frac{1}{3}$	1	Thin mass-transfer boundary layer.
$\frac{1}{2}$	$10^2 - 10^4$	Laminar flow, thin hydrodynamic and mass-transfer boundary layers.
$\frac{2}{3}$	$10^3 - \underline{Re}_{trans}$	Molecular and eddy diffusivities additive.
1	$\underline{Re}_{trans}$	Equating of molecular and eddy diffusivities defines the edge of the mass-transfer boundary layer.

The Reynolds number limits given in Table 1 are only approximate, for they depend on the free-stream and boundary-layer turbulence intensities as well as the Reynolds number of the averaged flow.

No precise data of $\underline{Sh}$ vs $\underline{Re}$ for spheres showing the above effect are available, but the data of Hilpert[8], which appear to have been obtained with care, for heat transfer from cylinders in cross-flow (Fig. 1) show a trend similar to that in Table 1 for turbulence intensities $\simeq 0.9\%$.

Curiously, heat transfer from spheres with varying incident turbulence has not been investigated, while considerable work has been done with cylinders and flat plates. Kestin, Maeder and Wong[9] found that changes of free-stream turbulence cause large variations in Nusselt number over flat plates when there is a pressure gradient in the boundary layer opposing the flow. For cylinders, Kestin, Maeder and Sogin[10] show a 40% increase in Nusselt number at the high but subcritical $\underline{Re} = 1.4 \times 10^5$ for turbulence intensities increasing from 1% to 2.2%. For $3 \times 10^3 < \underline{Re} < 3 \times 10^4$, a 70% Nusselt number shift is found by comparing Griffiths and Auberry's[11] data

obtained in the NPL wind-tunnel of rather high turbulence intensity with Hilpert's data in a low-intensity tunnel.

For spheres, heat (and mass) transfer rates from the front pole appear to be very sensitive to free-stream disturbances[12] for $5 \times 10^2 < \underline{Re} < 3 \times 10^4$: even the small-scale disturbances produced by straightening gauzes appear to be sufficient to influence significantly the transfer rates from the leading area of a sphere

In Rowe and coworkers' literature survey it is noted that Yuge[13] required two equations to describe his heat-transfer results.

$$\underline{Sh} = 2 + 0.493\ \underline{Re}^{0.5}, \quad 10 < \underline{Re} < 1.8 \times 10^3$$

$$\underline{Sh} = 2 + 0.30\ \underline{Re}^{0.5664}, \quad 1.8 \times 10^3 < \underline{Re} < 1.5 \times 10^5$$

The break at $\underline{Re} = 1.8 \times 10^3$ coincides with the change to the largest of the three wind tunnels. The kink could result from increased turbulence intensity in the longer tunnel for $\underline{Re} > 1.8 \times 10^3$ and similar discontinuities are detectable in Hilpert's data. Systematic Nusselt number differences between distributed and parabolic flows may be seen in the work on Garner and Suckling[4]. This also has been attributed to free-stream turbulence generated by the distributing screens[12]. For heat transfer to air, water and oil, Kramers[14] finds

$$\underline{Nu} = 2 + 1.3\ \underline{Pr}^{.15} + 0.66\ \underline{Re}^{\frac{1}{2}}\ Pr^{\frac{1}{3}}$$

The second term Rowe and coworkers suggest, with some evidence, is due to "inadvertent disturbance of the denser fluids by the H.F. field". The source of turbulence is not important to this discussion, but rather that turbulence in continuous media enhances transfer processes with spheres. The alternative explanation, that fluid properties change near the sphere, may be an additional consideration, as pointed out by Rowe and coworkers.

The data presented by Rowe and coworkers were obtained from a wind-tunnel and a water-trough operated with different flow straighteners, fluid velocities and differing geometries. While the authors state that both their flow straighteners gave a steady flow field for the working velocities, it seems possible from the limited constructional details given that the water-trough generated small-scale turbulence of greater scale and lower wave-number than the wind-tunnel.

Thus, if the postulate that free-stream turbulence enhances heat- (and mass-) transfer rates around spheres is accepted, then Rowe's data could be interpreted by differences in levels of turbulence rather than by errors in solution properties.

Nomenclature

B_1, B_2	constants in equation (1)
C	intercept of log Sh vs log Re plot
n	Reynolds number exponent (= [log Sh - C] /log Re)
Nu	Nusselt number
Pr	Prandtl number
Re	Reynolds number based upon sphere diameter and averaged incident flow
Re_{crit}	Reynolds number as above when latitude for separation increases due to boundary-layer turbulence
Re_{trans}	Reynolds number as above for transition from laminar to turbulent flow in the boundary layer
Sc	Schmidt number
Sh	Sherwood number
θ_s	Latitude for separation of forward flow

References

1. Rowe, P.N., Claxton, K.T., and Lewis, J.B., Trans. Instn Chem. Engrs, 1965, 43, T14.
2. Bird, R.B., Stewart, W.E., and Lightfoot, E.N., Transport Phenomena. 1960, p.637 (New York: Wiley & Sons Inc.)
3. Garner, F.A., and Keey, R.B., Chem. Engrg. Science, 1958, 9, 119.
4. Garner, F.A., and Suckling, R.D., A.I.Ch.E. Journal, 1958, 4, 114.
5. Wilke, C.R., and Chang, P., A.I.Ch.E. Journal, 1955, 1, 264.
6. Keey, R.B., and Glen, J.B., Can. J. Chem. Engrg., 1964, 42, 227.
7. Linton, M., and Sutherland, K.L., Chem. Engrg. Science, 1960, 12, 214.
8. Hilpert, R., mentioned in Schlichting, H., Boundary-Layer Theory, 1960, 4th edn, p.324 (New York: McGraw-Hill Book Co.)
9. Kestin, J., Maeder, P.F., and Wong, H.E., ibid, p.330
10. Kestin, J., Maeder, P.F., and Sogin, H.H., ibid, p.329
11. Griffith, E., and Awberry, J.H., Proc. Inst. Mech. Engrs (London), 1933, 125, 319.
12. Glen, J.B., and Keey, R.B., Chem. Engrg. Science, To be published.
13. Yuge, T., and associates, Refs.21-25 in Rowe, P.N., et al, op. cit.
14. Kramers, H., Physica 'sGrav., 1946, 12, 61.

APPENDIX 4

MASS TRANSFER FROM FIXED AND FREELY SUSPENDED PARTICLES IN AN AGITATED VESSEL

R.B. KEEY and J.B. GLEN, University of Canterbury, Christchurch, New Zealand.

Recently Middleman (1) has pointed out that mass-transfer relationships, deduced for flows around fixed spheres, may not be applied directly, if the particles are freely suspended in an agitated vessel. Rather than the mean bulk flow, it is the difference between the velocity of the particle and that of the mean local flow of the entraining fluid that controls the transfer process. The object of this note is to cite some further evidence to illustrate this difference.

For the fixed-sphere experiments, a lead spherule was electroplated in copper and attached to a thin support as shown in Fig. 1. This support occluded less than 2% of the surface of the sphere, which was used as the cathode in the reduction of ferricyanide ions to ferrocyanide ions in an indifferent electrolyte. This reaction has been shown to be mass-transfer controlled (2) and the arrangement was similar to that used previously by the authors (3).

As in that work, a series of experiments were done with the spherule held near the base and the walls of a rotating cylindrical vessel such that the local velocity was proportional to the rotational speed. The results of 26 data points gave

$$k = \frac{i_L}{ZFSc_o} \sim N^{0.47} \qquad (1)$$

for $440 < (2\pi rN)d_p/\nu < 2200$

and $\nu/\mathcal{D} = 1440$

The correlation coefficient for the logarithmic regression was 0.99. This regression could then be used to correlate mass-transfer coefficients with local mean velocities under similar flow regimes.

A second set of experiments was done with the same spherule held in a mixer in a vertical plane that bisected a segment bounded by neighbouring vertical baffles. The mixer consisted of a $7\frac{7}{8}$" x $7\frac{7}{8}$" diameter vessel, agitated by a centrally mounted, six-bladed paddle of $2\frac{7}{8}$" diameter and with a blade width/diameter ratio of $\frac{1}{8}$. The impellor was driven through a continuously variable gearbox that gave speeds between 0 and 1000 rpm. The sphere was held rigidly in various positions over the plane to give a grid of

locations that took in both the impellor stream and the ring-vortices surrounding it (see Fig. 2). To minimise disturbing the flow pattern forward of the spherule, the sphere support was placed "downstream" together with the anode and the salt-bridge from the calomel cell. Again the variation of mass-transfer coefficient with rotational speed was noted to yield the following results (12 data points in each set):

grid location	log. regression coefficient	correlation coefficient
C3	0.53	0.994
C5	0.44	0.993
D6	0.47	0.995
E3	0.53	0.994
F6	0.44	0.998

The difference between the regression coefficients is not statistically significant.

For the experiments with freely moving particles, o-nitrophenol was used. Technical grade material was purchased and steam-distillated to give a solid melting at 45.0± 0.2°C (reported value, 45°C (4)). Molten o-nitrophenol was injected into a saturated aqueous solution through an eye-dropper and the droplets so formed were allowed to freeze slowly during free fall. The particles were collected and the fraction between 16 and 22 mesh was kept for experiment. The same power unit was used as in the fixed-sphere experiments with six-bladed paddles for the following geometries:

vessel diameter, in.	impellor diameter, in.
$7\frac{7}{8}$	4
$7\frac{7}{8}$	$2\frac{7}{8}$
$5\frac{1}{2}$	$2\frac{7}{8}$

The continuous phase was distilled water, acidified to pH 3.5 ± 0.3 to suppress the dissociation of o-nitrophenol. The particles were introduced into the mixing vessel as quickly as possible and mixed for a set length of time, calculated from mass-transfer rates taken from Barker and Treybal's correlation (5). The dispersed-phase volume fraction was around 1.5%. At the end of each run the contents of the vessel were decanted and filtered through a fine mesh to separate the occasional chip of o-nitrophenol, the solution was quickly stirred to ensure uniformity and sampled for ultra-violet spectroscopy. In this way, it was possible to work with concentration driving forces that differed little from the saturation concentration at the surface of each particle, yet the final mean concentration

(ca. 7×10^{-4} g/ml) could be detected to within ± 3%.

The results for all geometries are plotted in terms of Sherwood number $k d_T/\mathfrak{D}$ against impellor Reynolds number (Nd_T^2/ν) in Fig. 3. It is seen that the results fall between those of Johnson and Huang (6) and those of Hixon and Baum (7) for similar conditions at the same Schmidt number ($\nu/\mathfrak{D}$ = 1240). The logarithmic regression coefficient is 0.80 with a correlation coefficient of 0.943: the standard deviation of the regression coefficient is 0.10.

The results of these and the previous experiments may be summarised:

Experiment	Impellor Reynolds Number	Schmidt Number	Regression Coefficient
held sphere	9,500-76,000	1,290-1,510	0.48 (av.)
free sphere	43,000-125,000	1240	0.80

These regression coefficients may be compared with values postulated from theoretical reasoning:

Experiment	Theoretical Regression Coefficient	Theory (8)
held sphere	0.5	laminar boundary layer with negligible wake effect
free sphere	0.875	boundary layer defined through skin-friction velocity in turbulent flow, $C_{DF} \sim N_{Re}^{-\frac{1}{4}}$

When the Reynolds number for local isotropic flow is based on the power dissipated per unit volume (9), we have

$$N_{Re}^* = \rho^{\frac{2}{3}} (P/V)^{\frac{1}{3}} d_p / \mu \qquad (2)$$

The logarithmic regression of $kd_p/\mathfrak{D}$ vs N_{Re}^* for the free spheres yields a regression coefficient of 0.77 with a correlation coefficient of 0.916. The theoretical regression coefficient is 0.75 (9). This result lends support to the usefulness of Kolmogoroff's (10) postulate of the local isotropy of turbulent flow at high Reynolds numbers, as suggested by Middleman (1).

However, the mass-transfer correlations for the free spheres suggest that the transfer rate is controlled through a turbulent boundary layer, while the bulk turbulence is not intense enough to penetrate the laminar boundary-layer around

a fixed particle. The difference between the fixed-sphere and free-sphere experiments also clearly shows that the slip velocity that governs the mass-transfer process for freely suspended particles may not be proportional to the mean bulk velocity of the fluid, as Middleman deduces (1). It would thus seem inappropriate to use correlations obtained for steady flows over particles as a starting point for describing transport processes in agitated vessels. For the leaching of particles suspended in a turbulent fluid, Levich (11) obtains expressions for the mass-transfer rate, when the particle size is much smaller or much larger than the dissipation scale of turbulence. The predicted dependence of particle diameter on mass-transfer coefficient differs from Harriott's experimental relationships (12) used by Middleman.

ACKNOWLEDGEMENTS

The authors wish to thank Mr T.P. Dobbie and Mr P.M. Farrier who carried out the experimental work described herein. The work was supported by a New Zealand University Grants Committee grant 62/169 and, in addition, one of us (J.B.G.) acknowledges the receipt of a U.G.C. Research Fund Fellowship.

NOTATION

C_{DF}	skin-friction drag coefficient
c_o	concentration at surface
d_I	diameter of impellor
d_p	diameter of particle
d_T	diameter of vessel
F	Faraday constant
i_L	limiting current
k	mass-transfer coefficient
N	speed of rotation
P	power dissipated
r	radial distance
S	surface area
V	volume
Z	valence change
$\mathcal{D}$	diffusivity
μ	viscosity
ν	kinematic viscosity
ρ	density

LITERATURE CITED

1. Middleman, S. A.I.Ch.E.J., 11, 750 (1965)

2. Lin, C.S., Denton, E.B., Gaskill, H.S., and Putnam, G.L., Ind. Eng. Chem., 43, 2136 (1951).

3. Glen, J.B., and Keey, R.B., Chem Eng. Sci., 20 444 (1965)

4. Hodgman, C.D. (ed.), Handbook of Chemistry and Physics, 40th edn, p.1156, Chem. Rubber Publishing Co., Cleveland (1958/9)

5. Barker, J.J., and Treybal, R.E., A.I.Ch.E.J., 6, 289 (1960)

6. Johnson, A.I., and Huang, C.J. A.I.Ch.E.J., 2, 412 (1956)

7. Hixon, A.W. and Baum, S.J., Ind. Eng. Chem., 33, 478 (1941)

8. Keey, R.B., and Glen, J.B., Can. J. Chem. Eng., 42, 227 (1964)

9. Calderbank, P.H., and Moo-Young, M.B., Chem. Eng. Sci., 16, 39 (1961)

10. Kolmogoroff, A.N., Compt. Rendu. Acad. Sci. U.S.S.R., 30, 301 (1941)

11. Levich, V.G., Physicochemical Hydrodynamics, pp.176-183, Prentice-Hall, New York (1962)

12. Harriott, P., A.I.Ch.E.J., 8, 93 (1962)

DIAGRAMS INCLUDED WITH APPENDICES 3 AND 4

Fig. A.1 Sphere used in electrochemical reduction measurements of mass transfer, Appendix 4.

Fig. A.2 Grid of mixer positions at which mass transfer measurements were made, Appendix 4.

Fig. A.3 Rate of o-nitrophenol dissolution in a mixer, Appendix 4.

Fig. A.4 Heat transfer data obtained by Hilpert for cylinders in wind tunnels, Appendix 3.

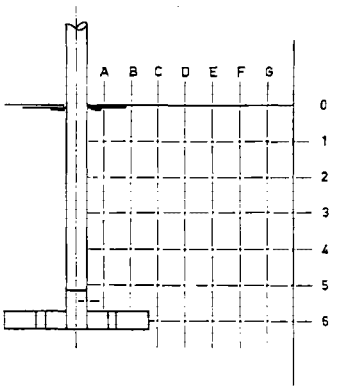

Fig. A4.2

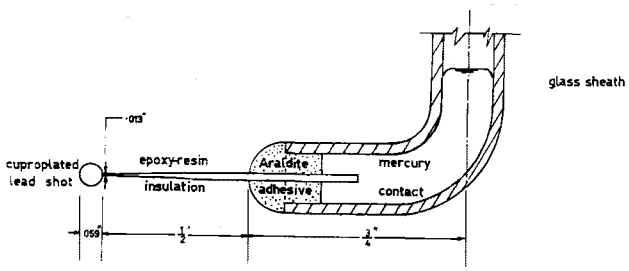

Fig. A4.1

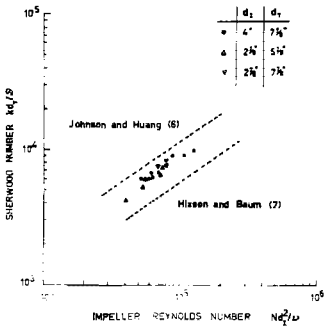

Fig. A4.3

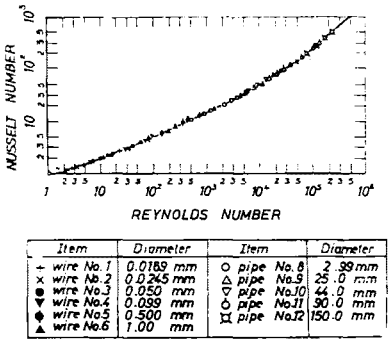

Item	Diameter	Item	Diameter
+ wire No.1	0.0169 mm	○ pipe No.8	2.39 mm
× wire No.2	0.0245 mm	△ pipe No.9	25.0 mm
● wire No.3	0.050 mm	▽ pipe No.10	44.0 mm
▼ wire No.4	0.099 mm	◇ pipe No.11	90.0 mm
◆ wire No.5	0.500 mm	⌑ pipe No.12	150.0 mm
▲ wire No.6	1.00 mm		

Fig. A3.1

APPENDIX 5

CONTINUOUS PHASE MASS TRANSFER WITH A CIRCULATING DROP

The mass transfer resistance in the continuous phase film around a mobile liquid interface, may be described by either of two mechanisms. The surface mobility may arise from internal circulation caused by the relative motion of the drop and the fluid, or from interfacial turbulence caused by surface tension gradients over the liquid interface.

The energy dissipation per unit volume of viscous fluid, is given by Levich (63), who develops these two models:

$$\epsilon = -\frac{dE}{dt} = \mu \int (\text{curl } u)^2 \, dV + \mu \int \frac{\partial u^2}{\partial n} \, ds + 2\mu \int (V \text{ curl } u) \, ds \qquad (A5.1)$$

n is the direction of the normal to the surface over which the fluid is flowing.

In the zone of viscous flow about a circulating drop, the deviation of the velocity from that of an ideal liquid may be neglected, for $Re_\lambda < 10^3$. The velocity of the undisturbed flow is irrotational, thus eqn. A5.1 may be simplified.

$$-\frac{dE}{dt} = \mu \int \left(\frac{\partial}{\partial r} (u_r^{(0)})^2 + \frac{\partial}{\partial r} (u_\theta^{(0)})^2 \right)_{r=a} 2\pi a^2 \sin\theta \, d\theta$$

$$= \mu \int \left(2 u_r^{(0)} \cdot \frac{\partial u_r^{(0)}}{\partial r} + 2 u_\theta^{(0)} \frac{\partial u_\theta^{(0)}}{\partial r} \right)_{r=a} 2\pi a^2 \sin\theta \, d\theta$$

$v_r^{(0)} = -3 v \cdot \frac{y}{a} \cos\theta$, where $y = r - a$ (ref.63)

$= 0$ at $y = 0$.

$$-\frac{dE}{dt} = \mu \, 4\pi a^2 \int v_\theta^{(0)} \frac{\partial v_\theta^{(0)}}{\partial y} \sin\theta \, d\theta \qquad (A5.2)$$

$$v_\theta^{(0)} = \frac{3}{2} v \left(1 - \frac{y}{a}\right) \sin\theta \qquad \text{(ref.63)}$$

Thus, eqn. A5.2 becomes,

$$\epsilon = -\frac{dE}{dt} = -12\pi a \mu v^2$$

Hence, the total dissipative force exerted on a drop becomes,

$$F = -\frac{1}{2}\frac{\partial}{\partial v}\left(\frac{dE}{dt}\right) = 12\pi\mu a v$$

A force balance, analogous to eqn. 3.27, may be written for the drop,

$$\frac{4\pi}{3}\rho_d a^3 \frac{dv}{dt} = (\rho_c - \rho_d)\frac{4\pi}{3}a^3\frac{du}{dt} - 12\pi a\mu v \qquad (A5.3)$$

The characteristic period T_λ, corresponding to the motion of scale λ, $\lambda > \lambda_o$, is a function only of the scale of motion λ, and the characteristic of the turbulent flow, $\frac{\epsilon}{\rho_c}$. Since $\lambda > \lambda_o$, T_λ is not a function of the fluid viscosity.

Dimensionally,

$$T_\lambda = \left(\frac{\lambda^2 \rho_c}{\epsilon}\right)^{\frac{1}{3}} \sim \frac{\lambda}{v_\lambda}$$

$$\text{or} \quad v = \frac{d\lambda}{dT} \sim \frac{\lambda}{T_\lambda}$$

The acceleration associated with eddies of scale λ may be written,

$$\omega_\lambda = \frac{dv_\lambda}{dt} \sim \frac{v_\lambda}{T_\lambda} \sim \frac{\lambda}{T_\lambda^2} \sim \left(\frac{\epsilon}{\rho_c}\right)^{\frac{2}{3}} \cdot \frac{1}{\lambda^{\frac{1}{3}}}$$

Thus eqn. A5.3 becomes,

$$\frac{4\pi}{3}\rho_d a^3 \frac{v}{T_\lambda} = (\rho_c - \rho_d)\frac{4\pi}{3}a^3\sqrt{\frac{\epsilon}{\rho_c T_\lambda}} - 12\pi\mu a v$$

which, with approximations similar to those used in Section 3.6, yields,

$$v \sim \frac{\rho_c - \rho_d}{\rho_d} \cdot \left(\frac{\epsilon}{\rho_c}\right)^{\frac{1}{2}} \cdot \frac{\sqrt{T_\lambda}}{\frac{9\nu T_\lambda}{a^2} + 1}$$

$$\text{or} \quad v_{max} \sim \frac{\rho_c - \rho_d}{d} \cdot a \cdot \sqrt{\frac{\epsilon}{\rho_c \nu_c}} \qquad (A5.4)$$

ϵ is substituted by eqn. 3.7, and U in eqn. 7.12 is substituted by v_{max}, to yield,

$$k_c \sim \sqrt{k_f'} \cdot \frac{\Delta\rho}{\rho_d} \cdot \frac{a}{\nu^{\frac{1}{2}}} \quad \frac{(ND_I)^{3/2}}{D_I^{1/2}}$$

$$\text{or} \quad Sh_{Imp} \sim \sqrt{k_f'} \; Re_{Imp}^{1.5} \; Sc^{0.5} \cdot \frac{\Delta\rho}{\rho_d} \cdot \frac{a}{D_I} \qquad 7.17$$

for mixers.

k_f' is constant for the Reynolds number range involved, $10^2 < Re_\lambda < 10^3$, (63).

The exponent of the Schmidt number is dependent on the viscous damping postulate assumed. From Ruckenstein's surface renewal models, it is apparent that 0.5 is the upper limiting value, see Sections 7.4 and 7.5.

The second model considers that the viscous damping, consequently the diffusion due to turbulence, near the interface is controlled by the interfacial tension. As before, the diffusion flux in a turbulent fluid is approximately determined by the turbulent notion near the interface. For $Sc \gg 1$, the diffusion resistance is considered to be within the diffusion sublayer, see Section 7.3.

The fluid velocity component normal to the surface must vanish at the liquid interface, the damping being determined from Piterskikh's relationship,

$$v_y = v_o \; {}^{y}/_{\lambda}$$

This condition arises as the velocity components must satisfy the continuity equation, and the x component of velocity is not a function of y.

x = distance along the surface

y = perpendicular distance from the surface.

Similarly, the scale of the turbulence eddies increases

with distance from the surface,

$$\lambda \sim y$$

Hence the effective kinematic viscosity, to which the turbulent diffusivity is analogous, is given by,

$$\nu_{turb} \sim \mathfrak{D}_{turb} \sim v_y \cdot y \sim v_o \frac{y^2}{\lambda} \qquad (A5.5)$$

If surface tension, rather than viscosity, controls the turbulence damping, then the depth λ, of the zone of damped turbulence near the interface, can be a function of only the eddy velocity v_λ, the liquid density ρ, and the surface tension σ,

$$\lambda \sim \frac{\sigma}{\rho v_o^2} \qquad (A5.6)$$

if a direct relationship between λ and σ is assumed.

Substitution of λ into eqn. A5.5 yields,

$$\mathfrak{D}_{turb} \sim \nu_{turb} \sim \frac{v_o^3 \rho y^2}{\sigma}$$

at $y = \delta$, $\mathfrak{D}_{turb} = \mathfrak{D}_{mol}$

$$\mathfrak{D} = \mathfrak{D}_{turb} \sim \frac{v_o^3 \rho \delta^2}{\sigma}$$

$$\text{or} \quad \delta \sim \left(\frac{\mathfrak{D}\sigma}{v_o^3 \rho}\right)^{\frac{1}{2}} \qquad (A5.7)$$

For control of the mass transfer rate by the diffusion sublayer, the mass transfer flux is approximated by,

$$j = \mathfrak{D}_{turb} \frac{\partial c}{\partial y} \sim \frac{\mathfrak{D}}{\delta}(c_b - c_o)$$

$$\sim \mathfrak{D}\left(\frac{v_o^3 \rho}{\mathfrak{D}\sigma}\right)^{\frac{1}{2}} \cdot (c_b - c_o)$$

$$\text{or} \quad k_c \sim \frac{\mathfrak{D}^{1/2} v_o^{3/2} \rho}{\sigma^{1/2}}$$

v_o may be substituted by eqn. 3.24 to yield,

$$k_c \sim \frac{(k_f')^{3/2}}{2^{3/2}} \cdot \frac{u^{3/2}\,\rho^{1/2}}{\sigma^{1/2}} \cdot \mathcal{D}^{1/2}$$

k_f' is again a constant.

For mixer conditions,

$$Sh_{Imp} \sim (k_f')^{3/2}\, Re_{Imp}^{1.5}\, Sc^{0.5} \cdot \frac{\rho^{\frac{1}{2}}\nu}{D_I^{\frac{1}{2}}\sigma^{\frac{1}{2}}}$$

$$\text{or } Sh_{Imp} \sim (k_f')^{3/2}\, Re_{Imp}^{1.5}\, Sc^{\frac{1}{2}} \cdot \frac{We^{\frac{1}{2}}}{Re} \qquad (A5.8)$$

The derivations of eqns. A5.8 and 7.17 differ in that in eqn. 7.17 the Reynolds number exponent arises from $v_{max} \sim (ND_I)^{3/2}$, with $\delta \sim 1/v_o$, while it arises in eqn. A5.8 because $\delta \sim 1/v_o^{3/2}$, and $v_o \sim (ND_I)$. In practice it is unlikely that this difference will be observed. Equation 7.17 however does predict $k_c \sim {}^{a}/_{l}$, whereas eqn. A5.8 does not. Again, with a range of drop diameters, as well as a range of inertial subrange eddy lengths, this difference may also not be found. Both mechanisms imply a low viscous energy dissipation in the mean velocity gradients through the drop boundary layers.

*University of Canterbury, Christchurch, New Zealand.

APPENDIX 6. Solute Distribution Data for the System. Isooctane/o-nitrophenol(solute)/Water (pH 3.5)

Temperature 18°C, pg. 153 Bk.I

Soln. No.	gm ONP / gm H_2O	gm ONP / gm isooct.	m_a
2	2.39×10^{-5}	1.049×10^{-4}	4.39
3	1.15 "	0.936 "	8.14
4	1.46 "	2.571 "	17.6
5	0.15 "	1.090 "	72.7
6	2.33 "	2.904 "	12.5
7	1.51 "	4.036 "	17.7
8	2.28 "	6.121 "	24.8
9	2.47 "	6.459 "	26.1
10	3.86 "	13.464 "	34.9
11	3.06 "	13.102 "	42.8
12	4.16 "	12.76 "	30.7
13	8.72 "	26.06 "	29.9
14	8.249 "	26.80 "	32.5
15	9.745 "	34.19 "	35.1
16	22.12 "	58.10 "	26.3
17	16.11 "	53.83 "	24.4
18	22.09 "	55.32 "	25.0
19	37.20 "	111.0 "	29.8
19a	40.52 "	110.5 "	27.3
20	35.65 "	113.0 "	31.7
21	23.32 "	113.6 "	48.7
22	70.29 "	226.7 "	32.2
23	65.28 "	220.0 "	33.7
24	62.09 "	216.7 "	34.9
25	103.6 "	410.4 "	39.6
26	110.8 "	410.8 "	37.1
27	112.7 "	407.7 "	36.2

Temperature 23.6°C, pg.157, Bk.I

21	1.89×10^{-5}	0.794×10^{-3}	42.0
23	7.05 "	2.93 "	41.5
24	9.46 "	3.69 "	39.0
25	11.47 "	4.87 "	42.4
26	14.27 "	5.76 "	40.4
27	16.17 "	6.70 "	41.4

Temperature 18°C, pg.157 BkI

Soln. No.	gm ONP / gm H_2O	gm ONP / gm isooct.	m_d
1	0.116×10^{-4}	0.382×10^{-3}	32.9
2	0.292 "	0.833 "	28.5
3	0.375 "	1.601 "	42.6
4	0.519 "	1.834 "	35.3
5	0.709 "	2.520 "	35.5
6	9.766 "	2.739 "	35.7
7	0.950 "	3.338 "	35.2
8	1.062 "	3.869 "	36.4
9	1.214 "	4.436 "	36.1
10	1.230 "	4.538 "	36.9
11	1.126 "	4.644 "	41.2
12	1.369 "	5.170 "	37.8
13	1.765 "	5.720 "	32.4
14	1.606 "	6.293 "	39.2
15	1.829 "	6.714 "	36.7
16	1.965 "	7.327 "	37.3
17	1.890 "	8.058 "	42.6
18	2.391 "	9.494 "	39.7
19	2.519 "	9.558 "	37.9
20	3.130 "	11.753 "	37.6

Temperature 18.3°C, pg.145 Bk.I

1	3.501×10^{-5}	1.418×10^{-3}	40.51
2	3.439 "	1.226 "	35.66
3	2.927 "	1.114 "	38.06
4	5.419 "	2.243 "	41.39
5	6.632 "	2.548 "	38.41
6	5.395 "	2.385 "	44.21
7	8.401 "	3.667 "	43.66
8	8.691 "	3.711 "	42.70
9	8.917 "	3.671 "	41.17
10	9.554 "	4.612 "	48.27
13	10.660 "	6.036 "	56.62
11	8.969 "	4.541 "	50.63
12	10.314 "	4.643 "	45.02
14	11.010 "	5.918 "	53.75
15	11.443 "	5.913 "	51.67

Temperature 17.7°C, pg.169 Bk.I

Soln. No.	gm ONP / gm H_2O	gm ONP / gm isooct.	m_d
36	3.49×10^{-5}	1.025×10^{-3}	29.4
41	2.02 "	0.557 "	27.6
52	5.99 "	1.756 "	29.3
53	6.68 "	2.218 "	33.2
54	7.55 "	2.570 "	34.1
55	7.694 "	2.885 "	37.5
56	10.35 "	3.423 "	33.1
57	15.17 "	5.004 "	33.0
58	13.80 "	5.865	42.5

Temperature 24.8°C, pg.167 Bk.I

14	2.36×10^{-5}	0.629×10^{-3}	26.6
15	3.49 "	1.157 "	33.1
18	5.36 "	1.794 "	27.0
2	6.64 "	2.350 "	29.6
13	7.93 "	2.768 "	34.9
10	9.043 "	3.38 "	37.4
1	11.24 "	4.08 "	26.3
11	3.38 "	0.860 "	25.4
39	13.94 "	5.53 "	34.7
40	10.78 "	3.05 "	29.3

Temperature 29.4°C, pg.157, Bk.I

28	2.68×10^{-5}	1.007×10^{-3}	37.9
29	5.053 "	1.925 "	38.1
30	6.838 "	2.756 "	40.3
31	9.545 "	3.775 "	39.5
32	11.84 "	4.950 "	41.8
33	13.69 "	5.717 "	41.8
34	8.819 "	3.679 "	41.7

APPENDIX 7. Density Data for the Solutions,(Isooctane + o-nitrophenol), (Water pH3.5 + o-nitrophenol).

Soln. No.	gm ONP / gm Isooct.	Density 18°C gm/cm³	Density 25.20°C gm/cm³
5	5.846×10^{-4}	0.6944	0.6873
6	11.111 "	0.6946	0.6883
7	19.29 "	0.6955	0.6876
8	27.87 "	0.694	0.6880
9	31.13 "	0.6961	0.6887
Isooctane		0.6936	0.6871
59	32.20 "	0.6946	0.6883
8	16.86 "	0.6944	0.6879
95	44.77 "	0.6954	0.6888
66	64.23 "	0.6961	0.6894
59	32.20 "	0.6950	0.6887
8	16.86 "	0.6948	0.6876
95	44.77 "	0.6954	0.6639
66	64.27 "	0.6961	0.6894
Isooctane		0.6934	0.6867
Isooctane		0.6942	0.6871
Isooctane		0.6935	

Aqueous phase, pg.161, Bk.I

2	10.109×10^{-5}	0.9994	0.9971
10	8.400 "	0.9989	0.9970
11	6.093 "	0.9988	0.9970
15	4.087 "	0.9975	0.9971
14	2.280 "	0.9991	0.9966
H_2O + acid		0.9996	0.9979

APPENDIX 8. Kinematic Viscosity Data for the Solutions,(Isooctane + o-nitrophenol), and Water pH3.5 + o-nitrophenol)

Soln. No.	gm ONP / gm H_2O	Kinematic viscosity 18°C cS.	25.20°C cS.
2	10.109×10^{-5}	1.066	0.899
10	8.400 "	1.055	0.907
11	6.093 "	1.089	0.897
15	4.087 "	1.057	0.907
14	2.280 "	1.056	0.904
H_2O + acid		1.063	0.903

Isooctane phase, Pg.162, Bk.I

5	5.846×10^{-4}	0.740	0.688
6	11.11 "	0.738	0.687
7	19.29 "	0.741	0.686
8	27.87 "	0.743	0.690
9	31.13 "	0.741	0.692
Isooctane		0.743	0.686
Isooctane		0.740	0.688

APPENDIX 9. Surface Tension Data for the System Isooctane/o-nitrophenol/Water

Two phases at equilibrium, temperature 18°C, pg.169, Bk.I

Soln. No.	gm ONP / gm isooct.	Surface Tension dynes/cm	
53	2.218×10^{-3}	49.22	
36	1.025 "	49.30	
56	3.423 "	48.90	
54	2.570 "	50.67	50.30
41	0.557 "	50.96	50.74
55	2.885 "	49.96	50.12
52	1.756 "	49.59	49.95
58	5.865 "	49.34	
57	5.004	48.91	49.34

Solute transfer from isooctane to aqueous phase, aqueous drops.

2	0.592×10^{-3}	50.37	
3	1.835 "	50.29	50.58
4	1.039 "	49.71	
5	2.586 "	50.39	49.81
6	3.635 "	47.55	49.37
V	4.128 "	50.02	

Solute transfer from isooctane to aqueous phase, isooctane drops. Temperature 18°C, pg.176, Bk.I.

3	1.835×10^{-3}	50.32	
2	0.592 "	50.39	
6	3.635 "	50.42	
4	1.039 "	50.23	50.53
5	2.586 "	50.36	
V	4.128 "	50.83	

APPENDIX 12. Hold-up Data

Agit. Speed RPM	Power gm cm/sec	Hold-up	Hold-up ratio ϕ	Temp °C
7½" Vessel, 4" Impellor				
143	6.11×10^3	0.0254	0.222	19.6
264	24.6 "	0.0437	0.382	19.7
183	10.7 "	0.0296	0.259	19.8
327	44.6 "	0.0500	0.688	19.9
416	88.0 "	0.0599	0.825	20.0
465	118.2 "	0.0625	0.875	20.2
636	318 "	0.0630	0.868	20.4
7½" Vessel, 2½" Impellor				
235	6.75×10^3	0.0343	0.300	20.6
329.5	14.18 "	0.0354	0.309	20.7
419	24.7 "	0.0338	0.465	19.4
502	39.0 "	0.0432	0.595	19.6
610	64.9 "	0.0547	0.753	19.7
729	106.2 "	0.0599	0.825	19.6
7½" vessel, 2½" Impellor				
318.5	7.53×10^3	0.0286	0.250	19.6
416	9.24 "	0.0333	0.291	19.7
518	12.9 "	0.0393	0.344	19.8
641	24.0 "	0.0443	0.387	19.8
750	35.0 "	0.0411	0.566	20.0
848	47.3 "	0.0495	0.681	20.2
5½" Vessel, 1½" Impellor				
472	8.34×10^3	0.0201	0.176	21.1
590	13.0 "	0.0295	0.259	21.2
693	18.0 "	0.0406	0.355	21.3
802	24.0 "	0.0491	0.430	21.3
900	30.4 "	0.0621	0.544	21.4
841	26.3 "	0.0479	0.420	21.6
8½" Vessel, 4½" Impellor				
133	8.42×10^3	0.0272	0.302	20.4
242.5	38.2 "	0.0539	0.598	20.5
187	19.2 "	0.0334	0.371	20.5
396	143 "	0.0632	0.870	20.5
510	304 "	0.0877	0.933	20.8
321.5	82.5 "	0.0571	0.786	20.7
635	591 "	0.0682	0.939	20.6
640	602 "	0.0677	0.932	21.0
8½" vessel, 3" Impellor				
187.5	5.02×10^3	0.0235	0.206	17.3
206	14.6 "	0.0305	0.266	17.4
458	36.9 "	0.0407	0.443	17.5
599	72.6 "	0.0595	0.820	17.6
678	100.9 "	0.0613	0.844	17.7
807	163 "	0.0640	0.882	17.8
8½" Vessel, 2 7/16" Impellor				
324	8.48×10^3	0.0236	0.206	19.4
444	17.19 "	0.0285	0.250	19.5
591	34.0 "	0.0401	0.351	19.6
721	55.8 "	0.0553	0.613	19.7
848	84.9 "	0.0562	0.774	20.1
5½" Vessel, 2½" Impellor				
207	5.13×10^3	0.0211	0.184	20.5
361	17.5 "	0.0571	0.500	20.5
445	28.6 "	0.0740	0.652	20.6
589	59.0 "	0.0763	0.835	20.6
697	93.7 "	0.0735	0.892	20.7
839	158.3 "	0.0635	0.798	20.8

APPENDIX 10. Vessel and Impellor Design Data

Ves. dia. cms.	Ves. ht. cms.	Ves. vol. litres	Baffle ratio D_T/D_B	Imp. dia. cms.	Blade width cms.	Boss dia. cms.	Scale Ratio D_T/D_I
14.05	14.37	2.090	8	4.49	0.561	1.087	3.13
"	"	"	"	7.26	0.894	1.811	1.94
19.76	19.9	5.875	"	5.43	0.721	1.451	3.64
"	"	"	"	7.26	0.894	1.811	2.72
"	"	"	"	10.29	1.270	2.532	1.93
22.20	22.5	8.408	"	6.27	0.820	1.633	3.54
"	"	"	"	7.66	0.953	1.920	2.90
"	"	"	"	11.83	1.422	2.710	1.88

Impellor Shaft diameter = 1.27 cms.

Diameter phase inlets to mixing vessel

Isooctane phase - 1.50 cms.
Aqueous phase - 2.82 cms O.D., 1.90 cms. I.D.

Nomenclature for Appendix 14.

		Read	Print
CIN	Concentration solute in inlet isooctane	$\frac{\text{gms ONP}}{\text{gms isooct.}}$	Mol/Mol
CIT	Concentration solute in outlet isooctane	"	"
CO	Mass transfer coefficient based on outlet concentrations.		M/hr
COA	CO x interfacial area/unit volume		hr^{-1}
COI	Mass transfer coefficient based on a fully mixed continuous phase and an unmixed dispersed phase		M/hr
COIA	COI x Interfacial area/unit volume		hr^{-1}
CWN	Concentration solute in inlet water	$\frac{\text{gm ONP}}{\text{gm } H_2O}$	Mol/Mol
CWT	Concentration solute in outlet water	"	"
DAB	Diffusivity of o-nitrophenol in water		M^2/hr
DENI	Density isooctane		Kg/M^3
DENS	Density dispersion		"
DSD	Mean drop diameter = $\frac{nd^3}{nd^2}$		cms.
DSV	Mean drop diameter log DSV = log d_{50} + 5.757 $\log^2 \frac{}{g}$		"
EFFY	Overall extraction efficiency		

		Read	Print
EFIN	Inlet extraction efficiency		
EFOUT	Outlet extraction efficiency		
EM	d_{50}	cms.	
FLOI	Flow rate of isooctane	ml/min	M^3/hr
FLOW	Flow rate of water	"	"
IMP	Impellor diameter	cm	M
PONO	Power Number		
POW	Power Input	$\frac{gm.cm}{sec}$	$\frac{Kg.M}{hr}$
RE	Impellor Reynolds Number		
REV	Impellor speed	R.P.M.	Rev/hr
RUN	Run number, (workbook 2, pg.no.)		
SCNO	Schmidt number =		
SIGMA	Particle size standard deviation = $\frac{d_{84}}{d_{50}}$		
TEMP	Temperature	°C	°C
VDIA	Vessel diameter	cms.	M.
VES	Vessel volume	ml.	M^3
VOLF	Dispersed phase volume fraction		

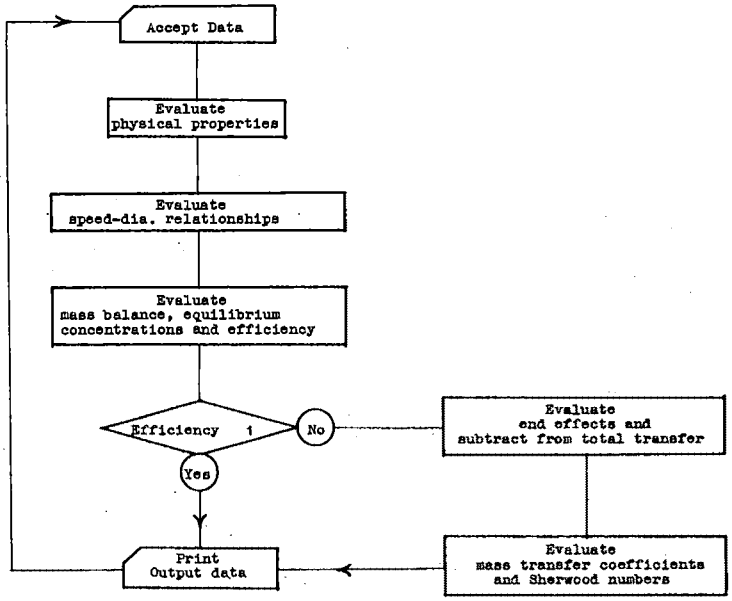

Appendix 14. Block diagram of mass transfer calculation program.

RUN NO	PHOTO NO	0-0.3	.3-.6	.6-1.0	1.-1.5	1.5-2.5	2.5-4.	NO DROP
29	1	.2102	.6938	.9503	.9951	1.0000	.0000	406
29	2	.3040	.7076	.9252	.9951	1.0000	.0000	434
29	3	.2512	.6504	.8928	.9867	.9999	.0000	487
29	4	.3252	.7266	.9420	.9948	1.0000	.0000	513
29	5	.2260	.6559	.8930	.9892	1.0000	.0000	508
29	6	.2733	.6884	.9071	.9883	.9999	.0000	462
29	7	.2142	.6082	.9060	.9837	.9999	.0000	344
29	8	.2708	.7327	.9376	.9952	1.0000	.0000	463
30	1	.4554	.8839	1.0000	.0000	.0000	.0000	435
30	2	.4484	.8372	1.0000	.0000	.0000	.0000	460
30	3	.5076	.8832	.9999	.0000	.0000	.0000	330
30	4	.4617	.8575	.9999	.0000	.0000	.0000	406
30	5	.5007	.8989	.9999	.0000	.0000	.0000	365
30	6	.4786	.8945	.9999	.0000	.0000	.0000	388
30	7	.4754	.8983	.9999	.0000	.0000	.0000	336
30	8	.4813	.8381	.9999	.0000	.0000	.0000	381
31	1	.2941	.8104	.9837	1.0000	.0000	.0000	383
37	1	.1228	.3872	.7049	.8829	.9661	1.0000	192
37	3	.1918	.4773	.6801	.8517	.9687	1.0000	231
37	4	.1645	.4488	.7054	.8766	.9654	1.0000	280
37	6	.1921	.4990	.7188	.8893	.9667	.9999	339
37	7	.2274	.5095	.7411	.9011	.9820	.9999	246
37	8	.2058	.4852	.7582	.9137	.9803	1.0000	223
37	9	.2791	.5385	.7711	.8970	.9618	1.0000	250
37	13	.2187	.4687	.6718	.8385	.9635	1.0000	192
39	3	.2061	.4685	.7559	.8975	.9600	1.0000	191
39	4	.2628	.5309	.7835	.9381	.9845	1.0000	208
39	6	.2036	.5187	.7612	.8872	.9672	.9999	214
39	7	.2512	.5467	.7684	.9211	.9704	.9999	203
39	9	.2352	.5346	.6971	.8768	.9692	.9999	241
39	10	.2197	.4875	.7674	.9209	.9819	.9999	344
39	11	.2221	.5082	.7176	.8861	.9693	1.0000	185
39	12	.2387	.5450	.7942	.9153	.9750	.9999	223
41	1	.3576	.7367	.8798	.9728	.9942	.9999	324
41	2	.2629	.6022	.8566	.9541	.9915	.9999	376
41	3	.2959	.6523	.8814	.9833	.9981	.9999	317
41	4	.2547	.5708	.8225	.9461	.9852	1.0000	340
41	6	.3208	.5762	.8349	.9528	.9823	.9999	312
41	8	.2678	.5783	.8384	.9657	.9910	.9999	281
43	1	.3877	.7309	.9470	1.0000	.0000	.0000	497
43	2	.4593	.7408	.9166	.9870	1.0000	.0000	519
43	3	.3796	.7272	.9150	.9840	1.0000	.0000	520
43	5	.4327	.7262	.9238	.9887	1.0000	.0000	551
45	1	.3840	.7869	.9548	.9959	.9999	.0000	467
45	2	.4380	.7737	.9318	.9961	.9999	.0000	379
45	3	.4214	.7812	.9430	.9948	1.0000	.0000	443
45	4	.3488	.7612	.9287	.9878	.9999	.0000	381
45	6	.4617	.7858	.9354	.9919	.9999	.0000	390
45	7	.4249	.8104	.9646	.9933	1.0000	.0000	510
45	8	.4385	.8039	.9529	.9933	1.0000	.0000	433
45	9	.4312	.7770	.9703	.9947	1.0000	.0000	531
47	1	.3918	.6989	.8502	.9399	.9799	1.0000	223
47	2	.3285	.5890	.7590	.8849	.9528	1.0000	187
47	3	.2358	.5085	.7223	.8418	.9504	.9999	152
47	4	.3578	.6105	.8105	.8631	.9368	.9999	95
47	5	.2619	.4789	.6510	.8456	.9438	.9999	137
49	1	.2259	.6071	.8613	.9823	.9964	.9999	324
49	3	.3805	.7164	.8768	.9543	.9912	.9999	293
49	4	.2905	.6753	.9162	.9790	.9947	.9999	320
49	5	.3544	.6820	.8860	.9774	.9947	.9999	326
49	6	.3156	.6980	.9292	.9885	.9974	.9999	271
49	7	.3510	.6834	.8864	.9692	.9957	.9999	381
49	8	.2549	.6561	.8923	.9729	.9962	.9999	314
51	1	.5963	.9455	1.0000	.0000	.0000	.0000	465
51	2	.5043	.9019	.9946	1.0000	.0000	.0000	484
51	3	.4244	.8351	.9892	1.0000	.0000	.0000	600
53	1	.5760	.8346	.9572	.9915	.9986	.9999	464
53	2	.4981	.8371	.9564	.9850	.9965	1.0000	486
53	3	.5869	.8614	.9755	.9945	.9999	.0000	408
53	4	.4541	.7922	.9445	.9948	1.0000	.0000	411
53	5	.5064	.8240	.9721	.9957	1.0000	.0000	479
53	6	.4419	.7993	.9452	.9958	1.0000	.0000	556
53	7	.4718	.7934	.9542	.9881	.9990	1.0000	404
55	1	.5051	.8499	.9760	.9999	.0000	.0000	454
55	2	.4507	.8179	.9522	.9999	.0000	.0000	351
55	3	.4661	.8202	.9680	.9999	.0000	.0000	484
55	4	.4908	.8456	.9817	.9999	.0000	.0000	447
55	5	.4878	.8482	.9728	.9999	.0000	.0000	402
55	6	.4739	.8140	.9776	1.0000	.0000	.0000	474
55	7	.4930	.8455	.9692	.9999	.0000	.0000	418
55	8	.4858	.8198	.9817	1.0000	.0000	.0000	371

RUN NO	PHOTO NO	0-0.3	.3-.6	.6-1.0	1.-1.5	1.5-2.5	2.5-4.	NO DROP
59	1	.2070	.5383	.8512	.9435	.9774	1.0000	243
59	2	.1660	.5147	.8025	.9333	.9771	1.0000	211
59	3	.1938	.6043	.7639	.8614	.9486	1.0000	164
59	4	.2123	.4869	.7288	.8781	.9656	1.0000	182
59	5	.2171	.5765	.7221	.8663	.9554	1.0000	158
59	7	.1752	.6219	.8481	.9409	.9873	1.0000	200
59	9	.2449	.5643	.7602	.8974	.9584	1.0000	146
59	11	.2216	.5115	.7285	.8813	.9711	1.0000	148
61	1	.1404	.4896	.7635	.9426	.9817	1.0000	183
61	2	.1796	.4969	.7815	.9285	.9902	1.0000	218
61	3	.2408	.5217	.8026	.9402	.9899	1.0000	223
61	4	.2569	.5878	.8207	.9366	.9851	.0000	241
61	5	.2556	.5432	.8361	.9462	.9817	1.0000	204
61	6	.3133	.5667	.7723	.9085	.9779	.9999	275
61	8	.2289	.5495	.7647	.9211	.9860	1.0000	201
61	10	.2836	.5814	.7814	.8268	.9871	.0000	201
63	1	.2158	.5691	.8203	.9478	.9892	.9999	244
63	2	.1848	.6740	.8869	.9690	.9948	.9999	346
63	3	.2344	.6496	.8525	.9781	.9963	.9999	302
63	4	.2668	.6132	.8698	.9724	.9941	.9999	249
63	5	.3471	.7541	.9177	.9800	.9960	.9999	267
63	6	.3522	.7602	.9226	.9762	.9964	1.0000	405
63	7	.2560	.6156	.8526	.9524	.9921	.9999	422
69	2	.2058	.5231	.7226	.8409	.9490	.9807	158
69	4	.3443	.5593	.7072	.8416	.9424	.9760	142
69	5	.2774	.5414	.7427	.8645	.9507	1.0000	165
69	6	.2357	.4796	.7317	.8373	.9268	.9999	123
69	7	.2284	.5711	.7680	.8804	.9648	1.0000	136
69	8	.2187	.4348	.6645	.8559	.9639	1.0000	182
69	9	.2722	.5143	.7349	.9088	.9779	.9999	136
69	11	.1788	.4764	.6846	.8379	.9518	1.0000	205
71	1	.2716	.7190	.9241	.9840	1.0000	.0000	385
71	2	.2461	.7015	.9107	.9846	1.0000	.0000	338
71	3	.3362	.7544	.9265	.9920	1.0000	.0000	394
71	4	.3280	.7558	.9445	.9921	1.0000	.0000	422
71	6	.3130	.7090	.9231	.9887	1.0000	.0000	452
71	7	.3078	.7535	.9431	.9918	1.0000	.0000	427
71	8	.2490	.7020	.9274	.9914	.9999	.0000	457
71	9	.3035	.7209	.9359	.9903	1.0000	.0000	427
73	1	.2386	.6893	.9132	.9751	.9941	.9999	288
73	2	.3412	.7599	.9348	.9922	.9986	.9999	383
73	3	.2971	.7235	.9308	.9821	.9964	.9999	424
73	4	.2863	.6710	.8857	.9752	.9976	1.0000	485
73	5	.3473	.6997	.8997	.9709	.9947	1.0000	445
73	6	.3449	.7186	.9330	.9890	.9970	1.0000	474
73	7	.3563	.7352	.8786	.9668	.9973	1.0000	523
73	8	.1890	.6155	.8418	.9695	.9948	.9999	291
75	1	.4505	.8455	.9738	1.0000	.0000	.0000	335
75	2	.3503	.7992	.9822	.9999	.0000	.0000	517
75	3	.3820	.8204	.9630	.9999	.0000	.0000	500
75	4	.4161	.8520	.9791	1.0000	.0000	.0000	442
75	5	.3844	.8018	.9716	.9999	.0000	.0000	436
75	6	.4094	.7849	.9745	1.0000	.0000	.0000	564
75	7	.3792	.8095	.9744	1.0000	.0000	.0000	593
75	8	.4141	.7940	.9679	.9999	.0000	.0000	451
77	1	.5192	.9258	.9862	.9999	.0000	.0000	369
77	2	.3286	.8544	.9765	.9999	.0000	.0000	218
77	3	.5936	.9010	.9863	.9999	.0000	.0000	333
77	4	.2762	.8081	.9667	.9999	.0000	.0000	202
77	5	.3421	.8677	.9735	.9999	.0000	.0000	286
77	6	.5635	.8729	.9804	.9999	.0000	.0000	313
77	7	.5365	.8692	.9711	.9999	.0000	.0000	318
77	8	.5700	.8847	.9781	.9999	.0000	.0000	328
79	1	.2340	.7433	.9490	1.0000	.0000	.0000	336
79	2	.2189	.7394	.9503	1.0000	.0000	.0000	387
79	3	.2079	.7147	.9278	.9917	1.0000	.0000	417
79	4	.3610	.8252	.9628	.9980	1.0000	.0000	426
79	5	.3265	.7951	.9560	.9967	1.0000	.0000	420
79	6	.3212	.7788	.9563	.9938	1.0000	.0000	525
79	7	.2770	.7808	.9553	.9962	1.0000	.0000	423
79	8	.2421	.8812	.9757	.9976	1.0000	.0000	481
83	1	.2612	.5348	.7252	.8168	.8778	.9694	87
83	2	.2453	.4906	.7185	.8762	.9393	.9818	65
83	3	.2828	.5387	.7407	.8585	.9292	.9685	88
83	4	.2289	.5036	.6868	.8241	.9194	.9560	78
83	5	.2295	.5409	.7868	.9016	.9508	.9999	61
83	6	.2773	.5630	.7226	.8487	.9243	.9663	119
83	7	.2604	.4895	.6145	.7916	.8750	.9791	96
83	8	.2345	.4567	.6913	.8148	.9135	.9753	81
83	9	.2137	.4274	.5877	.7633	.8778	.9770	131
83	10	.1538	.4153	.5615	.6769	.8153	.9615	130
85	2	.1513	.4221	.6929	.9160	.9565	.9797	144
85	3	.1546	.4426	.7519	.9333	.9786	.9919	200
85	4	.1942	.4703	.7924	.9233	.9718	.9948	217
85	5	.1835	.4993	.7416	.9104	.9664	.9832	156

RUN NO	PHOTO NO	0-0.3	.3-.6	.6-1.0	1.-1.5	1.5-2.5	2.5-4.	NO DROP
85	6	.1813	.4604	.6883	.8837	.9581	.9860	215
85	7	.1609	.4770	.7241	.9310	.9712	.9885	174
85	8	.1546	.4077	.6795	.8904	.9615	.9911	218
85	9	.2138	.4424	.6572	.8537	.9305	.9744	219
87	1	.2569	.6647	.9163	.9680	.9958	1.0000	425
87	2	.2788	.7132	.9047	.9766	.9942	1.0000	412
87	3	.3130	.7447	.9249	.9807	.9976	1.0000	461
87	4	.3086	.7016	.8969	.9674	.9971	1.0000	455
87	5	.2451	.6865	.9005	.9829	.9981	1.0000	509
87	6	.2380	.6438	.8584	.9855	.9968	.9999	289
87	7	.2627	.7173	.9144	.9866	.9984	1.0000	428
87	8	.2479	.7038	.9325	.9774	.9966	1.0000	432
89	1	.2725	.7012	.9515	.9929	1.0000	.0000	402
89	2	.2642	.7001	.9266	.9922	.9999	.0000	358
89	4	.2364	.7064	.9277	.9944	.9999	.0000	360
89	3	.2616	.7581	.9325	.9939	1.0000	.0000	333
89	5	.2061	.7321	.9240	.9941	.9999	.0000	264
89	6	.2353	.6910	.9711	.9964	.9999	.0000	349
89	7	.2434	.7481	.9500	.9963	.9999	.0000	366
89	8	.3091	.7314	.9036	.9924	1.0000	.0000	391
91	3	.2535	.7897	.9707	1.0000	.0000	.0000	447
91	4	.2395	.6881	.9047	.9965	1.0000	.0000	413
91	5	.2669	.7346	.9463	.9971	1.0000	.0000	485
91	6	.2964	.7687	.9527	.9854	1.0000	.0000	547
91	8	.3281	.7861	.9532	.9988	1.0000	.0000	520
91	9	.3507	.8164	.9587	.9991	1.0000	.0000	576
91	10	.3468	.7914	.9660	.9983	1.0000	.0000	574
91	11	.2650	.7620	.9511	.9970	1.0000	.0000	555
93	1	.2929	.8035	.9623	.9947	1.0000	.0000	390
93	2	.4007	.7562	.9275	.9964	.9999	.0000	263
93	3	.3867	.8465	.9676	.9963	1.0000	.0000	361
93	4	.3727	.8705	.9591	.9959	1.0000	.0000	434
93	5	.3254	.8025	.9433	.9926	.9999	.0000	392
93	6	.3461	.7949	.9612	.9977	1.0000	.0000	418
93	7	.3156	.7861	.9531	.9926	1.0000	.0000	407
93	8	.3337	.8111	.9699	.9929	1.0000	.0000	413
97	1	.1858	.4767	.7838	.9338	.9742	1.0000	137
97	2	.2561	.5335	.7695	.9289	.9908	.9999	136
97	3	.1713	.4697	.7605	.9196	.9770	1.0000	152
97	4	.1800	.4680	.7650	.9312	.9803	.9999	119
97	5	.1576	.4048	.6780	.8619	.9495	.9999	161
97	6	.1783	.3618	.6625	.8817	.9633	.9999	198
97	2	.2040	.4591	.7085	.8559	.9428	1.0000	189
97	4	.1848	.4620	.6733	.8927	.9630	1.0000	171
99	2	.0872	.4306	.7463	.9059	.9613	.9850	246
99	3	.1512	.5334	.8443	.9602	.9872	.9949	274
99	4	.1722	.4553	.7712	.9148	.9731	.9940	248
99	5	.1064	.4614	.7708	.9240	.9552	.9864	211
99	6	.1176	.4742	.8134	.9353	.9838	.9944	310
99	7	.2118	.5710	.7437	.9123	.9654	.9930	311
99	8	.2359	.6220	.8623	.9563	.9897	.9999	334
99	9	.2322	.5826	.8542	.9403	.9718	.9933	286
101	1	.3030	.7071	.9186	.9859	.9971	.9999	333
101	3	.2712	.7072	.9234	.9862	1.0000	.0000	312
101	4	.1770	.5739	.8475	.9583	.9905	.9999	224
101	5	.3134	.7561	.8969	.9707	.9938	.9999	417
101	6	.1939	.6166	.8881	.9773	.9959	.9999	298
101	7	.2608	.7071	.8999	.9825	.9959	.9999	386
101	8	.2018	.6587	.8926	.9697	.9944	.9999	395
101	9	.2568	.6432	.8500	.9674	.9939	1.0000	473
103	1	.3383	.7813	.9706	.9958	.9999	.0000	436
103	2	.3495	.7681	.9551	.9957	.9999	.0000	528
103	3	.3605	.7757	.9534	.9969	.9999	.0000	620
103	4	.1800	.6055	.9042	.9914	.9999	.0000	266
103	5	.2359	.8271	.9548	.9986	.9999	.0000	603
103	6	.3110	.7484	.9445	.9886	1.0000	.0000	560
105	1	.2112	.7835	.9637	.9953	1.0000	.0000	413
105	2	.1503	.7081	.9193	.9935	.9999	.0000	331
105	3	.1569	.7106	.9298	.9924	.9999	.0000	367
105	4	.2854	.7968	.9502	.9949	1.0000	.0000	519
105	5	.1379	.7330	.9305	.9954	.9999	.0000	335
105	6	.2897	.7231	.9425	.9930	.9995	.0000	392
105	7	.2204	.7313	.9384	.9937	.9999	.0000	399
105	8	.2665	.7673	.9453	.9945	1.0000	.0000	493
107	1	.2722	.7895	.9430	.9865	.9969	1.0000	452
107	2	.2796	.7659	.9311	.9878	.9987	.9999	449
107	3	.2762	.7983	.9420	.9884	.9977	.9999	424
107	5	.3122	.7805	.9301	.9821	.9981	1.0000	493
107	7	.3092	.7955	.9658	.9915	.9975	1.0000	472
107	8	.2824	.7916	.9606	.9953	.9999	.0000	452
107	9	.2562	.6915	.9278	.9847	.9961	1.0000	438
107	10	.2850	.7631	.9320	.9890	.9971	.9999	376

RUN NO	PHOTO NO	0-0.3	.3-.6	.6-1.0	1.-1.5	1.5-2.5	2.5-4.	NO DROP
113	1	.1369	.4358	.6413	.8356	.9439	1.0000	210
113	2	.1671	.3047	.5873	.7739	.9039	.9999	159
113	3	.2190	.4076	.6423	.8371	.9382	1.0000	161
113	1	.1504	.3008	.5929	.7876	.9026	1.0000	113
113	2	.0956	.2782	.6086	.8173	.9391	1.0000	115
113	3	.1176	.3686	.6432	.8315	.9413	.9962	129
115	1	.2287	.6049	.8591	.9790	.9949	.9999	241
115	2	.2474	.6505	.9179	.9817	.9965	.9999	283
115	3	.2799	.6264	.8735	.9815	.9973	1.0000	287
115	4	.2772	.6394	.8920	.9789	.9935	.9999	293
115	5	.2503	.5535	.8073	.9765	.9949	.9999	284
115	1	.3462	.7017	.9234	.9835	.9978	.9999	299
115	2	.3048	.6597	.8929	.9805	.9965	1.0000	267
115	3	.2241	.6489	.9137	.9790	.9916	.9999	346
115	4	.3015	.6104	.8714	.9724	.9951	.9999	380
115	5	.2555	.6218	.8339	.9872	.9950	.9999	316
119	1	.3605	.7679	.9809	.9967	1.0000	.0000	469
119	2	.3348	.7653	.9573	.9932	1.0000	.0000	413
119	3	.3314	.7704	.9710	.9937	1.0000	.0000	401
119	4	.3142	.7548	.9614	.9930	1.0000	.0000	362
119	5	.2865	.7449	.9598	.9927	.9999	.0000	350
119	6	.3029	.7556	.9395	.9965	.9999	.0000	338
119	7	.2678	.7529	.9575	.9878	.9999	.0000	251
119	8	.3653	.8592	.9601	.9922	1.0000	.0000	407
121	1	.2927	.8457	.9541	.9939	.9999	.0000	362
121	2	.2970	.8193	.9584	.9924	1.0000	.0000	400
121	3	.3040	.7204	.9450	.9961	1.0000	.0000	499
121	4	.4080	.8125	.9629	.9927	.9999	.0000	332
121	5	.2803	.7182	.9615	.9984	1.0000	.0000	378
121	6	.3073	.7299	.9206	.9978	1.0000	.0000	400
121	7	.3506	.7975	.9599	.9920	.9999	.0000	340
121	8	.3541	.8170	.9655	.9940	1.0000	.0000	396
123	1	.4982	.8619	.9917	1.0000	.0000	.0000	392
123	2	.4969	.8514	.9738	1.0000	.0000	.0000	360
123	3	.5098	.8887	.9931	1.0000	.0000	.0000	397
123	4	.5573	.9146	.9804	.9999	.0000	.0000	390
123	5	.4750	.9077	.9809	1.0000	.0000	.0000	498
123	6	.5187	.8824	.9842	.9999	.0000	.0000	453
123	7	.4926	.8892	.9873	.0000	.0000	.0000	543
123	8	.4153	.8148	.9790	1.0000	.0000	.0000	492
125	1	.3411	.8122	.9639	.9974	.9999	.0000	246
125	2	.2727	.7003	.8998	.9967	.9999	.0000	343
125	3	.4013	.8345	.9668	.9956	1.0000	.0000	294
125	4	.3101	.7753	.9567	.9956	1.0000	.0000	356
125	5	.3387	.8103	.9562	.9962	1.0000	.0000	425
125	6	.3135	.7678	.9406	.9950	1.0000	.0000	359
125	7	.3670	.7619	.9519	.9979	1.0000	.0000	531
125	8	.3652	.7961	.9553	.9988	1.0000	.0000	391
131	1	.3763	.7607	.9515	.9851	.9981	0000	366
131	1	.3491	.6255	.8219	.9474	.9848	1.0000	201
131	2	.1864	.4609	.7630	.9088	.9820	1.0000	238
131	3	.2504	.5448	.7863	.9522	.9888	1.0000	213
131	4	.2536	.5182	.7498	.9194	.9779	1.0000	179
131	5	.2343	.6160	.8606	.9645	.9893	1.0000	280
131	6	.2864	.5998	.8290	.9491	.9884	1.0000	226
131	7	.3073	.5781	.8663	.9824	.9999	.0000	305
131	8	.2806	.5519	.7577	.8774	.9875	1.0000	164
133	2	.2872	.7312	.9463	.9790	.9898	.9964	317
133	3	.3533	.7772	.9491	.9873	.9958	.9989	309
133	4	.3432	.5852	.8901	.9649	.9899	.9979	299
133	5	.3531	.7963	.9593	.9896	.9997	.0000	322
133	6	.3922	.7683	.8996	.9730	.9870	.9998	251
133	7	.3576	.7802	.9412	.9710	.9883	.9998	238
133	9	.2734	.7116	.9230	.9823	.9925	.9999	352
135	1	.2205	.6932	.9295	.9871	.9999	.0000	301
135	2	.2930	.7624	.9514	.9873	.9988	1.0000	373
135	3	.2627	.6532	.8860	.9777	.9981	.9999	317
135	4	.2937	.6795	.9525	.9905	.9990	.9999	421
135	5	.2749	.6640	.9364	.9865	.9989	.9999	384
137	1	.3569	.7657	.9516	.9591	1.0000	.0000	407
137	2	.3596	.8540	.9709	.9942	1.0000	.0000	410
137	3	.3015	.8316	.9670	.9933	.9999	.0000	366
137	4	.3998	.8347	.9720	.9912	1.0000	.0000	443
137	5	.4022	.8381	.9683	.9942	.9999	.0000	412
137	6	.4009	.8430	.9721	.9942	1.0000	.0000	450
137	7	.3549	.7690	.9799	.9975	1.0000	.0000	430
137	8	.4116	.8787	.9707	.9971	.9999	.0000	404
139	3	.3087	.8073	.9755	.9969	1.0000	.0000	440
139	4	.3565	.7761	.9734	.9958	1.0000	.0000	480
139	5	.3505	.7501	.9625	.9915	1.0000	.0000	471
139	6	.3794	.8041	.9667	.9974	.9999	.0000	487
139	7	.3567	.8501	.9597	.9972	.9999	.0000	426
139	8	.3704	.8323	.9719	.9967	.9999	.0000	326
139	9	.3854	.8041	.9572	.9948	1.0000	.0000	518
139	10	.3120	.7526	.9729	.9965	1.0000	.0000	437

APPENDIX 11, DROP SIZE DISTRIBUTION DATA

RUN NO	PHOTO NO	0-0.3	.3-.6	.6-1.0	1.-1.5	1.5-2.5	2.5-4.	NO DROP
143	1	.3009	.4805	.6650	.8155	.9271	.9757	206
143	2	.2148	.4958	.6611	.8099	.9421	.9834	121
143	3	.3597	.5467	.7194	.8705	.9280	.9640	139
143	4	.2448	.5034	.6326	.8095	.9251	.9591	147
143	5	.2348	.4090	.5833	.7651	.9015	.9848	132
143	6	.2654	.4567	.5925	.7777	.9506	.9938	162
143	7	.1504	.3539	.5929	.8053	.9646	1.0000	113
143	8	.1545	.3454	.5545	.7636	.9363	.9818	110
143	9	.1810	.3362	.5172	.7241	.9051	.9827	116
143	10	.1438	.3669	.5611	.8345	.9352	.9784	139
145	1	.2046	.4327	.7231	.9032	.9752	1.0000	161
145	2	.1534	.3986	.6863	.8747	.9514	.9933	192
145	3	.1744	.3647	.6897	.8681	.9325	.9875	183
145	4	.2119	.4662	.7064	.8548	.9537	.9961	134
145	5	.2423	.5229	.7484	.8988	.9730	1.0000	226
147	1	.3945	.7500	.9137	.9735	.9947	1.0000	342
147	2	.3417	.6520	.8858	.9676	.9928	.9999	277
147	3	.3041	.6027	.8424	.9509	.9930	.9999	316
147	4	.2614	.6245	.8608	.9673	.9847	1.0000	266
147	5	.2652	.6444	.9282	.9764	.9939	1.0000	449
147	6	.2757	.6107	.8491	.9785	.9933	.9999	351
147	7	.2741	.6182	.8870	.9659	.9874	.9999	333
149	1	.3142	.7227	.9322	.9924	.9999	.0000	430
149	2	.1796	.6683	.9189	.9909	.9999	.0000	383
149	3	.2908	.6552	.9461	.9908	.9982	.9999	352
149	4	.2514	.6515	.9532	.9864	.9963	1.0000	425
149	5	.2949	.7427	.9533	.9864	.9970	.9999	418
149	6	.3392	.7648	.9264	.9835	.9945	1.0000	360
149	7	.2899	.6438	.9438	.9767	.9935	.9999	346
149	8	.3727	.7615	.9559	.9784	.9930	.9999	387
151	1	.2195	.7430	.8894	.9512	.9918	.9983	279
151	2	.4128	.8210	.9156	.9723	.9930	.9982	338
151	3	.3875	.8349	.9560	.9856	.9976	1.0000	487
151	4	.2403	.6105	.8412	.9474	.9924	1.0000	276
151	5	.3616	.8148	.9409	.9840	.9970	.9999	431
151	6	.4251	.7923	.9183	.9819	.9903	1.0000	383
151	7	.4085	.7510	.9402	.9838	.9989	1.0000	341
151	8	.5856	.6464	.8905	.9705	.9919	.9986	351
151	9	.4470	.6887	.9238	.9801	.9975	.9999	247
153	1	.7391	.9278	.9861	.9977	1.0000	.0000	422
153	2	.3353	.8240	.9571	.9912	.9999	.0000	365
153	3	.5054	.8475	.9662	.9962	.9999	.0000	419
153	4	.5217	.8485	.9759	.9971	1.0000	.0000	429
153	5	.4976	.8957	.9824	.9968	1.0000	.0000	465
153	6	.4245	.8499	.9633	.9961	.9999	.0000	442
153	7	.5021	.9005	.9641	.9950	.9999	.0000	389
153	9	.4521	.8595	.9759	.9966	.9999	.0000	444
153	10	.4563	.8907	.9710	.9936	.9999	.0000	411
153	11	.4202	.8329	.9576	.9922	.9999	.0000	390
155	1	.2757	.7423	.9162	.9588	.9862	.9972	328
155	2	.3262	.7439	.9251	.9747	.9921	.9982	307
155	3	.2708	.7625	.9308	.9849	.9958	.9983	358
155	4	.3422	.7501	.9292	.9758	.9926	.9991	346
155	5	.3765	.7051	.8928	.9834	.9939	.9999	443
155	6	.3726	.7984	.9421	.9750	.9942	.9999	374
157	1	.2818	.7326	.9581	.9903	.9999	.0000	132
157	2	.2804	.7917	.9525	.9938	.9999	.0000	254
157	3	.3763	.8899	.9814	.9920	.9999	.0000	286
157	4	.4215	.8396	.9813	.9956	1.0000	.0000	337
157	5	.5364	.9181	.9861	.9940	1.0000	.0000	364
157	6	.4484	.9173	.9921	.9975	1.0000	.0000	336
157	7	.4396	.9236	.9926	1.0000	.0000	.0000	298
157	8	.4414	.9376	.9844	.9971	.9999	.0000	305
157	9	.4478	.9323	.9853	.9981	.9999	.0000	273

APPENDIX 14, PROGRAM FOR COMPUTING MASS TRANSFER COEFFICIENTS

```
  5 READ100,RUN,FV,TEMP,CIN,CWN,CWT,FLOW,FLOI,EM,SIGMA,VES
    READ10,POW,REV,DIA,VDIA,DPRO,RUN,IN,DSD
    VOLF=FV*FLOI/(FLOW+FLOI)
    DSL=LOGF(EM*.06411)+3.5*(LOGF(SIGMA))**2
    DSV=EXPF(DSL)
    DVL=LOGF(EM*.06411)+3.5*(LOGF(SIGMA))**2
    DV=EXPF(DVL)
    AREA=6.*VOLF/DSV
    ARE=6.*VOLF/DSD
    POW=1.113*POW
    DEN1=(.70984-TEMP*.000903)*(1.+CIN*.437)
    DENS=DEN1*VOLF+.9985*(1.-VOLF)
    VIS1=0.0146*EXPF(1036./(TEMP+273.3))
    VISW=100./(2.1482*(TEMP+81.97)-120.)
    VISS=VISW/(1.-VOLF)*(1.+1.5*VIS1*VOLF/(VIS1+VISW))
    DAB=2.722*(TEMP+273.3)*1.E-8/VISW
    SCNO=.01*VISW/(.9985*DAB)
    POW=POW*1.113
    PO=POW*2.12E+8/(REV**3*DIA**5*DENS)
    PONO=POW*2.12E+8/(REV**3*VDIA**5*DENS)
    POT=POW*2.12E8/(REV**3*VDIA**2*DIA**3*DENS)
    RE=REV*DIA**2*DENS*1.667/VISS
    REIV=DENS*(POW/(1.E+6*VES))**.1667*DSV**.667/SQRF(VISS*.01)
    REII=DENS*(POW/(DIA**5))**.1667*DSV**.667/SQRF(VISS*.01)
    REDSV=REV*DIA*DSV*DENS/(VISS*.6)
    REDSD=REV*DIA*DSD*DENS/(VISS*.6)
    RD=REV*DIA/60.
    R2D2=REV**2*DIA**2/(VDIA**3*3600.)
    RD3V3=REV*DIA**3/(VDIA**3*60.)
    R2D1=REV**2*DIA/(VDIA**2*3600.)
    DNT=(REV/60.)**1.4*DIA**1.6
    DNTR=DNT*(DIA/VDIA)**2.4
    DNS=(REV/60.)**1.8*DIA**1.6
    DNSR=DNS*(DIA/VDIA)**.84
    DN12=DIA**.4/(REV*DIA/60.)**1.2
    DNR=DN12*(VDIA/DIA)**1.2
    FLO=FLOW/FLOI*1106./((786.1-TEMP)*(1.+CIN*.437))
    CIT=CIN-(CWT-CWN)*FLO
    QEQN=CIN
    QEQT=0.
    DO1041=1,30
    QEQR=(QEQN-QEQT)*0.618+QEQT
    ERR=0.01877*QEQR**0.9329-(CIN-QEQR)/FLO
    IF(ERR**2-2.*10.**(-13))105,105,101
101 IF(ERR)102,105,103
102 QEQT=QEQR
    GO TO 104
103 QEQN=QEQR
104 CONTINUE
105 EFFY=(CWT-CWN)/(0.01877*QEQR**0.9329-CWN)
    IF(EFFY-1.)107,106,106
106 COA=.0
    CO=.0
    COIA=.0
    COI=.0
    GO TO 118
107 IF(EFFY-.2)131,121,121
121 IF(EFFY-.4)132,122,122
122 IF(EFFY-.6)133,123,123
123 IF(EFFY-.8)134,124,124
131 W=1.E+6
    V=1.E-6
    GO TO 117
132 W=5.E+5
    V=2.E-6
    GO TO 117
133 W=2.5E+5
    V=4.E-6
    GO TO 117
134 W=2.E+5
    V=5.E-6
    GO TO 117
124 W=1.66667E+5
    V=6.E-6
1170COIA=FLOW*6.E+3*(1.-.1295*CWT)/(VES*(1.-VOLF)*(.01877*CIN**.9329-C
   1WN-.01877*QEQR**.9329*.02)/LOGF(50.*(CIN/QEQR)**.9329))
    COI=COIA/(AREA*100.)
    RISE=11.66-FLOI*5.82E-3
    THETA=RISE/((FLOW+FLOI)*1.46E-3)+RISE/(FLOI*8.68E-2)
    COPEN=36.*(DAB/THETA)**.5
    TRIN=COPEN*(.01877*CIN**.9329-CWN)*3.66*RISE/FLOW
    EFIN=(TRIN-CWN)/(.01877*QEQR**.9329-CWN)
   OCOSAM=(DAB*VISW)**(-.67)*(VISW/VISI)**.254*(SCNO)**(-1.46)*(1./VIS
   1W)**.397*DAB*1170.
    TRSAM=COSAM*(.01877*CIT**.9329-CWT)*13.6
    EFPH=TRSAM/(.01877*QEQR**.9329-CWN)
    TAV=VOLF*VES*6.E+7/FLOI
```

```
    TOTDR=1.E-85
    EFD=1.E-85
   OTDF=.00971*(CIN**1.9329-(CWT/.01877)**2.073)/(CIN-(CWT/.01877)**1.
   1072)-CWT
    IF(TDF)27,27,11
 11 DCNT=FLOI*DPRO*3.82/((DV)**3*FLOW)
    CODR=35.2*DAB*(2.098E+5*SCNO/VISW)**.333
    DIMENSION DI(10)
    DI(1)=.0175
    DI(2)=.0156
    DI(3)=.0126
    DI(4)=.0108
    DI(5)=.0091
    DI(6)=.0079
    DI(7)=.0067
    DI(8)=.0057
    DI(9)=.0046
    DI(10)=.0032
    DO14I=1,10
    TS=DENI*DI(I)*(CIN-(1.02*CWT/.01877)**1.069)*6./(COI*TDF)
    IF(TS-.01*TAV)27,27,28
 28 TM=(TS-TAV+TAV*EXPF(-TS/TAV))/(1.-EXPF(-TS/TAV))
    XIN=CIN
    L=TM+.5
    DO12J=1,L
 12 XIN=XIN-COI*(.01877*XIN*.9329-CWT)*.9985/(6.0*DENI*DI(I))
    TDR=0.
    DO13M=1,20
    UDR=CODR*(.01877*XIN**.9329-CWT)*DI(I)**2*.0874
    XIN=XIN-1.91*UDR/(DI(I)**3*DENI)
 13 TDR=TDR+UDR
    EFM=TDR*DCNT/(.01877*QEQR**.9329-CWN)*.1
    EFD=EFD+EFM
    TOTDR=TOTDR+TDR*DCNT*.1
    IF(EFM-.0002)27,27,14
 14 CONTINUE
 27 FWN=CWN+TRIN
    FIN=CIN-TRIN*FLO
    FWT=CWT-TOTDR-TRSAM
    FIT=CIT+(TOTDR+TRSAM)*FLO
    IF(FWT-FWN)15,15,17
 15 PRINT16,RUN,FWN,FWT
    GO TO 5
 170COA=FLOW*6.E-5*(FWT-FWN)*(1.-.1295*FWT)/(.01877*FIT**.9329-FWT)/(V
   1ES*(1.-VOLF))
    CO=COA/(ARE*100.)
    KFIT=FIT*W+.5
    KFIN=FIN*W+.5
    N=KFIN-KFIT
    SFIT=FIT
    DF=0.
    DO25I=1,N
    DF=DF+1.E-8/(.01877*SFIT**.9329-FWT)
 25 SFIT=SFIT+V
    COIA=FLOW*6.E+3*(1.-.1295*FWT)*V*DF/(VES*FLO*(1.-VOLF))
    COI=COIA/(AREA*100.)
    SHTCO=CO*VDIA/(DAB*36.)
    SHTCI=COI*VDIA/(DAB*36.)
    SHICO=CO*DIA/(DAB*36.)
    SHICI=COI*DIA/(DAB*36.)
    CODSD=CO*DSD/(DAB*36.)
    CIDSD=COI*DSD/(DAB*36.)
    CODSV=CO*DSV/(DAB*36.)
    CIDSV=COI*DSV/(DAB*36.)
    EM=EM*.0641
    SIGMA=SIGMA+.005
118 DIA=DIA*.01
    VDIA=VDIA*.01
    REV=REV*60.
    POW=POW*.036
    FLOW=FLOW*6.E-5
    FLOI=FLOI*6.E-5
    CWT=CWT*.1295
    CIN=CIN*.647
    CIT=CIT*.647
    DAB=DAB*.36
    DENI=DENI*1000.
    DENS=DENS*1000.
    VISI=VISI*360.
    VISS=VISS*360.
    DR=DIA/VDIA
    EFOUT=EFPH+EFD
    IF(SENSE SWITCH 1)50,51
 51 PRINT23,RUN,SHTCO,SHTCI,SHICO,SHICI,CODSD,CIDSD,CODSV,CIDSV,DR,FV
    PRINT24,RUN,REDSD,REDSV,REII,REIV,RD,R2D2,RD3V3,R2D1,PONO,POT
    PRINT75,RUN,DNT,DNTR,DNS,DNSR,DN12,EM,DNR,SIGMA
    PRINT20,RUN,DIA,VDIA,REV,POW,VES,VOLF,FLOW,FLOI,DSD,DSV
    PRINT22,RUN,CWN,CWT,CIN,CIT,DAB,DENS,DENI,VISI,VISS,TEMP
 50 PRINT21,RUN,COA,CO,COIA,COI,PO,RE,SCNO,EFFY,EFIN,EFOUT
    PUNCH20,RUN,DIA,VDIA,REV,POW,VES,VOLF,FLOW,FLOI,DSD,DSV
    PUNCH22,RUN,CWN,CWT,CIN,CIT,DAB,DENS,DENI,VISI,VISS,TEMP
    PUNCH21,RUN,COA,CO,COIA,COI,PO,RE,SCNO,EFFY,EFIN,EFOUT
    PUNCH23,RUN,SHTCO,SHTCI,SHICO,SHICI,CODSD,CIDSD,CODSV,CIDSV,DR,FV
    PUNCH24,RUN,REDSD,REDSV,REII,REIV,RD,R2D2,RD3V3,R2D1,PONO,POT
    PUNCH75,RUN,DNT,DNTR,DNS,DNSR,DN12,EM,DNR,SIGMA
    GO TO 5
100 FORMAT(14,F5.4,F4.1,3E8.3,2F6.0,F6.5,F5.3,F6.5)
 10 FORMAT(F8.0,F6.1,F6.3,F6.3,F6.4,I4,I2,F6.4)
 16 FORMAT(I4,2F10.8)
103 FORMAT(2I4,7F7.4,F6.1,F10.4)
 20 FORMAT(I4,2F8.4,2F8.0,F8.6,F8.4,4F7.4)
 21 FORMAT(I4,F8.2,F8.4,F8.2,F8.4,F8.3,F8.0,F7.0,3F7.4)
 22 FORMAT(I4,F6.2,E10.3,2F8.6,E9.2,2F7.0,3F7.1)
 23 FORMAT(I4,4F8.0,2F8.1,2F7.1,2F7.4)
 24 FORMAT(I4,2F8.1,2F8.3,F8.2,F8.4,F7.4,F7.3,2F7.4)
 75 FORMAT(I4,2F8.2,F8.1,F8.2,2F8.5,F7.5,F7.4)
    END
```

APPENDIX 13, MASS TRANSFER DATA

RUN	IMP DIA	VES DIA	REVS	POWER	VES VOL	VOL FR	FLOW	FLOI	DSD CM	DSV CM
RUN	CWN	CWT	CIN	CIT	DAB	DENS	DENI	10^3VISI	10^3VISS	TEMP
RUN	COA	CO DSD	COIA	COI DSV	PONO DI	RE	SCNO	EFFY	EFIN	EFOUT
	MKH UNITS									
37	.0449	.1405	28680.	310.	.002090	.0207	.4536	.0583	.1293	.1650
37	0.00	8.935E-07	.002067	.002018	2.61E-06	992.	695.	187.1	403.7	16.7
37	17.19	.1698	17.16	.1698	9.184	14248.	1500.	.1009	.0004	.0094
39	.0449	.1405	35160.	467.	.002090	.0290	.4536	.0583	.1215	.1580
39	0.00	1.825E-06	.002067	.001966	2.59E-06	989.	696.	187.8	411.7	16.4
39	42.68	.2348	41.92	.2306	7.530	17086.	1522.	.2062	.0004	.0080
41	.0449	.1405	41520.	628.	.002090	.0446	.4536	.0583	.0949	.1123
41	0.00	2.421E-06	.002067	.001932	2.57E-06	984.	696.	188.5	424.5	16.1
41	63.76	.1870	61.17	.1798	6.170	19474.	1546.	.2735	.0004	.0071
43	.0449	.1405	47040.	834.	.002090	.0482	.4536	.0583	.0629	.0823
43	0.00	3.626E-06	.002067	.001865	2.57E-06	983.	696.	188.2	425.8	16.2
43	119.34	.2794	111.51	.2613	5.641	21973.	1538.	.4096	.0004	.0059
45	.0449	.1405	51900.	1015.	.002090	.0384	.8610	.0702	.0577	.0595
45	0.00	2.654E-06	.002067	.001834	2.55E-06	986.	696.	189.2	423.5	15.8
45	145.51	.3794	135.27	.3528	5.096	24447.	1570.	.3382	.0003	.0071
47	.0726	.1405	12900.	249.	.002090	.0267	.4536	.0583	.1402	.2620
47	0.00	8.676E-07	.002067	.002019	2.56E-06	990.	696.	188.7	414.2	16.0
47	16.82	.1287	16.75	.1281	7.376	16269.	1554.	.0980	.0004	.0088
49	.0726	.1405	19920.	504.	.002090	.0456	.4572	.0583	.0854	.0827
49	0.00	3.017E-06	.002067	.001898	2.57E-06	984.	696.	188.5	425.1	16.1
49	89.09	.2368	84.32	.2242	4.078	24334.	1546.	.3408	.0004	.0065
51	.0726	.1405	28080.	1169.	.002090	.0779	.4536	.0583	.0680	.0653
51	0.00	5.296E-06	.002067	.001772	2.57E-06	974.	696.	188.2	445.7	16.2
51	266.40	.2743	230.58	.2375	3.413	32391.	1538.	.5983	.0004	.0040
53	.0726	.1405	35040.	2129.	.002090	.0753	.7440	.0736	.0626	.0577
53	0.00	5.374E-06	.002067	.001678	2.58E-06	975.	696.	188.0	442.9	16.3
53	504.67	.4120	409.50	.3345	3.195	40716.	1530.	.6491	.0003	.0038
55	.0726	.1405	41160.	3060.	.002090	.0736	.9601	.0860	.0469	.0530
55	0.00	5.788E-06	.002067	.001604	2.57E-06	976.	696.	188.2	442.8	16.2
55	875.30	.6023	655.74	.4512	2.831	47861.	1538.	.7194	.0002	.0031
57	.0726	.1405	49080.	5313.	.002090	.0729	1.1118	.0960	.0415	.0485
57	0.00	6.280E-06	.002067	.001546	2.54E-06	976.	696.	189.4	447.5	15.7
57	1461.93	.8252	985.03	.5560	2.898	56482.	1578.	.7892	.0002	.0022
69	.1182	.2220	8160.	287.	.008410	.0259	.7452	.0717	.1346	.2531
69	0.00	1.042E-06	.002085	.002008	2.64E-06	990.	695.	185.9	402.2	17.2
69	8.50	.0765	8.37	.0754	2.936	28111.	1463.	.1257	.0003	.0104
71	.1182	.2220	15360.	1562.	.008410	.0569	.7452	.0717	.0612	.0632
71	0.00	5.840E-06	.002085	.001650	2.64E-06	981.	695.	185.9	421.6	17.2
71	157.83	.2814	121.90	.2338	2.416	49999.	1463.	.7044	.0003	.0035
73	.1182	.2220	12150.	820.	.008410	.0356	.7452	.0717	.0794	.1710
73	0.00	3.457E-06	.002085	.001828	2.57E-06	987.	696.	188.5	418.7	16.1
73	45.99	.1805	42.14	.1654	2.548	40083.	1546.	.4170	.0003	.0062
75	.1182	.2220	22800.	4800.	.008410	.0630	1.1430	.0893	.0464	.0465
75	0.00	7.951E-06	.002085	.001357	2.55E-06	979.	696.	189.2	439.7	15.8
75	0.00	0.0000	0.00	0.0000	2.273	71035.	1570.	1.0210	.0003	.0062
77	.1182	.2220	30480.	11156.	.008410	.0665	1.1430	.0893	.0440	.0488
77	0.00	7.381E-06	.002085	.001409	2.54E-06	978.	696.	189.4	443.1	15.7
77	1748.21	1.2521	583.10	.4180	2.214	94132.	1578.	.9478	.0002	.0005
79	.1182	.2220	19140.	2918.	.008410	.0599	1.1430	.0893	.0518	.0531
79	0.00	6.216E-06	.002085	.001516	2.52E-06	980.	696.	189.9	440.7	15.5
79	379.33	.5019	246.76	.3267	2.334	59550.	1594.	.7981	.0002	.0021
83	.0766	.2220	10830.	158.	.008410	.0232	.4536	.0583	.2369	1.4402
83	0.00	7.640E-07	.002085	.002043	2.59E-06	991.	695.	187.5	407.2	16.5
83	3.50	.0595	3.52	.0595	6.059	15475.	1515.	.0856	.0004	.0094
85	.0766	.2220	18540.	527.	.008410	.0304	.4536	.0583	.1992	.1851
85	0.00	2.784E-06	.002085	.001930	2.58E-06	989.	696.	188.0	413.5	16.3
85	18.87	.1270	18.01	.1213	4.033	26027.	1530.	.3120	.0004	.0069
87	.0766	.2220	27360.	1349.	.008410	.0524	.4536	.0583	.0776	.0731
87	0.00	6.734E-06	.002085	.001710	2.58E-06	982.	696.	188.0	427.6	16.3
87	133.17	.3278	102.28	.2520	3.233	36898.	1530.	.7546	.0004	.0024
89	.0766	.2220	35880.	2602.	.008410	.0588	1.1430	.0893	.0568	.0597
89	0.00	6.513E-06	.002085	.001488	2.55E-06	980.	696.	188.9	435.8	15.9
89	489.97	.7740	291.32	.4605	2.770	47375.	1562.	.8364	.0002	.0018
91	.0766	.2220	41040.	3683.	.008410	.0587	1.2138	.0905	.0529	.0542
91	0.00	6.759E-06	.002085	.001436	2.54E-06	980.	696.	189.4	437.9	15.7
91	745.01	1.0052	378.55	.5109	2.620	53940.	1578.	.8805	.0002	.0013
93	.0766	.2220	31620.	2000.	.008410	.0558	1.1430	.0893	.0540	.0497
93	0.00	5.633E-06	.002085	.001569	2.54E-06	981.	696.	189.4	435.9	15.7
93	249.56	.4842	182.24	.3541	3.109	41787.	1578.	.7233	.0002	.0030
225	202.53	.3421	140.00	.2366	3.280	37181.	1477.	.8486	.0005	.0015
225	.0726	.2220	31320.	1562.	.008410	.0724	.3476	.0576	.0708	.0718
225	0.00	7.731E-06	.002014	.001679	2.63E-06	976.	695.	186.4	433.8	17.0
23	.0726	.2220	39840.	2884.	.008410	.1172	.3476	.0576	.0560	.0543
23	0.00	8.806E-06	.002014	.001633	2.66E-06	962.	694.	185.2	460.2	17.5
23	1132.02	.8849	391.13	.3062	2.983	43966.	1441.	.9688	.0005	.0003
24	.0726	.2220	47160.	4728.	.008410	.0965	.5883	.0734	.0465	.0486
24	0.00	8.404E-06	.002014	.001531	2.64E-06	969.	695.	186.2	449.4	17.1
24	2812.59	2.1846	647.51	.5031	2.929	53643.	1470.	.9788	.0003	.0002
25	5060.05	3.2506	801.67	.5155	2.818	60215.	1500.	.9879	.0003	.0001
25	.0726	.2220	53760.	6731.	.008410	.0998	.5883	.0734	.0410	.0454
25	0.00	8.482E-06	.002014	.001527	2.61E-06	968.	695.	187.1	455.9	16.7
97	.0627	.2220	19440.	311.	.008410	.0237	.4536	.0583	.1213	.1562
97	0.00	1.463E-06	.002157	.002076	2.55E-06	991.	696.	189.2	414.2	15.8
97	7.57	.0941	7.42	.0923	5.616	18297.	1570.	.1585	.0004	.0080

APPENDIX 13. MASS TRANSFER DATA CONTD.

RUN	IMP DIA	VES DIA	REVS	POWER	VES VOL	VOL FR	FLOW	FLOI	DSD CM	DSV CM
RUN	CWN	CWT	CIN	CIT	DAB	DENS	DENI	10³VISI	10³VISS	TEMP
RUN	COA	CO DSD	COIA	COI DSV	PONO DI	RE	SCNO	EFFY	EFIN	EFOUT
	MKH UNITS									
99	.0627	.2220	26280.	554.	.008410	.0273	.4536	.0583	.1813	.1248
99	0.00	2.486E-06	.002157	.002019	2.55E-06	990.	696.	188.9	415.5	15.9
99	15.28	.1130	14.71	.1090	4.049	24631.	1562.	.2693	.0004	.0070
101	.0627	.2220	34920.	1276.	.008410	.0411	.4536	.0583	.0817	.0797
101	0.00	6.112E-06	.002157	.001817	2.57E-06	986.	696.	188.2	421.3	16.2
101	84.30	.2934	70.41	.2451	3.988	32146.	1538.	.6621	.0004	.0033
103	.0627	.2220	43020.	1885.	.008410	.0498	.7452	.0717	.0549	.0546
103	0.00	6.708E-06	.002157	.001658	2.55E-06	983.	696.	189.2	430.9	15.8
103	238.16	.5346	166.21	.3732	3.158	38611.	1570.	.7839	.0003	.0022
105	.0627	.2220	50640.	3012.	.008410	.0549	1.1430	.0893	.0557	.0542
105	0.00	6.449E-06	.002157	.001567	2.51E-06	981.	697.	190.3	439.5	15.3
105	386.14	.6452	249.51	.4174	3.098	44499.	1611.	.8023	.0002	.0020
107	.0627	.2220	39420.	1804.	.008410	.0748	.5430	.0893	.0706	.0614
107	0.00	4.856E-06	.002157	.001946	2.48E-06	975.	697.	191.3	457.5	14.9
107	56.09	.0930	51.68	.0858	3.959	33073.	1644.	.5000	.0003	.0041
59	.0627	.2220	20400.	319.	.008410	.0235	.4680	.0583	.1254	.2210
59	0.00	2.162E-06	.002067	.001943	2.56E-06	991.	696.	188.7	412.1	16.0
59	13.70	.1612	13.25	.1559	4.976	19299.	1554.	.2458	.0004	.0074
61	.0627	.2220	28200.	698.	.008410	.0299	.4536	.0583	.1073	.1160
61	0.00	4.687E-06	.002067	.001806	2.56E-06	989.	696.	188.7	416.2	16.0
61	47.48	.2955	42.53	.2654	4.131	26368.	1554.	.5296	.0004	.0046
63	.0627	.2220	35880.	1263.	.008410	.0314	.7452	.0717	.0871	.0939
63	0.00	4.739E-06	.002067	.001715	2.54E-06	989.	696.	189.4	420.1	15.7
63	87.69	.3871	74.62	.3296	3.628	33224.	1578.	.5763	.0003	.0043
113	.1028	.1976	8040.	197.	.005880	.0239	.4536	.0583	.1468	.2191
113	0.00	1.346E-06	.002545	.002470	2.56E-06	991.	696.	188.7	412.4	16.0
113	8.05	.0925	7.98	.0918	4.226	20452.	1554.	.1248	.0004	.0085
115	.1028	.1976	13140.	577.	.005880	.0368	.4536	.0583	.0809	.0785
115	0.00	4.182E-06	.002545	.002312	2.56E-06	987.	696.	188.7	420.5	16.0
115	38.40	.1564	36.03	.1469	2.847	32654.	1554.	.3878	.0004	.0059
117	.1028	.1976	10320.	325.	.005880	.0289	.4536	.0583	.1100	.1313
117	0.00	2.059E-06	.002545	.002430	2.59E-06	989.	696.	187.8	411.6	16.4
117	13.77	.0962	13.51	.0946	3.306	26261.	1522.	.1909	.0004	.0082
119	.1028	.1976	18450.	1364.	.005880	.0437	1.1430	.0893	.0549	.0523
119	0.00	5.063E-06	.002545	.002081	2.57E-06	985.	696.	188.2	422.9	16.2
119	156.71	.3572	133.51	.3045	2.434	45486.	1538.	.5376	.0002	.0052
121	.1028	.1976	16950.	1067.	.005880	.0378	1.1430	.0893	.0553	.0537
121	0.00	4.532E-06	.002545	.002129	2.56E-06	987.	696.	188.7	421.1	16.0
121	124.03	.3616	108.77	.3173	2.453	42045.	1554.	.4812	.0002	.0057
123	.1028	.1976	25080.	3350.	.005880	.0595	1.1430	.0893	.0424	.0416
123	0.00	6.967E-06	.002545	.001906	2.55E-06	980.	696.	189.2	437.4	15.8
123	391.39	.4531	280.66	.3253	2.391	59505.	1570.	.7397	.0002	.0028

RUN	IMP DIA	VES DIA	REVS	POWER	VES VOL	VOL FR	FLOW	FLOI	DSD CM	DSV CM
RUN	CWN	CWT	CIN	CIT	DAB	DENS	DENI	10³VISI	10³VISS	TEMP
RUN	COA	CO DSD	COIA	COI DSV	PONO DI	RE	SCNO	EFFY	EFIN	EFOUT
	MKH UNITS									
125	.1028	.1976	22050.	2283.	.005880	.0543	1.1430	.0893	.0535	.0594
125	0.00	6.617E-06	.002545	.001939	2.53E-06	982.	696.	189.6	435.9	15.6
125	323.44	.4838	242.88	.3633	2.394	52570.	1586.	.7026	.0002	.0031
129	8.90	.1008	8.79	.0996	5.523	17693.	1522.	.1354	.0004	.0087
129	.0726	.1976	13860.	231.	.005880	.0253	.4536	.0583	.1720	.2465
129	0.00	1.554E-06	.002715	.002628	2.59E-06	990.	696.	187.8	409.4	16.4
131	.0726	.1976	19080.	522.	.005880	.0356	.4536	.0583	.1021	.1145
131	0.00	2.797E-06	.002715	.002559	2.61E-06	987.	696.	187.1	412.9	16.7
131	19.19	.1042	18.53	.1010	4.797	24070.	1500.	.2441	.0004	.0079
133	.0726	.1976	24660.	868.	.005880	.0322	1.1430	.0893	.1008	.0751
133	0.00	3.237E-06	.002715	.002418	2.59E-06	988.	696.	187.5	412.7	16.5
133	62.75	.2746	58.45	.2558	3.688	31158.	1515.	.3236	.0002	.0079
135	.0726	.1976	29940.	1351.	.005880	.0434	1.1430	.0893	.0658	.0624
135	0.00	5.115E-06	.002715	.002246	2.55E-06	985.	696.	188.9	426.8	15.9
135	140.70	.3622	121.93	.3141	3.218	36546.	1562.	.5113	.0002	.0054
137	.0726	.1976	35220.	2196.	.005880	.0537	1.1430	.0893	.0520	.0619
137	0.00	6.941E-06	.002715	.002079	2.55E-06	982.	696.	189.2	433.5	15.8
137	308.94	.5273	233.59	.3993	3.222	42090.	1570.	.6938	.0002	.0033
139	.0726	.1976	32880.	1870.	.005880	.0509	1.1430	.0893	.0516	.0483
139	0.00	6.371E-06	.002715	.002131	2.53E-06	983.	697.	189.6	433.7	15.6
139	238.38	.4676	190.31	.3734	3.370	39311.	1586.	.6351	.0002	.0038
157	.0726	.1976	41940.	3435.	.005880	.0599	1.1430	.0893	.0476	.0485
157	0.00	7.252E-06	.002588	.001922	2.59E-06	980.	696.	187.5	430.5	16.5
157	431.28	.5395	301.07	.3768	2.991	50374.	1515.	.7581	.0002	.0028
143	.0542	.1976	19860.	209.	.005880	.0249	.4536	.0583	.2113	.2528
143	0.00	1.392E-06	.002588	.002510	2.64E-06	990.	695.	186.2	402.6	17.1
143	8.16	.1083	8.08	.1076	7.294	14389.	1470.	.1270	.0004	.0095
145	.0542	.1976	24960.	340.	.005880	.0294	.4590	.0583	.1532	.1858
145	0.00	2.110E-06	.002588	.002468	2.63E-06	989.	695.	186.4	406.2	17.0
145	14.06	.1209	13.79	.1187	5.991	17896.	1477.	.1929	.0004	.0087
147	.0542	.1976	31320.	564.	.005880	.0364	.4590	.0583	.0932	.0903
147	0.00	3.755E-06	.002588	.002376	2.63E-06	987.	695.	186.4	410.5	17.0
147	31.82	.1687	30.15	.1600	5.041	22172.	1477.	.3433	.0004	.0071
149	.0542	.1976	38460.	873.	.005880	.0440	.4590	.0583	.0734	.0705
149	0.00	6.086E-06	.002588	.002244	2.61E-06	985.	695.	187.1	418.2	16.7
149	78.00	.2649	68.81	.2338	4.218	26668.	1500.	.5564	.0004	.0046
151	.0542	.1976	44820.	1238.	.005880	.0414	1.1430	.0893	.0969	.0882
151	0.00	4.558E-06	.002588	.002170	2.54E-06	985.	696.	189.4	426.5	15.7
151	122.18	.3643	107.49	.3205	3.775	30500.	1578.	.4765	.0002	.0056
153	.0542	.1976	50520.	1678.	.005880	.0485	1.1430	.0893	.0512	.0503
153	0.00	5.426E-06	.002588	.002090	2.54E-06	983.	696.	189.4	431.1	15.7
153	177.77	.3922	148.93	.3289	3.582	33936.	1578.	.5672	.0002	.0046
155	.0542	.1976	38520.	873.	.005880	.0320	1.1430	.0893	.1125	.0828
155	0.00	3.146E-06	.002588	.002299	2.53E-06	988.	696.	189.6	421.4	15.6
155	64.56	.2988	60.23	.2790	4.183	26602.	1586.	.3289	.0002	.0071